TECHNISCHE
UNIVERSITÄT
DARMSTADT

ihwb

Modeling of Rain-Related Inundation Areas in Small Rural Catchments Using the Direct Rainfall Method

-

Modellierung von niederschlagsbedingten Überflutungsflächen in kleinen ländlichen Einzugsgebieten mit der Methode der direkten Beregnung

Vom Fachbereich Bau- und Umweltingenieurwissenschaften

der Technischen Universität Darmstadt

DISSERTATION

zur Erlangung des akademischen Grades Dr.-Ing.

von

Amrei Gesine David, M.Sc.

Erstgutachterin: Prof. Dr. habil. Britta Schmalz
Zweitgutachter: Prof. Dr.-Ing. Ernesto Ruiz Rodriguez

Darmstadt: 2023

Kurzfassung

Die modelltechnische, flächenhafte Ermittlung von Starkregengefahren ist für eine Vielzahl von planerischen wasserwirtschaftlichen Aufgaben von Bedeutung. Auf Basis von Überflutungskarten können Maßnahmen zum Überflutungsschutz geplant, Starkregenrisikomanagementpläne erstellt, Einsatzpläne und Evakuierungsstrategien entworfen oder stadt- und raumordnungsplanerische Entscheidungen getroffen werden. Vor allem für kleine, oberstrom gelegene Einzugsgebiete gibt es bisher noch keine einheitliche Methode zur Lokalisierung von durch Starkregen gefährdeter Gebiete (Starkregengefahrenkarten). Die vorliegende Doktorarbeit beschäftigt sich mit der Fragestellung, ob die Methode der direkten Beregnung (Direct Rainfall Method – DRM) einen geeigneten methodischen Ansatz darstellt, um Überflutungsbereiche in kleinen, ländlichen Einzugsgebieten flächenhaft zu ermitteln. Als Modellsystem wird das international weit verbreitete 2d Modell HEC-RAS als hydrologisch hydrodynamisches Niederschlags-Abflussmodell (Hydrological-Hydrodynamic Rainfall-Runoff Modell – HHDRRM) angewendet. Das Untersuchungsgebiet ist das Fischbach Einzugsgebiet (38 km²), ein Teileinzugsgebiet des Gewässersystems der Gersprenz (485 km²). Das Einzugsgebiet ist Teil des Feldlabors des Lehrstuhls für Ingenieurhydrologie und Wasserbewirtschaftung (IHWB) an der TU Darmstadt. In der Arbeit wird neben der Frage der generellen Anwendbarkeit von HEC-RAS als HHDRRM der Schwerpunkt auf die Abbildung der hydrologischen Komponenten im Modell und der flächenhaften Prozesse im Einzugsgebiet gelegt. Dabei wird die Forschungsfrage in drei Teilfragen mit folgenden Inhalten untergliedert: 1. Generelle Anwendbarkeit der Methode, 2. Räumliche Auflösung, Topographie und Modellsensitivität und 3. Flächenhafte, hydrologische Prozesse und Kalibrierung. Zur Beantwortung der drei Teilfragen wird jeweils eine eigene methodische Vorgehensweise innerhalb von drei Teilstudien entwickelt. Die Beantwortung der übergeordneten Forschungsfrage wird aus den Ergebnissen dieser drei Teilstudien abgeleitet. Durch diese Herangehensweise wird gezeigt, dass eine flächenhafte Ermittlung von Überflutungsbereichen mittels der DRM zusammen mit HEC-RAS im Untersuchungsgebiet möglich ist. Die Methode bietet ein großes Potenzial für die Starkregengefahrenanalyse in kleinen, ländlichen Einzugsgebieten. Die Modellergebnisse zeigen, ereignisabhängig gute bis sehr gute Übereinstimmungen mit den vorhandenen hydrologischen Messdaten. Auf Grundlage der durchgeführten Detailstudie zur Modellsensitivität können Empfehlungen zur räumlichen Auflösung der Topographie im Einzugsgebiet abgeleitet werden. Für ein aufgetretenes Starkregenereignis wird gezeigt, welchen Einfluss die Integration und Auflösung von flächenhaften, hydrologischen Prozessen (Catchment Hydrological Processes – CaHyPro) in das Modellgebiet auf die Modellergebnisse hat. Diese führen, unabhängig von einer Modellkalibrierung, zu einer deutlichen Verbesserung der Berechnungsergebnisse. Gleichzeitig werden Modelllimitationen und Verbesserungspotenziale von der DRM im Kontext der ereignisabhängigen, hydrologisch-hydrodynamischen Modellierung identifiziert. Diese zeigen sich in der im Vergleich zu

herkömmlichen Niederschlags-Abflussmodellen rechenzeitintensiven Anwendung, in den implementierten, aus der Gerinnehydraulik kommenden Gleichungsansätzen zur Oberflächenrauheit und in der Frage nach der Integration von weiteren abflussrelevanten, hydrologischen Komponenten. In der Thesis werden modelltechnische Lösungen zum Umgang der identifizierten Modelldefizite im Modellaufbau iterativ erarbeitet und abschließend der weitere Forschungsbedarf in der Anwendung von der DRM festgestellt.

Abstract

The model-based, spatially distributed determination of storm hazards is important for a variety of planning tasks in the field of water resource management. On the basis of flood maps, protective measures can be planned, storm risk management plans can be drawn up, emergency plans and evacuation strategies can be developed, or urban and spatial planning decisions can be made. Especially for small, upstream catchments, there is no standardized method for locating areas at risk from heavy rainfall (storm hazard maps). The scientific investigations presented herein address the question of whether the Direct Rainfall Method ('DRM') is a suitable methodological approach for identifying inundation areas in small, rural catchments. For this purpose, a case study is conducted using the internationally applied 2d model HEC-RAS as a Hydrological-Hydrodynamic Rainfall-Runoff Model ('HHDRRM'). The study area is the Fischbach catchment (38 km²) in Hesse (Germany), a subcatchment of the Gersprenz river system (485 km²). The catchment is part of the field laboratory of the Chair of Engineering Hydrology and Water Management (Fachgebiet Ingenieurhydrologie und Wasserbewirtschaftung – 'IHWB') at TU Darmstadt.

In addition to addressing the general applicability of HEC-RAS as a HHDRRM, the conducted research focuses on examining the representation of hydrological components and topographic data in the model. To this end, the study is divided into three research questions (sub-questions) concerning the 1. General Applicability, 2. Spatial Resolution, Topography and Sensitivity and 3. Catchment Hydrological Processes and Calibration. These questions are addressed in separate methodological approaches developed in sub-studies. The results of the sub-studies formed the basis for addressing the main objective of the study, namely the applicability of the DRM in the identification of storm hazards. The results obtained with this approach demonstrate that watershed-wide floodplain identification is possible by using the DRM in conjunction with HEC-RAS. It is shown that the proposed method offers great potential for storm hazard analysis in small rural catchments. The model results display good to very good agreements with the hydrological measurements, depending on the event. Through a detailed analysis of the sensitivity of the model, recommendations for the spatial discretization of the topography are derived. Based on an observed storm event it is shown which influence the integration and resolution of catchment hydrological processes ('CaHyPro') into the model domain has on the model results. It was shown that a higher spatiotemporal resolution of CaHyPro led to an improvement of the modeling results, independent of a model calibration. At the same time, model limitations and challenges of the DRM in the context of event-dependent hydrological-hydrodynamic modeling are identified. These arise mainly from the computationally intensive application of the DRM compared to conventional rainfall-runoff models, the implemented equation approaches for surface roughness coming from channel hydraulics, and the integration of further runoff-relevant hydrological components. The dissertation iteratively develops modeling solutions to address the identified model deficiencies and identifies further research needs in the application of the DRM.

Publications

I. David, A. & Schmalz, B. (2020). Flood Hazard Analysis in Small Catchments: Comparison of Hydrological and Hydrodynamic Approaches by the Use of Direct Rainfall. Journal of Flood Risk Management, 13(4), e12639. https://doi.org/10.1111/jfr3.12639

II. David, A. & Schmalz, B. (2021). A Systematic Analysis of the Interaction between Rain-on-Grid-Simulations and Spatial Resolution in 2d Hydrodynamic Modeling. Water, 13(17), 2346. https://doi.org/10.3390/w13172346

III. David, A. & Ruiz Rodriguez, E. & Schmalz, B. (2023). Importance of Catchment Hydrological Processes and Calibration of Hydrological-Hydrodynamic Rainfall-Runoff Models in Small Rural Catchments. Journal of Flood Risk Management, 16(3), e12901. https://doi.org/10.1111/jfr3.12901

Contents

List of Figures

List of Tables

List of Abbreviations

AP_I	Approach I
AP_II	Approach II
ATKIS	Official Topographic-Cartographic Information System/Amtliches Topographisch-Kartographisches Informationssystem
BC	Boundary Condition
BFD	Digital Soil Map/Bodenflächendaten
CaHyPro	Catchment Hydrological Processes
CN	Curve Number
CORINE	Coordination of Information on the Environment
CPU	Central Processing Unit
DEM	Digital Elevation Model
DRM	Direct Rainfall Method/syn. Direct Rainfall Modeling
DWA	German Association for Water, Wastewater and Waste e.V./Deutsche Vereinigung für Wasserwirtschaft, Abwasser und Abfall e.V.
DWD	German Weather Service/Deutscher Wetterdienst
DWE	Diffusive Wave Equation
EEA	European Environment Agency
FD-Models	Fully Distributed Models
FIM	Flood Inundation Modeling
GBII/GB2	Gauge of Groß-Bieberau 2
GIS	Geographical Information System
GLUE	Generalized Likelihood Uncertainty Estimation
GPU	Graphics Processing Unit
HEC-HMS	Hydrologic Engineering Center - Hydrologic Modeling System
HEC-RAS	Hydrologic Engineering Center - River Analysis System
HHDRRM	Hydrological-Hydrodynamic Rainfall-Runoff Model
HLNUG	Hessian Agency for Nature Conservation, Environment and Geology/Hessisches Landesamt für Naturschutz, Umwelt und Geologie
HPC	High Performance Cluster
HRU	Hydrological Response Unit

HVBG	Hessian Administration for Land Management and Geoinformation/Hessische Verwaltung für Bodenmanagement und Geoinformation
HWRM-RL	Flood Risk Management Directive/Hochwasserrisikomanagement-Richtlinie
IHWB	Chair of Engineering Hydrology and Water Management/Fachgebiet Ingenieurhydrologie und Wasserbewirtschaftung
IMI-CaHyPro	Approach of Iterative Model Improvement via Catchment Hydrological Processes
KOSTRA	Coordinated heavy precipitation regionalization and evaluation/ Koordinierte Starkniederschlagsregionalisierung und -auswertung
LAWA	German Working Group on water issues of the Federal States and the Federal Government/Bund-/Länder-Arbeitsgemeinschaft Wasser
MASL	Meters Above Sea Level
NSE	Nash-Sutcliffe Efficiency
RADOLAN	Radar Online Calibration/Radar Online Aneichung
RMS	Root Mean Square
SA	Sensitivity Analysis
SCS	Soil Conservation Service
SCS - CN	Soil Conservation Service - Curve Number
SD-Models	Semi Distributed Models
SW	Shallow Water
SWE	Shallow Water Equation
UA	Uncertainty Analysis
UH	Unit Hydrograph
USACE	U.S. Army Corps of Engineers
USDA	United States Department of Agriculture
WSE	Water Surface Elevation
ZI	Zero Inertia

1 Introduction

1.1 Motivation

Introduction – Flood Inundation Modeling

The modeling and graphical representation of flood plains resulting from storm events is of great importance for a variety of planning tasks in water resources management. This approach can be used to identify flood-prone areas and danger spots, understand the propagation of a flood wave in the watershed, develop risk management plans and evacuation strategies, and provide guidance for urban or regional planning decisions. Within the framework of the European Directive 2007/60/EC of the European Parliament and of the Council on the Assessment and Management of Flood Risks (Hochwasserrisikomanagementrichtlinie –'HWRM-RL'), a uniform procedure for dealing with fluvial flood hazards within the European Union has been established (EU, 2007). As a result of the European directive and in order to find a common national implementation of the directive, the "Recommendations for the creation, revision and updating of flood risk management plans" were formulated by the German Working Group on water issues (Bund/Länder-Arbeitsgemeinschaft Wasser - 'LAWA') (LAWA, 2018a). For the implementation of the HWRM-RL and the associated flood hazard maps, specific requirements exist in the respective federal states (e.g. UMBW, 2016). Considering these requirements, flood hazard maps can be prepared that include a graphical representation of the floodplains and thus form the basis for flood risk management plans. The floodplains are determined in advance using hydraulic models (LAWA, 2018a). Depending on the river structure and the associated flow regime, 1-dimensional (1d) or 2-dimensional (2d) hydrodynamic models are applied to determine flood hazards. 1d models are applied when the stream geometry is rather rectilinear. 2d models are mainly used for more complex flow conditions with water movements transverse to the main flow (UMBW, 2016).

From a technical point of view, hydrodynamic models represent an important tool for calculating flood hazards. They are often used together with rainfall-runoff models to determine the hydrological boundary conditions (David & Schmalz, 2020). This modeling procedure entails the separation of hydrological and hydrodynamic processes in two different modeling systems.

State of the Art: Storm Hazard Analysis – Direct Rainfall Method ('DRM')

Due to the devastating storm events and flash floods that have increasingly occurred in Germany and Europe in recent years, storm risk management strategies have been developed in parallel with flood risk management strategies. Although there is no European equivalent to the Flood Risk Management Directive for storm risk management, there is a LAWA guidance document on storm risk management as a national coping strategy for dealing with storm hazards (LAWA, 2018b). Furthermore, the guidelines were also additionally refined by the

federal states and thus adapted to regional specifics (e.g. LUBW, 2016). In addition to simplified hazard assessments based on site inspections and purely topographic, rainfall-independent methods, the basis for determining storm hazards continues to be hydrodynamic flood modeling based on 2d hydrodynamic models (LAWA, 2018b). In this case, the model area is directly irrigated and the hydrological processes are integrated in the 2d hydrodynamic model. This method is called the Direct Rainfall Method ('DRM') or the rain-on grid method (Ball et al., 2012). The advantage of the method is that the 2d model can be applied in small catchments as a Hydrological-Hydrodynamic Rainfall-Runoff Model ('HHDRRM'). This allows for integrated and spatially distributed modelling of runoff formation, concentration, and transformation in a singular model system. The advantage of the DRM comes into play especially in Flood Inundation Modeling ('FIM') in small, upstream catchments, when surface and channel runoff are difficult to separate spatially and the transitions between surface and channel runoff are ambiguous. In this case, the rainfall-runoff processes are not split into two different model systems.

2d Hydrodynamic Model HEC-RAS

The 2d model HEC-RAS, which is frequently used worldwide, was originally developed for the calculation of water surface elevations along the river line. The DRM was implemented in 2016 in HEC-RAS 5.0 for excess precipitation (HEC, 2016a). In 2021, spatially distributed rainfall and infiltration process integration was also introduced (HEC, 2021). However, the technically relatively "simple" model extension, where a source term is added, results in an application of the model for a variety of new use cases. This also includes the use of HEC-RAS as a HHDRRM. However, very little experience on model behavior, parameter estimation or sensitivity exists for the new application to date. This results in a knowledge gap with respect to modeling experience. Because of this lack of experience, especially among practicing modelers, the need for guidelines, experience, scientific investigations and recommendations in dealing with the DRM arises.

Study Area of Fischbach Catchment

The Chair of Engineering Hydrology and Water Management (Fachgebiet Ingenieurhydrologie und Wasserbewirtschaftung – 'IHWB') at Technical University of Darmstadt (TU Darmstadt) operates a river basin as a research field laboratory. Hydrological process analysis takes place in the research laboratory at two different spatial scales. The entire Gersprenz catchment covers an area of 485 km² (Schmalz & Kruse, 2019). The predominantly rural subcatchment of the Fischbach extends over 38 km² and is primarily cultivated for agricultural and forestry purposes. In the Fischbach catchment, flooding occurs as a result of storm events in addition to river flooding. A detailed spatially GIS-based analysis of flash flood hazards in the Gersprenz catchment shows that especially the upper, steeper catchments, as well as the heavily sealed areas are at risk of flooding from heavy rainfall events (Kleiber, 2018). For the subcatchment of the Fischbach River, the criteria for increased vulnerability due to storm events apply. An

example of this is provided by the storm event of April 23, 2018, which resulted in flooding not only from the Fischbach River itself, but also from surface runoff in the adjacent forest and on agricultural land (Echo, 2018; Bickelhaupt, 2018). Regarding the precipitation-related hazard situation, there is no statement on specific hazard locations, as flooding from storm events can occur anywhere (Winterrath, 2022).

Summarized Motivation

The motivation for this scientific work results from three research objectives. First, there is a methodological-scientific rationale to investigate the new method of direct rainfall and the use of a 2d model as HHDRRM (1. Methodological-scientific motivation). Second, there is an identified research gap in using the globally established 2d model HEC-RAS in combination with the DRM in terms of model behavior, parameter estimation, model parameterization, and model sensitivity (2. Model-specific motivation). Third, both pluvial and fluvial flooding occur in the field laboratory of the IHWB, which call for a methodological approach to determine storm-related floodplains. Therefore, especially for small, higher altitude catchments, an integrated approach to floodplain modeling is needed (3. Application-related motivation). The following **Figure 1** summarizes the three origins of motivation for this work. The practical approach of this research is intended to serve as an intermediary between scientific research and the applied engineering work of a practicing modeler.
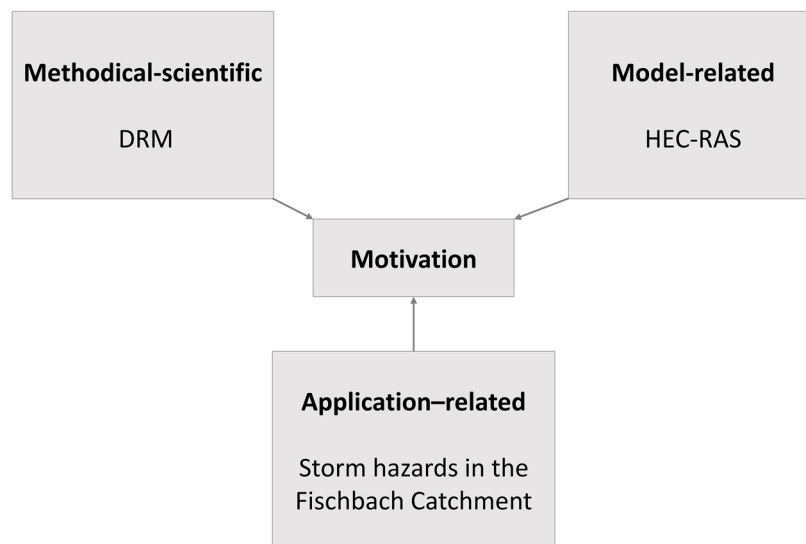
Figure 1: Graphical representation to illustrate the origin of the motivation of the research work

1.2   Research Questions and Objectives

In this doctoral thesis, the new and newly implemented Direct Rainfall Method is applied in the Fischbach River catchment using the 2d model HEC-RAS. Thereby the underlying question is whether the DRM is a suitable methodological approach to determine rain-related inundation

areas in small, rural catchments, such as the low mountain range Fischbach catchment and whether HEC-RAS can be used as HHDRRM. As a result, the study will help clarify the specifics and challenges of using HEC-RAS as a HHDRRM. Further, in addition to the general applicability of DRM in the Fischbach catchment, the work will focus on the parameterization of the catchment model. Here, the spatial resolution of topographic data as well as the hydrological processes are of major interest. This research emphasis is based on the consideration that although HEC-RAS has proven itself as a hydrodynamic model over many years, the hydrological modeling component has been added only recently. In the year 2016 for excess precipitation (HEC, 2016a) and in 2021 for gridded precipitation (HEC, 2021). The adding of the hydrologic model component and the integration of the hydrologic rainfall-runoff model and the 2d hydrodynamic model into one system allows for a variety of new use cases, but leads to a knowledge gap in the application of the new method.

For this reason, the research objective is divided into the following three sub-questions: 1. the question of the general applicability of the method, 2. the question of spatial resolution in terms of catchment topographic data and model sensitivity, and 3. the question of the integration of catchment hydrological processes and the subsequent model calibration. The three sub-questions are elaborated in more detail in the following:

1. **Question of Applicability:** Is it feasible to apply the DRM for the Fischbach River catchment using HEC-RAS? What are the challenges for small, rural catchments in terms of the model set-up, the approach of calibration and validation and the results compared to the classical, fluvial flood modeling approach?

2. **Question of Spatial Resolution of Topographic Data and Sensitivity:** Which model parameterization and spatial resolution with respect to the topographic data are reasonable when applying the DRM? Are there application-specific features and sensitivities regarding spatial resolution due to shallow water depths?

3. **Question of Catchment Hydrological Processes and Calibration:** What is the influence of the spatiotemporal resolution of the Catchment Hydrological Processes ('CaHyPro') of precipitation and runoff formation? Is there a possibility to integrate the event-based interflow (also referred to as subsurface stormflow) into the model system through an existing computational approach? How does the resolution and integration of the CaHyPro into the model domain interact with parameter estimation based on model calibration?

This work strives to combine an application and object-oriented approach. The compiled research results may be viewed as a summarized report of experience for practicing modelers. On this base, modeling experiences obtained during the application of the new method are compiled and application-oriented recommendations for the HEC-RAS model system and DRM in general are developed. Furthermore, the work aims to bridge the gap between model development and model application. It is intended to reinforce an existing, methodological approach with explicit modelling experience by means of a specific project area.

Each sub-question will be methodologically addressed separately in individual work packages.

1.3 Methodology and Structure

The central research objective is answered through the assessment of the three sub-questions mentioned in the previous chapter. This methodological approach serves to divide the set of questions arising from the new direct precipitation method into work packages. Each work package will answer one of the formulated sub-questions with an individual methodological approach. The sub-questions are dealt with one after the other so that the difficulties encountered and the results obtained can be incorporated into the structure of the subsequent investigation. This procedure makes it possible, on the one hand, to incorporate the challenges that arise during the processing time into the methodological procedure and, on the other hand, to ensure a consistent, continuous objective with the specified sub-questions.

The first sub-question addresses the question of applicability (**pp. 9 - 39**) by systematically comparing the decoupled and integrated approach to modeling storm events. 'Decoupled' is understood as the modeling of the rainfall-runoff process using two model systems: 1. The Rainfall-runoff model and 2. the 2d hydrodynamic model. Here, the runoff hydrographs generated in the rainfall-runoff model serve as inflow hydrographs for the 2d model. This approach is common in traditional fluvial flood hazard assessment. The 'Integrated method' combines the method of direct rainfall and the integrated modeling of hydrological and hydrodynamic processes in one modeling system. The model system HEC-RAS from USACE (U.S. Army Corps of Engineers) is used for this purpose. The field laboratory of the Fischbach catchment with a size of 38 km² serves as the study area. The entire study is presented in the second chapter of the compiled thesis and was published in 2020 in the Journal of Flood Risk Management from Wiley Online Library (David & Schmalz, 2020).

The second sub-question, the question of spatial resolution of topographic data and sensitivity (**pp. 40 - 86**) aims to develop a methodological approach in which the interaction between spatial resolution of the computational grid and the underlying terrain model is systematically investigated. During the development of the approach, the long computation times, which are the main challenge for a sensitivity analysis related to DRM, were to be taken into account. The study contains a detailed sensitivity study on topographic resolution in interaction with the computational mesh and further computational settings. Recommendations for spatial resolution, when the DRM is applied, are major findings from this study. For reasons of computational time, the spatial scale of the study area is reduced to a smaller subcatchment, the Messbach catchment with an extent of 2.1 km². The entire study is presented in the third chapter and was published in 2021 in the journal Water from the Multidisciplinary Digital Publishing Institute ('MDPI') in David & Schmalz (2021).

The third sub-question (**pp. 87 - 119**) addresses the spatiotemporal resolution of catchment hydrologic processes and their interaction with the parameter estimation after calibration. In the study, the CaHyPro of precipitation, runoff formation and event-related interflow with

various spatiotemporal resolutions are step by step added to the model area. The influence on the resulting runoff hydrograph at the gauging station is systematically investigated on the basis of the storm event of the April 23, 2018. In addition to the integration of radar precipitation data and a spatiotemporal differentiated runoff formation routine, the component of event based interflow (also referred to as subsurface stormflow), which has not been considered in the field of the DRM so far, is addressed. For this purpose, a procedure is developed to implement an existing, simplified approach into the model system HEC-RAS. Finally, the role of the integration of CaHyPro for the model parameterization after calibration is discussed. The following paragraph lists the three studies conducted and the associated publications.

Publication I, Sub-Question 1: Question of Applicability (pp. 9 - 39)
David, A. & Schmalz, B. (2020). Flood Hazard Analysis in Small Catchments: Comparison of Hydrological and Hydrodynamic Approaches by the Use of Direct Rainfall. Journal of Flood Risk Management, 13(4), e12639. https://doi.org/10.1111/jfr3.12639

Publication II, Sub-Question 2: Question of Spatial Resolution of Topographic Data and Sensitivity (pp. 40 - 86)
David, A. & Schmalz, B. (2021). A Systematic Analysis of the Interaction between Rain-on-Grid-Simulations and Spatial Resolution in 2d Hydrodynamic Modeling. Water, 13(17), 2346. https://doi.org/10.3390/w13172346

Publication III, Sub-Question 3: Question of Catchment Hydrological Processes and Calibration (pp. 87 – 119)
David, A. & Ruiz Rodriguez, E. & Schmalz, B. (2023). Importance of Catchment Hydrological Processes and Calibration of Hydrological-Hydrodynamic Rainfall-Runoff Models in Small Rural Catchments. Journal of Flood Risk Management, 16(3), e12901. https://doi.org/10.1111/jfr3.12901

The following **Figure 2** depicts the methodological framework of the thesis. The starting point is the central research objective, which is subdivided into the three sub-questions and set the focus of the thesis. For each sub-question a separate methodological approach is developed and the results were each published in an independent publication. The three publications are shown in the blue colored box. The challenges and difficulties encountered in each sub-study are incorporated into the design of the methodological approach for the subsequent study. The red colored arrow marks this approach. The spatial scale is adapted to the respective sub-questions. The entire Fischbach catchment with 38 km² serves as study area for the first investigation. The smaller subcatchment of the Messbach catchment with 2.1 km² is used for the detailed study of spatial resolution of topographic data. Finally, for the analysis on CaHyPro, the summarized findings of the first two case studies are again applied in the entire Fischbach catchment. The spatial scale of the sub studies is represented by the size of the black bordered

boxes at the left side in **Figure 2**. The final part of the thesis provides the summarized results, which contain methodological knowledge for the handling of the DRM, model experiences and guidelines for the model HEC-RAS in the use as HHDRRM, as well as explicit modeling experiences. These are summarized and discussed in Chapter 5. The green arrow added to the figure symbolizes the overall goal of improving flood inundation modeling, which is available to the modeler for future applications.

Research question: Is the DRM a suitable methodological approach to determine rain-related inundation areas in small, rural catchments, such as the low mountain range Fischbach catchment, and can HEC-RAS be used as HHDRRM?

Spatial scale

Sub-Question 1: Question of Applicability

38 km²

Publication I: Flood Hazard Analysis in Small Catchments: Comparison of Hydrological and Hydrodynamic Approaches by the Use of Direct Rainfall

Fischbach

Sub-Question 2: Question of Spatial Resolution of Topographic Data and Sensitivity

2.1 km²

Publication II: A Systematic Analysis of the Interaction between Rain-on-Grid-Simulations and Spatial Resolution in 2d Hydrodynamic Modeling

Messbach

Sub-Question 3: Question of Catchment Hydrological Processes and Calibration

38 km²

Publication III: Importance of Catchment Hydrological Processes and Calibration of Hydrological-Hydrodynamic Rainfall-Runoff Models in Small Rural Catchments

Fischbach

Summary, discussion and outlook

- Methodological knowledge on DRM
- Model experience with HEC-RAS in use as HHDRRM
- Explicit experience and guidelines for practicing modelers

Improvement of Flood Inundation Modeling (FIM)

Figure 2: Framework of the thesis with key research question and methodological overview; DRM – Direct Rainfall Method, HHDRRM – Hydrological-Hydrodynamic Rainfall-Runoff Model, HEC-RAS – Hydrologic Engineering Center – River Analysis System

1.4 Author Contributions

The main part of the thesis consists of three manuscripts, which have been submitted to international peer-reviewed journals. The three manuscripts passed a double-blind peer review process each and were published in two different professional journals. The author herself is responsible for the principal part of the work presented. All listed co-authors contributed to the manuscripts through their ideas, comments, discussions, and review of the final manuscripts. The author contributions of the first author and the supporting co-authors of the three manuscripts are listed below.

Publication I: Conceptualization: David, A. and Schmalz, B.; Methodology: David, A. and Schmalz, B.; Software: David, A., Investigation: David, A.; Data curation: David, A. and Schmalz, B.; Visualization: David, A.; Writing — Original draft: David, A.; Writing — Review & Editing: David, A. and Schmalz, B.; Supervision: Schmalz, B..

Publication II: Conceptualization: David, A. and Schmalz, B.; Methodology: David, A. and Schmalz, B.; Software: David, A., Investigation: David, A.; Data curation: David, A. and Schmalz, B.; Visualization: David, A.; Writing — Original draft: David, A.; Writing — Review & Editing: David, A. and Schmalz, B.; Supervision: Schmalz, B..

Publication III: Conceptualization: David, A., Schmalz, B., Ruiz-Rodriguez, E.; Methodology: David, A., Schmalz, B., Ruiz-Rodriguez, E.; Software: David, A., Investigation: David, A.; Data curation: David, A. and Schmalz, B.; Visualization: David, A.; Writing — Original draft: David, A.; Writing — Review & Editing: David, A., Schmalz, B., Ruiz-Rodriguez, E.; Supervision: Schmalz, B., Ruiz-Rodriguez, E..

All authors have read and agreed to the published versions of the manuscript.

2 Flood Hazard Analysis in Small Catchments: Comparison of Hydrological and Hydrodynamic Approaches by the Use of Direct Rainfall

Abstract

The classical 'decoupled' approach for fluvial flooding makes use of hydrographs as input boundary conditions. The catchment hydrology is determined by empirical semi-distributed rainfall–runoff models, the flood processes by the use of hydrodynamic models. However, for urban floods, the distributed rainfall is set directly as input (Direct Rainfall Modelling – DRM) to the elements of the 2d model. This 'integrated approach' aims to include hydrological and hydraulic processes in one single model. In this study, both modelling approaches are applied and evaluated for their suitability to determine flood hazards in small, rural catchments. The resulting flood maps and flow hydrographs are compared for selected rainfall–runoff events in a catchment located in Central Germany. In the first approach, the hydrological model (HEC-HMS) from the Hydrologic Engineering Center (HEC) is used to generate the inflow boundary hydrographs for the 2d model (HEC-RAS), which is then used to simulate the flow variables for the river network and its floodplains. For the second approach, the DRM is applied over the whole catchment by the use of HEC-RAS. Special focus is given for the integrated approach to the difficulties occurring during the model optimization and calibration. The comparison of the results and modelling processes of both approaches give insights into the advantages, disadvantages and difficulties or limitations of each presented approach.

Keywords: Direct Rainfall Modelling (DRM); flash flood; Flood Inundation Modelling (FIM); HEC-RAS; hydraulic modelling; hydrological modelling; pluvial flooding

2.1 Introduction

2.1.1 Motivation and Research Gap

Since the institutionalized initiation of fluvial flood hazard mapping by the European Union Floods Directive (2007/60/EC), a standardized procedure has been established for the generation of flood maps along large rivers. In 2010, the German working group on water issues (Bund-/Länderarbeitsgemeinschaft Wasser) published a document addressing a standardized methodology on the production of flood hazard – and risk maps (LAWA, 2010). In addition, the ministries of the federal states published several documents to improve the quality of the flood risk maps and give recommendations within their area of administration (compare LUBW, 2012; MKULNV, 2014). Internationally, the need for standardization and improvement of flood risk mapping led to the benchmarking of 2d surface water models and 2d hydrodynamic models for urban flooding (compare Hunter et al., 2008; Néelz & Pender, 2013). The procedure to determine fluvial flood hazards can be divided into two main steps. Firstly, the determination of flow rates of single runoff events, using hydrological rainfall–runoff models (e.g., HEC-HMS, WaSiM-ETH, LARSIM) and, secondly, using the calculated hydrographs as inflow boundary condition to the 2d hydrodynamic model (e.g., HEC-RAS, TUFLOW, MIKE21). This well-established flood inundation modelling (FIM) using two separate models has been subject to various international studies. In Thakur et al. (2017), Elfeki et al. (2017), Tahmasbine et al. (2012), Gül et al. (2010) or Knebl et al. (2005) examples can be found in which the hydrological analysis is based on HEC-HMS while hydrodynamic modelling of the floodplains is done using HEC-RAS.

The increasing availability of detailed observation data, advancing methods in flow observation and terrestrial surveys, increasing computational power by the use of GPU (graphics processing unit)-based simulations and better parallelization techniques have led to an ongoing optimization of FIM (García-Feal et al., 2018; Loretz & Volz, 2017; Cea & Bladé, 2015; Faber et al., 2012; Neal et al., 2010; Rauchlatner & Höppl, 2009; Mandlburger et al., 2009). The coupling procedure has been further developed to more integrated concepts by the use of distributed hydrological models and integrated hydrological and hydrodynamic modules in one model system only (Bates & De Roo, 2000; Howes et al., 2006; Cea et al., 2008; Cea & Bladé, 2015). In Nguyen et al. (2016), Nguyen et al. (2015) or Segura-Beltrán et al. (2016), examples can be found where a distributed hydrological model is coupled with an 2d hydrodynamic model via subcatchment hydrograph point source. The development of the different coupling methods between raster-based hydrological and hydrodynamic models is not focus in this study. However, the more classical described method of using a lumped hydrological model and a 2d hydrodynamic model consecutively will be further investigated and called decoupled approach in the following.

Due to a rising number of hazardous non-fluvial flood events in the past and present (Bronstert et al., 2017; GDV, 2017; Schanze, 2018; Vogel et al., 2017) in combination with a forecasted increase of extreme events due to climate change (Hübener et al., 2017), there is a growing

awareness in Germany and Europe on different types of flooding. These floods originate from heavy rainfall events bearing different characteristics than fluvial floods. They occur apart from large rivers and are often characterized as urban, flash or pluvial floods. In small catchments, a combination of all three flood types can occur whereas the definition of pluvial floods is often considered to be a part of the main river network (Schanze, 2018). There is an increasing application of a storm risk management besides the mentioned classical flood risk management. In the last years several technical papers and authoritative guidelines were published to give recommendations on the procedure of storm hazard analysis and risk management (LAWA, 2018; Tyrna et al., 2018; LUBW, 2016; Fritsch et al., 2016; Assmann et al., 2012; Falconer et al., 2009). Apart from analyses based on Geographical Information Systems (GIS) of the digital elevation model (DEM), the key features of the storm risk management are again the 2d surface water models based on the 2d St. Venant equations. Non-fluvial floods with strongly interconnected rainfall–runoff processes are modelled with an integrated modelling approach which is also known as direct rainfall modelling - 'DRM' (Babister & Barton, 2012) or *'rain-on-grid'* approach (Taylor et al., 2014). Here, the hydrological and hydrodynamic flood processes are not modelled in two different model systems, they are modelled entirely with the 2d hydrodynamic model. This approach is meanwhile widely used to determine the rainfall–runoff processes of watersheds with different sizes (e.g., Cea & Bladé, 2015; Fernández-Pato et al., 2016; Howes et al., 2006; Kivva & Zheleznyak, 2005). Hall (2015) presents a comprehensive overview on the current state of the art and experiences of the application of the DRM on a large scale. Thereby, he gives a concise summary about the advantages ('the good') and disadvantages ('the bad and the ugly') which lie in the application of this method. Rehmann et al. (2003) carried out a comparison between traditional hydrological and 2d hydrodynamic routing methods. Van Drie et al. (2011) and Van Drie et al., (2010) compared the 2d model ANUGA and the role of roughness coefficients with the traditional hydrological model WBNM. Further successful applications of the integrated approach can be found in Tyrna et al. (2018). Some long-term experiences of the pluvial flood risk management are presented in Fritsch et al. (2016).

Also on an urban scale a similar development from semi-distributed (SD) to fully distributed (FD) stormwater models can be observed in Pina et al. (2016). The FD models make use of the DRM and rainfall is directly applied to the elements of the 2d hydrodynamic model. Due to the high relevance of the sewer system the studies often focus on the concept of dual drainage (Djordjevi et al., 1999; Djordjevi et al., 2005). Many studies apply the bi-directional coupling of 1d sewer system and 1d/2d surface flow models (Fan et al., 2017; Leandro & Martins, 2016; Seyoum et al., 2012; Chen et al., 2010; Li et al., 2009 or Leandro et al., 2009). Fully integrated urban 2d applications of direct rainfall with integrated determination of the infiltration processes can be also found in Leandro et al. (2016), Pina et al. (2016), Fernández-Pato et al. (2016), Chang et al. (2015) or in Cea et al., (2010b). Cea et al., 2010a validate the numerical results of the dynamic and a diffusive wave model by an experimental small-scale laboratory configuration with a 3d rainfall simulator.

Despite the fast ongoing development and widespread parallel application of either fluvial or storm hazard analysis in all different kinds of catchments, a clear delimitation of the two mentioned approaches and a comparison of their suitability is needed in terms of: the exact type of flooding which is to be modelled, the catchment size, the dominating hydrological processes and the computational effort of each approach.

2.1.2 Objectives

The purpose of this study is to contrast and compare the two mentioned different flood modelling approaches in a small rural catchment area ($38\,km^2$) in Hesse, Germany.

The aim of the work is to apply the integrated hydrodynamic approach which is mainly used for urban flooding in a rural, gauged catchment. This model set-up will be compared with the application of the more classical decoupled approach for fluvial flooding. HEC-HMS 4.2.1 (HEC, 2016d) from the Hydrologic Engineering Center (HEC) was chosen as hydrological rainfall–runoff model. HEC-RAS 5.0.6 was used as 2d hydrodynamic model (HEC, 2016a).

The summarized objectives are:

- to model similar observed rainfall–runoff flood events in an exemplary small catchment with the use of the two different modelling techniques (Approach I: Decoupled approach; Approach II: Integrated approach);
- to evaluate whether the use of HEC-HMS as rainfall–runoff model in combination with HEC-RAS as 2d hydrodynamic model and only HEC-RAS are suitable to apply Approaches I and II;
- to compare the modelling process and the results of the two different modelling approaches and to give recommendation on the use of the integrated approach in comparison to the decoupled approach for flood inundation modelling in small catchments;
- to make 'a first step' towards the use of DRM in combination with HEC-RAS in application in this area ($38\,km^2$) and to find suitable model settings. The case study is seen as a proposal of how the integrated methodology can be principally applied with this model.

The Fischbach catchment is part of a field observatory of the Chair of Engineering Hydrology and Water Management (IHWB) from Technical University of Darmstadt (Schmalz & Kruse, 2019).

2.2 Materials and Methods

In this section, materials and methods involved in the realization of the project's objectives are presented. An overview on the modelling procedure and the evaluation of the results are given in **Figure 3**. The main part consists of two model set-ups based on different modelling principles. The first approach (Approach I) involves the decoupled hydrological–hydrodynamic modelling with HEC-HMS and HEC-RAS successively. The second approach (Approach II) involves an integrated approach of only hydraulic modelling with direct (effective) precipitation in HEC-RAS.
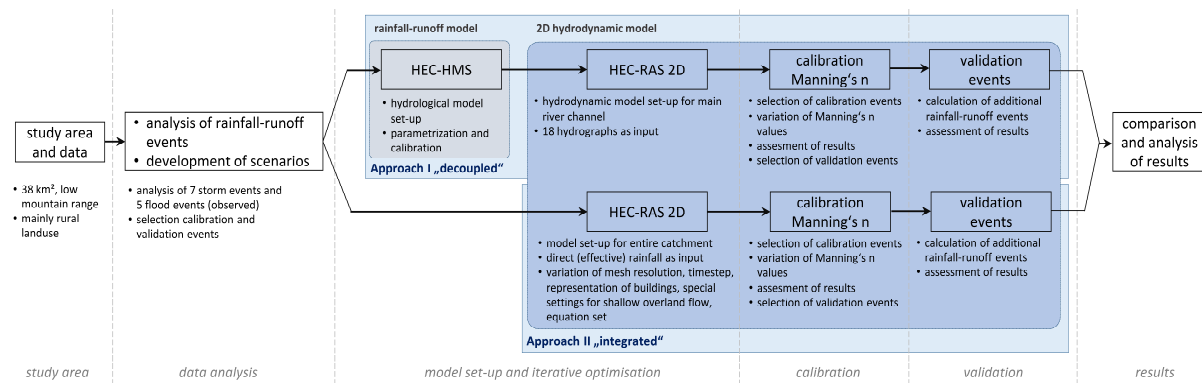
Figure 3: Methodical overview to compare the 'decoupled' hydrological–hydrodynamic Approach I and the 'integrated' Approach II with direct rainfall for event based modelling

2.2.1 Study Area and Data

The Fischbach catchment (**Figure 4**) is located in the south of Hesse in Germany in the low mountain range of the Odin forest ('Odenwald'). Water level and discharge data provided by the Hessian Agency for Nature Conservation, Environment and Geology (HLNUG) was utilized. Time series for Groß-Bieberau2 (GBII) were made available from 1985 to 2018 in 15-min intervals (HLNUG, 2020a). The gauging station GBII delineates 93.2 % of the Fischbach catchment area. The highest recorded winter floods were 22 and 20 m³/s in the years 1995 and 1983, respectively. The highest discharge in summer measured 12.8 m³/s in 1998 (HLNUG, 2011). Due to reoccurring high winter floods, a flood retention basin with 220.000 m³ storage volume was constructed in 2016 and is in operation since 2017.
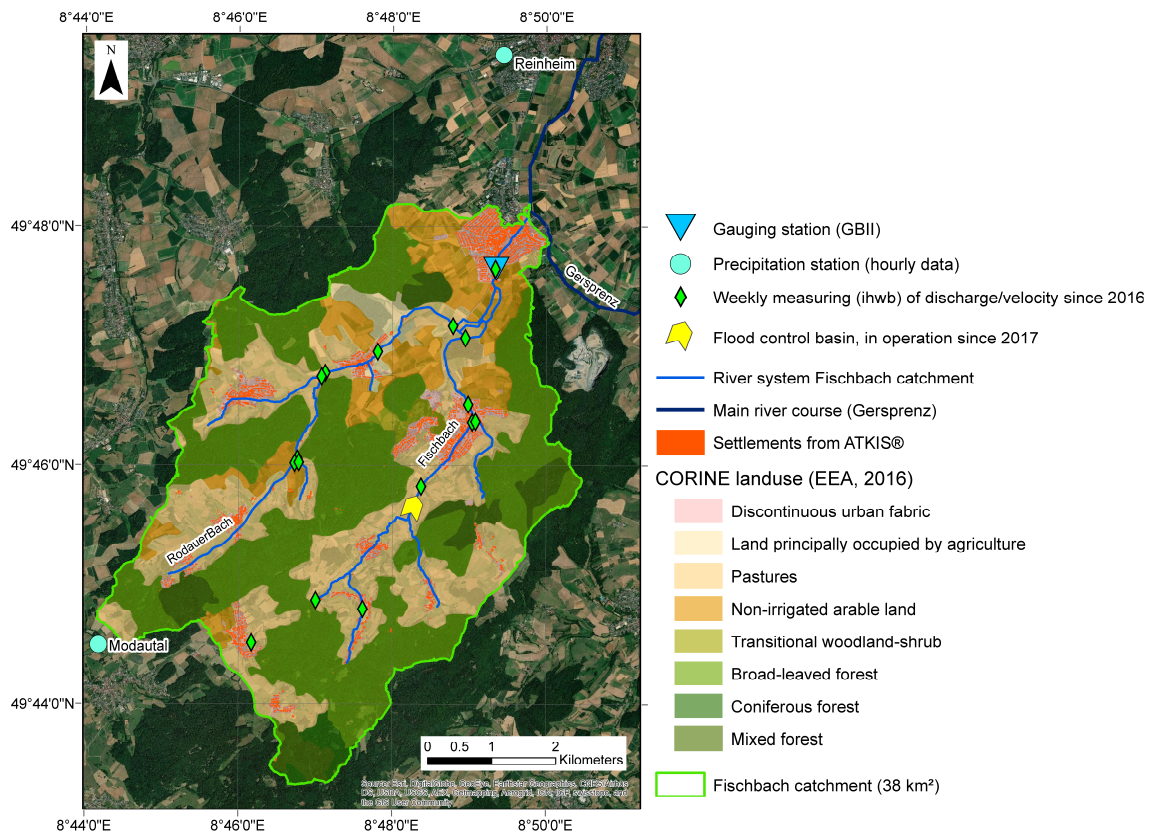
Figure 4: Study area of Fischbach catchment (38 km³) with river system (HVBG, 2017a), land use and location of precipitation stations Modautal (HLNUG, 2020b), Reinheim (DWD, 2018) and gauging station GBII (HLNUG, 2020a)

As precipitation data, the two closest precipitation stations, Reinheim, from the German Meteorological Service (DWD, 2018) and Modautal–Brandau–Kläranlage (in the following called Modautal) (HLNUG, 2020b) from HLNUG are used. The highest recorded hourly rainfall intensities for the evaluated time period (2004–2016) are 32 mm/h at the Reinheim station and 39.8 mm/h at the Modautal station.

Table 1 summarizes the maximum observed events during the observation period for precipitation and runoff.

Table 1: Discharge and precipitation data and maximum values during observation period

Measuring station	Analyzed period	Time step	Max. value	100 a event
Gauging station I (GBII)	1985–2016	15 min/1 h/1 day	22 m³/s	23.5 m³/s
Precipitation Station I (Reinheim)	2004–2016	10 min/1 h/1 day	32 mm/h	49.5 mm/hr[a]
Precipitation Station II (Modautal)	2004–2016	1min[b] /1 h /1 day	39.8 mm/h	43.3 mm/hr[a]
Radar measurement, RADOLAN-RW (1 km²) (Winterrath et al., 2018a)	2005–2016	1 h	67.4 mm/h	50.2 mm/hr[a]
KOSTRA-2010 (67 km²) (DWD, 2017)	1951–2010	1 h	–	55.2 mm/h

[a] Schürmann (2018), [b] Scenario 10: April 23, 2018.

The topography was analyzed based on a DEM provided by the Hessian Agency for Land Management and Geoinformation (HVBG, 2017b) with a 1-m raster resolution.

Land use data were retrieved from the CORINE classification for land cover from the European Environment Agency (EEA, 2016). Analysis of this data showed that local conditions were not accurately presented. Therefore, official topographical data (ATKIS®) provided by HVBG (2017a) were used to improve the data set. About 90% of the catchment is not sealed and there is no wastewater treatment plant within the catchment. Therefore, effects of sewer system drainage were neglected within this study.

For soil classification, the digital soil map BFD50 (1:50,000) was used from (HLNUG, 2017a). The catchment's soil is predominantly silt and clay. Over 70% of the soils are categorized as medium clay or sandy loamy silt.

2.2.2 Cross-sectional Data and River Bathymetry

From previous studies, data from the HLNUG on cross sections are available along 6.5 km of the Fischbach River (**Figure 5**). For the remaining kilometers, additional cross sections were recorded by own geodesic surveys. The satellite-based measurements were carried out with a real-time kinematic receiver from JAVAD (2017). The average distance between the profiles was set to be 110 m. At river segments with jumps and strong profile changes, distances were set lower. Due to the very small river size, with cross section widths of only 1–2 m in the upper region and 5–6 m in the lower region, there are many bridges and culverts along the smaller tributaries. For economic reasons, it was not possible to survey the geometries of existing structures in detail.
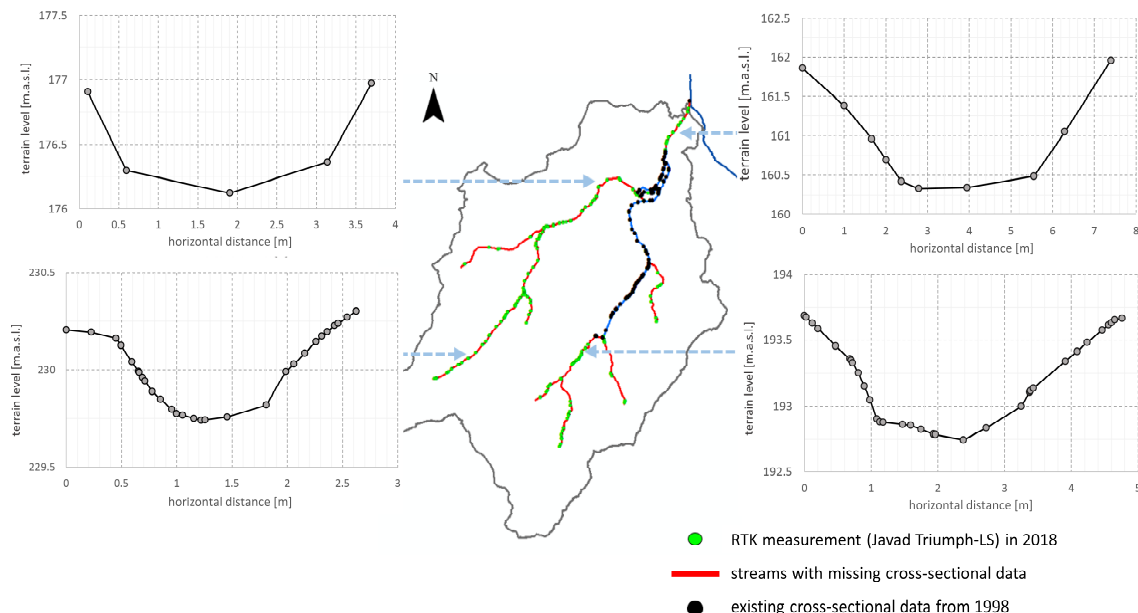
Figure 5: Locations of terrestrial cross-sectional survey with RTK receiver JAVAD Triumph-LS and exemplary cross-sectional profiles within the catchment

2.2.3 Event Analysis and Selection of Modelling Events

With the objective to investigate the effects of extreme rainfall events on flooding, the time series were analyzed to depict exemplary events for the calibration and validation. A threshold for the variable precipitation was set in accordance to the DWD Alert level 3 ($>25\,\mathrm{mm/h}$ or $>35\,\mathrm{mm/6\,h}$). Flooding was defined as an event characterized by discharges measuring more than two years return period ($Q_2 = 5\,\mathrm{m^3/s}$). From 2004 to 2016 six storm events and five flood events were identified. The characteristics of each flood and storm event area are summarized in **Table 2**. The runoff coefficient Ψ for each event was determined via the direct runoff divided by the total precipitation. The hydrograph separation followed the methodology proposed by Blume et al. (2007).

Table 2: Analysis of flood and storm event characteristics within observation period (2004–2016); the storm event on April 23, 2018 occurred during editing time and was added to extend the list of rainfall–runoff events

	Date	Pev_area (mm)	PDur (h)	I_{max} (mm/h)	T_I_{max} (a)	API, 21 (mm)	API, 30 (mm)	Q_{ev_tot} (mm)	Q_{max} (m³/s)	T_Q_{max} (a)	Q_0 (m³/s)	BLag (min)	Ψ (–)
Storm events	10 June 2004	20.1	6.5	30.8	7.6	3.2	6.1	0.8	1.6	1.0	0.08	60	0.03
	27 July 2006	9.5	2	32.0	8.9	8.0	17.1	No flood	–	–	0.08	–	–
	9 June 2007	36.9	5	39.8	24.9	6.0	17.6	1.4	1.7	1.0	0.15	240	0.03
	23 June 2007	32.8	12	14.3	0.8	30.3	52.9	6.0	5.7	2.4	0.58	540	0.14
	3 August 2010	18.5	4.5	31.2	8.0	28.2	48.4	1.4	2.0	1.1	0.42	180	0.03
	5 December 2011	54.8	22	13.3	0.7	42.7	44.2	3.8	4.7	1.9	0.10	300	0.06
	23 April 2018	20.5	1	29.2	6.1	9.2	15.4	8.5	12.5	9.9	0.5	165	0.35
Flood events	10 May 2007	48.1	18.5	18.4	1.5	17.3	18.5	4.9	6.4	2.8	0.20	300	0.09
	13 June 2007	32.8	12	14.3	0.8	30.3	52.9	6.0	5.7	2.4	0.58	540	0.14
	13 January 2011	30.6	29	3.2	0.2	21.6	26.5	14.8	6.7	2.9	1.28	420	0.28
	31 May 2013	35.0	14	6.6	0.3	35.5	54.3	7.5	6.7	2.9	0.59	660	0.17
	1 June 2013	21.9	12	5.4	0.3	39.4	58.5	12.1	8.6	4.4	2.18	420	0.30

Abbreviations: Pev_area, total event areal precipitation determined with Thiessen polygons in [mm]; Pdur, total rainfall event duration in [h]; I_max, maximum rainfall intensity per event in [mm/h]; T_Imax, return period of max. rainfall intensity in [a] by KOSTRA-2010 (DWD, 2017); API, 21, 21 days antecedent precipitation index by (Zaiß, 1989); API, 30, 30 days antecedent precipitation index; Qev_tot, total event runoff in [mm]; Qmax, max. event discharge in at GBII [m³/s]; T_Qmax, return period in [a] of peak discharge with log-distribution, plotting positions m/N+1 (Makkonen, 2006); Q0, pre-event discharge in [m³/s]; Blag, basin lag time in [min]; Ψ, runoff coefficient determined based on Blume et al. (2007).

For the hydrological modelling, event-based calibration was possible for all events, due to low computational time. For the modelling in HEC-RAS, events were selected in respect to their suitability for calibration and validation. The rainfall–runoff events from 23 June 2007 (Scenario 04) and 23 April 2018 (Scenario 10) fit the set criteria for storm and flood events and were thus utilized for calibration in Approaches I and II. The other summer storm events with high precipitation are characterized by very low runoff coefficients combined with low

antecedent precipitation indexes (APIs). This is assumed to be difficult to model accurately by the integrated approach. Therefore as validation events for Approach I the two observed events of 9 June 2007 (Scenario 03), 1 June 2013 (Scenario 09), and two statistical events (Scenarios 11 and 12) were investigated. For the integrated approach, for reasons of computational time, only the flood event of 1 June 2013 (Scenario 09) is analyzed. **Table 3** gives an overview of all events used in calibration and validation in this study.

Table 3: Selection of modelling events for calibration and validation (Approach I: 'decoupled' and Approach II: 'integrated')

#	Date	Calibration data	Approach I (decoupled)		Approach II (integrated)
			HEC-HMS	HEC-RAS	HEC-RAS
Scenario 01	10 June 04	Yes	Yes[a]	No	No
Scenario 02	10 May 2007	Yes	Yes[a]		
Scenario 03	9 June 2007	Yes	Yes[a]	Yes[b]	
Scenario 04	23 June 2007	Yes	Yes[a]	Yes[a]	Yes[a]
Scenario 05	3 August 2010	Yes	Yes[a]	No	No
Scenario 06	13 January 2011	Yes	Yes[a]		
Scenario 07	5 December 2011	Yes	Yes[a]		
Scenario 08	31 May 2013	Yes	Yes[a]		
Scenario 09	1 June 2013	Yes	Yes[a]	Yes[b]	Yes[b]
Scenario 10	23 April 2018	Yes	Yes[a]	Yes[a]	Yes[a]
Scenario 11	100a, 1 h	No	Yes	Yes[b]	No
Scenario 12	100a, 6 h	No	Yes	Yes[b]	

[a] Used for calibration.
[b] Used for validation.

2.2.4 Approach I ('decoupled'): HEC-HMS and HEC-RAS

Hydrological Modeling (HEC-HMS)

For spatial discretization and the differentiation of input hydrographs, the catchment was divided into 19 subcatchments (**Figure 8**). The discretization was primarily done due to topographical data. At each inflow stream delineating to the main river course an outlet point was set. Additionally the location of the IHWB's observation stations (**Figure 4**) was used as extra criteria to add outlet points. The parameterization for each subcatchment was done on the basis of topographical data, such as channel and catchment slope, flow length, land use and soil. The areal information was assigned to each catchment and transport segment using HEC-GeoHMS (HEC, 2012). For the spatial rainfall distribution, each subcatchment is assigned to one gauging station based on the Thiessen Polygons. **Table 4** summarizes the averaged assigned parameters for each considered hydrological process.

Table 4: Calculation methods and parametrization to calculate hydrological catchment response via the hydrological model HEC-HMS (HEC, 2000). A short summary of the underlying mathematical model of HEC-HMS can be found in **Appendix A**.

Hydrological process: calculation routine	Parametrization
Runoff formation: **SCS[a] - Curve Number Method**	• SCS-CN values for each subcatchment: 67.6–78.6 based on (Melenti et al., 2011) • Initial abstraction I_a: 13.8–24.3 mm ($I_a = 0.2 * S_{max}$)
Runoff concentration: **Clark Unit Hydrograph**	• Time of concentration t_c (h) (watershed lag method): 0.4–1.3 h (USDA, 2010) • Storage coefficient R (h): 0.4–1.3 h (initially set as t_c, calibration parameter)
Runoff routing: Kinematic Wave	• Manning's n value: 0.029–0.045 • Sub-reaches: 1–2, Shape: triangle, trapezoid • Side slope (×H:1V): 0.3–2.3, slope (M/M): 0.002–0.09, length: 0.5–2.1 km
Baseflow: Constant Monthly	• Constant baseflow for each subcatchment: 0.001–0.039 m³/s

[a] SCS - Soil Conservation Service.

After the set-up, each event was calibrated individually in HEC-HMS using the objective functions of Nash-Sutcliffe efficiency (NSE), root mean square (RMS) and volume residual (Vol. Residual) to evaluate the 'goodness of fit' for each event. The calibration was conducted based on the processes of runoff formation (SCS-CN values, initial abstraction I_a), runoff concentration (storage coefficient R, concentration time t_c), channel routing (Manning's n) and baseflow (constant flow Q_B). Parameters were increased or decreased uniformly for the different subcatchments and transport segments. The baseflow was set as constant baseflow for each subcatchment as a percentage of the pre-event discharge Q_0 (**Table 2**). The percentage of the 19 subcatchments is determined via analysis of the IHWB's discharge measurements. All weekly measurements (2016 – 2017) are sorted by range and the percentage of the lowest discharges is calculated at each station as a percentage in comparison to the total low flow rate at the catchment's outlet. The calibration process was terminated for the event when the change of the evaluated parameter did not have a positive impact on the objective functions. The objective functions of all calibrated events of NSE are in a range of 0.68–0.98, RMS in a range of 0.1 to 1.0 m³/s and volume residuals of 0.1–0.3 mm.

Table 5 provides an overview on the final calibrated parameters. Due to the very different event characteristics, no sophisticated long-term soil moisture routine and the event-based calibration procedure, the parameter set varies for each event. Therefore, no validation is done for the hydrological model. As parameter set for the statistical event, the one from the runoff event of 23 June 2007 is selected.

Table 5: Calibration parameters and range of calibrated values for hydrological modelling

Calculation routine	Calibrated parameter	Calibrated average value range for *flood events*	Calibrated average value range for *storm events*
SCS Curve Number Method[a]	SCS-CN values	55.5–86.5	34.6–74.2
	Initial abstraction I_a	0.4–19.2 mm	13.9–30.1 mm
Clark unit hydrograph	Storage coefficient R	3.2–5.7 h	1.9–4 h
	Time of concentration t_C	0.5–2.6 h	0.6–5.6 h
Kinematic wave	Manning's n	0.029–0.040	0.028–0.060
Baseflow	Initial baseflow	0.2–2.18 m³/s	0.08–0.58 m³/s

[a] SCS - Soil Conservation Service.

Figure 6 and **Figure 7** show the results for the calibrated hydrographs in HEC-HMS of a representative storm event (10 June 2004) and flood event (01 June 2013).
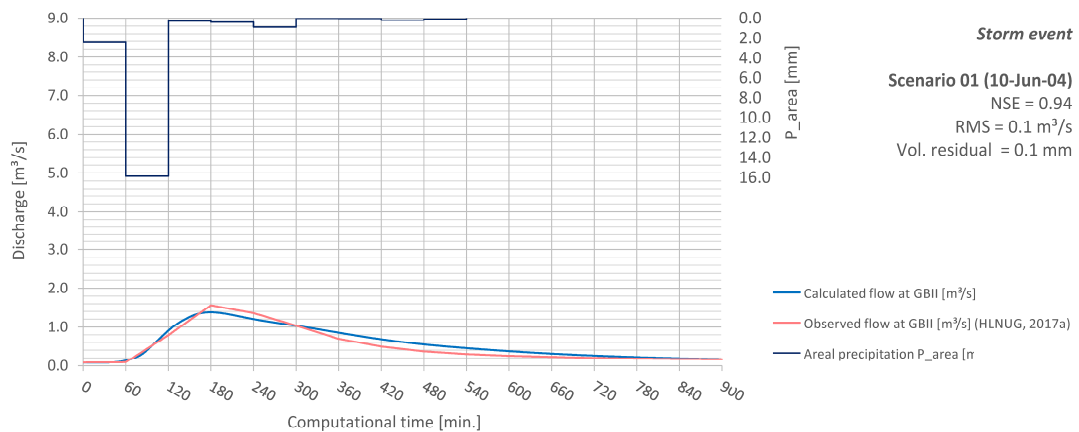
Figure 6: Representative, calibrated *storm event* (10 June 2004) of the hydrological model with objective functions and observed hydrographs at gauging station GBII (HLNUG, 2020a)
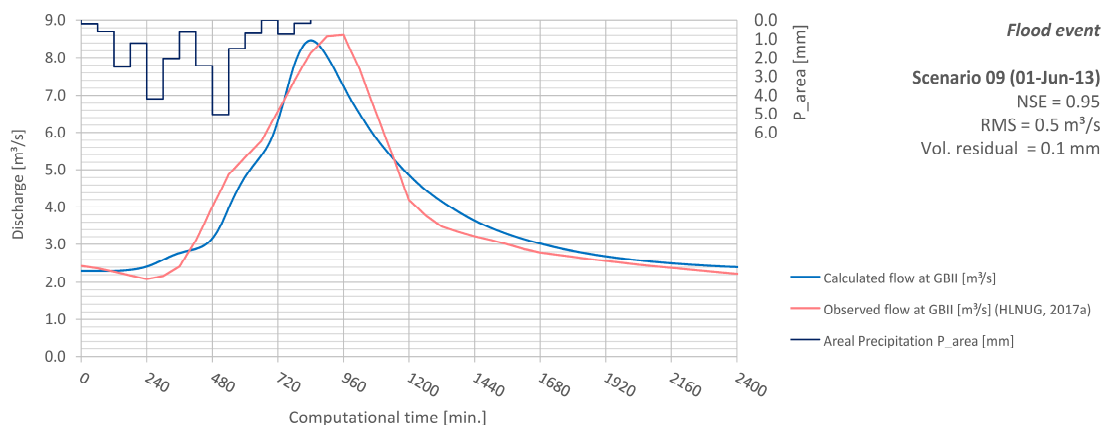
Figure 7: Representative, calibrated *flood event* (01 June 2013) of the hydrological model with objective functions and observed hydrographs at gauging station GBII

2.2.4.1 Hydrodynamic Modeling (HEC-RAS)

3d Channel Geometry and Terrain Model

For all surveyed tributaries listed in **Figure 5**, a separate channel geometry was created based on cross-sectional data. At locations in which the surveyed cross-sectional distance was found too large to represent irregularities in the DEM, additional profiles were interpolated and fitted manually to the elevation height of the terrain model. The final river channel was created with a mesh resolution of 0.25 m. Along the tributaries, culverts and bridge passages were modelled as open channel flow. Surveyed bridges of the village downstream were analyzed for the occurrence of pressurized flow and the resulting necessity for inclusion in the model. However, the events used for calibration measured maximum water surface elevations below the lower edge of the bridge deck, which is why the effect of backwater was neglected. All buildings of the village were added as flow barriers with a height of 40 m via DEM manipulation. Levees were set as manually digitized break lines to the 2d model area. All pre-processing was performed using the ArcGIS extension HEC-GeoRAS, the HEC-RAS Geometry editor and RASMapper (HEC, 2011 in combination with HEC, 2016a).

Land Use and Manning's n

The land use was generated on the basis of CORINE land use data (EEA, 2016) and ATKIS© (HVBG, 2017a). Manning's n roughness coefficients (**Table 6**) were assigned according to roughness values for natural streams and floodplains. The river course is classified with bed material of gravel with 2–64 mm ($n = 0.029$) based on LUBW (2003) in combination with Arcement & Schneider (1989). For the floodplains the selection for pastures, cultivated areas and brushes was set between $n = 0.034$ and $n = 0.05$ based on Chow (1985). The residential areas ('discontinuous urban fabric') were defined with $n = 0.038$ due to the existence of several gardens and green area. For the forest areas, the initial n value is set to 0.056 as minimum average value for trees in the overbank areas with sprouts and heavy stand of timber, flood stage below branches Chow (1985). The same initial roughness values were selected as part of the first parameterization for the decoupled and the integrated approach.

Table 6: Initially assigned Manning's n roughness for different types of land use for the hydrodynamic modeling of Approaches I + II. A short summary of the underlying mathematical model of HEC-RAS can be found in **Appendix A**

CORINE ID	Description	Manning's n
112	Discontinuous urban fabric	0.038
211	Non-irrigated arable land	0.040
231	Pastures	0.034
243	Land principally occupied by agriculture	0.042
311	Broad-leaved forest	0.056
312	Coniferous forest	0.056
313	Mixed forest	0.056
324	Transitional woodland-shrub	0.050
–	River channel	0.029

2d Flow Area, Mesh and Boundary Conditions

The 2d area (**Figure 8**) for Approach I was defined along the main river channel with a cell size of 5 and 2 m refinement. Refinement along the main channel was created by a 60-m buffer zone to both sides of the water body. The entire mesh contains a total of 582,600 cells and covers an area of 4 km². Boundary conditions (BCs) were set from the corresponding event hydrographs of the calibrated hydrological model output at the outlet point of each subcatchment. In total, there were eight tributaries defined as external BC and 10 internal outlets, which are set as internal BC (**Figure 8**).
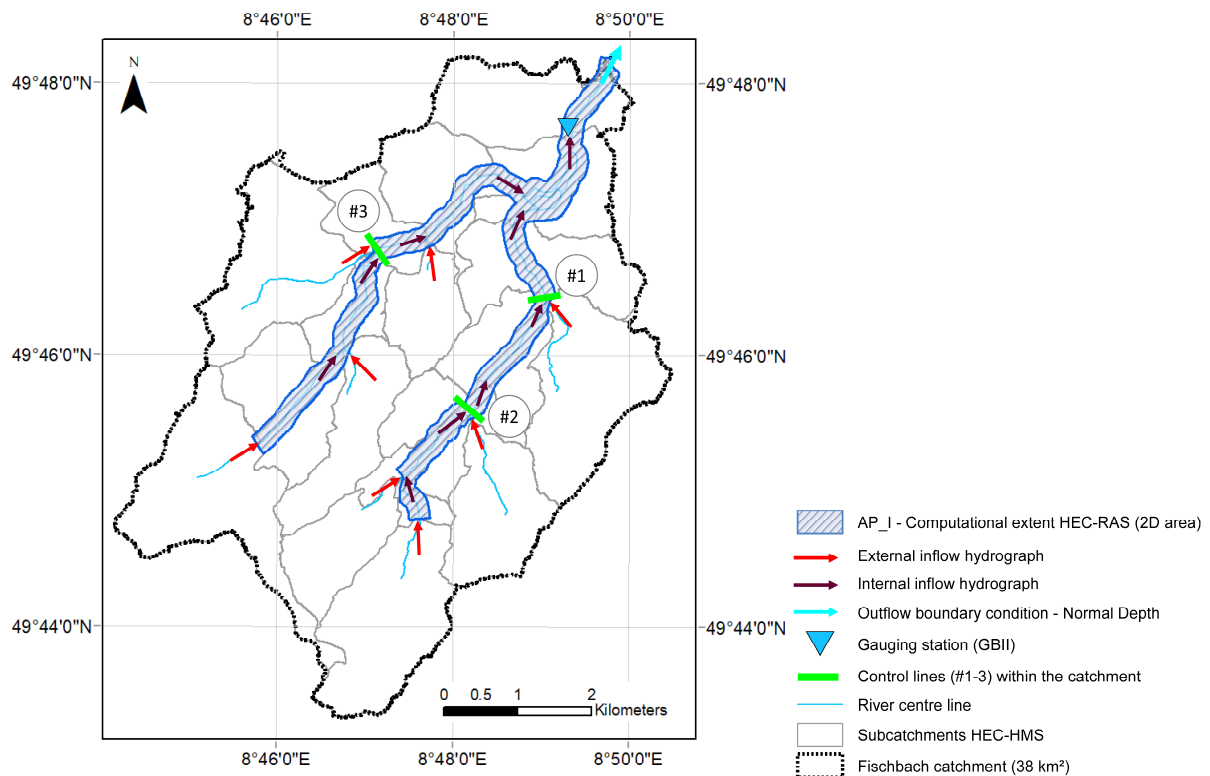
Figure 8: Subcatchments (HEC-HMS), computational extents (HEC-RAS) and boundary conditions – Approach I

Computational Settings, Model Optimization and Calibration of 2d Model (HEC-RAS)

Model parametrization and optimization were conducted based on experience and iterative optimization. The time step is set to 10 s (adaptive time step option) with a Courant range from 0.6–1.0. For the decoupled approach, the diffusive wave equation (DWE) and the shallow water equation (SWE) were evaluated subsequently. For the model calibration, the initial assigned Manning's n value (**Table 6**) was changed uniformly for the entire 2d model area in steps of 10%. Each run was assessed by NSE (Nash-Sutcliffe Efficiency), Vol% (total volume balance based on: % of total outflow volume (m³) from total inflow volume (m³) for entire simulation time) and Δh difference in (m) of calculated maximum water level at maximum discharge $Q_{\max}$ to rating curve's water level at $Q_{\max}$). The model run that performed best on all three criteria was rated as 'best fit' and used for validation.

2.2.5 Approach II ('integrated'): HEC-RAS

2.2.5.1 Hydrodynamic Modeling (HEC-RAS)

2d Flow Area, Mesh and Boundary Conditions

The 2d model area for Approach II is the entire catchment (**Figure 9**). HEC-RAS makes use of the 'high-resolution subgrid model' (Casulli, 2009), which will have distinct impacts at low water levels where experience is lacking. Therefore, two different mesh resolutions were evaluated. The coarser set-up uses grid cells with 100 and 5 m refinement. It has a total number of 246,100 cells. The finer set-up uses a cell resolution of 3 and 30 m refinement. It has a total number of 687,800 cells. The refinement was applied along the main river channels as well as for the settlement areas with a buffer zone of 60 m. The terrain model used in this approach is the same as in the decoupled model set-up.
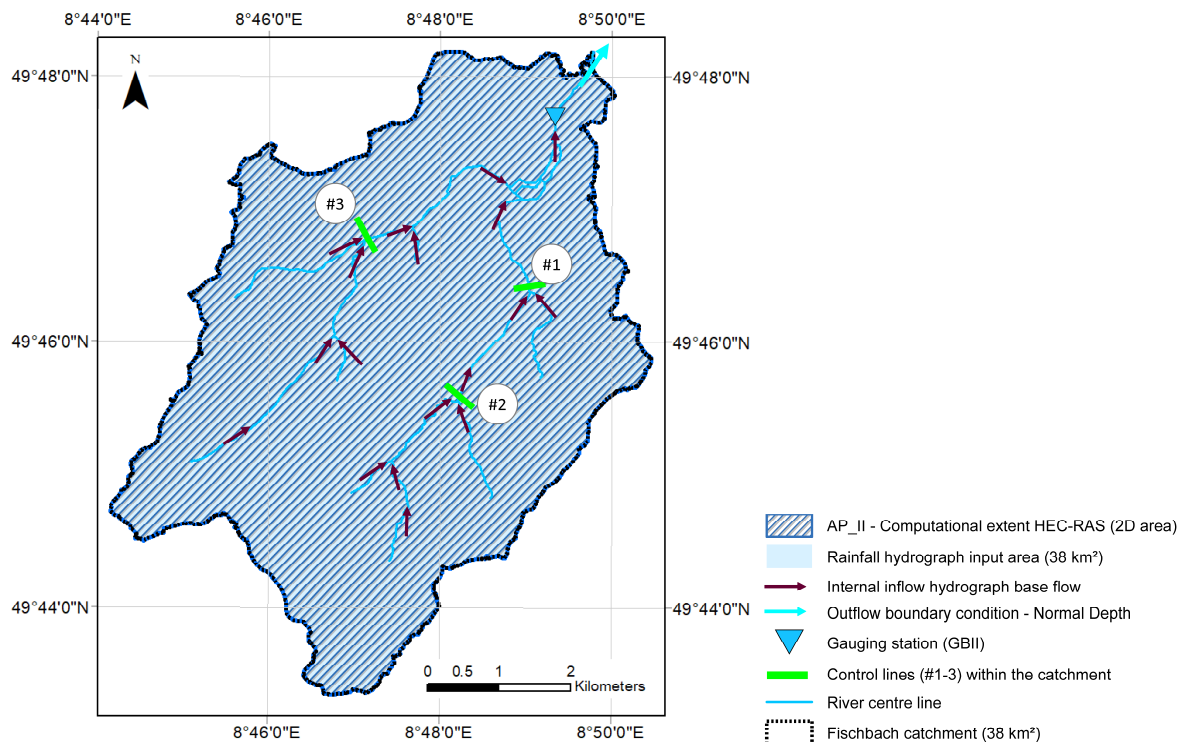
Figure 9: Computational extents (HEC-RAS) and boundary conditions – Approach II

Two suitable boundary conditions were applied, namely, the input of precipitation (P) over the entire 2d model area and the baseflow (Q_b) hydrographs at each tributary. Up to now, there is no method to calculate spatially distributed losses due to infiltration or losses to the sewer system implemented in HEC-RAS. For this reason, it was decided to apply the effective precipitation (P_{eff}) as direct rainfall to the 2d area. P_{eff} was evaluated in two manners: Firstly, with the help of a constant runoff coefficient which was determined for each event individually and secondly, via the extended SCS method (Zaiß, 1989) with temporally variable runoff coefficients. The effective rainfall volume corresponds to the volume of the gauged direct runoff. For this reason, no additional calibration of the infiltration approach was prosecuted.

The baseflow $Q_{b, \text{subcatchment}}$ is set as constant baseflow rate at each institute's observation point. The spatial distribution of the $Q_{b, \text{subcatchment}}$ input was set as described above as a percentage of the gauges pre-event discharge Q_0.

Computational Settings, Model Optimization and Calibration of 2d Model (HEC-RAS)

A major challenge of this study was to implement a suitable model set-up and to evaluate appropriate computational settings for the integrated approach. Due to necessary limitations of computational costs, a detailed sensitivity analysis for the entire catchment was not realizable. The adjusted default settings from Approach I were applied also in the second approach, however, an additional model optimization was pursued with the objective to obtain a satisfactory model set-up. The following parameter changes were evaluated:

1. Computational mesh: $100 + 5\,\text{m}$ refinement, $30 + 3\,\text{m}$ refinement – Approach II (**Table 7**).
2. Time step: $5\,\text{s}$, $3\,\text{s}$, ($1\,\text{s}$ for SWE) – Approach II (**Table 8**).
3. Representation of buildings: DEM, Manning's n value – Approach II (**Table 9**).
4. Setting for shallow overland flow: Computational tolerances, filter tolerances – Approach II (**Table 10**).
5. Equation set: SWE, DWE – Approaches I + II (**Table 11**).
6. Runoff formation: constant Ψ, Ψ (SCS, Zaiß) – Approach II (**Table 12**).
7. Manning's n values – Approaches I + II (**Table 14** and **Table 15**).

After each model run the results were assessed by NSE, Vol% and Δh. If the results improved for the evaluated parameter, this setting was used in the model set-up for evaluation of the next parameter. For the calibration process, the model run that performed best on all three criteria was rated as 'best fit' and used for validation.

2.3   Results and Discussion

In the following, the computational results of the model optimization, calibration and validation runs for Approach I (*AP_I*) and Approach II (*AP_II*) are presented and discussed comparatively.

2.3.1   Model Optimization Runs: Scenario 04 (23 June 2007)

Mesh Resolution (Approach II)

For the coarse set-up (*AP_II_v01*) a high discrepancy between the model outflow (*Vol%* at 55.1 %) and the model inflow volume was detected (**Table 7**). For the fine set-up (*AP_II_v02*), the same effect is detected but with less intensity (*Vol% at 77.8 %*). This 'volume loss' effect was observed in previous studies by Clark et al. (2008) for the 2d models TUFLOW and SOBEK. Both models show an increasing discharge volume with decreasing cell size. For the decoupled modelling procedure, the volume difference *Vol%* measured 97.8 % of the model inflow (s. *AP_I_v01*, s. **Table 11**). The strong correlation between the two model set-ups and the model

volume's output can be seen as an indicator of the difficulties of representing flow at very shallow depth. The model calculates with one water elevation for each cell. If water is stored due to the high impact of surface roughness or lost due to limited computational tolerances in a large cell the impact of the missing volume is much higher than if the cell has a smaller size. The coarse set-up was not further considered for optimization.

The computational time for the 26-h event plus 3-h warm-up time increased from 6.15 h for the coarse set-up (246,100 cells) to 25.25 h for the fine set-up (687,800 cells) with 5 s constant time step each.

Table 7: Comparison of hydrograph with coarse (100 + 5 m) and fine (30 + 3 m) mesh resolution – Approach II

| mesh: **v01**: 100m + 5m, **v02**: 20m + 3m |
| time step: 5 s |
| output interval: 5 min. |
| inititial condition time: 3 h (100 %) |
| max. iterations: 40 |
| all other settings: default |
| buildings: included in DEM |
| runoff formation: constant Ψ |

AP_II_v01	**AP_II _v02**
NSE: -0.19	NSE: 0.38
V %: 55.1	V %: 77.8
Δh [m]: 0.32	Δh [m]: -0.16
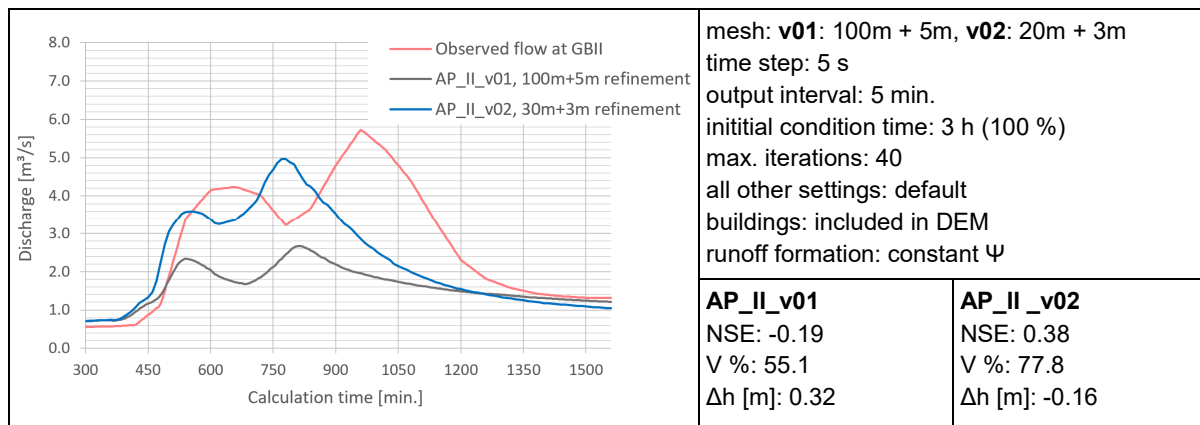
Time Step (Approach II)

For the integrated approach, two different time steps were evaluated. The results of the two different time steps did not show significant differences at the gauging station and in the regions with flat topography (**Table 8**). Both model outputs show consistent and robust results. Whereas in the upper, hillier parts of the catchments (**Figure 9**, Control lines #1–3) with higher velocities the model output with 3-s time step was more stable. For the Control line #2 and further upstream the velocities at some locations were even higher so that both defined time steps were still too large. For computational reasons the time step was not set lower or further evaluated with adaptive time steps at this stage. During the evaluation of the equation set the time step for the calculation with the SWE was reduced to 1 s (compare **Table 11**).

The computational time increased from 25.25 h for 5-s time step to 42.9 h for 3-s time step.

Table 8: Results of model output with 5 and 3 s time step at gauging station and control lines #1–3 – Approach II

time step: **v02:** 5s, **v03:** 3s all other settings: **AP_II _v02**
AP_II _v03 NSE: 0.36 V %: 77.8 Δh [m]: -0.16
For locations of control lines #1-3, s. **Figure 9**
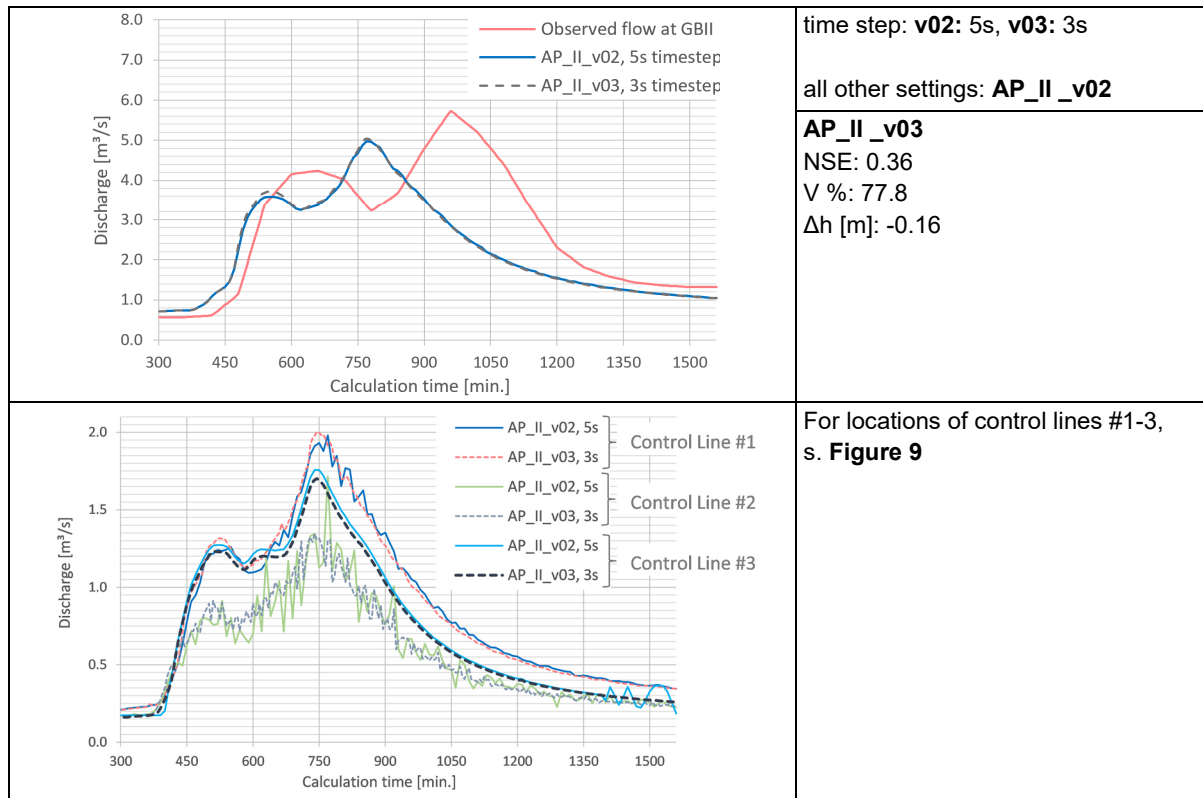
Representation of Buildings (Approach II)

Two model set-ups for the integration of buildings were evaluated for the integrated approach. In the first set-up on the left (**Table 9**), the buildings were added as a flow barrier with 5 m height to the DEM. The result maps of the water depth and elevations were then interpolated to the wet, higher roof of the building, which resulted in deep ditches around the buildings envelope. In HEC-RAS, there is no way to deactivate single cells or include holes in the 2d area at the buildings locations. Therefore the buildings were then integrated as high roughness values with Manning's $n = 10$. The model changes did not have any effect on the hydrographs or computational times.

Table 9: Representation of buildings as flow barriers in the digital elevation model (DEM) and high roughness values – Approach II

v03: buildings in DEM **v04:** buildings as Manning's *n* all other settings: **AP_II _v03**
AP_II _v04 NSE: 0.41 V %: 76.9 Δh [m]: -0.17

AP_II _v03, buildings included in DEM as flow barriers | **AP_II_v04**, buildings included as surface roughness (n=10)
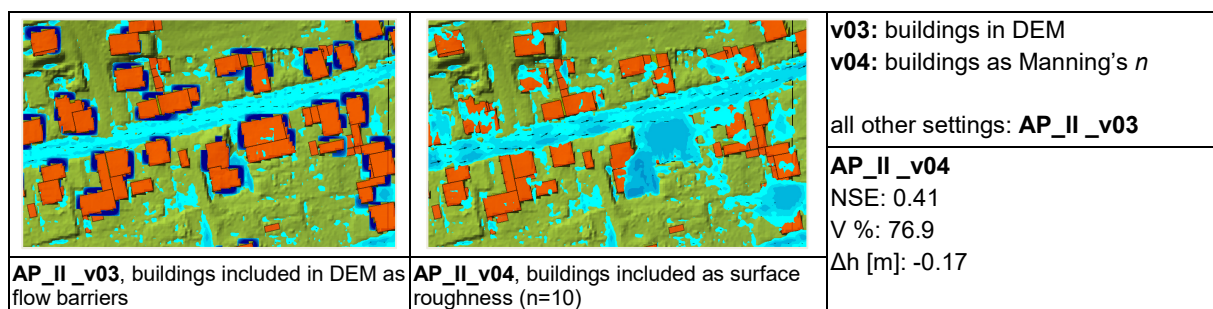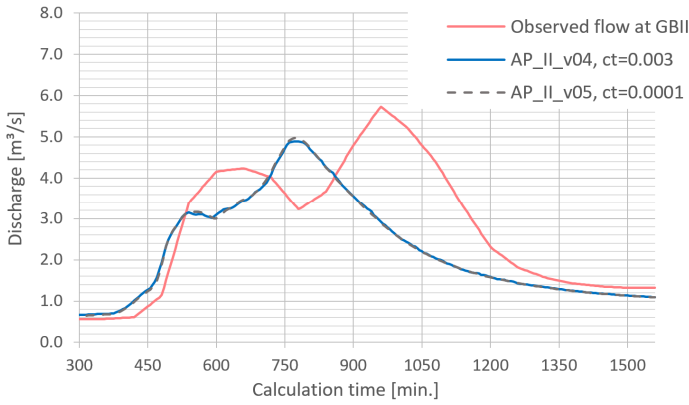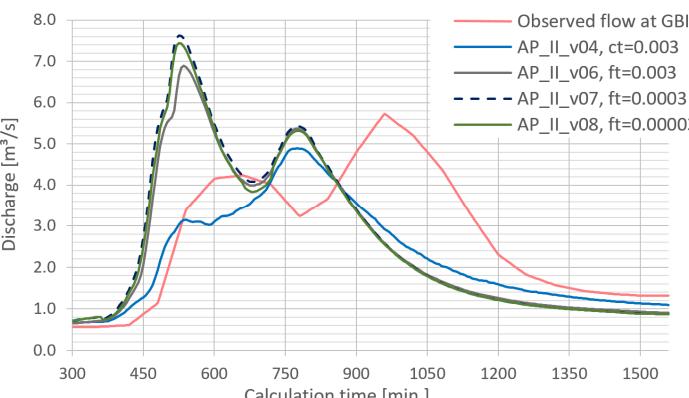
Further Settings for Shallow Overland Flow (Approach II)

Two further settings were evaluated for the integrated approach to investigate possible influences on the problem of the water volume output. Two parameters were chosen since due to their definition they were assumed to be sensitive to water flow and volumes at shallow water depths. The first parameter, the computational tolerances ct define the limit when the solver stops to iterate in comparison to the numerical error. It was reduced from the default value of $ct_{default} = 0.003$ m for water surface and volume tolerance to $ct = 0.0001$ m. The model results were hardly sensitive towards changes in computational tolerances (**Table 10**). The computational time increased to 48 h compared to 42.9 h in the previous simulation. The second evaluated parameters were the subgrid filter tolerances ft, which define the level of detail the DEM subgrid is considered in the computation. In the first run, the default settings from $ft_{default} = 0.003$ m were applied also for the *cell minimum surface area fraction* (default value 0.01 m). Then they were uniformly reduced to $ft_1 = 0.0003$ and $ft_2 = 0.00003$. The different values for the subgrid filter tolerances visibly influenced the results. Especially errors regarding the model volume outputs were affected by changes of the subgrid filter tolerances. While for the default settings the Vol% accounted for 75.9 % of inflow volume, a reduction of all filter tolerances to 0.003 increased the volume outflow to 86.9 % and a change to 0.0003–89.3 % of the model inflow. It is highly likely that this effect was mainly caused by the filter tolerances for shallow water stability, which were used to calculate the subgrid hydraulic property tables. The parameter is not known to be sensitive to normal fluvial flooding application, but was detected sensitive to DRM calculation in this study. It was shown that it was impossible to use the model with the same parametrization for the integrated approach as it is common for normal flood inundation application.

The computational time increased from 47.1 h for $ft_{default} = 0.003$ to 55.6 h for $ft_1 = 0.0003$ and 63.7 h for $ft_2 = 0.00003$.

Table 10: Further settings for shallow overland flow: computational tolerances and subgrid filter – Approach II

computational tolerances (*ct*)	**v04:** ct = 0.003, **v05:** ct = 0.0001
	all other settings: **AP_II _v04**
	AP_II_v05 NSE: 0.40 V %: 75.9 Δh [m]: -0.17

filter tolerances (*ft*), subgrid tables	**v06:** ft = 0.003, **v07:** ft = 0.0003, **v08:** ft = 0.00003	
	all other settings: **AP_II_v04**	
	AP_II_v06 NSE: -0.21 V %: 86.9 Δh [m]: -0.22	**AP_II_v07** NSE: -0.47 V %: 89.3 Δh [m]: -0.26
	AP_II_v08 NSE: -0.39 V %: 89.3 Δh [m]: -0.24	

Equation Set (Approaches I + II)

Both approaches were run with the two equation sets, the DWE and the SWE. For the SWE calculations the model stability decreased with divergent numerical solutions at maximum iterations in both approaches (**Table 11**). The numerical problems were detected by the displayed convergence and a water surface elevation error in the computational messages of HEC-RAS. The time step for the DRM calculation was reduced to 1 s which reduced the number of cells which were not solved within the numerical tolerance though increased the computational time. For the regions with higher slopes and flow velocities at the upper part of the catchment (s. **Figure 8** and **Figure 9**: Control lines #2 and #3) both model set-ups had difficulties to reproduce the flow patterns without hydrograph oscillations and would have required even lower time steps. In both approaches, the results of the SWE fit better to the water elevation of the gauge's rating curve whereas the DWE reproduces much lower water depth. For this reason, the SWE was selected for the following computations.

For Approach I, the computational time with adaptive time step increased from 14.7 h for DWE to 24.4 h for the SWE calculation. For Approach II, the computational cost increased significantly due to the lower time step of 1 s. The calculation took 188.1 h in comparison to 55.6 h for the DWE calculation with 3-s time step.

Table 11: Comparison of model results with diffusive wave approximation (DWE) and shallow water equations (SWE) – Approaches I + II

Approach I		Approach II	
(graphs: Observed flow at GBII; HEC-HMS, calibrated [a]; AP_I_v01, DWE [b]; AP_I_v02, SWE [b])		*(graphs: Observed flow at GBII; AP_II_v07, DWE; AP_II_v09b, SWE)*	
AP_I_v01 [c] NSE: 0.77 V %: 97.8 Δh [m]: -0.34	**AP_I_v02** [c] NSE: 0.74 V %: 96.6 Δh [m]: 0.02	**v07:** DWE (3s), **v09a:** SWE (3s) **v09b:** SWE (1s) all other settings: **AP_II_v07**	**AP_II_v09b** NSE: -0.04 V %: 90.3 Δh [m]: 0.15
(graphs: HEC-HMS, calibrated; AP_I_v01, DWE; AP_I_v02_SWE; #1[d], #2, #3)		*(graphs: AP_II_v07, DWE; AP_II_v09a, SWE, 3s; AP_II_v09b, SWE, 1s; #1[d], #2)*	

[a] The blue hydrograph 'HEC-HMS, calibrated' for Approach I represents the calibrated output of the hydrological model HEC-HMS

[b] DWE: Diffusive Wave Approximation, SWE: Shallow Water Equations

[c] NSE, V %, Δh [m] are calculated for the output hydrograph of the 2d model HEC-RAS in comparison to the observed flow at the gauge

[d] #1-3 show the hydrographs at the control lines within the catchment (**Figure 8, Figure 9**). For better readability #3 was not added to the graph of Approach II.

Runoff Formation (Approach II)

For the uncalibrated version, the effects of time-dependent runoff coefficients for the rainfall–runoff event on 23 June 2007 were significant. This effect is shown in **Table 12**: *AP_II_v09* in comparison to *AP_II_10*. Both runoff formation routines applied in this study gave low accordance for the objective functions. For the time-dependent Ψ, the general shape of the hydrograph for the longer event without calibration can be interpreted a little better, whereas the effect for the event of April 23, 2018 was less significant due to its short duration. Generally both applied runoff formation routines in this study cannot be interpreted as a satisfactory replacement of the hydrological model due to the model limitations. The effective rainfall is applied uniformly. Local land use and soil characteristics were not considered for the infiltration process, as they are considered in the HEC-HMS hydrological model for the decoupled

approach. This simplification is made for both approaches. Tyrna et al. (2018) or Caddis et al. (2008), examples can be found for a more sophisticated physical-based DRM infiltration routine for 2d hydrodynamic modelling.

Table 12: Comparison of runoff formation – Approach II

v09b: constant Ψ v10: Ψ (SCS, Zaiß) all other settings: AP_II_v09b
AP_II_v10 NSE: 0.02 V %: 90.2 Δh [m]: 0.22
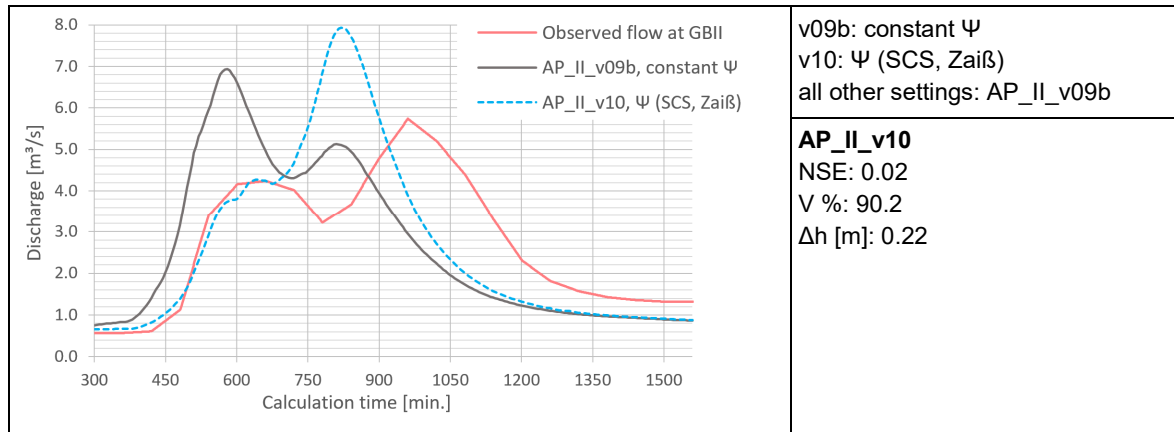
During the calibration process, the effect of the two different runoff formation routines was neutralized due to the increasing impact of the change of roughness coefficients (**Table 14**: *AP_II_v11–v14*). The risk is to calibrate the effects of catchment runoff formation due to hydrological processes based on adaption of the roughness values. For Approach II, the hydrological and the hydraulic component of the hydrograph is calibrated jointly in one model, whereas for the decoupled approach the calibration process is separated into the calibration of the hydrological and the hydrodynamic model. In this study, it is shown that for the integrated approach the runoff formation, concentration and the effects of the hydrodynamic processes are interdependent.

2.3.2 Results of Calibration Runs: Scenario 04 (23 June 2007)

Manning's n Roughness

For Approach I, the calibrated roughness coefficients were in a similar range as the initially assigned values for natural channels and floodplains (**Table 13** for initially and calibrated Manning's n – values).

Table 13: Comparison of initially assigned and calibrated Manning's n values for hydrodynamic modeling – Approaches I + II

CORINE ID	Description	Manning's n	Approach I calibrated[a]	Approach II calibrated
112	Discontinuous urban fabric	0.038	0.034[b]	0.076
211	Non-irrigated arable land	0.040	0.036[b]	0.080
231	Pastures	0.034	0.031	0.068
243	Land principally occupied by agriculture	0.042	0.038	0.084
311	Broad-leaved forest	0.056	0.05[b]	0.112
312	Coniferous forest	0.056	—[c]	0.112[b]
313	Mixed forest	0.056	0.05[b]	0.112
324	Transitional woodland-shrub	0.050	—[c]	0.100[b]
–	River channel	0.029	0.026	0.026

[a] The values are only used in the calibration process of the 2d hydrodynamic model.
[b] The area of this land use type had only minor contribution (<1.5 %) to total inundated area.
[c] This land use type was not present in the floodplain area.

For Approach II, one of the major obstacles was the calibration and validation process of the rainfall–runoff events. The calibration routine resulted in roughness values for the catchment area up to 100–200 % larger than the initially assigned values (**Table 14**). Thus, it was necessary to define different *n* values for the channel and the catchment.

Table 14: Comparison of calibration runs for Scenario 04 (23 June 2007) – Approaches I + II

Approach I

Chart legend:
- Observed flow at GBII
- AP_I_v02, original n [a]
- AP_I_v03, n -20%
- AP_I_v04, n -10%
- AP_I_v05, n +10%
- AP_I_v06, n +20%

X-axis: Calculation time [min.], Y-axis: Discharge [m³/s]

all other settings: **AP_I_v02**

AP_I_v03	**AP_I_v04**
NSE: 0.75	NSE: 0.75
V %: 95.9	V %: 95.7
Δh [m]: -0.03	Δh [m]: 0.002

AP_I_v05	**AP_I_v06**
NSE: 0.74	NSE: 0.73
V %: 95.3	V %: 95.1
Δh [m]: 0.04	Δh [m]: 0.07

Approach II, constant Ψ

Chart legend:
- Observed flow at GBII
- AP_II_v09b, original n [a]
- AP_II_v11, n + 20%
- AP_II_v12, n +40%
- AP_II_v13, n +100%, channel -10%
- AP_II_v14, n +200%, channel -10%

X-axis: Calculation time [min.], Y-axis: Discharge [m³/s]

all other settings: **AP_II_v09b**

AP_II_v11	**AP_II_v12**
NSE: 0.20	NSE: 0.39
V %: 89.3	V %: 88.4
Δh [m]: 0.21	Δh [m]: 0.32

AP_II_v13	**AP_II_v14**
NSE: 0.57	NSE: 0.73
V %: 87.3	V %: 84.4
Δh [m]: 0.1	Δh [m]: 0.1

Approach II, Ψ (SCS, Zaiß)

Chart legend:
- Observed flow at GBII
- AP_II_v10, original n [a]
- AP_II_v15, n +100%, channel -10%
- AP_II_v16, n +200%, channel -10%

X-axis: Calculation time [min.], Y-axis: Discharge [m³/s]

all other settings: **AP_II_v10**

AP_II_v15	**AP_II _v16**
NSE: 0.48	NSE: 0.61
V %: 87.1	V %: 83.8
Δh [m]: 0.18	Δh [m]: 0.14

[a] Compare with **Table 6** for initially assigned n - values 'original n'

Many studies of the DRM (Van Drie et al., 2011; Caddis et al., 2008; Clark et al., 2008 or Muncaster et al., 2006) compare the hydrological lumped model output to the output of the 2d hydrodynamic model without discharge measurements. This makes general statements about calibration routines difficult in terms of the correct representation of the hydrograph and Manning's n values. The catchment roughness values need to be increased to fit the requirements for overland flow. In Engman (1986), there are recommended Manning's roughness coefficients for overland flow. Generally, the recommended values are much higher than for normal channel flow. For different types of grass, the values are in a range of 0.15 for short grass and 0.45 for 'Bluegrass sod' (0.3–0.48 for 'Bermuda Grass' by Palmer, 1946). However, the values for floodplains in Chow (1985) are 0.030 for short grass and 0.035 for

high grass. Similar roughness coefficients for overland flow can be found in Downer & Ogden (2006). The values for pastures are in a range between $n = 0.235$–0.271 (Senarath et al., 2000) and $n = 0.30$–0.4 (HEC, 1998). For forest areas the n value for overland flow is recommended in a range between $n = 0.184$ and 0.198 (Senarath et al., 2000). The calibrated values of the integrated approach were still lower but much closer to the recommended than the initially assigned values. Due to the additional effect that the increase of the surface roughness had a negative impact on the model's volume output, the roughness values were not considered to be increased higher than 200%.

2.3.3 Results of Calibration Runs: Scenario 10 (23 April 2018)

The second calibration event was the storm event of 23 April 2018 where the flood control basin was added to the hydrological model and the hydrodynamic model for Approach I and the hydrodynamic model for Approach II. For Approach I, the model output fits well to the observed hydrograph at the gauge and the outlet of the flood control basin with the same range of Manning's n values. The NSE for the hydrodynamic model is 0.85 at the gauge and 0.8 at the outlet of the flood control basin. For Approach II the results during the calibration process are similar as for Scenario 04. The calibration process results in much higher roughness values to have consistent results with the discharge measurements. In both approaches, this event results in better accordance with the measurements (NSE, Vol%, Δh) than the Scenario 04 because of its one peak characteristic and fast rainfall–runoff process (**Table 15**).

Table 15: Comparison of calibration runs for Scenario 10 (23 April 2018) – Approaches I + II

Approach I		
Discharge at gauge GBII	all settings: **AP_I_v04,** Manning's *n*: n -10%	
	AP_I _v07 NSE: 0.85 V %: 99.0 Δh [m]: 0.05	
Discharge at outlet, flood control basin (**Figure 4**)	**AP_I _v07** NSE: 0.80	
Approach II, constant Ψ		
Discharge at gauge GBII	all other settings: **AP_II_v09b**	
	AP_I _v17 NSE: 0.45 V %: 91.3 Δh [m]: 0.21	**AP_I _v18** NSE: 0.74 V %: 90.6 Δh [m]: 0.32
	AP_I _v19 NSE: 0.86 V %: 90.1 Δh [m]: 0.38	**AP_I _v20** NSE: 0.93 V %: 90.8 Δh [m]: 0.29
	AP_I _v21 NSE: 0.88 V %: 89.4 Δh [m]: 0.3	
Discharge at outlet, flood control basin (**Figure 4**)	**AP_I _v17** NSE: 0.47	**AP_I _v18** NSE: 0.49
	AP_I _v19 NSE: 0.54	**AP_I _v20** NSE: 0.65
	AP_I _v21 NSE: 0.74	
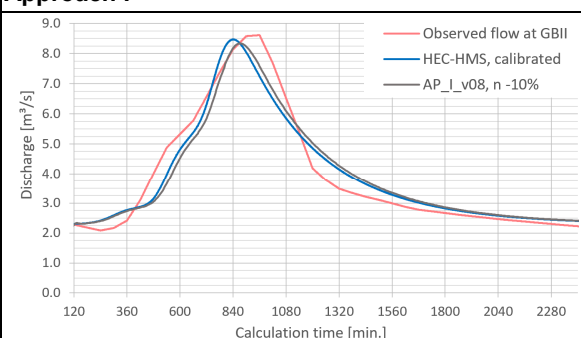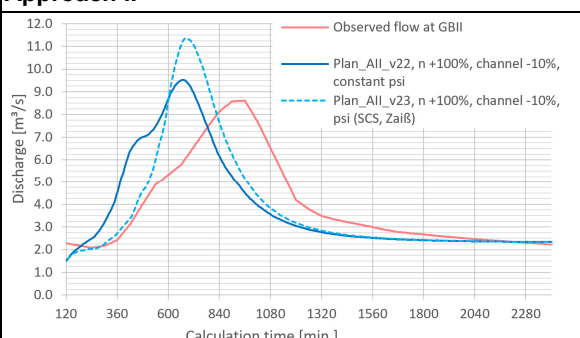
[a] Compare with **Table 6** for initially assigned n - values 'original n'

2.3.4 Results of Validation Runs: Scenario 09 (01 June 2013)

Scenario 09 (01 June 2013)

The results of the validation event of 01 June 2013 of Approach I with the same settings in HEC-RAS as for the calibrated events of Scenarios 04 and 10 showed very good accordance with the observed and the calibrated hydrological output of HEC-HMS. Whereas for the decoupled Approach II, the results with the two different runoff formation routines and an increase of 100% of the Manning's n values (channel −10%) the reproduced hydrographs (**Table 16:** AP_II_v22–23) still showed large discrepancies with the measurements.

Table 16: Comparison of validation runs for Scenario 09 (01 June 13) – Approaches I + II

Approach I		Approach II	
All settings: **AP_I _v04**	**AP_I _v08** NSE: 0.93 V %: 98.8 Δh [m]: 0.03	All settings: **v22: AP_II _v13** **v23: AP_II _v15**	**AP_II_v22** NSE: 0.19 V %: 93.5 Δh [m]: 0.26
			AP_II _v23 NSE: 0.31 V %: 93.2 Δh [m]: 0.28

2.3.5 Comparison of Validation Runs with Rating Curve at Gauge GBII

The evaluated, calibrated events with Approach I showed all very good consistency with the gauge's rating curve. For a broad range of events, the hydrodynamic model was able to reproduce the depth – discharge relationship of the gauge very well. Whereas for the decoupled Approach II, the model output of the water level of the evaluated events was in each run higher than the relationship of the rating curve. The integrated model of Approach II was less capable of reproducing the flow characteristics at the gauge (**Table 17**).

Table 17: Comparison of validation runs with gauge's rating curve from HLNUG (2017b) – Approaches I + II
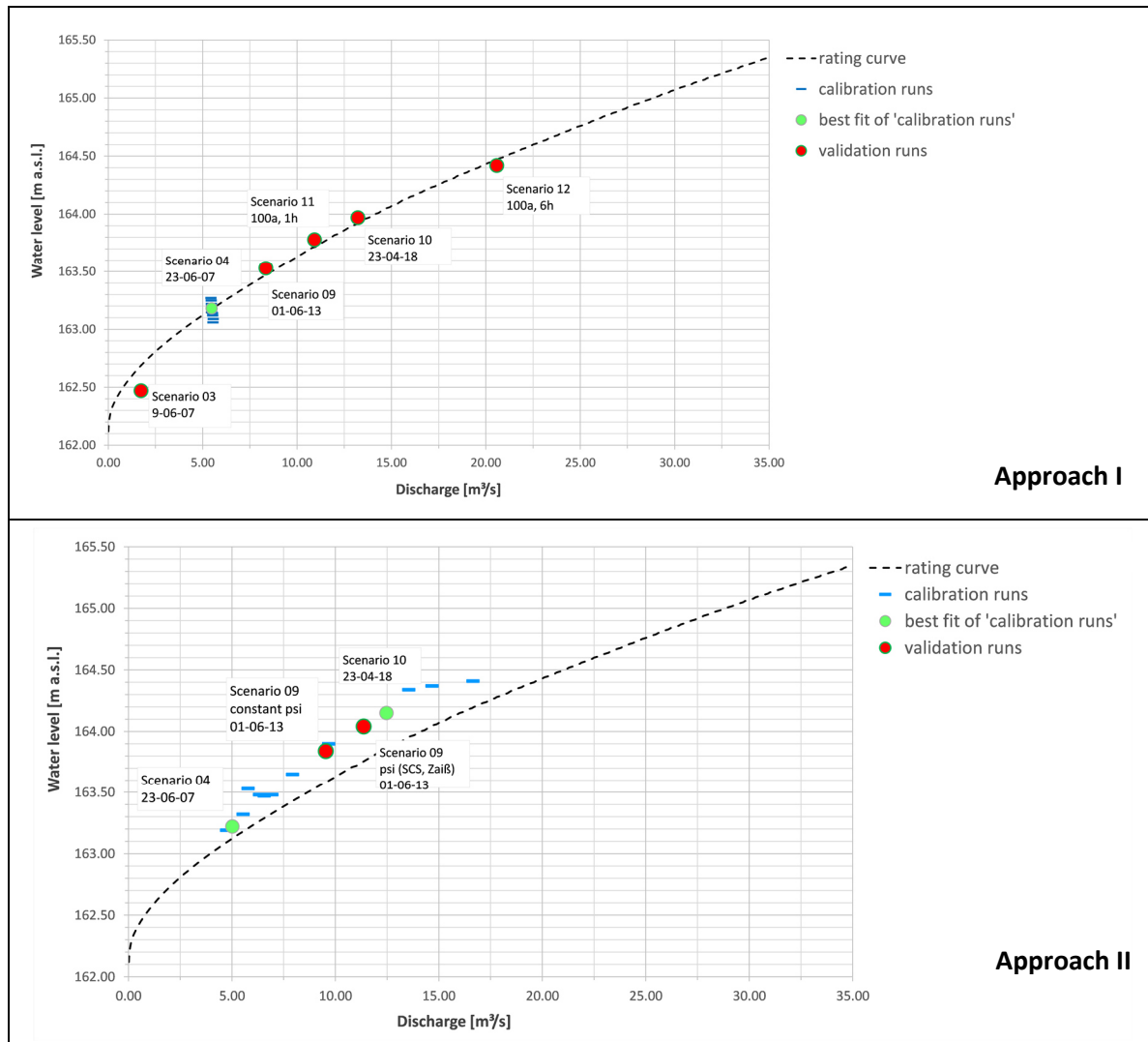
2.3.6 Flood Extents, Water Depth and Velocities

Flood Extents and Water Depths

For the integrated Approach II, it was possible to get a very detailed picture on flood formation within the catchment, the main flow paths and water depths apart of the channel (**Table 18**). The total inundated area with water depth larger than 0.1 m was 0.7 km². Whereas for the decoupled Approach I, no flooding apart of the river is detected. The model output of 23 June 2007 resulted in only 0.06 km² of inundated area with depth >0.1 m. For the storm event of April 23, 2018, the same findings were made. Here, it was possible to compare the model outputs with the pictures made from the use of the local fire brigade. At one location, the streets in the village were flooded by surface flow. The model outputs of Approach II showed good correlation to the water depth on the flood picture. Whereas the model output of Approach I showed only minor fluvial flooding along the channel.

Table 18: Comparison of flood extents and water depths for Scenario 04 (23 June 2007) and Scenario 10 (23 April 2018) – Approaches I + II, Picture from Bickelhaupt (2018)

■ Total inundated area [km²]: 0.075	■ Total inundated area [km²]: 1.42
■ Inundated area > 0.1 m [km²]: 0.061	■ Inundated area > 0.1 m [km²]: 0.7
■ Inundated area > 0.3 m [km²]: 0.049	■ Inundated area > 0.3 m [km²]: 0.38
■ Inundated area > 0.5 m [km²]: 0.036	■ Inundated area > 0.5 m [km²]: 0.24
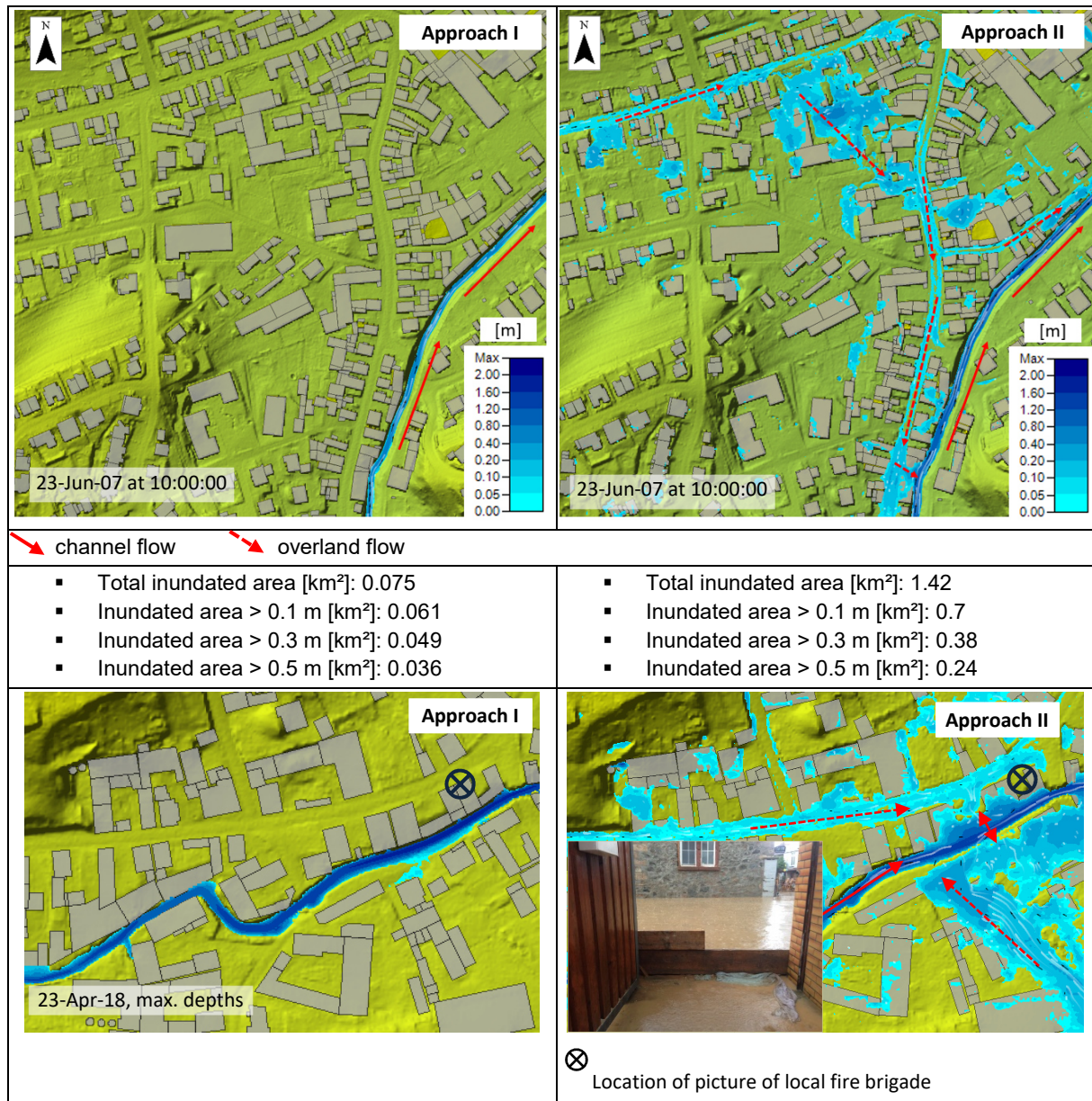
Maximum Water Depths h_{max}

The distribution of the maximum water depths during the simulation for 23 June 2007 (**Table 19**) is very different for both approaches. The decoupled Approach I has 25–35% of the total inundated area in water depth between <0.2 and <1 m. The distribution within the first three classes is relatively equable. Whereas the evaluation of the water depth of the integrated Approach II showed over 65% of inundated areas with depths <0.2 m. This approach is dominated by very shallow water flow, which has very different flow characteristics and influence of roughness values than flow processes with higher water depth. The difficulties during the calibration processes for this approach can be explained by this difference between the two approaches.

Table 19: Comparison of maximum water depths h_{max} – Approaches I + II
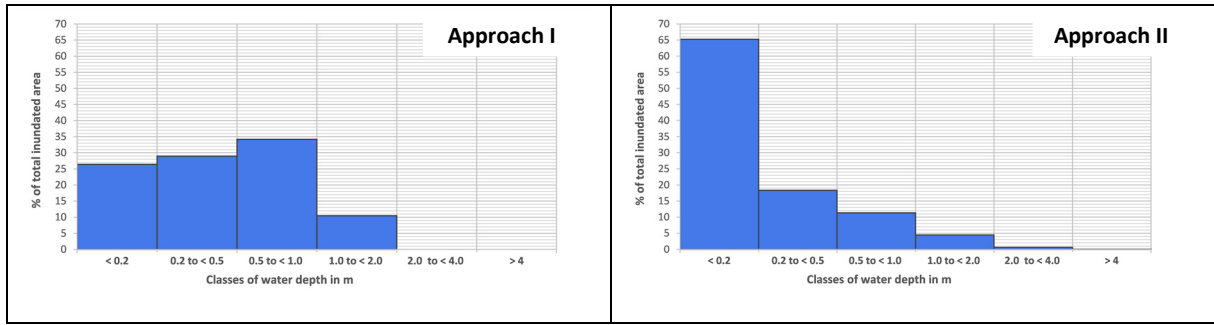
Reynolds Numbers Re

As indicator for the classification of the flow regime the maximum Reynolds number Re_{max} was analyzed (**Table 20**). For the Reynolds number >85% of the inundated area is larger than 20,000 which can be seen as definitely turbulent. For the integrated approach >25% of the inundated area has Reynold numbers <500 which is interpreted as laminar flow. This comparison shows the two different flow regimes that can occur for very shallow water flows. This difference to the more applied decoupled approach makes the 1:1 use of common approaches as the Manning's equation problematic.

Table 20: Comparison of max. Reynold numbers Re_{max} – Approaches I + II
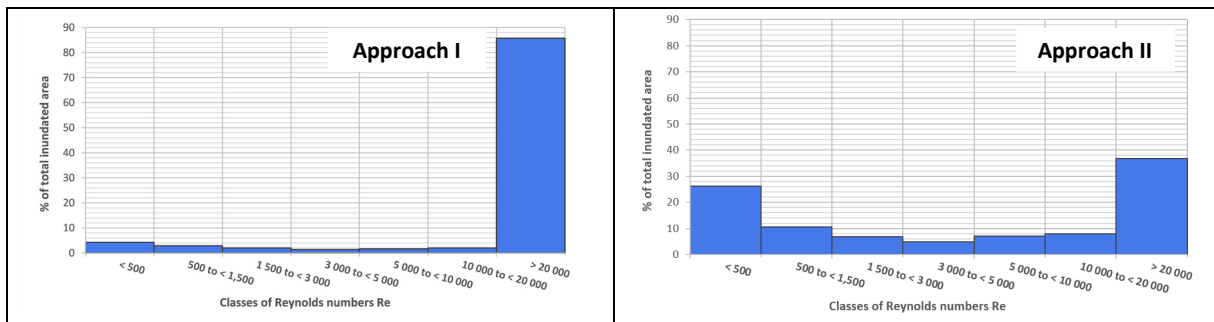
L is set as water depth [m], ν is set to $1.3*10^{-6}$ m²/s for T_{Water} = 10° C

2.4 Conclusions and Future Work

The objective of this study was to model, calibrate and validate single rainfall–runoff events with a more traditional, decoupled approach and to set the modelling process and the results in comparison to an integrated modelling procedure.

As a conclusion, the results of the initially specified objectives will be summarized as followed:

- In general, the decoupled Approach I gave better results on hydrographs than Approach II, but the integrated approach gave more detailed and realistic information on floodplains and the origin of overland flow in the catchment. For the decoupled approach, the use of HEC-HMS to determine the calibrated hydrographs in combination with HEC-RAS as hydrodynamic model provides consistent results for the catchment

over a large range of rainfall–runoff events. The modelling process of the integrated approach in HEC-RAS produces detailed flood inundation maps within the subcatchments. It was much better possible to reproduce the highly dynamic and interconnected flow processes of runoff formation, concentration and routing in a small catchment. Therefore, regarding urban, pluvial and flash floods in small catchments it is recommended to further focus on the integrated approach.

- The model optimization process of the integrated approach has shown that special attention must be paid to the selection of suitable model parameters and computational settings. The mesh resolution was shown to have a high impact on the model's output flow volume. The model-specific parameters of subgrid filter tolerances are detected as a sensitive parameter to control the model's outflow volume. The comparison of water depths, flow velocities and Reynolds numbers showed different flow characteristic for the event of 23 June 2007 for both modelling approaches. The ranges of Reynolds numbers for the integrated approach where significantly lower which indicates a different flow regime than for the fluvial flood applications. For this reason, it is concluded that it is not possible to transfer the more investigated parameters for the application of fluvial flooding 1:1 to the integrated approach. For further investigations, the effect of sensitive parameter ranges and combinations needs to be clarified for the integrated approach.

- The model calibration process showed very different results for the two applications. The initially assigned roughness values for Approach I were in a similar range as the calibrated n values. Whereas for the decoupled approach special focus needs to be set on the selection and effect of Manning's n values. The n values were initially selected for natural channels and floodplains. This is shown to be inadequate for the DRM application. Therefore, the roughness coefficients needed to be increased to fit the requirements of overland flow. They were then comparable to Engman (1986) and the summarized recommendations for overland roughness coefficients in Downer & Ogden (2006) or HEC (1998). If the approach to determine friction losses is generally applicable in combination with 2d models in the context of overland flow should be further investigated.

- To make valid comparisons and further investigate the newly proposed methodology, the integrated approach should be applied in other equipped study areas with different sizes, topography and land uses. The study also showed that the integrated approach has much higher computational times than the decoupled approach, due to larger model extents and higher number of grid cells. The reduction of the computational cost can be achieved by the progressive use of GPU based calculation (e.g. García-Feal et al., 2018; Loretz & Volz, 2017 or Kalyanapu et al., 2011) or by the implementation of more effective numerical schemes as for example presented in Cea & Bladé, (2015). The contribution of rainfall heterogeneity, runoff formation routines and subsurface flow in

rural areas should be investigated in further studies. To expand the 'model-specific view', a model intercomparison on catchment scale would provide an enhanced overview on model-specific problems.

3 A Systematic Analysis of the Interaction between Rain-on-Grid-Simulations and Spatial Resolution in 2d Hydrodynamic Modeling

Abstract

A large number of 2d models were originally developed as 1d models for the calculation of water levels along the main course of a river. Due to their development as 2d distributed models, the majority have added precipitation as a source term. The models can now be used as quasi-2d hydrodynamic rainfall–runoff models ('HDRRM'). Within the direct rainfall method ('DRM'), there is an approach, referred to as 'rain-on-grid', in which input precipitation is applied to the entire catchment area. The study contains a systematic analysis of the model behavior of HEC-RAS ('Hydrologic Engineering Center—River Analysis System') with a special focus on spatial resolution. The rain-on-grid approach is applied in a small, ungauged, low-mountain-range study area (Messbach catchment, 2.13 km^2) in Central Germany. Suitable model settings and recommendations on model discretization and parametrization are derived therefrom. The sensitivity analysis focuses on the influence of the mesh resolution's interaction with the spatial resolution of the underlying terrain model ('subgrid'). Furthermore, the sensitivity of the parameters interplaying with spatial resolution, like the height of the laminar depth, surface roughness, model specific filter-settings and the precipitation input-data temporal distribution, is analyzed. The results are evaluated against a high-resolution benchmark run, and further criteria, such as 1. Nash–Sutcliffe efficiency, 2. water-surface elevation, 3. flooded area, 4. volume deficit, 5. volume balance and 6. computational time. The investigation showed that, based on the chosen criteria for this size and type of catchment, a mesh resolution between 3 m to 5 m, in combination with a DEM resolution from 0.25 m to 1 m, are recommendable. Furthermore, we show considerable scale effects on flooded areas for coarser meshing, due to low water levels in relation to topographic height.

Keywords: hydrodynamic modeling; hydrological modeling; storm hazard analysis; Direct Rainfall Method; rain-on-grid; sensitivity analysis; overland flow; spatial resolution

3.1 Introduction

3.1.1 Motivation and Research Gap

The use of 2d hydrodynamic models to determine storm hazards in rural and urban catchments based on the Direct Rainfall Method (in the following called DRM or 'rain-on -grid', (compare Ball et al. (2012)) has become state-of-the-art in storm hazard flood modeling in recent years. The DRM has meanwhile established itself and is included in the mainstream commercial and non-commercial 2d software packages for urban or river flooding. Examples of applications of DRM together with a Hydrological-Hydrodynamic Rainfall-Runoff Model (HHDRRM) or "hydro-inundation model" (Yu & Coulthard, 2015) can be found for urban and rural areas in Zeiger & Hubbart (2021), Krvavica & Rubini (2020), David & Schmalz (2020), Broich et al. (2019), Jia et al. (2019), Tyrna et al. (2018), Yu & Coulthard (2015), Cea et al. (2010) or Hunter et al. (2008).

The models for fluvial flood hazard assessment were often originally designed as 1d models to determine the water levels and floodplains along the 1d river stream. With the increased availability of high resolution data of the terrain ('digital elevation model', DEM) and the surface ('digital surface model') the models also increased their level of detail with the extension from 1d to 2d (Mandlburger et al., 2009). With this extension, also the floodplains and backwater effects are modeled in high resolution. Due to the simultaneous increase of flood events apart from large rivers (urban, pluvial or flash floods according to Schanze, 2018), the 2d models were expanded to include the source term of precipitation. This enables the models to be used in the context of storm hazard analysis within the entire catchment area (David & Schmalz, 2020).

The problem of the application of 2d hydrodynamic models for the use of catchment hydrology and determination of shallow overland flow is that the model is applied in ways for which it was not originally developed. However, the flow behavior of the thin-layer runoff differs greatly from the flow process in a 'normal' river due to the very low flow depths (Oberle et al., 2021; Grismer, 2016). The model user must consider this different way of application and need to take care of a suitable model parametrization. During the process of model creation details such as spatial resolution, computational settings or roughness values have to be determined by the user. These should be suitable, on the one hand, to best represent the characteristics of the catchment, but on the other hand, also need to consider the special type of application of direct precipitation. It can be seen, for example, in Broich et al. (2019) or in David & Schmalz (2020), that with the use of a 2d model as 2d HHDRRM the model shows a different behavior than for fluvial flood hazard assessment. For this way of application, other model settings are necessary and model parameters that have so far been ignored may be sensitive. For this reason, before using the DRM in combination with a 2d model, the model should first be evaluated extensively with regard to its model behavior in relation to the parameterization and parameter's sensitivity.

Additional challenges of using a 2d model as 2d HHDRRM are the catchment size and the spatial resolution. The application of the DRM throughout the entire catchment covers significantly larger model extents. Therefore, the consideration of a suitable representation of catchment topography with the simultaneous regard to computational times and possible interplay with further model settings becomes of increased importance.

In the following, examples of the application of the DRM method in urban areas for gauged and ungauged catchments are evaluated, with special regard paid to how the model parameterization and the parameter sensitivity is addressed in the modeling process. In the literature review, particular attention is paid to how detailed different spatial resolutions are considered to be in their modeling. The research contributions are classified as 'urban' when the sewer network has been integrated into the model (so-called 'dual drainage modeling' according to Djordjevi et al. (1999)) or the runoff process is significantly affected by urban structures. Since the focus of this work is an application of the DRM in a 'real' catchment area, the literature review does not contain any laboratory or purely numerical test cases.

- Zeiger & Hubbart (2021) evaluated an integrated modeling approach, using a coupled-modeling routine. The river basin model SWAT ('Soil and Water Assessment Tool') was used to determine effective rainfall rates and HEC-RAS 2d was used as for the rain-on-grid simulations. The Hinkson Creek Watershed (232 km²) was discretized with 10 m mesh and 1 m DEM as underlying subgrid.

- Krvavica & Rubinić (2020) applied HEC-RAS with direct precipitation in a small ungauged catchment of 3.08 km². The focus of the research project was the evaluation of the influence of different storm designs and rainfall durations on the catchment outflow. A mesh with an average grid size of 10 m and local refinements of 5 m was used with a 2 m subgrid DEM for topographic details.

- Rangari et al. (2019) applied HEC-RAS as HHDRRM for different storm events in the highly urbanized area of Hyderabad. The model was set up for an area with 47.08 km², a fixed mesh resolution and underlying DEM of each 10 m and 139,487 computational cells.

- Caviedes-Voullième et al. (2020) compared the impact of the application of zero-inertia ('ZI') and shallow-water ('SW') models. The results of six different benchmarking test cases were analyzed. One of the test cases included the application in an urban area in Glasgow with a catchment size of 0.4 km². The study was conducted for four different (1. 'very-coarse'—4 m, 2. 'coarse'—3 m, 3. 'medium'—2 m, 4.'fine'—1 m) model-set-ups.

- Tyrna et al. (2018) applied the 2d hydraulic model FloodArea in an ungauged urban area with a study area of 144 km² to provide "large-scale high-resolution fluvial flood hazard mapping". They presented a method that involves a precipitation model, a hydrological model, a digital elevation model and a hydraulic model component. The model set-up consisted of a 1 m raster-based model.

- Pina et al. (2016) used two case studies to compare a semi ('SD')—and a fully ('FD')—distributed model. The study consists of two model set-ups with the focus of the comparison of the SD and FD approaches and the integration of a sewer-system network. The first FD model has an average resolution of 61 m² with a catchment size of 8.5 km². The second FD model has a size of 1.5 km² with an average cell size of 89 m². The focus of the modeling processes is the comparison of the two different model types.

- Cea & Rodriguez (2016) present the development of a 2d distributed hydrologic-hydraulic model ('GUAD-2d') with the objective to model the rainfall–runoff process within a catchment. The presented model was tested in a 12.97 km² large urban catchment, an ungauged area with a cell size of 4 m and a 500-year storm event. The model was evaluated against a model-set up without DRM.

- Fraga et al. (2016) conducted a global sensitivity and uncertainty analysis for a 2d-1d dual drainage model (Fraga et al., 2015) using the GLUE ('Generalized Likelihood Uncertainty Estimation', compare Beven & Binley (1992)) method which is developed for distributed models. For the surface model the sensitivity of the Manning's n coefficient and the infiltration parameters were analyzed. The study was conducted in a motorway section with an area of 0.049 km². The model geometry consists of an unstructured mesh with a fixed mesh resolution of circa 3 m.

- Leandro et al. (2016) introduced a methodology that stepwise increases the model complexity in different modeling levels to evaluate the impact of 'spatial heterogeneity of urban key features'. The 2d overland flow model P-DWave (Leandro et al., 2014) was set-up for a catchment area ('Borbecker Mühlenbach', 4.9 km²). The model was systematically extended in five stages with focus on the representation of buildings and land surfaces. The model geometry was created with a fixed grid with 2 m resolution.

- Yu & Coulthard (2015) applied the hydro-inundation model FloodMap in an urbanized area in Kingston upon Hull (UK). The influence of improved urban and rural drainage and storage capacity was investigated in a stepwise manner. During the modeling, process the model sensitivity to roughness and mesh resolution was determined.

- Néelz & Pender (2013) analyzed various 2d hydrodynamic model in eight different benchmark test cases. The last test case includes an application of the 2d models by direct precipitation in a small urban area in Glasgow with a total size of 0.384 km². The same test case was further evaluated for various models in Broich et al. (2018) and for HEC-RAS in HEC (2018). For most of the models, a fixed spatial resolution and roughness values were used with a 2 m grid. For HEC-RAS two different mesh resolution (2 m, 4 m) were evaluated, which showed minor sensitivity on model run times and sensitivity on water level time series (HEC, 2018).

- Chen et al. (2010) applied the integrated 1d sewer and 2d overland flow model SIPSON/UIM in a small urban catchment area ('Stockbridge', ca. 0.18 km²) close to a riverside. The model is set-up with a fixed resolution of 2 m. The focus of the study is

given on the impact of different design storms and floods for an area which is affected by combined pluvial and fluvial flooding.

In the following case studies, applications of the DRM in rural catchment areas are presented. The studies are classified as 'rural' when there are mainly agricultural and forest-covered areas in the catchment. Special focus on the literature review is again set on the model parametrization, the spatial resolution and parameter sensitivity during the modeling process.

- David & Schmalz (2020) evaluated the application of the modeling software HEC-RAS in a low mountain-range study area with a catchment size of 38 km². Various model settings were tested for the specific application of DRM and a model calibration was carried out based on the Manning's n roughness. It is shown that internal model parameters are sensitive for the application of hydrodynamic rainfall–runoff modeling and must be adapted to a different value range. Due to the size of the area and the resulting extensive computational times, no detailed sensitivity analysis was carried out.

- Jia et al. (2019) developed the model system for surface and channel runoff CCHE2d. It was applied to a subcatchment of the Mississippi River, with a catchment size of 18 km². In the study, a local sensitivity analysis for the Manning's n roughness was carried out. The evaluated values were in a range between 0.03 and 0.3 s × m−1/3. The model was set up with a fixed mesh resolution between 3.8 and 5 m.

- Broich et al. (2019) developed an approach for the implementation of the DRM in the 2d hydrodynamic model TELEMAC-2d. They applied the extended model to the catchment areas of Simbach (45.9 km²) and Triftern (90.1 km²). Furthermore, alternative approaches for the roughness calculation for sheet water flow were implemented as new calculation routines. Additionally the impact of model intern ('hidden') parameters on the modeling results were evaluated. The model geometry was based on a 5 m DEM with 1 s timestep.

- Hall (2015) conducted a DRM application in the Birrega catchment with an area of ca. 185 km². For the model application, the 2d model MIKE from the Danish Hydraulic Institute ('DHI') was used. The model geometry consists of a grid with a constant resolution of 20 m. In the modeling process, design floods with different return periods were evaluated. In a simplified local sensitivity analysis of the impact of 1. rainfall, 2. Manning's n roughness, 3. infiltration and 4. groundwater inundation. Each model set-up was tested for a large- (176 km²) and small- (7 km²) scale catchment area.

- Cea & Bladé (2015) developed a discretization scheme ('Decoupled hydrological discretization', DHD) to solve the 2d SWE for hydrodynamic rainfall–runoff applications. They applied the model to five test cases, where two test cases involved application in small rural basins. The first catchment has a size of 4 km² with an average cell size of 15.5 m. The second catchment has a size of 5 km² with an average cell size of 20 m. The model was calibrated by the infiltration rate and the Manning's n values.

In the study, the alternative discretization scheme is evaluated against three other methods.

- Clark et al. (2008) compare the two 2d models TUFlow and SOBEK with a traditional lumped hydrological rainfall-runoff model. In a 11.85 km² large catchment area a local sensitivity analysis is performed considering various parameters. The spatial resolution is evaluated for mesh resolution between 10 m and 100 m (TUFlow) and 5 m and 100 m (SOBEK). It has shown that both models are sensitive towards the mesh resolution.

The summary of the studies shows that there is a broad scattering of different model extents from 0.049 km² to 232 km², with spatial resolutions varying between 1 m and 30 m. The number of cells varies between 5444 and 144,000,000 cells. The parameter's sensitivity and model output uncertainty is regarded sparely in the modeling process when applying the DRM in a new catchment. Some studies as Clark et al. (2008), Hall (2015), Yu & Coulthard (2015), Fraga et al. (2016), Jia et al. (2019) and David & Schmalz (2020) have evaluated the Manning's n sensitivity. The studies of Clark et al. (2008), Yu & Coulthard (2015) and Caviedes-Voullième et al. (2020) evaluated different spatial resolutions during the modeling process and one study conducts a detailed global sensitivity and uncertainty analysis based on the GLUE method (Beven & Binley, 1992). None of the studies has applied a sensitivity or uncertainty analysis together with the free software HEC-RAS from the U.S. Army Corps of Engineers (HEC, 2020). The key facts of the results of the literature study are summarized in **Table 21** for urban applications and **Table 22** for rural applications. In case studies in which no information on the cell size or the number of cells was available, it was determined by use of the computational area and the spatial resolution. For the case studies with an unstructured mesh, the average cell size is given.

Table 21: Overview of case studies 2d rainfall–runoff modeling ('Direct Rainfall Method') - Urban applications

Reference	2d Model (s)	Catchment: Size	Spatial Resolution (Number of Cells)	Rainfall Input	Rainfall Loss Approach	Roughness Values [s×m$^{-1/3}$]	Sensitivity Analysis	Calibration Data
Zeiger & Hubbart (2021)	SWAT/ HEC-RAS	Hinkson Creek, MO: 232 km²	DEM: 1 m Mesh: 10 m	10 historical storm events	long term hydrological modeling (SWAT) SCS-CN method	Manning formula n from 0.003 (barren land) to 0.092 (Herbaceous); calibrated values	Computational interval	gauging stations
Krvavica & Rubinić (2020)	HEC-RAS	Novigrad: 3.08 km²	DEM: 2 m Mesh: 10 m, 5 m refinement (38,499 cells)	2 historical events 6 statistical events	SCS-CN method	Manning formula n = 0.015 (roads) n = 0.2 (agriculture)	6 different design storms 4 different rainfall durations	none
Caviedes-Voullième et al. (2020)	in-house development	Glasgow: 0.384 km²	4 m (24,100) 3 m (42,693) 2 m (96,400) 1 m (384,237)	1 rainfall event	none	Manning formula n = 0.02 (roads) n = 0.05 (other)	SWE and ZI ('zero inertia') solver mesh resolution	none
Rangari et al. (2019)	HEC-RAS	Hyderabad: 47.08 km²	DEM: 10 m Mesh: 10 m (139,487)	3 historical events 3 statistical events	no information	Manning formula n = 0.025	none	none
Tyrna et al. (2018)	FloodArea	Unna: 144 km²	1 m (144,000,000)	1 statistical event 1 fictional event	simplified physical approach based on Green and Ampt and Darcy	Manning formula from n = 0.013 (roads) to n = 0.250 (forest)	none	none
Pina et al. (2016)	Infoworks ICM v.5.5	Cranbrook: 8.5 km² Zona central: ca. 1.5 km²	Cranbrook: avrg. 8.5 m (117,712) Zona central: avrg. 11.8 m (10,741)	Cranbrook: 3 historical events, 5 statistical events Zona central: 4 historical events, 6 statistical events	fixed runoff coefficient	no information	SD/FD approach different design storms	gauging station
Cea & Rodriguez (2016)	GUAD-2d	Alginet: 12.97 km²	4 m (ca. 810,625)	500-year event	SCS-CN method Green-Ampt Horton Philip	Manning formula	hydraulic-hydrological calculation	none
Fraga et al. (2016)	in-house development	Motorway section: 0.049 km²	avrg. 3 m (ca. 5444)	7 historical events	initial-constant approach	Manning formula n = 0.02–0.1 (impervious surface) n = 0.02–0.5 (pervious surface) n = 0.008–0.025 (conduits)	Manning's n Infiltration rates Discharge coefficients	discharge data
Leandro et al. (2016)	P-DWave	Borbecker Mühlenbach: 4.9 km²	2 m (ca. 1,225,000)	1 historical event	Green-Ampt	Manning formula	5 modeling levels, increasing complexity of key urban features	none

Reference	2d Model (s)	Catchment: Size	Spatial Resolution (Number of Cells)	Rainfall Input	Rainfall Loss Approach	Roughness Values [s×m−1/3]	Sensitivity Analysis	Calibration Data
Yu & Coulthard (2015)	FloodMap	City of Kingston/Hull: -	10 m 20 m	1 historical event	Green-Ampt	Manning formula	Mesh resolution Manning's n Hydraulic conductivity	inundation areas
Néelz & Pender (2013) Broich et al. (2018) HEC (2018)	Various	Glasgow: 0.384 km²	2 m (ca. 97,000) HEC-RAS: DEM: 0.5 m Mesh: 2 m, 4 m	1 event	none	Manning formula 0.02 (roads) 0.05 (area)	HEC-RAS: mesh resolution	none
Chen et al. (2010)	Sipson/UIM	Stockbridge: ca. 0.18 km²	2 m (ca. 45,000)	statistical events	no information	no information	design storms flood types	none

Table 22: Overview of case studies 2d rainfall–runoff modeling ('Direct Rainfall Method') - Rural applications

Reference	2d Model (s)	Catchment: Size	Spatial Resolution (Number of Cells)	Rainfall Input	Rainfall Loss Approach	Roughness Values [s×m−1/3]	Sensitivity Analysis	Calibration Data
David & Schmalz (2020)	HEC-RAS	Fischbach: 38 km²	DEM: 1 m Mesh: 100 m, 5 m refinement (246,100) 30 m, 3 m refinement (687,800)	3 historical events	constant psi SCS-CN method with modification [33]	Manning formula final range from n = 0.07 for pastures to n = 0.11 for forest-covered areas	Manning's n model specific parameters: computational and filter tolerances	gauging station
Jia et al. (2019)	CCHE2d	Howden Lake: 18 km²	from 3.76 to 4.98 m (ca. 942,600)	historical events	no loss (clayey soils)	Manning formula initial value from 0.03 to 0.3 final value n = 0.3 (catchment area), n = 0.16 (channel)	Manning's n	gauging station
Broich et al. (2019)	TELEMAC 2d	Simbach a. Inn: 45.9 km² Triftern: 90.1 km²	5 m (ca. 1,836,000) 5 m (ca. 3,604,000)	1 historical event	SCS-CN method	DWA, (2020), [34] Machiels et al. (2009), [35] Lawrence, (1996), [36] Lindner, (1982), [37]	model specific parameters: fricti.f (H0), steep slope correction (SSC)	gauging station
Hall (2015)	MIKE Flood	Birrega: 185 km²	20 m (ca. 462,500)	2 historical events 5 statistical events	constant infiltration rate	Manning formula calibrated n from n = 0.022 (roads) to n = 0.059 (urban/native vegetation)	rainfall depth Manning's n Infiltration rate Groundwater inundation	gauging station
Cea & Bladé (2015)	in-house development	Solivella: 4 km² Maior River: 5 km²	Solivella: avrg. ca. 15.5 m (17,926) Maior River: avrg. ca. 20 m (24,676)	Solivella: 1 fictional storm event Maior River: 1 historical event	Solivella: no infiltration (fully saturated soil) Maior river: constant infiltration rate	Manning formula Solivella: n = 0.15 Maior river: from n = 0.3 to n = 0.5	four different discretization schemes	none
Clark et al. (2008)	TUFLOW, SOBEK	Boembee Valley: 11.85 km²	5 m, 10 m, 20 m, 50 m, 100 m	design storm: 100-year event, 2 h	constant infiltration rate	constant Manning's n values: 0.04, 0.06, 0.08	timestep Manning's n mesh resolution run length slope return period	none

3.1.2 Objectives

The goal of this study is the systematic analysis of the model behavior of the 2d hydrodynamic model HEC-RAS by applying the DRM in a small, ungauged rural catchment in the low mountain range. In this context, special focus is given on the spatial resolution in interplay with the underlying 'subgrid' (Casulli, 2009) topography of the DEM and further model parameters. In a first step (Step 1), seven different resolutions of DEM are combined with seven different mesh resolutions. The model results of the 49 model runs are evaluated against a high resolution benchmark (DEM 0.25 m, mesh: 1 m). From this pool of simulations the most suitable combinations of mesh and subgrid resolution are identified based on fixed criteria. They are further investigated and combined in a second step (Step 2) for their model sensitivity concerning 1. laminar depth, 2. Manning's n roughness values, 3. model-specific filter settings and 4. precipitation data. As a result, the model parameter sensitivity is quantified based on selected local sensitivity indices. Finally, together with a qualitative assessment of the results a recommendation for a good model-set up applying the DRM is given. Furthermore, the study should lead to a better model understanding of this specific 2d model and parameter interaction without the use of the computationally high demanding statistical methods. As model, the 2d hydrodynamic model HEC-RAS 6.0 from the Hydrologic Engineering Center (HEC) is used (HEC, 2020). The summarized objectives of the study are:

- To introduce a stepwise methodology which allows a systematic analysis of model behavior and parameter sensitivity when applying HEC-RAS and the DRM in a small rural catchment.
- To reduce the number of model runs in order to manually execute the methodology.
- To evaluate the parameter sensitivity of: 1. mesh resolution, 2. subgrid topographical data, 3. laminar depth, 4. Manning's n values, 5. model-specific filter settings and 6. precipitation data.
- To give recommendations on suitable spatial resolution and identify sensitive model settings when applying the 2d model HEC-RAS for storm hazard analysis in small catchments of low mountain range areas.

This study can be seen as a suggestion of how a systematic analysis of model behavior can be principally applied for the mentioned model parameters in combination with the spatial resolution. The study catchment is part of the field laboratory of the Chair of Engineering Hydrology and Water Management (IHWB) from Technical University of Darmstadt (Schmalz & Kruse, 2019; Kissel & Schmalz, 2020 and Grosser & Schmalz, 2021).

3.2 Materials and Methods

3.2.1 Model Behavior, Sensitivity Analysis and Model Uncertainty

The most common methods to assess model behavior and to quantify the model output limitations due to the inexact representation of the real world phenomena is the Uncertainty Analysis (UA) in combination with the Sensitivity Analysis (SA) (Savage et al., 2016). While the uncertainty analysis quantifies the uncertainty in the model output, the sensitivity analysis focusses on the relative contribution of each model parameter to the model output. Both methods are applied for a better model understanding and to explore a broad spectrum of parameter ranges. Ideally, uncertainty and sensitivity analysis are run in tandem. The uncertainty analysis is often applied in hydraulic modeling in flood forecasting to quantify the uncertainty of the predicted result (Savage et al., 2016). Whereas sensitivity analysis is more often applied to identify the most influential parameters, to simplify the calibration process and therefore to reduce the number of calculation runs (Savage et al., 2016).

SA can be divided into two main categories, local and global-sensitivity analysis. The local SA is defined as a 'a local measure of the effect of a given input on a given output' (Saltelli, 2004, p. 42). It means that 'one point of the factors' space is explored' and 'factors are changed one at a time' (Saltelli, 2004, p. 42). The parameter sensitivity is determined using the first-order sensitivity index, which measures the effect of a local change on the model output (Beven, 2012). The advantage of this local sensitivity approach is the simplicity and the reduced number of simulations. The disadvantage of this method is that it has a limited epistemic value, since it focusses on the 'response surface' of only one single parameter (Beven, 2012). The effect of the interaction of parameter variations on the modeling results cannot be investigated by this method. Therefore and due to the increasing complexity of numerical models the local SA was extended to the more complex global SA (Saltelli, 2008, as cited in Savage et al. (2016)). The method of the global SA makes it possible to investigate the model output over a broad range of parameter values and its interactions. The advantage of the global SA is that it allows a much more sophisticated analysis of the model behavior. The disadvantage of this method is that the amount of simulations is increasing exponentially and therefore it needs much longer computational times.

Uncertainty analysis is often applied for flood hazard models to give a quantitative statement about the accuracy of the modeling results (Willis et al., 2019). In Willis et al. (2019) there can be found an example of the application of an uncertainty analysis for different sources of uncertainty. He gives the classification by Willems (2012) of four different types of uncertainty from 1. input data, 2. parameter, 3. model structure and 4. model assessment. A systematic analysis of the model uncertainty in a stepwise manner with special focus on model structure can be found in Willis et al. (2019). Even though in the computationally simplified methodology, still 3010 model runs were persecuted for six different parameter types. This makes it difficult to apply the method in contexts of limited resources in terms of time and hardware in combination with the computationally demanding 2d hydrodynamic models.

In hydrology a widely used method of the global SA and uncertainty analysis is the broadly applied Generalized Likelihood Uncertainty Estimation ('GLUE') method (Beven, 2012) or its precursor the Hornberger-Spear-Young ('HSY') method (Hornberger & Spear, 1981 as cited in Beven (2012)).

3.2.2 Systematic Analysis of Model Behavior

Due to the fact that the application of hydrodynamic models as rainfall–runoff models needs long computational time, the number of simulations is limited for computational reason. Furthermore, the model HEC-RAS runs on CPU (central processing unit) - based office-desktop PCs and not on high-performance clusters (HPC). Therefore, a full global sensitivity or uncertainty analysis based on statistical methods was not feasible in this study. Furthermore, the focus of the study should lie on a pragmatic, but systematic approach, which can be principally applied, in a hydraulic modeler's everyday practice. The results should help model users to decide on suitable model settings when applying the DRM together with a 2d HHDRRM. As a result, we can become more sensitive on the choice of model settings and parameters. However, since the parameter interaction on the results should not be neglected, a simplified systematic sensitivity analysis should be conducted. By the introduced methodology (compare **Figure 10**), special focus will be given on the impact of the spatial resolution of meshing and subgrid on the modeling results ('Step 01'). The methodology is able to assess the parameter interaction in context of spatial resolution (DEM, mesh) for a broad range of DEM (0.5 m, 1 m, 2 m, 3 m, 4 m, 5 m) and mesh (2 m, 3 m, 4 m, 5 m, 10 m, 20 m, 30 m) resolution. The results are analyzed based on six different criteria, which are presented in the following section. Three indices allow the comparison with the high-resolution benchmark (1 m mesh, 0.25 m DEM). The other three criteria are absolute indices. In a second step ('Step 02') a predefined selection of suitable model runs will be further evaluated in terms of parameter sensitivity. Therefore, model runs with different realizations of mesh and DEM resolution are analyzed towards its sensitivity on four different categories: 1. Laminar depth, 2. Manning's n, 3. Model-specific filter settings and 4. Precipitation data. The further sensitivity analysis was carried out with this selection of parameters in order to identify further model settings, which might have to be taken into account during the calibration process. The selection was done because it was assumed, due to their mode of action, that they could affect the model results using rain-on-grid simulation. The sensitivity of the variables of the runoff formation routine was not part of the study. For all model configurations, the identical effective precipitation is applied.

Step 1: DEM vs. mesh resolution

DEM resolution „subgrid"

| 0.25 m | 0.5 m | 1 m | 2 m | 3 m | 4 m | 5 m |

MESH resolution

| 1 m (Benchmark) | 2 m | 3 m | 4 m | 5 m | 10 m | 20 m | 30 m |

∑ 50 sim.

A Assessment of results
Quantitative assessment of results:
- o Indices relative to benchmark: 1. Nash Sutcliffe Efficiency (NSE), 2. Difference in maximum Water surface Elevation (ΔWSE), 3. Flooded Area (F²)
- o Absolute indices: 4. Volume Deficit (VD), 5. Volume Balance (VB), 6. Computational Time (CT)

B Definition of threshold
1. $NSE_{outlet} \geq 0.8$, $NSE_{village} \geq 0.8$
2. $\Delta WSE_{stream} \leq 0.05m$, $\Delta WSE_{road} \leq 0.05m$
3. $F^2 \geq 0.3$
4. $VD \leq 5\%$
5. $VB \geq 95\%$
6. $CT \leq 1$

C Exclusion of non-suitable combinations
- o Selection of parameter ranges (DEM and MESH resolution) for further investigation

Step 2: Spatial resolution, model parametrization and parameter sensitivity

Laminar depth	Manning's n	Model specific Filter settings	Precipitation data
1. Default (0.06)	1. Original	1. 0.0003	1. Euler II
2. 0.04	2. Plus 20%	2. Default	2. Initial
3. 0.08	3. Plus 10%	3. 0.003	3. End
4. 0.1	4. Minus 20%		4. Block
	5. Minus 10%		
∑ 36 sim.	∑ 40 sim.	∑ 27 sim.	∑ 36 sim.

A Assessment of results
Quantitative assessment of parameter sensitivity (S_i):
- o Volume deficit (S-VD)
- o Flooded Area (S-F²)
- o Flood peak (S-Qmax)

Step 3: Evaluation of results and suitable parametrization

A Recommendation of suitable parametrization
- o Mesh resolution
- o DEM resolution
- o Sensitive parameters

B Discussion of applicability of the Direct Rainfall Method
- o General conclusion
- o Model specific results
- o Catchment specific results

Figure 10: Schematic overview method for systematic analysis of model behavior

3.2.3 Hardware

In the study four different hardware configurations were used, which are summarized in the following **Table 23**. To speed up the computational time each investigated parameter of Step 2 was outsourced on a single PC.

Table 23: Hardware configurations used in the study

	PC-1	PC-2	PC-3	PC-4
System	ThinkStation P330	ThinkStation P520c	ThinkStation P330	ThinkStation P520c
CPU	I9-9900, 3.10 GHz	Xeon W-2125, 4.00 GHz	i7-9700, 3.00 GHz	Xeon W-2125, 4.00 GHz
GPU	Nvidia Quadro P2000	Nvidia Quadro P2000	Nvidia Quadro P620	Nvidia Quadro P2000
RAM	16 GB	16 GB	16 GB	32 GB
Used for	DEM vs. Mesh resolution Precipitation data	Filter parameters	Manning's n	Laminar depth

3.2.4 Evaluation of Results

The model results of Step 1 are analyzed based on the following criteria. Three following indices are evaluated against the high-resolution benchmark run with 1 m mesh resolution and 0.25 m underlying subgrid: 1. Nash–Sutcliffe efficiency ('NSE', compare **Eq. 1** and **Eq. 2**), 2. Difference in maximum water-surface elevation ('ΔWSE', compare **Eq. 3** and **Eq. 4**) and 3. Flooded area ('F2′, compare **Eq. 5**). A further three indices are evaluated based on absolute values: 4. volume deficit ('VD', compare **Eq. 6**), 5. Volume balance ('VB', compare **Eq. 7**) and 6. Computational time ('CT', compare **Eq. 8**). In Step 2 local sensitivities are determined based on absolute and relative sensitivity indices (compare **Eq. 9** and **Eq. 10**).

Nash–Sutcliffe Efficiency (NSE)

The results are analyzed using the Nash–Sutcliffe Efficiency (NSE). The modeled time series (Q_M) will be set in relation to the results of the high-resolution benchmark run (Q_B). The NSE index is criticized to overestimate the peak value (Pappenberger et al., 2008) as cited in (Willis et al., 2019). Since the peak valued plays an important role in storm hazard analysis, this index was chosen to analyze the results. Furthermore, this index allows to compare the model output over the entire simulation time with the benchmark run. The NSE for the stream discharge will be computed at two different locations, the NSE_{outlet} (**Eq. 1**) is computed at the outlet of the catchment (compare **Figure 11**), the $NSE_{village}$ (**Eq. 2**) is computed at the control point in the village in the upper part of the catchment.

$$NSE_{outlet}\ (\text{-})=1-\frac{\sum_{t=1}^{T}(Q_B^t\ -Q_M^t)^2}{\sum_{t=1}^{T}(Q_B^t\ -\overline{Q_B^t})^2} \qquad \textbf{Eq. 1}$$

$$NSE_{village}(\text{-})=1-\frac{\sum_{t=1}^{T}(Q_{B,village}^t\ -Q_{M,village}^t)^2}{\sum_{t=1}^{T}(Q_{B,village}^t\ -\overline{Q_{B,village}^t})^2} \qquad \textbf{Eq. 2}$$

Difference in Maximum Water-Surface Elevation (ΔWSE)

The difference in maximum water-surface elevation (ΔWSE) is compared with the high-resolution benchmark run at two different locations (**Figure 11**). The first location is at the flow control point (ΔWSE$_{max,stream}$, **Eq. 3**) in the stream, close to the village. The second location (ΔWSE$_{max,road}$, **Eq. 4**) is on the main road in the village. To determine the change of water-surface elevation the maximum value during the simulation time of the benchmark run (WSE$_{max,Benchmark}$) is subtracted from the maximum water-surface elevation of the model run (WSE$_{max,model\ run}$). The index was chosen as further criteria to compare the differences of water depth of the evaluated model configurations.

$$\Delta \text{WSE}_{\text{stream}}(\text{m}) = s\text{WSE}_{\text{max,model run}} - s\text{WSE}_{\text{max,Benchmark}}$$

Eq. 3

$$\Delta \text{WSE}_{\text{road}}(\text{m}) = r\text{WSE}_{\text{max,model run}} - r\text{WSE}_{\text{max,Benchmark}}$$

Eq. 4

Flooded Area (F2)

To compare the model output and the flooded area within the entire catchment area one area based index was chosen to evaluated the model runs against the benchmark run. The flooded area F² based on Bates & De Roo (2000), as cited in Aronica et al. (2002) and Willis et al. (2019) is added to evaluate the spatial distribution of the model results. This index (Eq. 5) is seen to be important since the spatial distribution of flooded area in the entire catchment is considered whereas the first two indices of NSE and ΔWSE only consider the model output at single locations. F² is determined for the maximum water depth larger than 0.05 m.

$$F^2\ (-) = \frac{\sum_i P_i^{B1M1}}{\sum_i P_i^{B1M1} + \sum_i P_i^{B1M0} + \sum_i P_i^{B0M1}}$$

Eq. 5

P$_i^{B1M1}$ – inundated pixel present in the model M1 and present in the benchmark run B1
P$_i^{B0M1}$ – inundated pixel present in the model M1 and absent in the benchmark run B0

Volume Deficit (VD)

The volume deficit VD (%) considers the difference of the input volume (V$_{in}$) in comparison to the accumulated output volume (V$_{out}$) at the end of the simulation. The index is seen important to identify the water volume, which is kept in the catchment or lost during the simulation. It is calculated using the following equation (**Eq. 6**).

$$VD\ (\%) = \frac{Vin - Vout}{Vin} * 100$$

Eq. 6

Volume Balance (VB)

The volume balance VB (%) is chosen as index to identify if the determined volume deficit (Equation (6)) is lost or kept in the catchment at the end of the simulation. Therefore, a volume balance is calculated which divides the sum of the total output volume (V_{out}) plus the water volume which is kept in the model area (V_{area}) at the end of the simulation by the total input volume (V_{in}). It is calculated using the following equation (**Eq. 7**).

$$VB\ (\%) = \frac{Vout + Varea}{Vin} * 100 \qquad \textbf{Eq. 7}$$

Computational Time (CT)

The computational time index CT (**Eq. 8**) is chosen to select simulation runs with reasonable run time. The index sets the computational time ($CT_{modeled}$) in relation to the real time ($CT_{realtime}$). All simulations were calculated for a real time of 24 h.

$$CT\ (-) = \frac{CTmodeled}{CTrealtime} \qquad \textbf{Eq. 8}$$

Local Model Sensitivity (e)

To investigate the model sensitivity towards changes of parameter input in Step 2 the relative, local sensitivity index, the elasticity index e1 (Maidment & Hoogerwerf, 2002; Walega et al., 2014; Ouédraogo et al., 2018) is determined by the following equation (**Eq. 9**). The model output Y can be classified as sensitive toward changes of the parameter X if $|e1| \geq 1$. If $|e| < 1$ the model output is only weak or insensitive towards changes of the input parameter.

$$e1\ (-) = \frac{\frac{\Delta Y}{Y_0}}{\frac{\Delta X_i}{X_i}} = \frac{\%change_{output}}{\%change_{input}} \qquad \textbf{Eq. 9}$$

For the non-scalable input parameter the different filter setting configurations and the precipitation distributions the output sensitivity e2 (**Eq. 10**) is determined based on the absolute change of model output.

$$e2\ (\%) = \frac{\Delta Y}{Y_0} = \%change_{output} \qquad \textbf{Eq. 10}$$

The parameter sensitivity is determined for the three different criteria: change in peak flow (S-Qmax), volume deficit (S-VD) and flooded area (S-F2) in comparison to the corresponding model run with the same spatial resolution of Step 01.

3.2.5 2d Hydrodynamic Model: HEC-RAS

2d overland flow is determined by the hydrodynamic model HEC-RAS from the U.S. Army Corps of Engineers (USACE). The theoretical basis for the 2d unsteady flow hydrodynamics is documented in detail in the technical reference manual (HEC, 2020). The mathematical model consists of the 2d equations of the continuity of mass and momentum, the 2d shallow water equation (SWE) and their simplification, the diffusion wave approximation (DWE). For the current version of HEC-RAS 6.0 there are two different versions of the SWE, the SWE-ELM (shallow water equations, the Eulerian–Lagrangian method) and the more momentum-conservative SWE-EM (shallow water equations, Eulerian Method). For the equation sets, the model makes use of the subgrid bathymetry approach (Casulli, 2009).

The approach takes into account the fine underlying topography of each cell by a characteristic cell volume property table. This makes it possible to define a coarser mesh resolution than the resolution of the digital elevation model. HEC-RAS solves the equations by a hybrid discretization scheme combining finite differences and finite volumes. The hybrid discretization makes advantage of the orthogonality of the grid. If the grid is orthogonal, the normal derivatives are determined by a finite difference approximation. If the grid is not orthogonal a finite volume approximation is used. The numerical methods to solve the underlying mathematical equations are described in detail in the hydraulic reference manual of the model (HEC, 2020).

3.3 Case Study, Data and Model Set-up

3.3.1 Messbach Catchment

The Messbach catchment has an area of 2.13 km² (**Figure 11**) and is part of the larger river system of the Gersprenz river. It is located in the south of Hesse in the low mountain range of the Odin forest (germ. 'Odenwald'). The Messbach is a small, ungauged creek of ca. 0.7 to 1.5 m channel width and around 1860 m channel length. It forms an inflow to the tributary of the Fischbach tributary of the Gersprenz river which was subject to former studies of Grosser & Schmalz (2021), Kissel & Schmalz (2020), David & Schmalz (2020) and Schmalz & Kruse (2019).

In the past, the Fischbach catchment area was subject to frequent flooding due to river floods and heavy rainfall events. One recent storm event with resulting flooded streets and houses took place on the April 23, 2018 (Echo, 2018). In 2017, a retention basin with a size of 220,000 m³ was taken in operation on the main stream of the Fischbach River. There are no retention basins in the Messbach catchment itself.
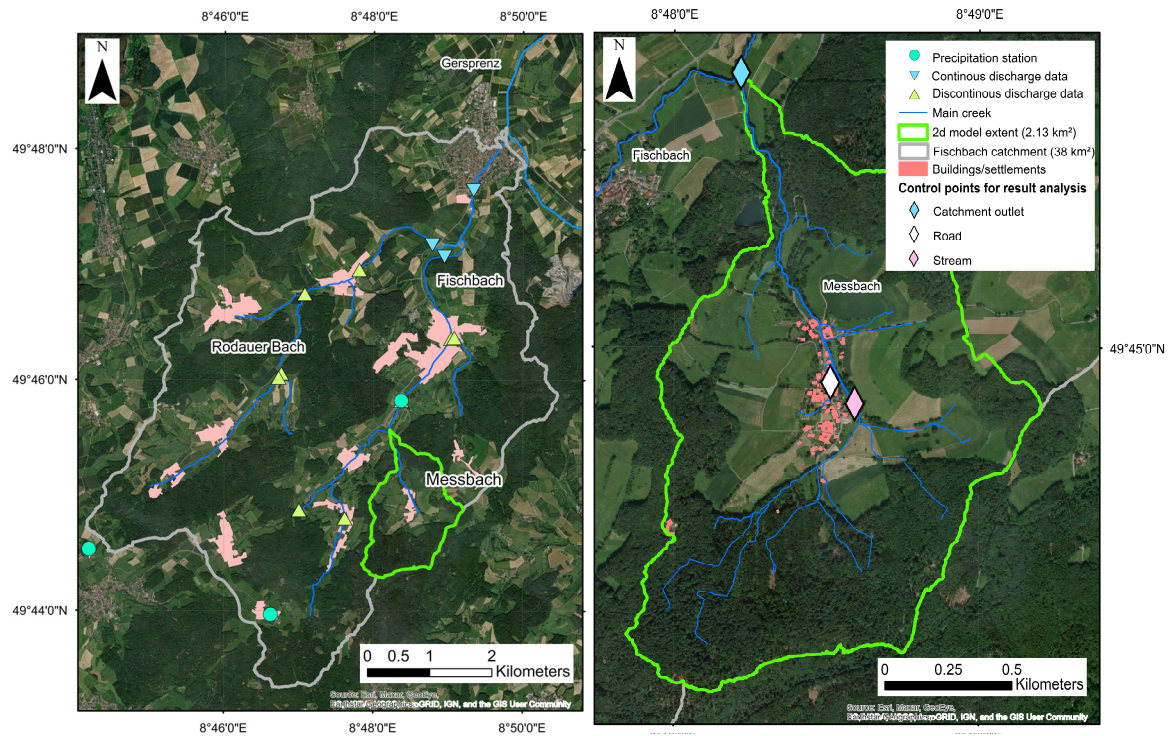
Figure 11: Study area of Messbach catchment

The topography (**Figure 12**) was analyzed based on the Airborne Laser scan data (LAS Version 1.3) from the Hessian Agency For Land Management and Geoinformation (Hessische Verwaltung für Bodenmanagement und Geoinformation, 'HVBG') (HVBG, 2019). The original point cloud of the received dataset was already classified in terms of ground-, non-ground and other points. The achieved accuracy of the measuring procedure is approx. 15 cm in height and approx. 30 cm in horizontal position. (HVBG, 2019) The catchment topography varies from 498.8 m above sea level ('masl') at the upper hills to 187.6 masl at the outlet of the catchment. The village is at a height of 305 masl. The steepest slopes in the catchment are up to 50 % on the forest-covered hillsides. In average, the catchment has a slope of 24.7 %. The longest flow path of the Messbach catchment has a length of L = 3.29 km with an average slope of 9.4 %. The steepest slope of the creek itself is around 20 %. The elevation within the catchment, along the longest flowpath and the position of the village can be seen in **Figure 12**.

The catchment area is predominately constituted by wooded area (ca. 54.0 % of total area) followed by agricultural area of farmland with field crops (ca. 18.8 %) and grassland (ca. 18.3 %). There are a few agricultural and forestry trails that make up around 4.2 % of the total area. In the center of the catchment there is located the small, Messbach, with a size of ca. 100 inhabitants. The area of the settlements has only minor effects on the overall catchment runoff characteristics and makes 1.9 % of the total area. As land-use data the official topographical data (ATKIS®) provided by HVBG was used (HVBG, 2017a). A summary of the different land-use categories within the catchment is presented in **Figure 13** and **Table 24**.
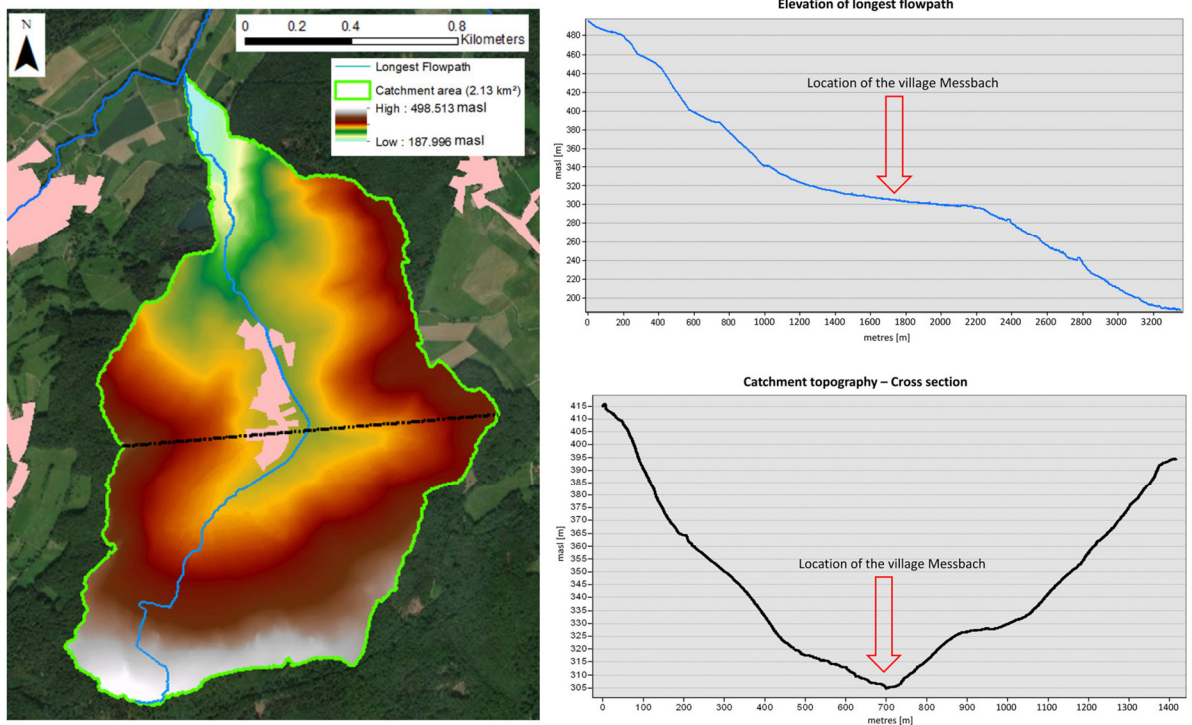
Figure 12: Topography of the Messbach catchment and location of Messbach village (HVBG, 2019)
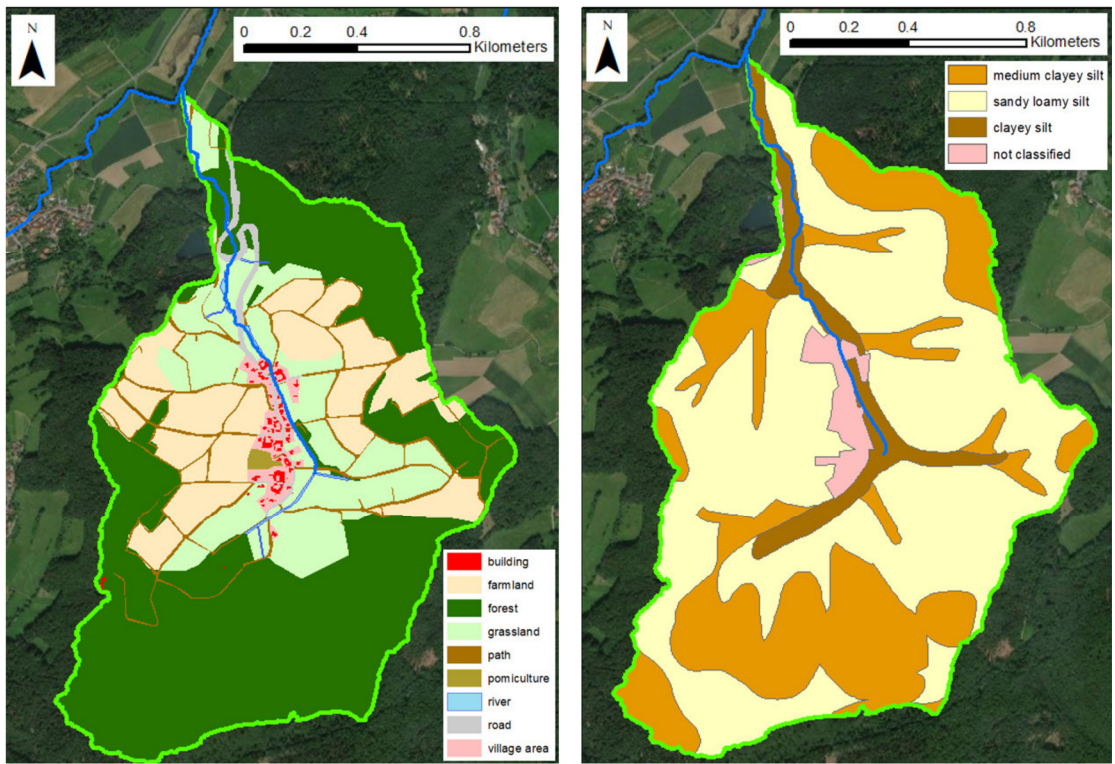
Figure 13: Map of land-use and soil data in the Messbach catchment

For soil classification, the digital soil map BFD50 (1:50,000) was used from the Hessian Agency for Nature Conservation, Environment and Geology (Hessisches Landesamt für Naturschutz, Umwelt und Geologie, 'HLNUG') (HLNUG, 2017a). The catchment's soil is predominantly silt with different compositions: sandy loamy silt (ca. 58.7 %), medium clayey silt (ca. 32.4 %) and clayey silt (ca. 6.1%). The infiltration capacity of the soil can be classified as moderate (ca. 59.0 %) with slower infiltration rates in the sinks of the hills (ca. 20.0 %) and very slow infiltration rates in the valley and the floodplains of the brook (ca. 21.2 %) (HLNUG, 2017a). A summary of the different soil categories within the catchment is presented in **Figure 13** and **Table 24.**

Table 24: Summary of landuse (HVBG, 2017a) and soil (HLNUG, 2017a) in the Messbach catchment

Landuse Classification (HVBG, 2017a)			Soil Classification (HLNUG, 2017a)
Description	Area [km²]	Percentage [%][a]	Description
Wooded area	1.15	54.0	sandy loamy silt
Farmland: field crops	0.40	18.8	medium clayey silt
Farmland: grassland	0.39	18.3	clayey silt
Trails	0.09	4.2	Not classified
Settlements Thereof buildings	0.04 0.01	1.9 0.5	-
Roads	0.03	1.4	-
Water bodies	0.02	0.9	-

[a] of total catchment area (2.13 km²)

As precipitation data the statistical dataset KOSTRA-DWD-2010R from the German Meteorological Service ('Deutscher Wetterdienst'—'DWD') was used (DWD, 2017). The KOSTRA dataset is a statistical precipitation dataset, which provides rainfall heights and rates for the different rainfall durations from 5 min to 72 h and return period from 1-year to 100-years. The 100-year event in the catchment has a rainfall height of 50.2 mm, the 50-year event a height of 45.0 mm, the 10-year event a height of 34.4 mm. (DWD, 2017)

In the catchment, there are no measurements of runoff. In the Fischbach catchment runoff coefficients for storm and flood events were determined by David & Schmalz (2020). In the observation period of 2004 to 2016 there were average runoff coefficients between 0.11 for the summer storm and 0.2 for the winter flood events. Maximum runoff coefficients are 0.35. The Messbach catchment has comparable land use.

To get an impression about typical concentration times within the catchment a unit hydrograph based on Wackermann (1981) as cited in DWA (2008) was determined (**Eq. 11**):

$$U(t) = \alpha * \frac{t}{k_1^2} * e^{\frac{-1}{k_1}} + (1 - \alpha) * \frac{t}{k_2^2} * e^{\frac{-t}{k_2}}$$

<div align="right">**Eq. 11**</div>

The storage coefficients k1 (Eq. 12), k2 (Eq. 13) and the weighting factor α (Eq. 14) were determined based Schröder & Euler (1999) as cited in DWA (2008):

$$K1 = \frac{0{,}555}{\left(\frac{L}{\sqrt{J}}\right)^{0{,}61}} + 0{,}511 * \ln\left(\frac{L}{\sqrt{J}}\right) - 0{,}355$$

<div align="right">**Eq. 12**</div>

$$K2 = 3 * k_1^{1,3}$$

<div align="right">**Eq. 13**</div>

$$\alpha = \frac{3{,}91}{\left(\frac{L}{\sqrt{J}}\right)^{0{,}86}} + 0{,}1 \text{ ;for } \frac{L}{\sqrt{J}} > 10km$$

<div align="right">**Eq. 14**</div>

With L: longest flowpath [km] and J: average slope of the catchment [-].

For the Messbach catchment with L = 3290 m and J = 0.095 the determined storage coefficients of the catchment are k1 = 0.99 h and k2 = 2.95 h. The weighting factor α = 0.61. The determined hydrograph is shown in **Figure** 14. In **Figure 15** there is an example of the outlet hydrograph for the 50-year event with a runoff coefficient of Ψ = 0.22.
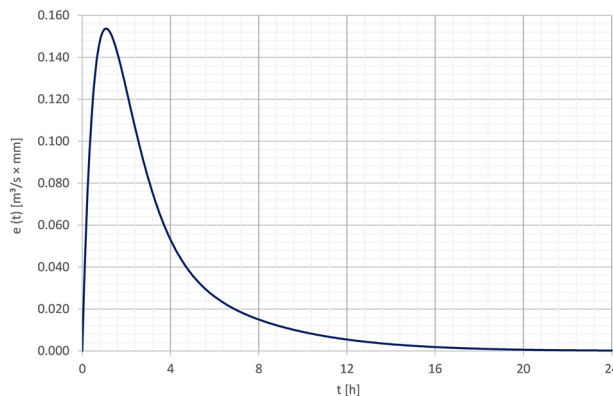
Figure 14: Determined unit hydrograph e (t) in [m³/s × mm] for the Messbach catchment.
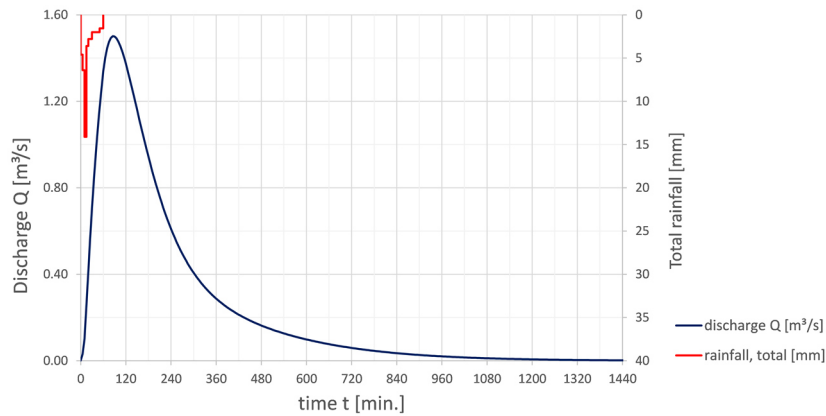
Figure 15: Determined hydrograph for the 50-year rainfall event with runoff coefficient $\Psi = 0.22$.

Base- and interflow are not considered in this study since this is not the main purpose of this paper.

3.3.2 Model Set-Up

From the original point cloud the ground points were extracted to build the Digital Elevation Models ('DEM') with seven different spatial resolutions: '0.25 m', '0.5 m', '1 m', '2 m', '3 m', '4 m', '5 m' (compare **Figure 10**). This procedure was done using the ArcGIS Toolset from ESRI 'LAS Dataset to Raster' using the binning interpolation-type with linear-void fill method and IDW cell assignment. (ESRI, 2021)

Buildings were integrated to the DEM from the original LAS surface model. For each resolution a DEM was created from the 'first return' surface point with the help of the LAS Toolset from ESRI 'LAS Dataset to Raster'. The shape of the buildings was clipped using the ATKIS® landuse data and then added to the original surface DEM. This procedure was made for reasons of comparability so that there is for each created DEM only one consistent raster resolution. In **Figure 16** there is shown the DEM with included buildings with a resolution of 0.25 m in comparison to the DEM with 2 m.
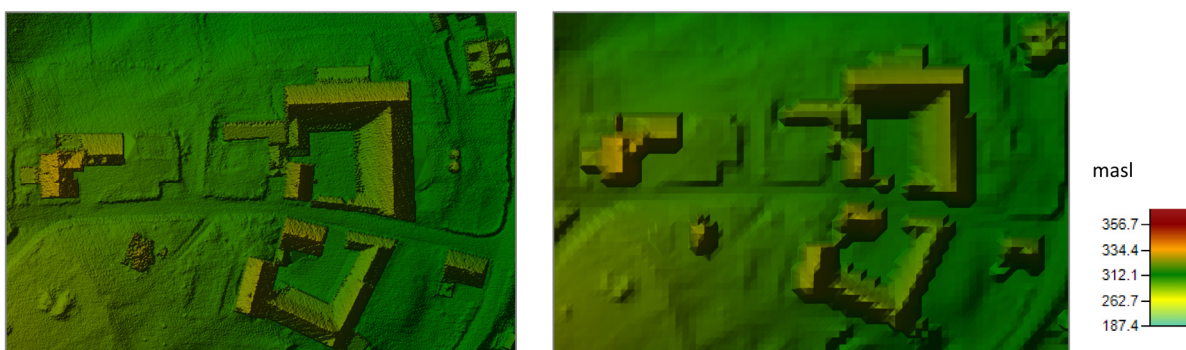
Figure 16: Buildings in the modeling domain using different DEM resolution: on the left: 0.25 m resolution, on the right 2 m resolution.

Culverts and bridges were integrated to the model domain by creating open channels with linear slope from the inlet to the outlet of the construction. This was done by creating a TIN with the

TIN Toolset from ArcGIS ESRI (ESRI Inc., 2021a). The TIN contains the linear topography of the digitized 26 culverts in the catchment and was added in a second step to the main topography of the model domain.

The mesh was created using the geometry editor from HEC-RAS. For each resolution for reasons of comparability one consistent mesh with one single mesh resolution was created. The finest mesh resolution is 1 m, which makes 2,128,354 cells for the catchment area. The coarsest mesh resolution is 30 m, which makes 2299 cells. It was evaluated to create even a finer mesh resolution but this led to the program's capacity being exceeded. A summary of all different computational grids and resulting number of cells is shown in **Table 25.**

Table 25: Mesh resolution and number of cells for each computational grid.

#	File Name*	Mesh Resolution	Number of Cells
1	0_25 m_1 m	1 m	2,128,354
2	0_25 m_2 m	2 m	531,489
3	0_25 m_3 m	3 m	236,035
4	0_25 m_4 m	4 m	132,652
5	0_25 m_5 m	5 m	84,810
6	0_25 m_10 m	10 m	21,102
7	0_25 m_20 m	20 m	5236
8	0_25 m_30 m	30 m	2299

* for 0.25 m DEM.

The initial Manning's n values for the different landuse categories (**Figure 13, Table 26**) were defined based on the values for overland flow roughness from Engman (1986) summarized in Downer & Ogden (2006). For the Messbach itself the initial roughness value was defined for 'coarse gravel' based on (Patt & Jüpner, 2013).

Table 26: Initially assigned Manning's n value based on Engman (1986), Downer & Ogden (2006), Patt & Jüpner (2013)

Landuse Category	Manning's n Value
wooded area	0.198
farmland: arable land	0.18
farmland: grassland	0.15
trails	0.03
settlements, buildings	0.1, 0.013
roads	0.013
river	0.029

As precipitation input, a storm event with a 50-year return period and 1 h duration and a total sum of 45 mm rainfall height and 5 min timestep is set. For Step 1 (compare **Figure 10**) the

temporal distribution of rainfall is set as Euler Type II (DWA, 2006). In Step 2 there are investigated four further temporal rainfall input distributions, the Alterning Block Method ('ABM'), an rainfall distribution with initial peak rate ('initial'), an rainfall distribution with end peak rate ('end') and a block precipitation input ('block').

The excess rainfall is determined by the SCS-CN method with an initial abstraction of $I_a = 0.05$. Soil and landuse data (compare **Table 24**) is preprocessed using the ArcGIS plugin from HECGeoHMS (HEC, 2012). The SCS-CN value is aggregated to one single value of CN = 69 for the catchment. All simulations were run with the same sum of excess rainfall for the event. The different input rainfall distributions are shown in **Figure 17**.
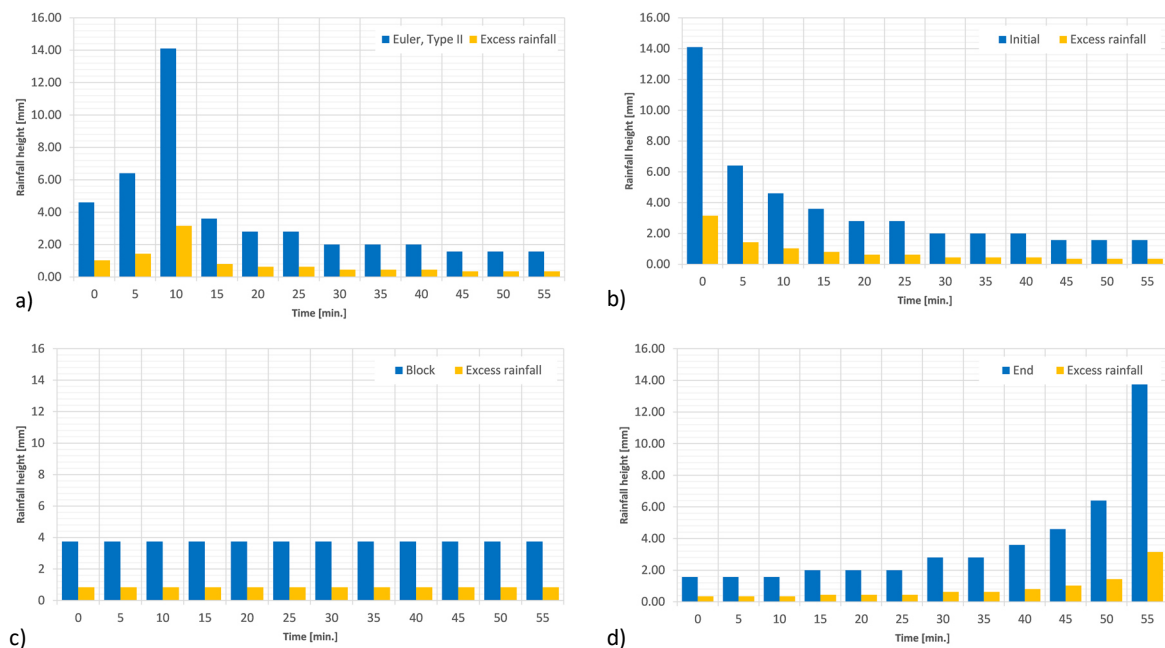
Figure 17: Temporal rainfall distributions (a): Euler Type II, (b): Initial, (c): Block, (d): End distribution.

As further model settings, a timestep was defined for each mesh resolution, based on the Courant criteria and an assumed maximum velocity within the catchment and stream flow of 5 m/s. The simulation time for the 1 h rain event is set to 24 h so that it is assured that the rainfall-runoff event is completed after the end of the simulation. The computational tolerances for water surface and volumes are set to 0.0001 m. The subgrid filter tolerances are reduced to 0.0003 m. Both adjustments are made to assure that shallow water precipitation heights are considered in the computational routine. For the main part, the Diffusion wave approximation is used as an equation set. This adaption is made to accelerate the runtimes and is considered to be physically justifiable, since slope and surface roughness are considered to be the most important driving forces for overland flow in the low mountain range. Furthermore, in Caviedes-Voullième et al. (2020) it is shown that model applications with DRM show comparable results between Zero-inertia (ZI, diffusive wave) and SWE solvers.

3.4 Results and Discussion

3.4.1 Pre-Study: Comparison of HEC-RAS 5.0.7 and 6.0

Since the current version of HEC-RAS, 6.0, came out during the case study, the seven test runs (mesh resolution 2 m, 3 m, 4 m, 5 m, 10 m, 20 m, 30 m), plus the high resolution benchmark in combination with a DEM of 0.25 m, were evaluated for their computational times. In average, for the evaluated test cases, the version 6.0 runs 25 % faster than the version 5.0.7. For the hydrograph at the catchment outlet and for the flooded area within the catchment there was no difference between the two software versions. For this reason, the main study was carried out using the current version of HEC-RAS 6.0.

3.4.2 Step 1—DEM vs. Mesh Resolution

Nash–Sutcliffe Efficiency (NSE)

        a) NSE_{outlet}

The NSE was selected as an index to compare the correspondence of the hydrograph at two locations in the catchment area with the high-resolution benchmark. The simulations with a grid resolution of 2 m show a very good agreement ($NSE_{outlet} \geq 0.98$) for all seven terrain models at the outlet of the catchment (**Figure 18**). There was no sensitivity with regard to the various terrain models. The runoff dynamics and the peak values ($Q_{max} = 4.24$ m³/s) of the seven model runs are almost identical with the benchmark run. The group of simulations, with a computational grid of 3 m, show very good agreement with the benchmark (NSE ≥ 0.92) as well. For this group of simulation it was found that the simulations with a DEM between 1 m and 4 m reproduce well the runoff dynamics of the catchment. It is better reproduced than for the very finely resolved DEM of 0.25 m and 0.5 m. The maximum runoff decreases and is in the order of 3.65 m³/s (4 m DEM) and 3.93 m³/s (2 m DEM). For the group of simulations with a computational grid of 4 m and 5 m, the values for NSE decrease in an order of magnitude of approx. 0.05. All simulations are above the value of NSE > 0.8, which can be regarded as good agreement for hydrological calculations. Furthermore, the simulations with a coarser DEM have slightly better values for NSE (0.87 for the 0.25 m DEM and 0.90 for the 5 m DEM with a 4 m calculation grid). For the simulations with a calculation grid coarser than 10 m, there is a clear decrease in the correspondence with the benchmark. The reason for this jump is also because that there is a larger jump from the 5 m to the 10 m calculation grid. Here, the hydrographs only have a correspondence of 0.62 for the 0.25 m terrain model and 0.66 for the 5 m terrain model. The same tendency can be seen for the calculation runs with a mesh resolution of 20 m and 30 m. For the simulations between 2 m and 5 m the NSE value decreases by approx. 0.05 for each model group when the calculation grid is increased by 1 m. For the simulations between 10 m and 30 m the NSE value decreases by approx. 0.25 for each model group when the calculation grid is increased by 10 m.
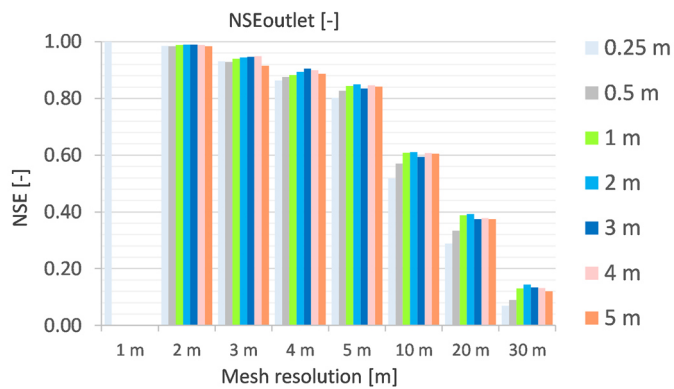
Figure 18: Overview of results of NSE (flow hydrograph) at the outlet of the catchment for the different mesh and DEM resolutions (DEM: colored legend).

A qualitative examination of the hydrographs (**Figure 19**) shows that the decrease of the NSE is mainly due to a delay and reduction in the peak runoff. All hydrographs tend to zero at 24 h of simulation time. From a hydrological point of view, the coarser computational grid results in a prolonged stay of the water in the catchment area. The finely resolved models have a concentration time and the maximum peak runoff at approx. 50 min, which is in good correspondence with the determined time of concentration. The models with a resolution of 30 m have a concentration time of approx. 2.3 h. The peak runoff is clearly flattened (maximum flow rate at approx. 0.7 m³/s) and reproduced with a time delay of more than one hour in comparison to the benchmark. The model thus shows a strong sensitivity in the reproduction of the hydrograph depending on the individual cell resolution. It can be generalized that cell resolutions larger than 10 m result in a significantly delayed and flattened hydrograph. This effect is caused by the changed model geometry and the resulting different detection of the terrain geometry. It cannot be traced back to different physical characteristics in the catchment.
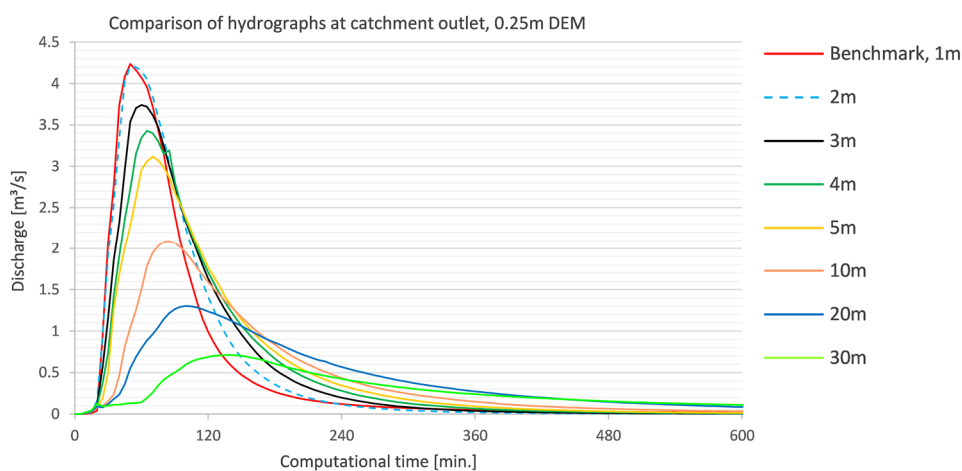
Figure 19: Overview of hydrographs at the outlet of the catchment for DEM 0.25 m and different mesh resolutions (mesh: colored legend).

b) NSE$_{village}$

For the control point in the village itself, there is the same tendency of the runoff dynamics as for the catchment outlet (**Figure 20**). The peak runoff is flattened for each coarser cell resolution by approx. 0.13 to 0.28 m³/s (**Figure 21**). At the same time, the time of concentration increases up to a maximum of approx. 1.8 h for the 30 m mesh resolution. This leads to a decrease of the NSE from 0.98–0.99 (DEM 0.25 m to 5 m, 2 m mesh resolution) to 0.80–0.85 (DEM 0.25 m to 5 m, 5 m mesh resolution). For the coarser resolutions of 10 m to 30 m, the lowest values of NSE are determined in a range of NSE from 0.67 (10 m mesh, 3 m DEM) to the lowest value of 0.3 (30 m mesh, 0.25 m DEM). In summary, it can be said that the runoff dynamics up to a cell resolution of 5 m is in a comparable range with the benchmark (NSE > 0.8).
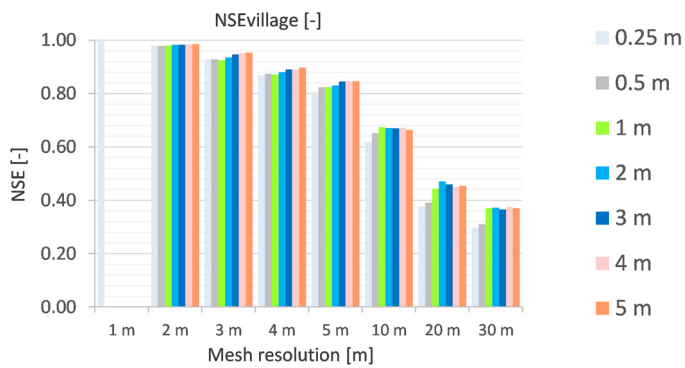
Figure 20: Overview of results of NSE (flow hydrograph) at the control point in the village for the different mesh and DEM resolutions (DEM: colored legend).
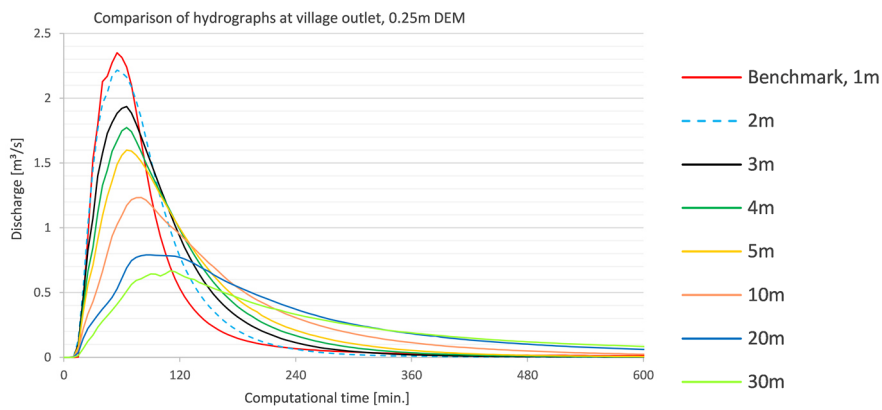
Figure 21: Overview of hydrographs at the control point in the village for DEM 0.25 m and different mesh resolutions (mesh: colored legend).

Difference in Maximum Water-Surface Elevation (ΔWSE)

a) ΔWSE$_{stream}$

The deviations of the maximum water level at the control point in the stream are in a very low range up to a mesh resolution of 5 m (**Figure 22**). For the group of simulations with a DEM between 0.25 m and 4 m, they are each at 0 m. For the terrain model of 5 m, the water level

deviates from the benchmark by 0.03 m up to a cell resolution of 5 m. For the coarser cell resolutions of 10 to 30 m, the deviations of the maximum water level increase from 0.1 (10 m mesh) up to 0.6 m (30 m mesh) and the respective flooded areas can no longer be seen comparable with the reference run. The total water depth is at 0.43 m at this location. In summary, it can be said that up to a mesh resolution of 5 m and up to a DEM of 4 m, very good results are obtained with regard to the comparison of the maximum water levels. A mesh resolution of 10 m provides comparable results up to a terrain model of 0.5 m. With a cell resolution of 20 m or 30 m, the deviations are over 100 % of the total water depth and the mesh resolution is seen as too coarse for a catchment area of this size and type.
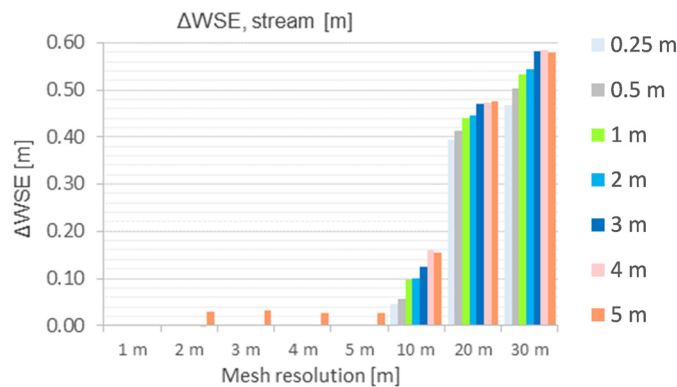
Figure 22: Overview of results of ΔWSE at the control point in the stream for the different mesh and DEM resolutions (DEM: colored legend).

b) ΔWSE_{road}

For the deviation of the maximum water levels at the control point within the village itself, all values for the fine mesh resolutions are in a value range between 0.003 m (0.25 m DEM) to 0.037 m (2 m DEM) with a maximum water depth of 0.10 m for the benchmark (**Figure 23**). Even for the coarser mesh resolutions between 3 and 5 m, there are overall slight deviations in the water level compared to the benchmark of 0.03 m. From a cell resolution of 5 m with a 5 m terrain model and a coarser cell resolution of 10 to 30 m, the deviation increases to up to 0.66 m (10 m mesh, 1 m DEM), which indicates a lack of model performance for the benchmark at a maximum water depth of 0.10 m. In summary, it can be said that the deviations in water level on the street in the locality, as a percentage of the total water depth, are in a significantly higher order of magnitude and fluctuate more strongly than in the water course itself.
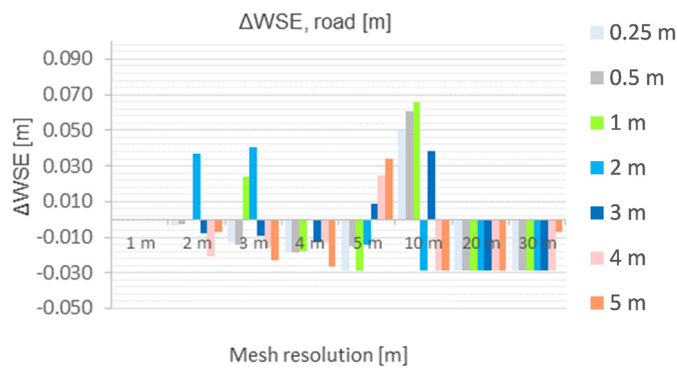
Figure 23: Overview of results of ΔWSE at the control point on the road for the different mesh and DEM resolutions (DEM: colored legend).

Flooded Area (F2)

The pixel-based indicator F^2 compares the flooded area with the benchmark run. Generally, the correspondence of the flooded area is relatively poor for all simulation runs (**Figure 24**). In addition, also the model runs with fine meshing have low correspondence in a range between 0.3 and 0.5 ('1' stands for the identical flood plains as the benchmark). Furthermore, for a grid resolution between 2 m and 5 m there is a clear decrease in the correspondence of the floodplain areas. The best match with the benchmark run is $F^2 = 0.55$ for the model with a cell resolution of 2 m and a terrain model of 0.25 m.
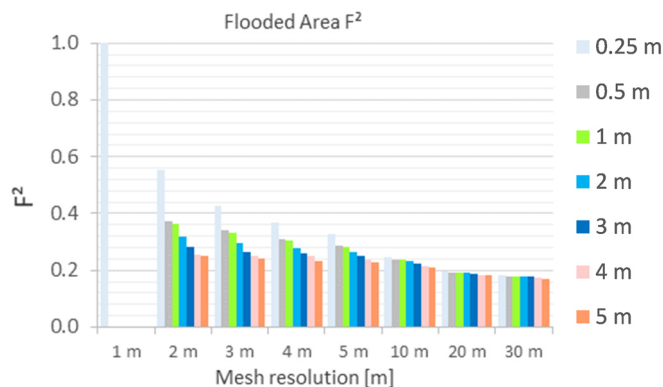
Figure 24: Overview of results of flooded area F^2 for the different mesh and DEM resolutions (DEM: colored legend).

A more qualitative look at the floodplains itself, **Figure 25** for 0.25 m DEM and **Figure 26** for 1 m DEM, provides further information. By this, the reason for the large deviations from the benchmark are identified. It is clarified that a basic comparability between the models is still given. Despite the large deviation from the benchmark, the general flooded areas match well. The differences are mainly because the benchmark run can finely resolve a multitude of microsinks. This recording of microsinks with shallow water depths decreases sharply from 5 m. At 30 m mesh resolution, the wet areas are no longer represented (compare **Figure 26, d**).
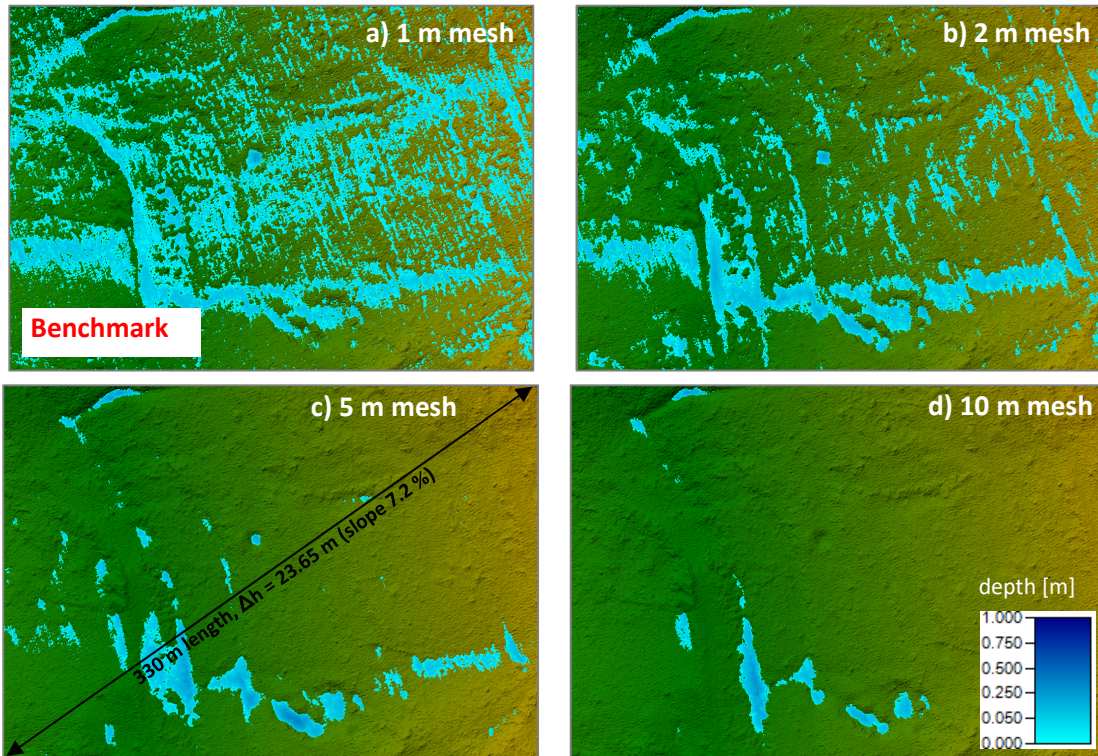
Figure 25: Qualitative comparison of flooded area (max. flood depth during overall simulation time) for four different mesh resolution (a): 1 m, (b): 2 m, (c): 5 m, (d): 10 m and 0.25 m DEM.
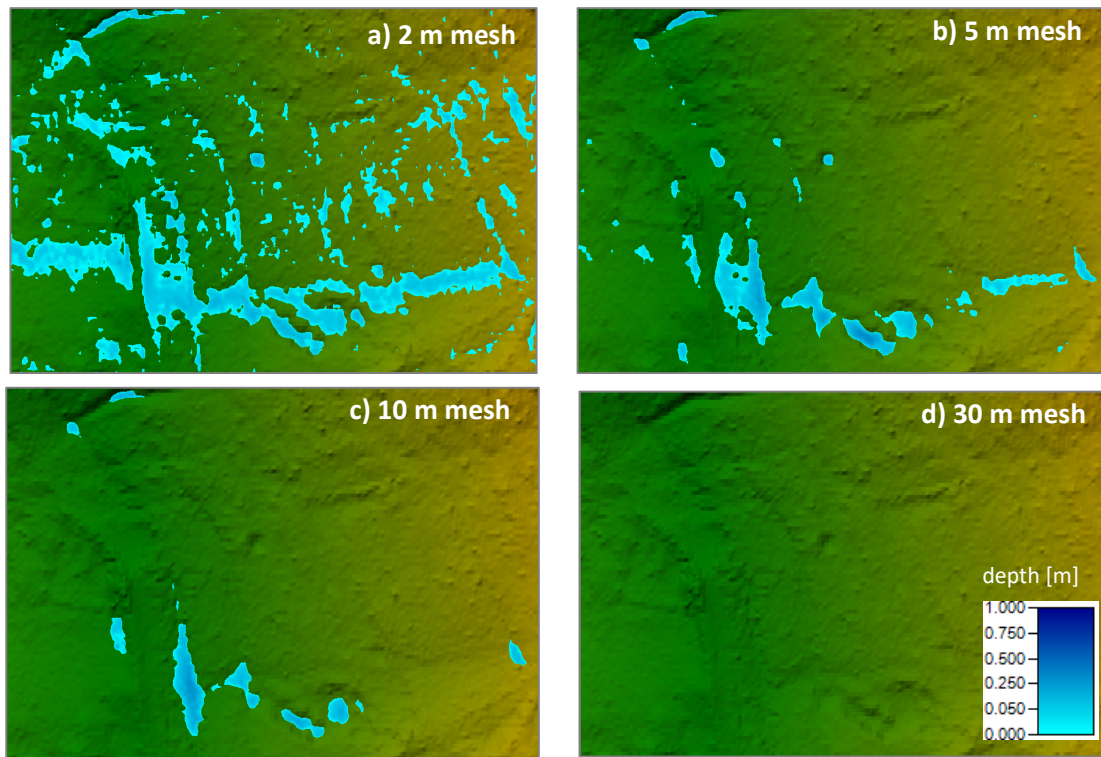
Figure 26: Qualitative comparison of Flooded area (max. flood depth during overall simulation time) for four different mesh resolution (a: 2 m, b: 5 m, c: 10 m, d: 30 m) and 1 m DEM

In summary, the pixel-by-pixel comparison of wet cells using F^2 also includes differences of very shallow water depths in individual cells. Most of the cells have water depths lower than 5 cm, which is a great requirement of accuracy for the surface runoff model. In areas of larger sinks or the course of the river itself, there is a fundamental correspondence with the benchmark run-up to a cell resolution of 5 m. The main reason for the large deviation F^2 is due to the large number of flooded individual cells in the benchmark itself. In addition, there is an increase in the deviation of the floodplain areas around the buildings. Since the buildings were inserted into the terrain model as block elements with a height of 5 m, interpolation is made in the model between the wet cells on the building itself and the closest cells close to the ground. This leads to artificial moats around the building, the size of which depends on the cell size. Therefore, the informative value of F^2 is only possible if the cause of the deviation and the comparison of the actual flood areas are taken into account.

Volume Deficit (VD)

For the majority of the simulations, the volume deficit has a low value—below 2 %, which corresponds to approximately 450 m³ water volume (**Figure 27**). This is held back in the catchment area because the volume control for all simulations is maintained (compare results for the volume balance VB). The benchmark run with the very fine resolution of the terrain model and the coarsest mesh resolution of 30 m calculation grid (approx. 6.4 %, 1380 m³) have the highest retention volume in the catchment area. Furthermore, with the same mesh resolution, the finer terrain models have a larger proportion of water that remains in the catchment area than the coarser terrain models. The evaluation of the results show that a consideration of the characteristic values alone is not meaningful, as they do not provide any information about how and where the water is held back in the area.
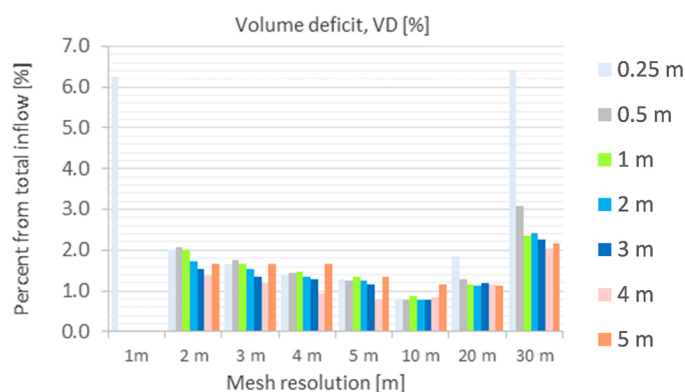
Figure 27: Overview of results of VD for the different mesh and DEM resolutions (DEM: colored legend).

A qualitative analysis of the water levels that did not leave the catchment during the simulation period shows that the way in which the volume is distributed in the catchment area is very different for the individual mesh resolutions. For the finest mesh resolution in combination with the 0.25 m DEM, there are numerous microsinks distributed over the entire catchment (compare **Figure a–d** in **Figure 28**).
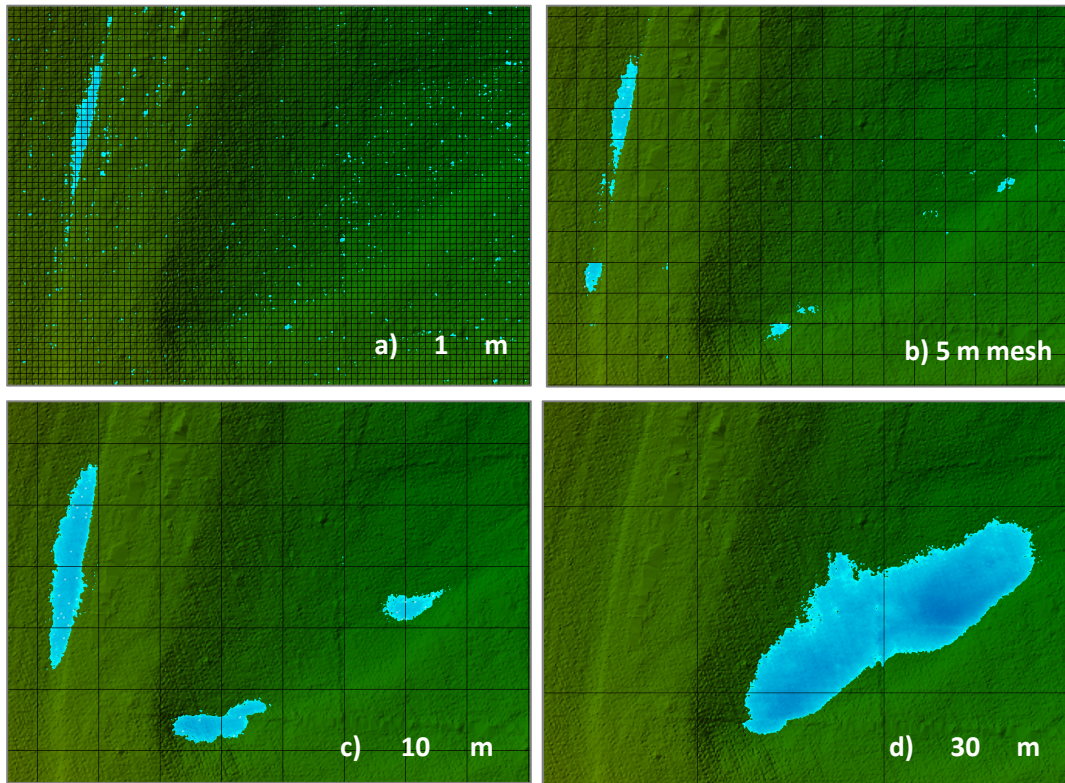
Figure 28: Remaining water in microrelief (a): 1 m, (b): 5 m mesh of the 0.25 m DEM and shallow artificial sinks (c): 10 m, (d): 30 m mesh at the end of the simulation time.

It can be said that the computational grid captures the microrelief of the fine terrain model very well. With the coarser computational grids (approx. from 10 m mesh resolution) instead larger, local sinks are formed which store the drainage volume and only release it with a considerable delay or not at all. These coarser sinks are artificially created by the computational grid and cannot be identified visually or computationally with the tool 'fill sinks' from ArcGIS (results in **Figure 29 a–d**). The effect of the artificially created sinks on the flat surface can be explained by the different capturing of the terrain geometry by the coarse grid. The water in a grid cell can only leave the cell via the cell edge. With a fine grid resolution, there is a larger number of flow paths than for the depressions generated in the coarse model, through which the water can flow to the next lower point. In the case of a coarse resolution, it happens that the randomly placed cell edges show slightly higher terrain topographies than the area of the cell itself. Due to the very shallow water depths, a height of 5–10 cm means that a water volume of 45–90 m³ is trapped in a cell of 30 m resolution. Thereby, a coarse computational grid in combination with a fine resolution of the terrain model creates artificial depressions in the terrain.
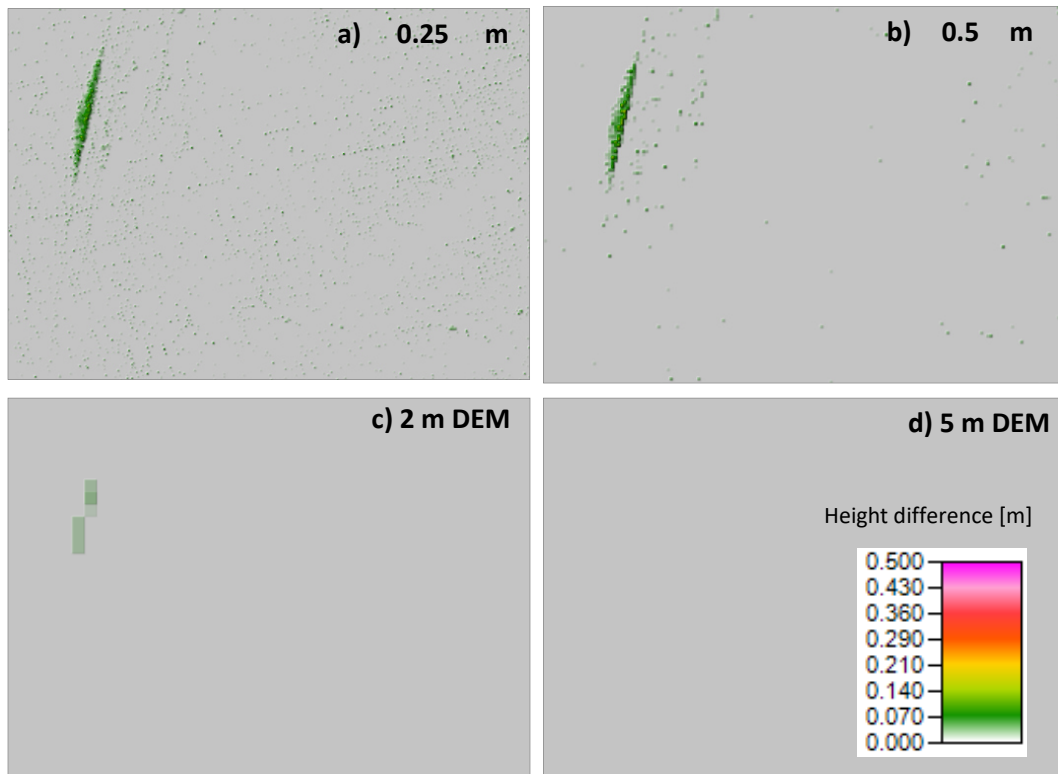
Figure 29: Identified sinks for DEM with (a): 0.25 m, (b): 0.5 m, (c): 2 m and (d): 5 m spatial resolution.

Figure 28 and **Figure 29** illustrate the effects that occurred during the flood event: (a) simulations with very fine and coarse computational grids have an increased volume deficit and (b) the volume deficit for the finer compared to the coarser terrain model is higher. Furthermore, it can be seen in **Figure 28** that the larger the cells become, the more water is retained in artificial sinks at the end of the simulation time. For the 1 m computational grid, the water volume is held back in actually existing and many small microsinks. Whereas for the 10 m grid, there is a concentration of water in three and for the 30 m computational grid in only one large sink. These sinks cannot be identified by the substraction of a filled with an unfilled DEM in **Figure 29** shows the difference between the filled sinks and the unfilled terrain model for the same section as shown in **Figure 28**. This evaluation shows where the actual sinks are in the selected area. It can be seen that the many small microsinks that existed in the 0.25 m DEM are lost due to the conversion to the coarser resolution. Therefore, the number of actually existing sinks and consequently the volume deficit for the coarser terrain models becomes smaller. The comparison with the results from **Figure 29** shows that the local runoff concentrations generated with the coarse computational grid do not correspond to the actual high and low points of the terrain. These effects are not known in the field of fluvial flood-hazard mapping, since the water levels are usually significantly higher in relation to the changes in elevation in the terrain. For high points in the terrain that are not recorded due to the coarse cell resolution, breaklines can be specifically inserted in the calculation grid.

For the catchment-based modeling, due to the effects mentioned, it is not recommended to combine cell resolutions coarser 10 m with a terrain model finer than 0.5 m. Furthermore, microsinks can be lost due to the coarsening of the terrain model. The volume deficit indicator is not sufficient for the comprehensive consideration of the results and a qualitative analysis of the water volumes remaining in the catchment area should be carried out.

Volume Balance (VB)

The volume balance (**Figure 30**) is maintained for all simulations. The indicator VB is independent of cell resolution and the DEM. No water loss occurs during the simulation.
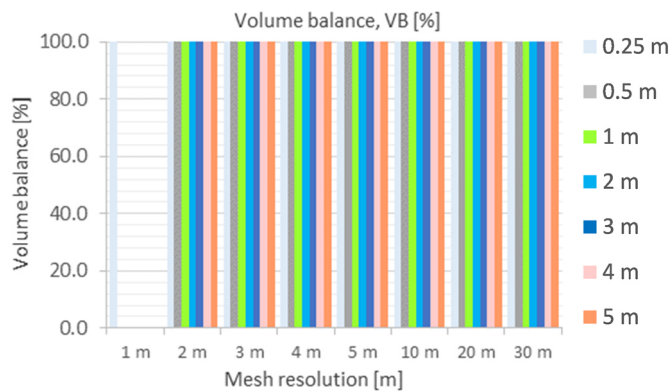
Figure 30: Overview of results of VB for the different mesh and DEM resolutions (DEM: colored legend).

Computational Time in Comparison to Real Time (CT)

The computational time (used hardware s. **Table 23**) increases exponentially with a finer cell resolution (**Figure 31**). The high-resolution benchmark run has the longest computational times with a value of 12.4 times longer than the simulation period of 24 h. This makes in total 297 h and is not feasible for a day-to-day modeling practice with limited hardware resources. The simulations with a mesh resolution of 2 m are over the simulation period of 24 h. This group of simulations shows that there is a clear increase in the simulation time when the cell resolution is finer than the terrain model. The computational time within the group of 2 m simulations is 1.2 times real time (1 m DEM) to 2.55 times the real time for the 5 m terrain model. Also for the group of simulations with a computation grid of 3 m, the computation time increases from 0.32 times real time (1 m DEM) to 0.7 (5 m DEM) within the terrain models. The simulations with the computational grid of 3 m are all below the simulation period. The group of simulations with a computing grid of 4 m has a computational time between 0.16 (1 m DEM) and 0.37 (5 m DEM) times the real time. For the group of simulations from 5 m to 30 m, the computational time decreases exponentially by a factor of $17.103 \, x^{-3.308}$ ($R^2 = 0.99$) if the mean values of the individual cell resolutions are used as a basis.
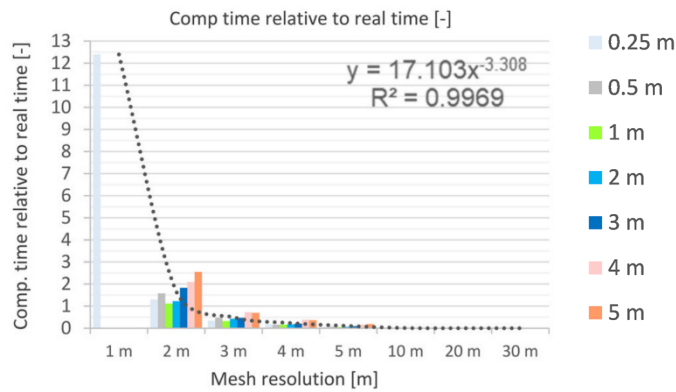
Figure 31: Overview of results of computational time CT for the different mesh and DEM resolutions (DEM: colored legend).

In summary, it can be said that the trade-off between accuracy requirements and cell resolution has limits with regard to the cell resolution. A cell resolution of 3 m that can be implemented in practice is determined for this catchment. Due to comparability between model runs, no calculations were performed with local refinements of the computational grid. This adjustment can be made for larger catchment areas.

3.4.3 Criteria for the Selection of Suitable Model Configurations

In order to reduce the number of simulations and thus the computational time for the parameter-based sensitivity analysis, unsuitable simulations were removed from the first part of the investigation (compare Step 1, C in **Figure 10**). This is done using established criteria for the 'goodness of fit' parameters examined. All quality parameters were set in such a way that they contain an acceptable deviation from the benchmark run and that simulations are still left for further investigation. This resulted in:

- $NSE_{village/outlet} = 0.8$,
- $\Delta WSE_{road} = 0.03$ cm,
- $\Delta WSE_{stream} = 0.05$ cm,
- VD = 5%, VB = 95 %,
- CT = 1

For the floodplain area F^2, the criterion had to be reduced due to the poor agreement with the benchmark. Since the qualitative evaluation showed that there is agreement of the inundation areas up to a resolution of 5 m and 1 m DEM, $F^2 = 0.28$ was set. This corresponds to the top third of the simulations with the best agreement with the benchmark. Based on the criteria introduced, the following model configurations were selected for further investigation:

- 3 m mesh with 0.25 m, 0.5 m, 1 m terrain model,
- 4 m mesh with 0.25 m, 0.5 m, 1 m terrain model,
- 5 m mesh with 0.25 m, 0.5 m, 1 m terrain model.

3.4.4 Step 2 - Further Parameter Sensitivity

Laminar Depth

For the laminar flow depth, the calculation was carried out with the standard settings from Step 1 (model default value = 0.06 m) with three additional values of 0.04 m, 0.06 m and 0.1 m. The laminar flow depth was so changed in 2 cm intervals. A qualitative comparison of the resulting hydrographs at the outlet of the catchment is shown in **Figure 32**.

Figure 32: Qualitative comparison of the hydrographs and model sensitivity for laminar depth at the catchment outlet for 3 m mesh and 0.5 m DEM.

The model sensitivity was determined with regard to the maximum outflow at the catchment outlet (S-Qmax, **Figure 33**), the volume deficit within the model region (S-VD, **Figure 34**) and the deviation of the flooded area (S-F2, **Figure 35**) with the respective initial run with corresponding spatial resolution. It is shown that the height of the laminar flow depth can be viewed as weakly sensitive for the parameter maximum outflow (**Figure 33**). The elasticity ratio for the total mean values is in the order of e = 0.32. By reducing the laminar flow depth by 2 cm, the flow peak is reduced by approx. 0.4 m³/s and increasing the laminar flow depth by 2 cm it is increased by approx. 0.4 m³/s. This corresponds to an average of 10–15 %.
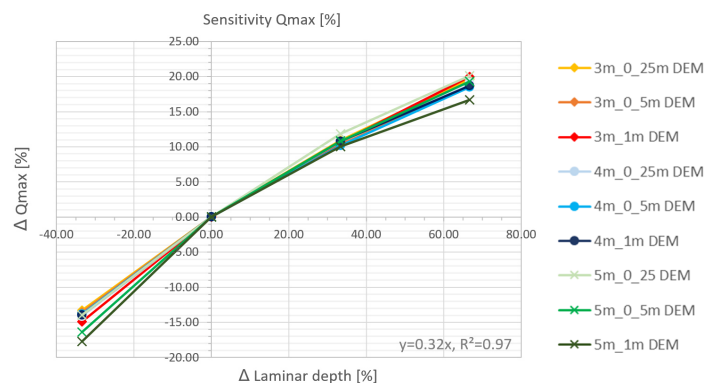
Figure 33: Comparison of the model sensitivity (S-Qmax) for laminar depth and the evaluated mesh and DEM resolutions with the averaged elasticity ratio e.

A change in the laminar flow depth has hardly any effect on the volume deficit (**Figure 34**). The elasticity ratio is only on the order of e = 0.08.
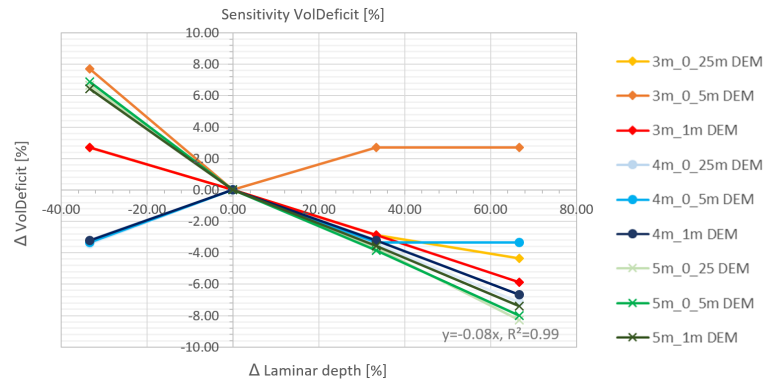
Figure 34: Comparison of the model sensitivity (S-VD) for laminar depth and the evaluated mesh and DEM resolutions with the averaged elasticity ratio e.

For the pixel-by-pixel comparison of the floodplain areas, the elasticity ratio is in the order of e = 0.13 to e = 0.21. The comparison between the model resolutions shows that the computational grids and terrain models have model sensitivities of a similar order of magnitude. Only a low sensitivity with regard to the spatial resolution is found here. The distributions can be described well with an approximation function (R2 S-Qmax = 0.97, R2 S-VD = 0.99) in order to describe the basic characteristics of the model behavior with regard to the change in the laminar flow depth in combination with the different spatial resolutions.
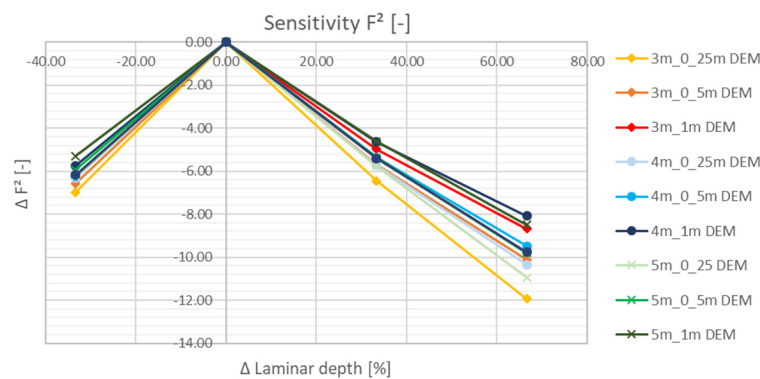
Figure 35: Comparison of the model sensitivity (S-F²) for laminar depth and the evaluated mesh and DEM resolutions.

In general, it can be summarized that the determination of the laminar flow depth for the model results must be given significantly more consideration than is currently the case. On the basis of a series of test runs in a runoff simulation flume, Grismer (2016) showed that the simulated thin-layer runoff resulted in laminar runoff. This coincides with the Reynolds numbers determined over a large area from David & Schmalz (2020) for simulated and calibrated storm events. The sensitivity analysis carried out has shown that the determination of the laminar flow depth in a value range of 4-10 cm has an influence on the model results. This agrees with the information from Grismer (2016) and recommendations from Oberle et al. (2021). The simulated thin-layer runoff needs to be adapted and checked in relation to the implemented roughness approaches and basic flow characteristics (Oberle et al., 2021).

Manning's n Roughness Values

The evaluation of the model's sensitivity with regard to the parameter, Manning's n, shows that an increase of the Manning's n values in the order of 10 % results in a reduction of the discharge peak of approx. 5–7 % (**Figure 36** and **Figure 37**).
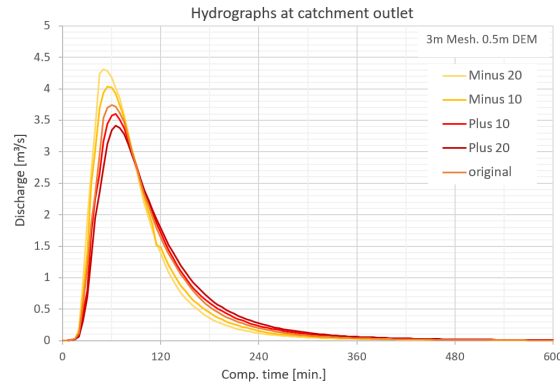
Figure 36: Qualitative comparison of the hydrographs and model sensitivity for Manning's n values at the catchment outlet for 3 m mesh and 0.5 m DEM.

A reduction of the surface roughness (increase of Manning's n values) by 20 % results in a reduction of the discharge peak by approx. 10–14 %, depending on the model resolution. A 10 % decrease in the Manning's n values increases the discharge peak by 6–8 %. A reduction in the Manning's n values of 20% results in an increase in the discharge peak between 14–20 %. Overall, the surface roughness can be viewed as sensitive in relation to the maximum flow. An elasticity ratio of 0.68 ($R^2 = 0.98$) is determined for the mean values of all simulations.
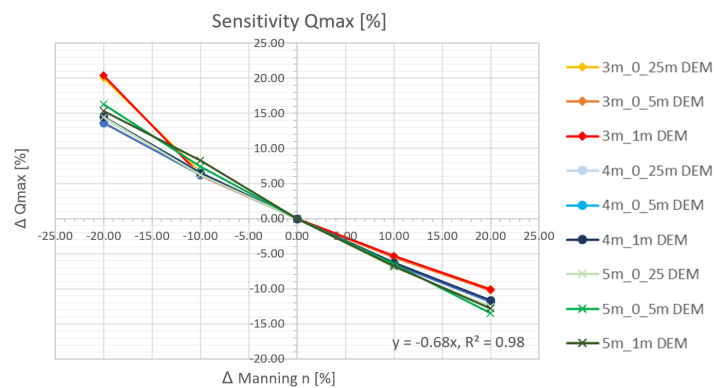
Figure 37: Comparison of the model sensitivity (S-Qmax) for Manning's n values and the evaluated mesh and DEM resolutions with the averaged elasticity ratio e.

With regard to the volume deficit S-VD (**Figure 38**), it is shown that there is a significantly lower sensitivity (e = 0.12). A reduction in the roughness values results in a reduction in the volume deficit, as the water can flow away faster. Conversely, an increase in surface roughness leads to slower drainage and thus greater amounts of water remaining in the catchment area after the simulation has been completed.
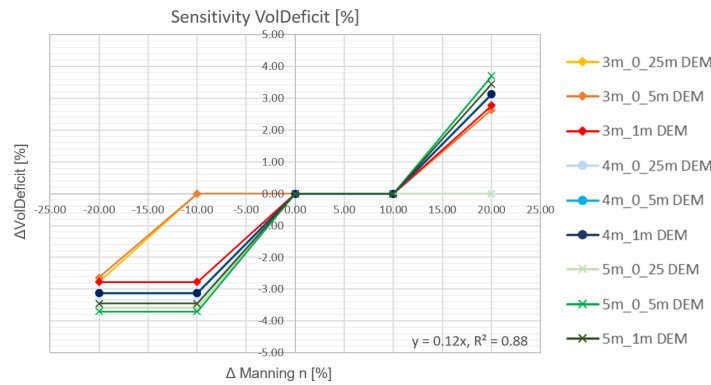
Figure 38: Comparison of the model sensitivity (S-VD) for Manning's n values and the evaluated mesh and DEM resolutions with the averaged elasticity ratio e.

The evaluation also showed that the influence of the change in roughness values on the floodplain is rather small and is only in the order of magnitude of e = 0.15–0.2 (**Figure 39**). The evaluation showed that the influence of the roughness values on the model results of Qmax (**Figure 37**) is greatest. The actual roughness values should therefore be taken into account in the calibration process and in the subsequent uncertainty analysis. The influence for the model geometries with a 3 m computational grid is somewhat greater when the Manning's n values are reduced. Overall, however, there is no clear tendency for the three quality criteria with regard to differences in terms of the various spatial resolutions.
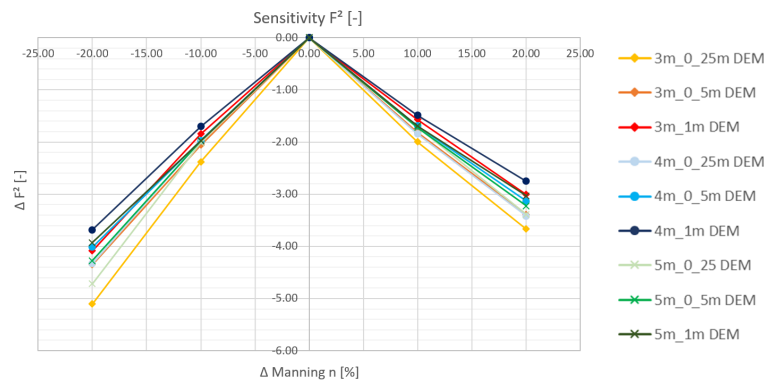
Figure 39: Comparison of the model sensitivity (S-F2) for Manning's n values and the evaluated mesh and DEM resolutions.

Since the model calibration often takes place on the basis of the roughness values, this and the implemented approaches must be taken into account. It is shown that in relation to the parameters examined here, roughness values have one of the greatest influences on the model results. The correct selection of the roughness values cannot be considered separately from the flow characteristics (laminar/turbulent) and the implemented surface roughness equation. Therefore, a further review and discussion of the adaption or general applicability of the Manning's equation is recommended in Grismer (2016) or Oberle et al. (2021). The results of the sensitivity analysis in this study only relate to the current loss approach, which is implemented in the model calculation routine.

Filter Settings

The evaluation of the model behavior for the three different configurations of the cell-based filter settings (ft) to take into account the level of detail of the subgrid shows that the model sensitivities are different for the different quality criteria. For the respective hydrographs, there are hardly any deviations from the standard values for ft = 0.003 m or ft = 0.0003 m (**Figure 40**).
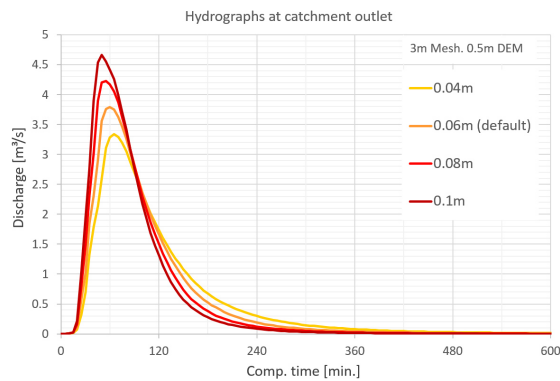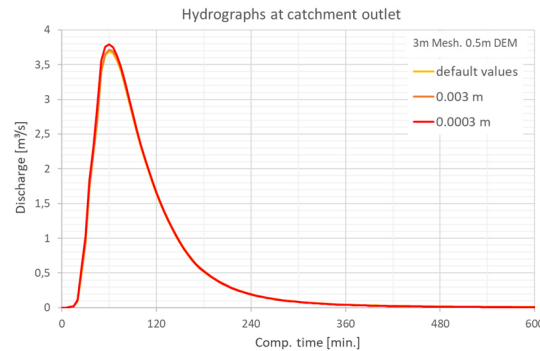

Figure 40: Qualitative comparison of the hydrographs and model sensitivity for the filter settings at the catchment outlet for 3 m mesh and 0.5 m DEM.

For the default settings, there is a reduction in the maximum discharge heights of between approx. 2–3 %. For ft = 0.003 m there is a reduction in the discharge heights of between 1–3 % which corresponds to an absolute value of a maximum of 0.1 m³/s and is classified as very low (**Figure 41**). In David & Schmalz (2020), a significant influence of the filter settings on the model results with regard to the volume deficit and corresponding reduction of the flow peak was found. There, however, the spatial resolution of the computational grid was about 30 m in the catchment area and 3 m along the stream, so that there may be a cell size dependency here. Therefore, the statement that these model settings are not significantly sensitive only applies to the model simulations of 3 m, 4 m, and 5 m computational grids performed in this study.
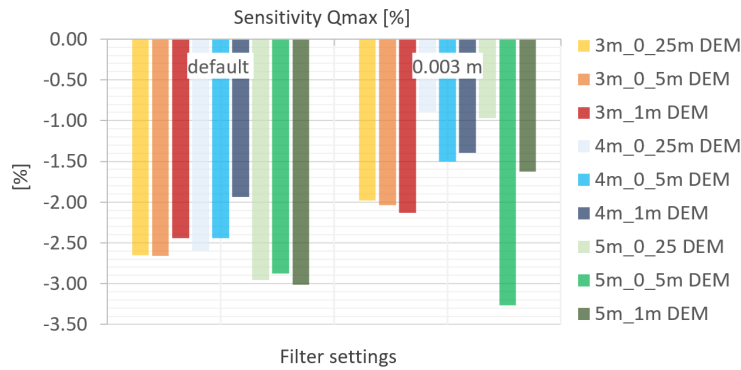
Figure 41: Comparison of the model sensitivity (S-Qmax) for the filter settings and the evaluated mesh and DEM resolutions.

With regard to the volume difference, this tendency can be identified as well when the values of the filter settings are reduced. For the standard settings, the volume deficit (S-VD, **Figure 42**) increases by an order of magnitude of 70–170 %, whereas for the settings with ft = 0.003 m it only increases by an order of magnitude of 30–40 %. The absolute value ranges for the volume deficit are then 2.9–3.0 % for the standard settings and approx. 1.8 % for ct = 0.003 m. This effect is significantly higher for the standard settings and the 5 m calculation grid with values between 140–170 % increase in volume deficit compared to the group of simulations with 3 m calculation grid. From these results, it can be seen that there is a dependency of the mesh resolution and the terrain model, which should be recorded in the process of calibration, especially with computational grids larger than 5 m resolution.
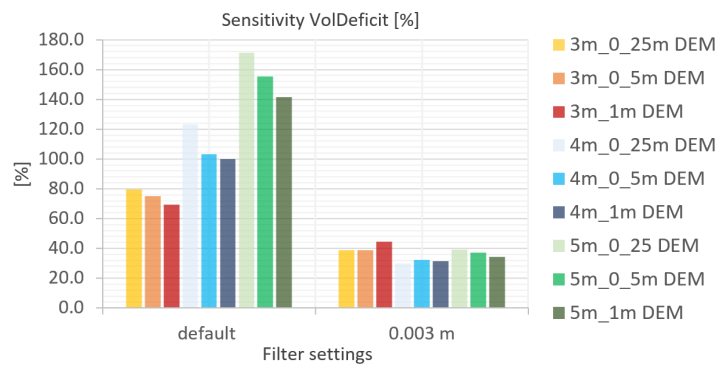
Figure 42: Comparison of the model sensitivity (S-VD) for the filter settings and the evaluated mesh and DEM resolutions.

With respect to the floodplains, there are only minor deviations from the respective comparison run in the order of magnitude of 1–1.5 %, which is the smallest change compared to the other sensitivity studies conducted (**Figure 43**).
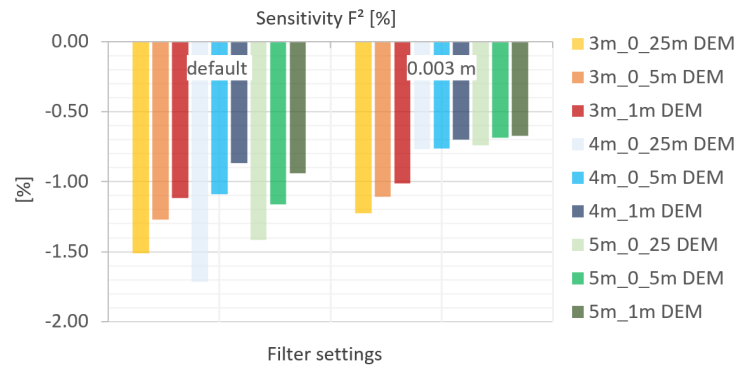
Figure 43: Comparison of the model sensitivity (S-F²) for the filter settings and the evaluated mesh and DEM resolutions.

Precipitation Input

The comparison of the model results of the four different precipitation input data shows that the highest runoff values (Qmax = 3.6–4.4 m³/s) occur for the precipitation event with the intensity peak at the end of the event. The outflow increases in an order of magnitude of up to 23 %, especially for the cells with a lower resolution of 3 m. At the same time, the time of peak is delayed by approx. 25 min (**Figure 44**).
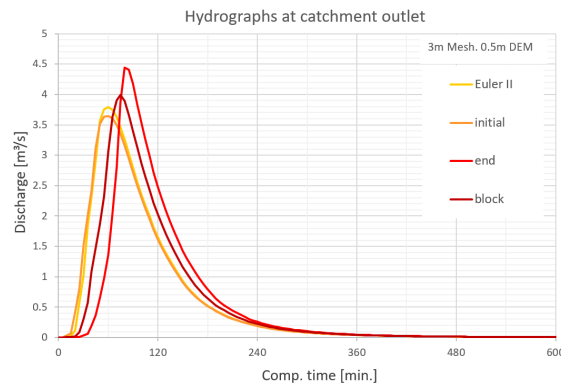
Figure 44: Qualitative comparison of the hydrographs and model sensitivity for the precipitation distribution at the catchment outlet for 3 m mesh and 0.5 m DEM.

With the coarser cell resolutions, the increase in the flood peak is only in an order of magnitude of 9–12 %. In this sense, it can be stated that the precipitation distribution has a greater influence on the finer grid. For the block precipitation event there is a slight delay of the flood peak by approx. 15 min. At the same time, the flood peak increases by 2–9 % for the various spatial resolutions, resulting in increased absolute peak flow of 3.37 to 4.0 m³/s (**Figure 45**).
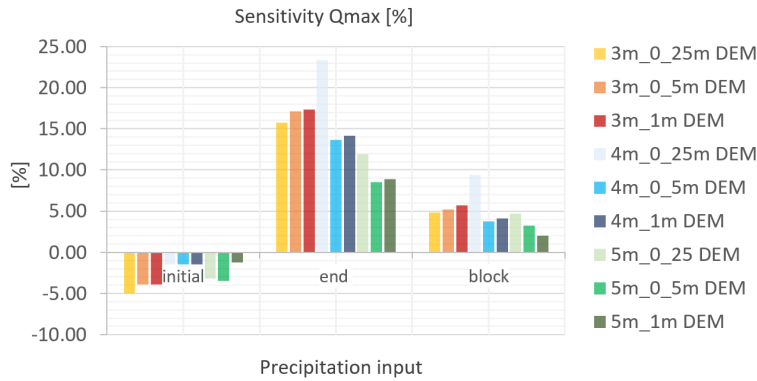
Figure 45: Comparison of the model sensitivity (S-Qmax) for the precipitation distribution and the evaluated mesh and DEM resolutions.

For the initial peak precipitation event, there is the least change in the resulting runoff hydrograph. The resulting peak flow changes by 1–5 %. The comparability is given since the initial peak precipitation event most closely corresponds to the Euler-II model rain. For the volume deficit, there are only minor deviations from the initial run and no systematic change with regard to the model sensitivity can be identified (**Figure 46**).
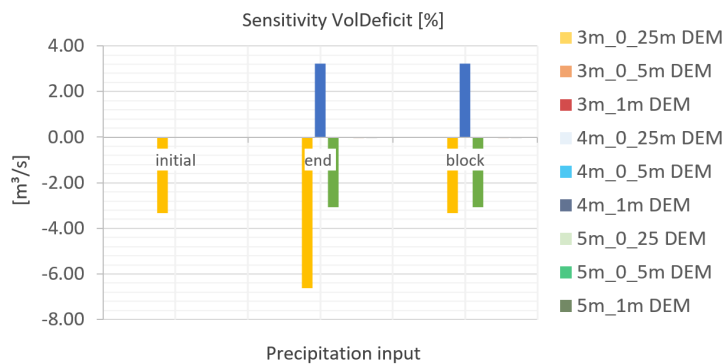
Figure 46: Comparison of the model sensitivity (S-VD) for the precipitation distribution and the evaluated mesh and DEM resolutions.

Three simulations have slightly larger deviations. However, since these are not systematic, they can be more related to the numerical calculation method rather than a systematic model response with respect to the precipitation input data. For F^2 similar effects can be recognized as for the change of maximum discharge (**Figure 47**). For the end peak rainfall event, the highest deviation to the initial run is recognized with a value between 5.5–7 %. For the block rainfall event there are deviations from 4–7 % recognized in comparison to the Euler II floodplains. For the initial distributed rainfall event, the deviations in F^2 are in the order of magnitude between 2.5–3.8 %. For all three rainfall events there is a slight dependency on the spatial resolution. It can be said that the finer the mesh and the DEM the higher the sensitivity is for the three evaluated rainfall distributions.
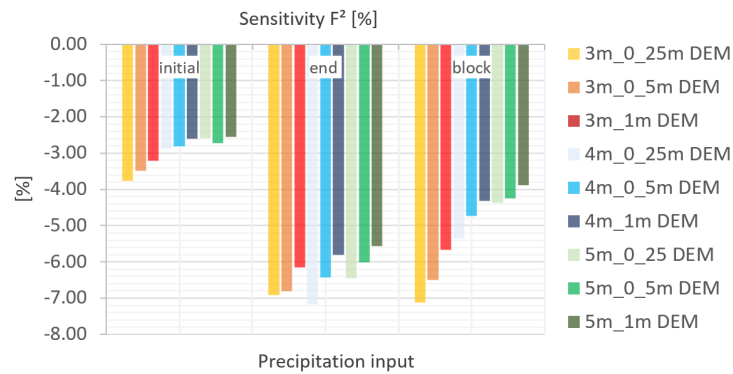
Figure 47: Comparison of the model sensitivity (S-F²) for the filter settings and the evaluated mesh and DEM resolutions.

In summary, it can be stated that the temporal distribution of precipitation has a relatively high influence on the model results with regard to the general runoff dynamics. The results of this study are in accordance with the BLUE hyetograph theory by Villani & Veneziano (1999) for linear basin response and low correlated space-time precipitation (Veneziano & Villani, 1999). In Veneziano & Villani (1999) the hyetograph is "the mirror image of the instantaneous unit hydrograph". This agrees also to the results founded in Krvavica & Rubini (2020). However, a closer comparison with the results from Krvavica & Rubini (2020) shows the duration dependency of the resulting hydrograph. For the hyetograph with 1 h duration, the Huff-Curve, an end based precipitation event has the largest flow rates. Whereas for the 6 h rainfall event the Euler II hyetograph has largest flow rates (Krvavica & Rubini , 2020).

3.4.5 Discussion of the Results in the Context of Rain-On-Grid Simulations

In the studies summarized in **Table 21** and **Table 22**, there are different combinations between the size of the catchment area and the spatial resolution chosen. The spatial discretization for all studies is summarized in **Figure 48**. The majority of the studies contains mesh resolutions in the order of magnitude of up to 5 m, which also corresponds to the spatial resolution (3 m, 4 m, 5 m) which is recommended in this study here. However, there is still a model difference, since HEC-RAS also takes into account the more finely resolved DEM through the subgrid. The recommended grid resolutions are highlighted in color in **Figure 48**. For the HEC-RAS applications the DEM resolutions vary between 0.5 m (HEC, 2018) and 10 m (Rangari et al., 2019). The coarser parametrization differs much from the recommended DEM resolution from 0.25 m to 1 m in this study. However, the spatial resolution of the DEM is also highly dependent on the available data in the study area. If a fine resolution as 0.25 m is used by the modeler, he need to take into account the microstorage effects, which are modeled in more detail. Further, it should be noted that the most commonly used and recommended mesh resolutions of finer than 5 m for storm hazard analysis are significantly different from the more studied area of flood modeling.
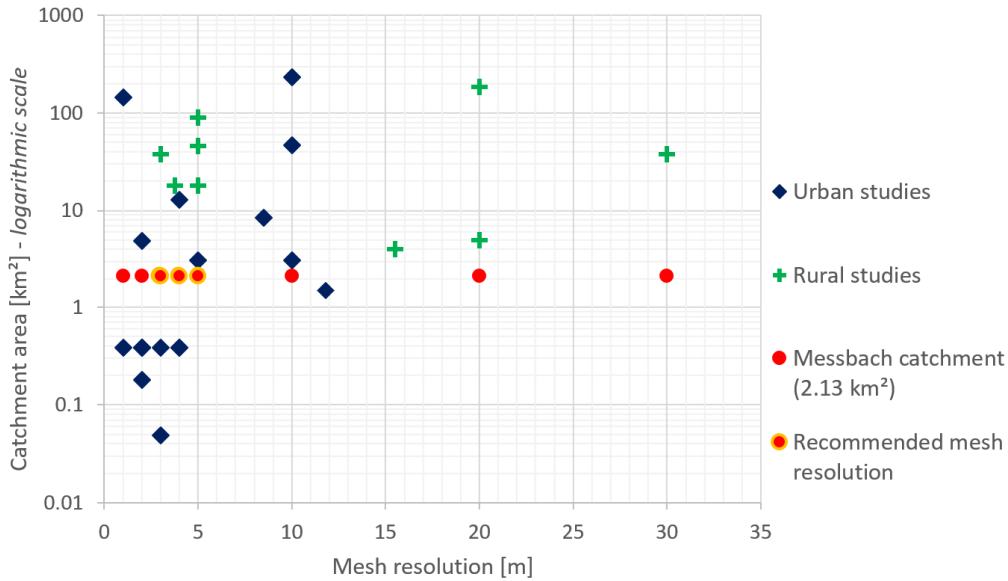
Figure 48: Spatial resolution and catchment size of the results of the literature review (summary of results of Table 21 and Table 22) and evaluated and recommended mesh resolution (orange outlined dot) for HEC-RAS in the Messbach catchment, 2.13 km²)

In Savage et al. (2016) it is detected for the model LISFLOOD-FP that the model results become high deviations to the finer discretization from mesh resolutions coarser than 50 m. This effect is caused by a poorer representation of the channel itself. The recommendation of such a coarse spatial discretization results from a study for large fluvial flood events. This shows that the correct choice of spatial discretization is not only "scale-dependent" on the size of the catchment, but also "use-dependent" on the type of flood to be modeled.

Only few studies investigated model sensitivity towards spatial discretization together with the application of rain-on-grid simulations. Clark et al. (2008) detected model sensitivity with regard to the spatial resolution for the 2d models TUFlow and SOBEK. It was found in Clark et al. (2008) that a coarser cell resolution resulted in a delay and reduction of the resulting hydrograph for the SOBEK model whereas TUFlow showed decreasing peak discharge rates for the finer mesh resolution. For both models and the coarser resolutions a reduction of the discharge volume at the end of the simulation time is determined. This is identical to the finding in this study here. In addition, the mesh-dependent increased time to peak is similar to what is detected here (compare **Figure 19** and **Figure 21**). Caviedes-Voullième et al. (2020) show varying results for the four evaluated spatial discretization. The results of the finest mesh of 1 m are significantly different from the coarse mesh resolutions of 2 m, 3 m and 4 m. While similar results for the models with 2 m, 3 m and 4 m mesh resolution are obtained, the overlapping flood distributions of the model with the finest mesh varies for the two solving algorithms. Here a dependency from the mesh resolution and the solver is detected, which Caviedes-Voullième et al. (2020) traces back to a "mesh-induced diffusivity or viscosity" and resulting "overestimation of friction forces in the SWE model". In HEC (2018) two different

spatial resolutions (2 m and 4m, 0.5 m DEM) are evaluated together with HEC-RAS in the Glasgow Test case. There are minor sensitives detected towards the change of spatial resolution. Four of the six presented Test Points show lower water surface elevations for the coarser mesh resolution. This trend is confirmed in this study. In Yu at al. (2015) very low sensitivities are determined for the total inundated area for the two evaluated spatial resolutions of 10 m and 20 m in combination with various roughness values. With the 10 m mesh the inundated area is likely smaller. For the relative indices as RMSE and the F statistics, a model sensitivity was determined. Here it was detected a combined sensitivity of mesh resolution and Manning's n values. In a more detailed sensitivity analysis for 5 m, 10 m, 50 m and 100 m DEM greater inundation is detected which confirms the statement of the "channel effect" of Ozdemir et al. (2013) for urban fluvial flooding and can also be detected in this study. Furthermore, it is recommended due to the spatiotemporal variability of the included hydrological processes (precipitation, infiltration, evapotranspiration) more attention should be given to the sensitivity of the spatiotemporal hydrological distribution of the hydrological processes. These are not considered in this study and need to be investigated in more detail in future studies.

3.4.6 Comparison with Determined Unit-Hydrograph

In the subcatchment-based rainfall-runoff models, the runoff formation within the catchment area for small catchments is often determined using storage-based approaches e.g., the concept of the Unit Hydrograph ('UH') (as referred in DWA (2008) and Chow et al. (1988)). In the data section (compare **Figure** 14 and **Figure** 15), a UH is applied to the Messbach catchment using the parallel storage cascade according to Wackermann (1981). This resulted in concentration times of k1 = 0.99 h for the fast cascade and k2 = 2.95 h for the slower cascade. In the first part of the study, however, the model results were not compared with the hydrograph from the determined UH, but with the finely resolved benchmark run. The main reason for this is that by the UH the fast, event-dependent interflow is mapped due to the two different storage coefficients. With the 2d hydrodynamic rainfall-runoff model only the surface runoff is taken into account. Here, the storage time within the catchment is produced by the surface roughness values. This results in two different model concepts taking into account different hydrological processes: (a) UH: surface runoff + event-based fast runoff = entire direct runoff (b) 2d hydrodynamic model: surface runoff. For this reason, the results were compared only with the results of the model with the same representation of hydrological processes. In addition, this study focuses on the effects of spatial resolution. However, due to the relatively high proportion of interflow in low mountains (Chifflard, 2016), it is also necessary to further investigate the influence of interflow and the effect on the calibration of Manning's n values on the model results.

3.5 Conclusions

The study has shown that a large number of simulations for sensitivity analyses are possible within the framework of 2d hydrodynamic surface runoff simulation by reducing the size of the catchment area and manually combining selected spatial resolutions. The influence of the mesh resolution in interaction with the resolution of the terrain model was investigated in detail. In the first part, model runs with spatial resolutions between 2 m and 30 m and terrain models between 0.25 m and 5 m were combined and evaluated based on various quality criteria. For this purpose, a high-resolution benchmark (1 m mesh, 0.25 m terrain model) was used for comparison. The model results showed strong sensitivity to spatial resolution on F^2 as well as to point-by-point evaluation at different control points in the catchment via the NSE. The main results of this study are presented below:

- For the coarser grids from 10 m mesh, the runoff is significantly delayed at the catchment outlet. The results showed that this effect is caused by a very low water layer that is computationally kept in the cells. The comparison with the benchmark run showed that comparable results were achieved up to a mesh resolution of 5 m and a terrain model up to 1 m (NSE $\geq$ 0.8).

- For the water levels in the channel, there is very good agreement (Δ WSE $\leq$ 0.03 m) with the benchmark run up to a spatial resolution of 5 m mesh.

- The area-based index F2 shows large deviations from the benchmark for all simulations. The study has made evident that deviations are sourcing mainly from a large number of microsinks in the 0.25 m DEM. The latter are mapped well using a 1 m mesh. The detailed display of microsinks reduces with increasing DEM and mesh resolutions.

- The study emphasized that the volume deficit as indicator was only partially meaningful. A qualitative analysis was additionally necessary to interpret the results adequately. It is shown that artificial depressions are detected for the mesh resolution coarser than 10 m. These are caused due to the very low water levels (<10 cm) in comparison to changes in topography.

- With regard to the computational time, model resolutions in the order of 3 m or higher are considered acceptable for a catchment area of this size (A = 2.13 km², CT < 1 and thus smaller than 24 h of computational time).

- The laminar flow depth is viewed as weakly sensitive with regard to the maximum discharge height. The roughness values are considered sensitive with respect to the discharge height. The filter settings show only a very low sensitivity for the calculated resolutions with respect to the runoff height and the floodplains. For the precipitation distributions, it is shown that the initially peak precipitation event has only a very small effect on the runoff height. For the 1 h-event, the end peak rainfall event results in the highest peak flow.

In summary, the study showed how a manual, systematic sensitivity analysis was performed with focus on spatial resolution. By the introduced methodology, valuable information for correct model parametrization and model sensitivities in the context of rain-on-grid simulations were obtained. Based on the results, clear recommendations for suitable spatial resolution and sensitive parameters for model calibration were made. The results obtained in this study are useful for daily engineering practice in conducting storm hazard analysis. Due to the limited extent of this study future studies were undertaken to evaluate: (i) the spatiotemporal model sensitivity towards hydrological processes as precipitation and runoff formation, (ii) the impact on model sensitivity towards catchment variability (size, slope), (iii) the model specific impact on the determined spatial effects, and (iv) a strategy to effectively consider the results of the sensitivity analysis in the framework of calibration.

4 Importance of Catchment Hydrological Processes and Calibration of Hydrological-Hydrodynamic Rainfall-Runoff Models in Small Rural Catchments

Abstract

In recent years, many two-dimensional (2d) hydrodynamic models have been extended to include the direct rainfall method (DRM). This allows their application as a hydrological-hydrodynamic model for the determination of floodplains in one model system. In previous studies on DRM, the role of catchment hydrological processes (CaHyPro) and its interaction with the calibration process was not investigated in detail. In the present, case-oriented study, the influence of the spatiotemporal distribution of the processes precipitation and runoff formation in combination with the 2d model HEC-RAS is investigated. In a further step, a conceptual approach for event-based interflow is integrated. The study is performed on the basis of a single storm event in a small rural catchment (low mountain range, 38 km²) in Hesse (Germany). The model results are evaluated against six quality criteria and compared to a simplified baseline model. Finally, the calibrated improved model is contrasted with a calibrated baseline model. The results show the enhancement of the model results due to the integration of the CaHyPro and highlight its interplay with the calibrated model parameters.

Keywords: Direct rainfall modeling ('DRM'), hydrological processes, radar data, calibration, 2d hydrodynamic modeling, runoff formation

4.1 Introduction

The rain-on-grid method, also known as Direct Rainfall Modeling ('DRM') has become the state of the art for storm hazard analysis in urban and rural catchments (Costabile et al., 2021; David & Schmalz, 2020; Cea & Rodriguez, 2016). In this method, a 2d hydrodynamic model is applied as a 2d hydrologic-hydrodynamic rainfall-runoff model ('HHDRRM'). The advantage of the modeling method is that hydrological processes are considered together with the hydrodynamic floodplain flow routing in one modeling system. The method can be applied to determine inundation areas caused by storm events within the entire catchment area (David & Schmalz, 2020). The size of the catchments, in which the DRM is applied, varies considerably. So does the spatial variability of the distribution of hydrological input parameters and the subsequent calibration routine. For catchments with predominantly agricultural or forestry land use, the catchment size varies from 4 km² (Cea & Bladé, 2015) to 185 km² (Hall, 2015). For catchments with more mixed and urban land use, the size varies even more from 0.049 km² (Fraga et al., 2016) to 232 km² (Zeiger & Hubbart, 2021). In David & Schmalz (2021), examples with applications of the rain-on-grid method were compared with focus on how the spatial discretization of the computational mesh and topography took place in the modeling process. A detailed sensitivity analyses was conducted in the study with focus on the interaction of computational mesh and underlying subgrid.

The integration of Catchment Hydrological Processes ('CaHyPro') has been established within the framework of spatially distributed hydrological modeling (Guse et al., 2019). There are different spatial scales in which hydrological modeling has evolved. The development went from the original lumped or subcatchment based modeling approach over the so-called semi-lumped models over HRUs to fully 2d distributed models (Guse et al., 2019). Meanwhile, in the field of hydrological modeling, a large number of applications exists for the spatially distributed representation of hydrological processes. Well-known modeling systems in the German-speaking area are, for example, RoGeR, WaSiM-ETH, NASIM or SWAT (Guse et al., 2019).

In the field of 2d hydrodynamic modeling, the DRM has evolved over the past decade due to increased computational power. The analysis of 20 applications with DRM by David & Schmalz (2021) showed that the integration and spatiotemporal resolution of CaHyPro using DRM varies considerably. Two of the studies use radar data as input data. Half of the studies use gauging station data, but only four studies consider spatially distributed rainfall data. In terms of runoff formation, seven studies use a method with spatially distributed runoff coefficients and nine use a spatially uniform runoff coefficient. In six of the studies, the temporal variation of the runoff coefficient during the event was integrated. None of the studies evaluates event-related fast interflow as component of the runoff hydrograph. The state of the art of the calibration of the DRM is summarized as the following. The fully integrated method implies that hydrological and hydrodynamic processes are modeled and calibrated in one modeling system together. Here, a parameter based calibration technique of the dominant processes and parameters (mostly roughness and infiltration values) takes place. Examples can be found in Fraga et al.

(2016), Yu & Coulthard (2015) and Jia et al. (2019). The method of effective rain-on-grid modeling instead implies that effective precipitation is set as input variable directly to the 2d model. The hydrological parameters, respectively the effective rainfall rates are determined externally via a separate modeling system or a simplified infiltration approach. Examples of this approach can be found in Hall (2015), Zeiger & Hubbart (2021) or David & Schmalz (2020). Here, the calibration takes place in two separate model systems.

The internationally used 2d hydrodynamic model HEC-RAS has the capability for rain-on-grid modeling with spatially homogeneous effective precipitation since 2016 (HEC, 2016a). With the version 6.0 (2021) there is the possibility of an integrated routine for runoff formation as well as spatially distributed rainfall (HEC, 2020).

If the rain-on-grid model does not take into account the spatiotemporal heterogeneity of CaHyPro processes that are not actually implemented in the modeling structure might be induced by the calibration of free model parameters of other processes. An example can be that precipitation volumes are adjusted by calibrating the parameters of the runoff formation routine (e.g. SCS-CN values). These parameters may not need to be calibrated if radar rainfall was used as input data. The process of subsurface stormflow or fast event-based interflow can be mentioned as another example. The process can contribute significantly to the runoff event (Weiler et al., 2005). The time to maximum discharge in the model is too short compared to the measured discharge curve. This can be related to the event-dependent interflow. If the process is not included in the model, the modeler might increase the surface roughness values to produce the delay in the runoff hydrograph.

To highlight this problem, the following study investigates the importance of CaHyPro and its interaction with the subsequent calibration routine together with the meanwhile widely used DRM. The question is how a stepwise integration of CaHyPro influences the model results and the final parametrization using the 2d hydrodynamic model HEC-RAS as HHDRRM.

4.2 Objectives

The objective of the study is to analyze the importance of different levels of spatiotemporal representation of CaHyPro with the application of DRM in a small rural catchment. In order to elaborate the respective effect of the integration of CaHyPro, a method should be developed that allows a step-by-step investigation. As a result, a résumé should be drawn on the importance of CaHyPro and its interaction with the calibration process in combination with the DRM. Besides the hydrological scientific investigation of the integration of CaHyPro, the study serves to gain experience with the new technical possibilities of HEC-RAS 6.0 (HEC, 2021). For this purpose, technical issues of the processing of radar data in the GIS should be addressed. A simplified approach for the calculation of storm-related interflow based on the parallel cascades of linear reservoirs is proposed. The summarized objectives are the following:

- To develop a methodology which allows a step-by-step investigation of the impact of the integration of CaHyPro and its interplay with the calibrated model parametrization together with the DRM in a small rural catchment.
- To integrate radar rainfall, spatially distributed process of runoff formation and a simplified, conceptual approach of interflow to HEC-RAS 6.0.
- To give a résumé on the impact of spatiotemporal resolution of CaHyPro, its interaction with the calibration process and the final model parametrization.

The study is conducted as a case study in the Fischbach catchment. The catchment is part of the field observatory of the Chair of Engineering Hydrology and Water Management (Fachgebiet Ingenieurhydrologie und Wasserbewirtschaftung – 'IHWB') from Technical University of Darmstadt (see details in David & Schmalz, 2021; Grosser & Schmalz, 2021; Scholand & Schmalz, 2021; Kissel & Schmalz, 2020; Schmalz & Kruse, 2019).

4.3 Materials and Methods

4.3.1 Project Area of Fischbach Catchment

The Fischbach catchment has a total area of 38 km² (**Figure 49**). It is part of the Gersprenz river system and is located in the Odenwald region of Hesse in Germany. 93 % of the catchment area is covered by a state gauge from which discharge is available since 1985 in a time interval of 15 minutes (HLNUG, 2020a). These are supplemented by water level observations with five minutes intervals since 2018 from IHWB (2020). Within the catchment area, a flood retention basin with a capacity of 220,000 m³ was built in the year 2016 (in operation since 2017). The elevations of the watershed range from 592 to 158 masl (mean 283 masl). A terrain model with a resolution of 1 m is provided from HVBG (2017b). The CORINE land cover ('CLC') (EEA, 2016) is available as land use data and supplemented by the local ATKIS landuse data set (Amtliches Topographisch-Kartographisches Informationssystem – 'ATKIS') (HVBG, 2017a). The catchment area is predominantly rural with 43.8 % agricultural and farmland, 46.3 % forest area and 9.6 % areas belonging to settlements including buildings and roads. As precipitation data, the two nearby precipitation stations of Modautal-Brandau-Kläranlage (HLNUG, 2020b) and Reinheim (DWD, 2022) are applied. For the respective model extensions, the radar data (RADOLAN-YW) from Winterrath et al. (2018b) with 5 min temporal and 1 km x 1 km spatial resolution is used. For soil data, the official soil map with a scale of 1:50,000 from HLNUG (2017) is taken. As there are no sewage treatment plants in the catchment area, no drainage system was integrated into the model.
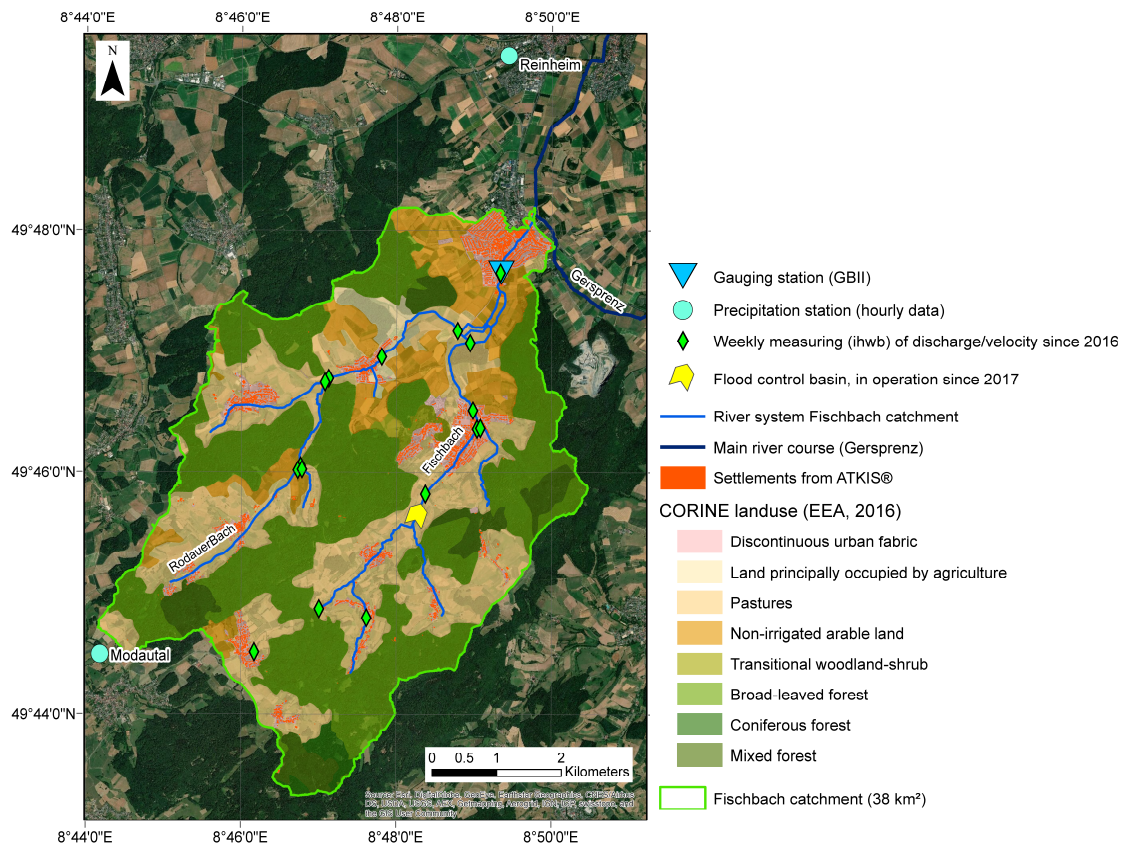
Figure 49: Project area of Fischbach catchment in Central Germany (38 km²)

4.3.2 Rainfall Event of April 23, 2018

The observed rainfall event occurred on April, 23 2018. The precipitation station of Modautal-Brandau-Kläranlage recorded a total precipitation sum of 29.2 mm from 3:00 p.m. to 4:00 p.m.. According to the official German storm hazard statistics of KOSTRA-2010R (DWD, 2017), this corresponds to a return period of four years. The precipitation station of Reinheim recorded a total height of 11.3 mm in the period between 2:00 p.m. to 4:00 p.m.. The radar precipitation data have maximum values of 52 mm in the period between 3:00 p.m. to 4:00 p.m.. At the gauge of Groß-Bieberau 2 ('GB2'), the observed discharge increased to a level of 12.5 m³/s. This corresponds to a return period of ten years (David & Schmalz, 2020). As a result of the event, flooding occurred on the slopes, on the forest trails and there was flooding of private buildings, bridges and roads (Bickelhaupt, 2018) (**Figure 50**).
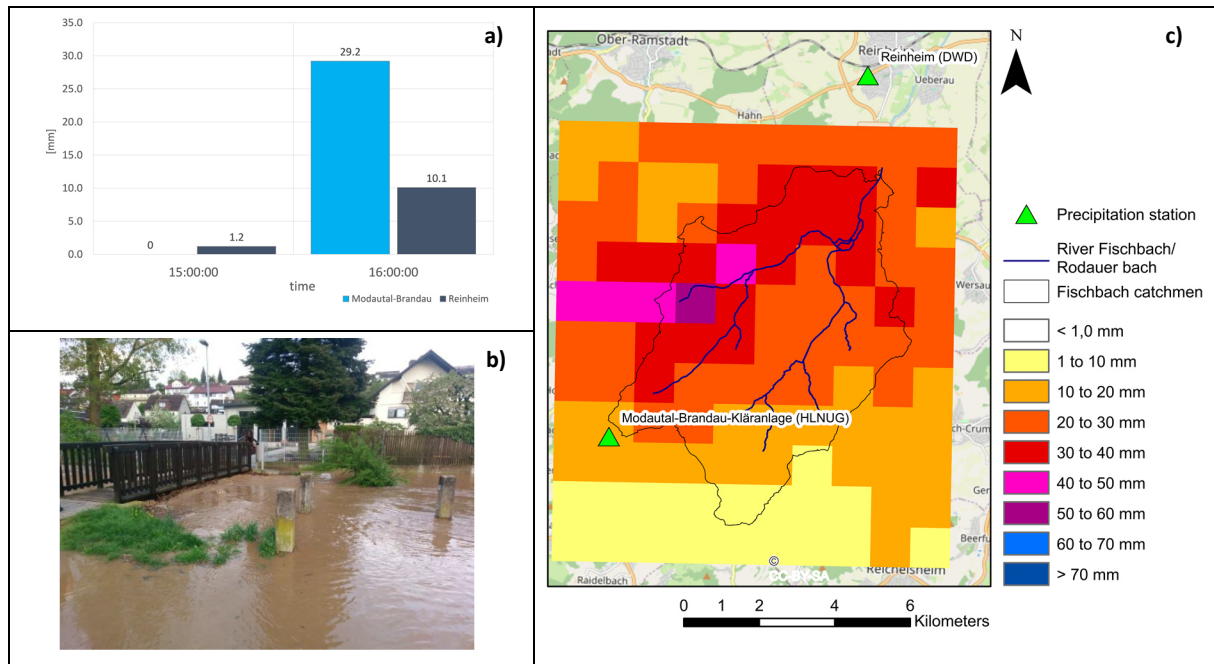
Figure 50: a) Recorded precipitation data at the precipitation stations of Modautal-Brandau-Kläranlage and Reinheim of the April 23, 2018, b) Flooded areas in the village of Groß-Bieberau (Fischbach) near the gauging station GB2, c) Recorded radar rainfall event from the April 23, 2018 with pixel-based accumulated rainfalls sums based on 1 km x 1 km DWD Radolan Raster (Winterrath et al., 2018a)

4.3.3 2d Hydrodynamic Model HEC-RAS

The 2d hydrodynamic model HEC-RAS is used as HHDRRM in this study. The free model was extended in 2016 with the model version 5.0 (HEC, 2016c) by the 2d hydrodynamic solution of the shallow water equations. Furthermore, the possibility of DRM was added to the model capabilities. In the year 2021 (HEC, 2021) with model version 6.0, the model was extended by spatially distributed precipitation input and three different loss methods. The model is used in numerous scientific publications worldwide. Examples on the use of HEC-RAS as HHDRRM can be found in Rangari et al. (2019), David & Schmalz (2020), Zeiger & Hubbart (2021) and Costabile et al. (2021). The technical details and mathematical principles of HEC-RAS are documented in the Technical Reference Manual (HEC, 2020).

4.3.4 Iterative Model Improvement via CaHyPro

The introduced method of Iterative Model Improvement via Catchment Hydrological Processes ('IMI-CaHyPro') carried out here involves the application of DRM together with HEC-RAS based on an observed storm event on April 23, 2018. A schematic overview of the method can be found in **Figure 51**. In the first part, a simplified model (*Baseline model*) is set up in HEC-RAS as a reference model. This contains a common model set-up with simplified implementation of CaHyPro. The model is calibrated using observed discharge time series available for the project area (HLNUG, 2020a). The calibration of the baseline model takes place as parameter based calibration via SCS-CN values [-] for the runoff formation and Manning's n values [s×m$^{-1/3}$] for the runoff concentration. In the second part, the hydrological processes of precipitation, runoff

formation and event-related interflow are iteratively improved and added to the HEC-RAS baseline model. The integration of CaHyPro takes place successively. The model improvement is conducted in HEC-RAS. In order to accurately study the effect of each added hydrologic process, they are added stepwise before the actual calibration is performed. The following model improvements were made:

1. Precipitation
   1.1. 1 h radar data
   1.2. 5 min radar data
2. Runoff formation
   2.1. Spatial SCS-CN values
   2.2. Spatiotemporal SCS-CN values
3. Interflow
   3.1. Catchment based
   3.2. Subcatchment based.

The improved model (*IMI-CaHyPro model*) is then calibrated using the parameters of runoff formation (SCS-CN values [-]), event-related interflow (storage coefficients k_2 [h]) and runoff concentration (Manning's n values [$s \times m^{-1/3}$]).

Subsequently, a) the model results of the uncalibrated baseline model and the modified model set-ups are compared, b) the influence of the approach of IMI-CaHyPro on model parametrization is discussed, and c) a general conclusion is drawn on the integration of CaHyPro in combination with the application of DRM.
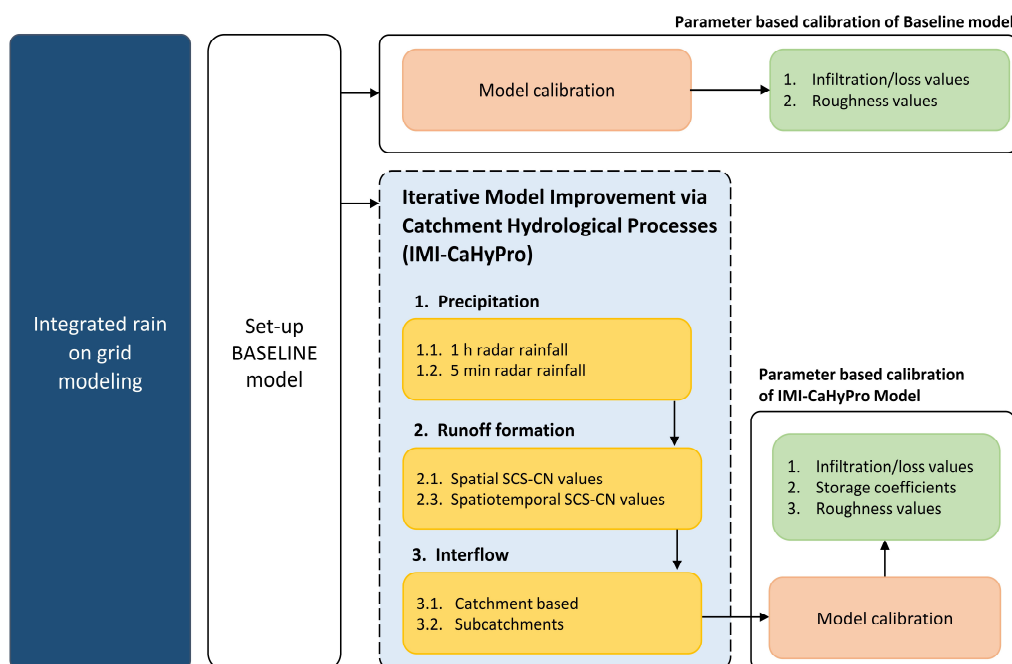
Figure 51: Overview of the Iterative Model Improvement via Catchment Hydrological Processes (IMI-CaHyPro)

In the following, the technical details of the baseline model and the stepwise model improvements for the processes of precipitation, runoff formation, and interflow processes of the IMI-CaHyPro approach will be explained.

4.3.5 Baseline Model

The model area (38 km²) is spatially discretized with a computational grid with 5 m resolution. According to David & Schmalz (2021) this corresponds to the coarsest recommended resolution for the application of DRM and is still acceptable with regard to the computational times. The underlying terrain geometry ('subgrid', according to Casulli (2009)) is defined with a resolution of 1 m. The river course is burned into the model domain using supplementary terrestrial cross-section surveys (David & Schmalz, 2020). The time step is set to 1 s for numerical solution of Diffusion Wave approximation and expected maximum velocities of 5 m/s in the catchment. By this time step selection the Courant criteria with CFL ≤ 1 is fulfilled. The selected time step is within the recommendations of Rangari et al. (2019) and David & Schmalz (2020) for applications of DRM together with HEC-RAS. The model area is assigned roughness values (Manning's n values) for surface runoff according to Downer & Ogden (2006) and for channel flow according to Patt & Jüpner (2013). SCS-CN values using the SCS method from USDA (1986) are assigned according to DVWK (1984) and USDA (1986, p. 55). For the model, a mean SCS-CN value is determined for the entire catchment area. Precipitation data from the two precipitation stations (**Figure 50**) with an hourly time interval are used. Interpolation between the stations is done using Thiessen polygons. The following **Figure 52** shows the total and effective input precipitation of the baseline model.
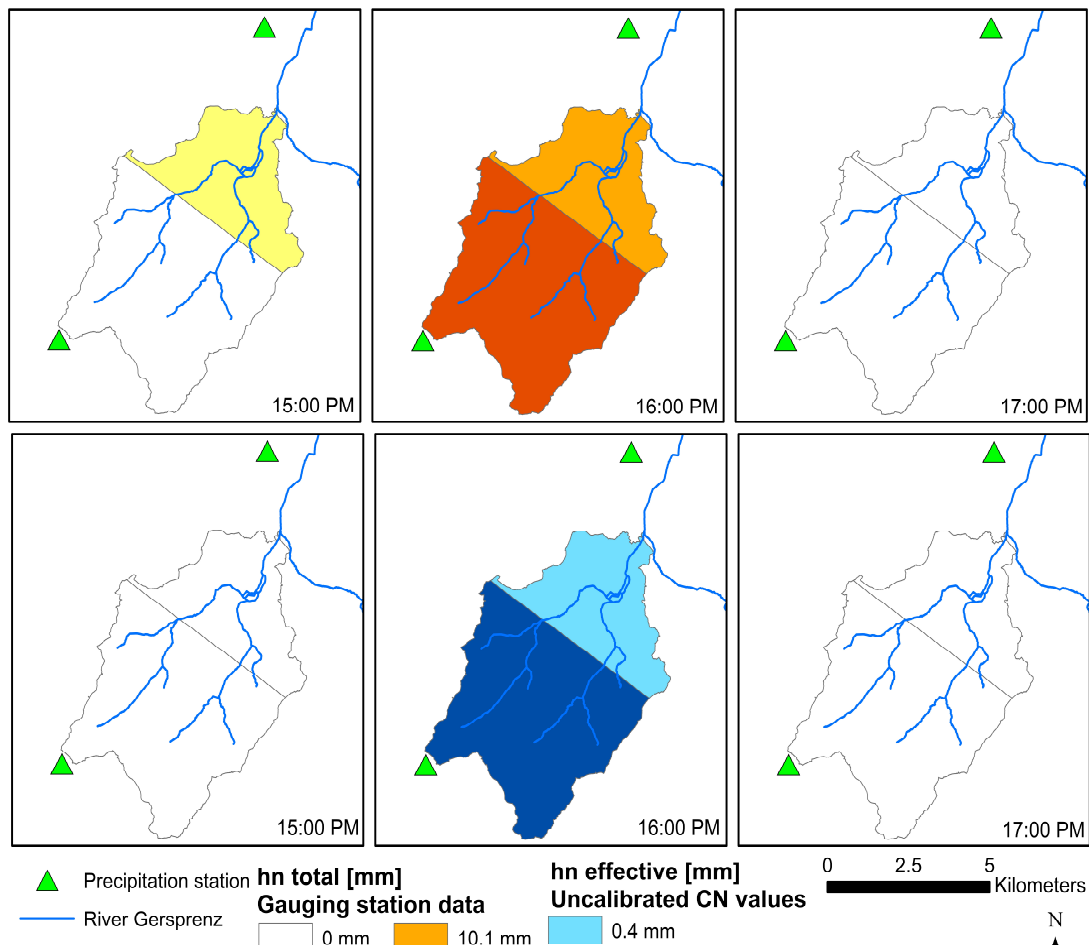
Figure 52: Precipitation input for April 23, 2018 of Baseline model with Thiessen-Polygons and averaged CN-value for total (above) and effective (below) precipitation

4.3.6 Technical Implementation of Iterative Model Improvement

4.3.6.1 Precipitation

One hour radar rainfall

As model extension (Precipitation I), precipitation is integrated to the model domain as spatially distributed precipitation data. For this purpose, the data set is integrated as a grid with an hourly resolution (**Figure 53a**). The five minutes radar data from Winterrath et al. (2018b) was aggregated to hourly input data to get time-consistent time-intervals as for the precipitation station data of the baseline model. The general preprocessing for the creation of the input data is performed using ArcGIS. The original data set is available for each time step as *.ascii-file for the whole of Germany in a polar stereographic coordinate system. This is first converted as *.tif-file and then projected into the project-related coordinate system (UTM) via GIS. The resulting data set is cut out with the model area and reconverted as *.ascii-file. The conversion tool ('asc2dss.exe') from HEC (HEC, 2017) is used to convert each *.ascii-file into a *.dss file. The *.dss file is imported into HEC-RAS as precipitation input data set. The technical details are presented in (HEC, 2017).

Five minutes radar rainfall

For the next model extension, five minutes radar rainfall time series from Winterrath et al. (2018b) are created as input data instead of hourly rainfall data (**Figure 53b**).
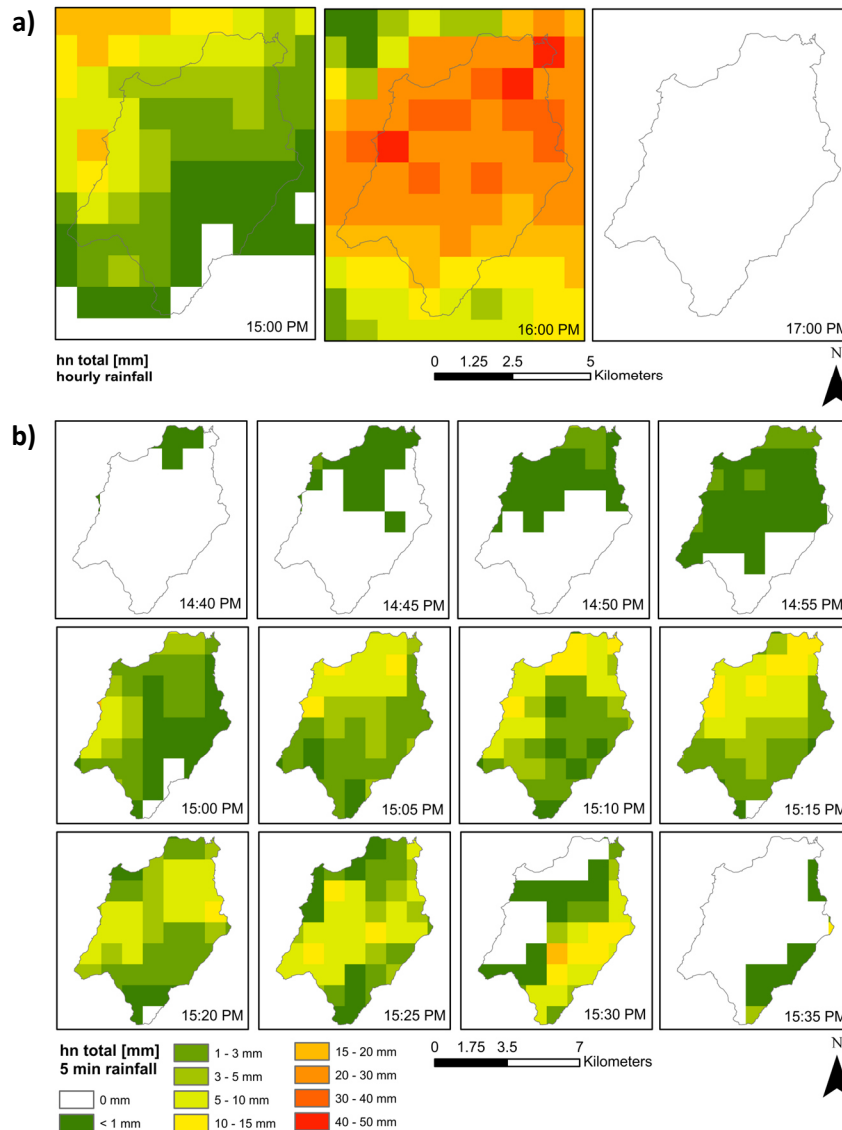
Figure 53: Gridded precipitation data: a) Hourly precipitation input for April 23, 2018 based on Winterrath et al. (2018a), b) Five minutes precipitation input for April 23, 2018 based on Winterrath et al. (2018b)

4.3.6.2   Runoff Formation

Spatial SCS-CN values

As further model extension, spatially distributed CN values were added to the model area. This results in a cell-by-cell calculation of runoff coefficients depending on the individual land use and soil classes (**Figure 54**). Time invariable runoff coefficients were calculated based on rainfall sums of each cell applying the widely used SCS-CN method (USDA, 1986, p. 55). The underlying equations are presented in **Eq. 15** - **Eq. 17**. The resulting effective precipitation rates in **Figure 55**.

$$h_{n,effective} = \frac{\left(h_{n,total} - I_a\right)^2}{\left(h_{n,total} - I_a\right) + S_{max}}$$ **Eq. 15**

$$S_{max} = \frac{25400}{CN} - 254$$ **Eq. 16**

$$I_a = a * S_{max}, \, a=0.05$$ **Eq. 17**

$h_{n,effective}$ – Effective precipitation height [mm]
$h_{n,total}$ – Total precipitation height [mm]
I_a – Initial abstraction [mm]
S_{max} – Potential maximum retention [mm]
a – Constant to determine initial abstraction; a=0.05 (DWA, 2008)
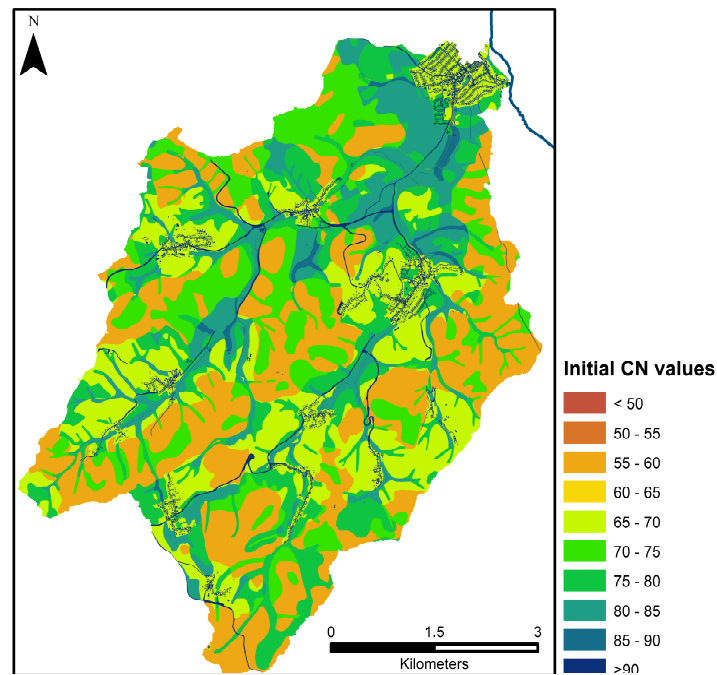
Figure 54: Spatially distributed CN-values based on the different soil (HLNUG, 2017a) and landuse (EEA, 2016), (HVBG, 2017a) categories
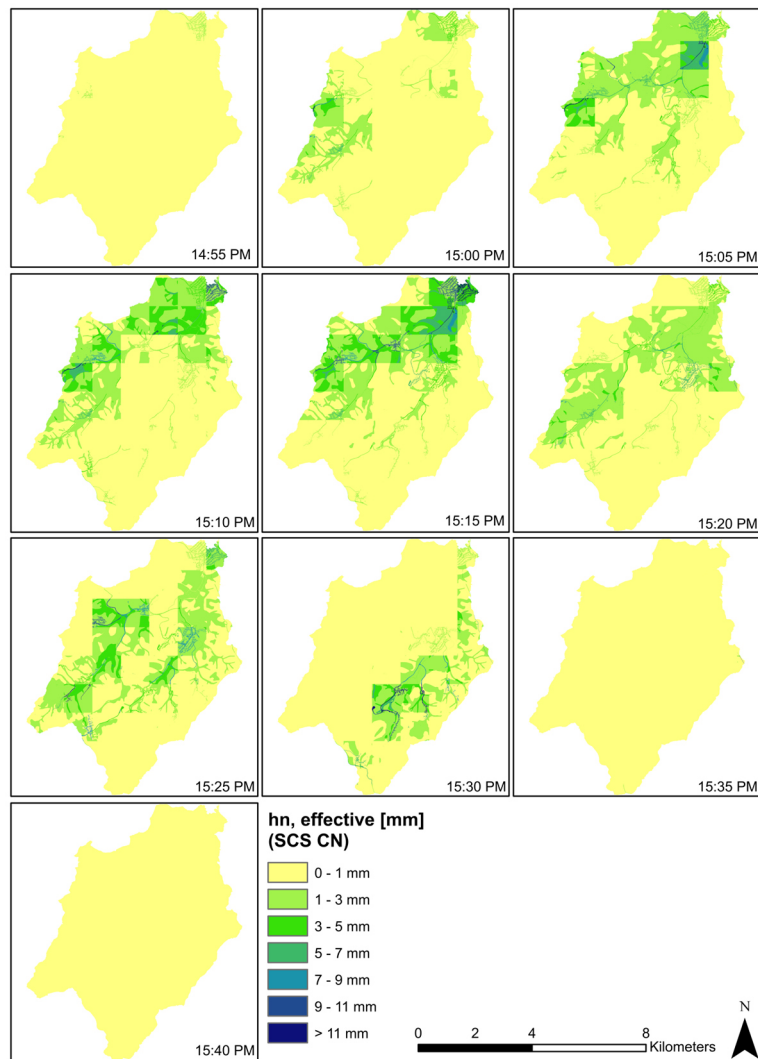
Figure 55: Effective rainfall (SCS-CN method) based on spatially distributed SCS-CN-values (**Figure 54**) and temporally invariant runoff coefficients for April 23, 2018

Spatiotemporal SCS-CN values

For the next model improvement, the temporal distribution of the runoff formation process during the precipitation event is considered (**Figure 56**). For this purpose an extended version of the SCS-CN method (Zaiß, 1989 as cited in DWA, 2008) is used. This method recalculates the runoff coefficient after each time step for the accumulated rainfall sum instead of a constant value for the entire event (**Eq. 18**). The total rainfall raster is then multiplied with the runoff coefficient for each time step (**Eq. 19**). The original method by Zaiß (1989) additionally includes the initial soil moisture condition in the determination of the SCS-CN values. This was not integrated in the routine here since the impact of the initial state of the catchment is not focused on in this study.

$$\psi_i = 1 - \left(\frac{I_a}{0.05 * \sum h_{ni} + 0.95 * I_a}\right)^2 \qquad \textbf{Eq. 18}$$

$$h_{n,effective,i} = \psi_i * h_{ni} \qquad \textbf{Eq. 19}$$

$\boldsymbol{\psi_i}$ – Runoff coefficient for each timestep [-]

$\boldsymbol{h_{ni}}$ – Total rainfall height for each timestep [mm]

$\boldsymbol{h_{n,effective,i}}$ – Effective rainfall height for each timestep [mm]
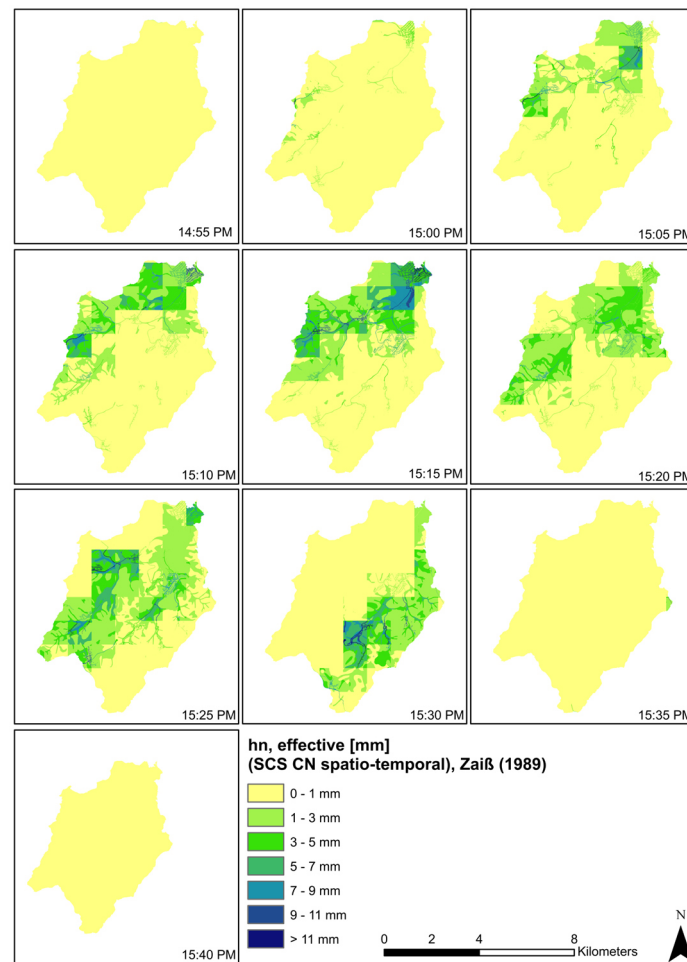
Figure 56: Effective rainfall (extended SCS-CN method) based on spatially distributed CN-values and temporally variable runoff coefficients for April 23, 2018

4.3.6.3 Interflow

A simplified procedure based on two parallel cascades of linear reservoirs is used to obtain the event-based interflow (Becker & Glos, 1969 as cited in Wackermann, 1981). The conceptual hydrological approach assumes that the direct runoff can be divided into a fast and a slow cascade via two different storage coefficients (k_1, k_2) (DWA, 2008). Even though the simplified conceptual approach with two different storage times does not allow 1:1 transferability on the

corresponding physical hydrological components, the slower cascade will be defined in the following as fast, event-based interflow. HEC-RAS computes surface roughness on a cell-by-cell basis, resulting in runoff retention. It is difficult to add another subsurface runoff component on a cell-by-cell basis with the existing model set-up. Therefore, as a first model extension (Interflow I) a catchment based simplified approach was implemented. As a second extension (Interflow II) interflow is added via subcatchments to the model area. The following equations (**Eq. 20** - **Eq. 27**) based on DWA (2008) and Wackermann (1981) are used to determine (sub -) catchment based interflow.

$$U(t) = \alpha * \frac{t}{k_1^2} * e^{\frac{-t}{k_1}} + (1 - \alpha) * \frac{t}{k_2^2} * e^{\frac{-t}{k_2}}$$ **Eq. 20**

$$k_1 = \frac{0.555}{\frac{L}{\sqrt{J}}^{0.61}} + 0.5111 * ln\frac{L}{\sqrt{J}} - 0.355$$ **Eq. 21**

$$k_2 = 3 * k_1^{1.3}$$ **Eq. 22**

$$\alpha = 1 - 0.02425 * (ln\frac{L}{\sqrt{J}})^{3.2444}, \frac{L}{\sqrt{J}} \leq 10 \ km$$ **Eq. 23**

$$\alpha = \frac{3.91}{(\frac{L}{\sqrt{J}})^{0.86}} + 0.1, \frac{L}{\sqrt{J}} > 10 \ km$$ **Eq. 24**

$$k_1^* = 4.38 - 2.25 * ChDe$$ **Eq. 25**

$$k_2^* = 0.0168 * \frac{L}{\sqrt{J}} + 2.5$$ **Eq. 26**

$$\alpha^* = 0.323 * e^{-0.00765 * \frac{L}{\sqrt{J}}}$$ **Eq. 27**

* For catchment areas larger than 10 km²

$U(t)$ – Unit Hydrograph [1/h]
α – Distribution factor for fast and slow cascade [-]
k_1, k_2 – Storage coefficients for fast and slow cascade [h]
L – Longest flowpath [km]
J – Slope [-]
$ChDe$ – Channel density [km/km²]

Catchment based interflow

For the model extension of interflow, the unit hydrograph is calculated for the entire catchment with a fixed factor $\alpha = 0.18$ and $k_2 = 3.84 \ h$. The raster of each timestep with the effective rainfall is multiplied with α to get the proportion of the fast surface runoff and the event-related interflow.

Subcatchment based interflow

For the following model extension, the process is repeated with a fixed α and factor of the slow cascade k_2 for each subcatchment (**Figure 57**). The subcatchments were divided at each inflow according to David & Schmalz (2020). The separate slow cascade with the interflow runoff fraction is added to the model area at each node. The effective precipitation is multiplied with α for each subcatchment, so that subcatchment-based adjusted effective precipitation is added to the model area. In **Figure 57** the subcatchments and their respective calculated slow retention constants (**Eq. 22**) and individual division factors (**Eq. 23** and **Eq. 24**) are summarized. **Figure 58** contains the resulting spatially distributed interflow hydrograph for each subcatchment.
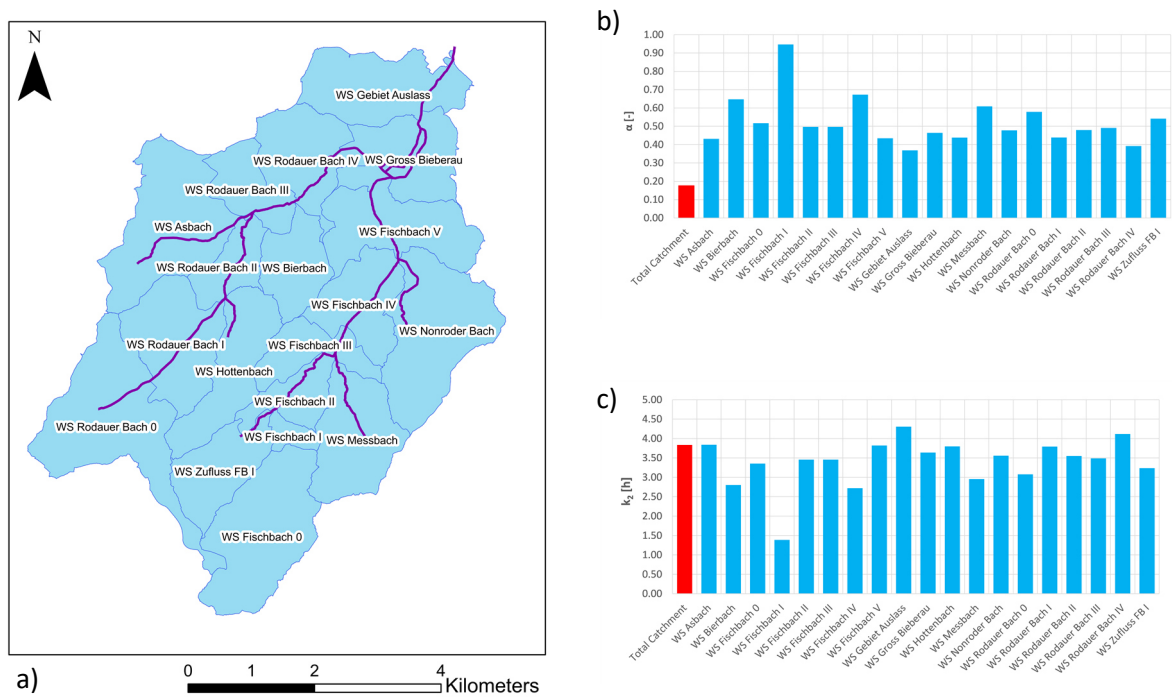
Figure 57: Subcatchments and parameters for conceptual interflow approach: a) Subcatchments for determination of slow cascade, b) Factor alpha α [-] to split effective rainfall in fast and slow cascade, c) Storage coefficient k_2 [h] for slow cascade
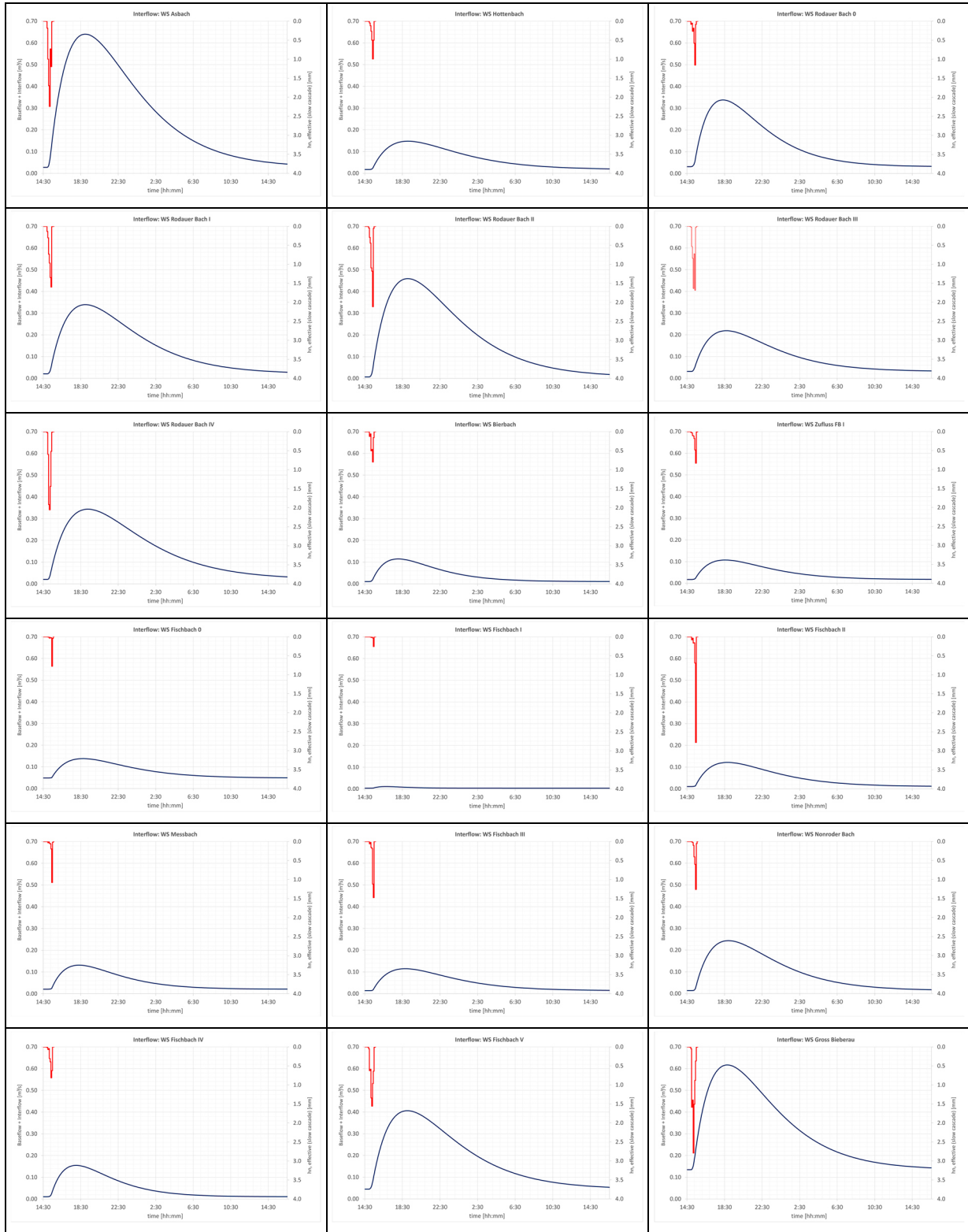
Figure 58: Spatially distributed interflow for the different subcatchments

4.3.7 Procedure for the Evaluation of Results

The results of the non-calibrated baseline model as well as the results of the model improvements via the approach of IMI-CaHyPro are analyzed in **Chapter 4.4** systematically. First, there will be a detailed evaluation of the changes in the output hydrograph and distribution of effective rainfall rates due to the implemented model improvements (**Chapter 4.4.2, Figure 59** - **Figure 72**). Afterwards, the results of the individual model runs are evaluated on the basis of six quality criteria (**Chapter 4.4.3, Figure 73** - **Figure 77**). For the model calibration process, the result analysis takes place for the baseline model by the change in output hydrographs (**Chapter 4.4.4.1, Figure 78)** and the change of quality criteria (**Table 29**)**. The same analysis is applied similarly for the calibrated IMI-CaHyPro model (**Chapter 4.4.4.1, Figure 79, Table 30**)**. The influence of the approach of IMI-CaHyPro on the parameter estimation of the calibrated IMI-CaHyPro model is analyzed in **Table 31** (**Chapter 4.4.4.2**). For this purpose, the free model parameters initially assigned based on literature values to the baseline model are compared with the parameter-set of the calibrated baseline model and the parameter-set of the calibrated IMI-CaHyPro model. The evaluation of the general model results takes place based on six standardized quality criteria (**Eq. 28** - **Eq. 33**). The used indices are briefly presented in the following paragraph.

4.3.7.1 Comparison with Gauging Station Data GB2

Nash-Sutcliffe Efficiency, NSE [-]

The *NSE* (**Eq. 1**) is used to allow a comparison of the modeled time series ($Q^t_{modeled}$) with the measured time series at the gauge (Q^t_{Obs}) where $\overline{Q^t_{Obs}}$ is the mean of observed discharges. The *NSE* is criticized for overestimating the peak flow (Pappenberger et al., 2008). Since the present study focuses on the mapping of extreme events, the *NSE* can be used for comparison with the measured data.

$$\text{NSE [-]} = 1 - \frac{\sum_{t=1}^{T} (Q^t_{Obs} - Q^t_{modeled})^2}{\sum_{t=1}^{T} (Q^t_{Obs} - \overline{Q^t_{Obs}})^2} \qquad \textbf{Eq. 28}$$

In order to be able to determine the development and possible improvement of the model results by integrating the CaHyPro, the NSE is determined one after the other. This results in seven different analyses for NSE for the model improvement process plus the determination of NSE in the calibration process. They are summarized in **Table 27**. The reference observed values for all NSE indices (Q^t_{Obs}) are the discharge values from the gauging station GB2.

Delta peak flow, ΔPF [m³/s]

The deviation of the calculated maximum discharge ($PF_{modeled}$) from the measured maximum discharge (PF_{obs}) is evaluated in absolute terms and given as ΔPF in [m³/s] (**Eq. 29**). For the measured event on April 23, 2018, the maximum discharge at the gauge GB2 is 12.5 m³/s. For

the simulated events, the discharge value and the respective deviation are determined and compared after each model extension.

$$\Delta\text{PF} \ [m^3/s] = PF_{obs} - PF_{modeled}$$

<div align="right">**Eq. 29**</div>

Delta time of Peak, ΔTP [min]

As a further criterion, the deviation of the time of occurrence of the peak flow at the gauge is evaluated. This is formed as the difference (ΔTP) of the modeled time (TP$_{modeled}$) and the observed time (TP$_{obs}$) and the deviation is given as delta in minutes (**Eq. 30**).

$$\Delta\text{TP} \ [min] = TP_{obs} - TP_{modeled}$$

<div align="right">**Eq. 30**</div>

Delta direct runoff volume, ΔDV [%]

The direct runoff volume is determined in each case by subtracting a constant base flow from the total runoff hydrograph. Then, the deviation of the direct runoff of the simulated runoff hydrograph (DV$_{modelled}$) from the volume of direct runoff of the observed hydrograph (DV$_{obs}$) is calculated. The thus determined value for ΔDV [%] (**Eq. 31**) is calculated in percent from the observed volume.

$$\Delta\text{DV} \ [\%] = \frac{DV_{obs} - DV_{modelled}}{DV_{obs}} * 100$$

<div align="right">**Eq. 31**</div>

Total precipitation volume, TPV [m³]

The total precipitation volume TPV [m³] is calculated as absolute index via the total rainfall heights for each time step (h$_{Ni}$) and the corresponding areas (a). This index is calculated for the three different rainfall scenarios of: 1. Thiessen polygons of the baseline model, 2. Hourly radar rainfall and 3. Five minutes radar rainfall.

$$\text{TPV} \ [m^3] = \sum_i h_{Ni}*a$$

<div align="right">**Eq. 32**</div>

Effective precipitation volume, EPV [m³]

The effective precipitation volume EPV [m³] is calculated as absolute index via the effective rainfall heights for each time step (h$_{N,effective,i}$) and the corresponding areas (a). This index is calculated for the different scenarios: 1. Uniform SCS-CN value as mean value for the entire catchment, 2. Spatially distributed SCS-CN value, 3. Spatiotemporal SCS-CN value,

4. Calibrated SCS-CN values for Baseline model runs, 5. Calibrated SCS-CN values for integrated model runs.

$$\text{EPV } [\text{m}^3] = \sum_{i} h_{N,effective,i} * a$$

In summary, the following indices (**Table 27**) are used for the comparison with the measured data at the gauge and the relative change of the input parameters due to iterative model improvement. The indices are determined after each step of model improvement and for the different stages of model calibration.

Table 27: Criteria for the evaluation of results and numbering for the different model runs (Note: In the following results and discussion chapter, the abbreviations and notations are used according to this table.)

Baseline model	
NSE^1, ΔPF^1, ΔTP^1, ΔDV^1, TPV^1, EPV^1	1. Uncalibrated Baseline model
Model extension of Precipitation I/II	
NSE^2, ΔPF^2, ΔTP^2, ΔDV^2, TPV^2, EPV^2	2. 1 h radar rainfall
NSE^3, ΔPF^3, ΔTP^3, ΔDV^3, TPV^3, EPV^3	3. 5 min radar rainfall
Model extension of Runoff formation I/II	
NSE^4, ΔPF^4, ΔTP^4, ΔDV^4, TPV^4, EPV^4	4. Spatial SCS-CN values
NSE^5, ΔPF^5, ΔTP^5, ΔDV^5, TPV^5, EPV^5	5. Spatiotemporal SCS-CN values
Model extension of Interflow I/II	
NSE^6, ΔPF^6, ΔTP^6, ΔDV^6, TPV^6, EPV^6	6. Catchment based interflow
NSE^7, ΔPF^7, ΔTP^7, ΔDV^7, EPV^7, EPV^7	7. Subcatchments based interflow
Calibration process	
NSE, ΔPF, ΔTP, ΔDV, TPV, EPV [a]	8. Calibration runs of *Baseline model*
NSE, ΔPF, ΔTP, ΔDV, TPV, EPV [a]	9. Calibration runs of *IMI-CaHyPro model*

[a] The results of the model runs for the calibration of the baseline model are presented in Table 29 and in Table 30 for the IMI-CaHyPro model. Since there are several model runs, they are not distinguished again with an abbreviation.

4.3.7.2 Comparison of Model Parametrization after Calibration

The effect of the approach of IMI-CaHyPro on the finally calibrated model parameters of runoff formation (SCS-CN values) and runoff concentration (Manning's n value) is evalauted. For this comparison, the three parameter sets: 1. Baseline model, 2. Calibrated Baseline model, and 3. Calibrated IMI-CyHyPro model are compared. The notation according to **Table 28** will be used.

Table 28: Evaluated parameter sets after calibration routine

$CN_{Baseline}$ $n_{Baseline}$	1. Initial parameter set for uncalibrated baseline model
$CN_{Baseline, calibrated}$ $n_{Baseline, calibrated}$	2. Parameter set for calibrated baseline model
$CN_{IMI-CaHyPro}$ $n_{IMI-CaHyPro}$	3. Parameter set for calibrated IMI-CaHyPro model

4.4 Results and Discussion

4.4.1 Baseline Model

The uncalibrated baseline model shows a temporally delayed runoff peak and a significantly too low effective precipitation and direct runoff (**Figure 59**). The effective precipitation results from the amount of input precipitation (**Figure 60**) associated with runoff losses due to initial parametrization of runoff formation. Therefore, the excessively low direct runoff can result either from the input precipitation being too low or from the SCS-CN values not being calibrated. The difference between effective input precipitation and direct runoff at the gauging station can be attributed to losses due to sinks and depressions in the unfilled terrain model. The poor correspondence of the model results with the measured data is also reflected by the quality criterion of the NSE[1] = -0.36 (For notations of the result analysis of the model runs, see **Table 27**).
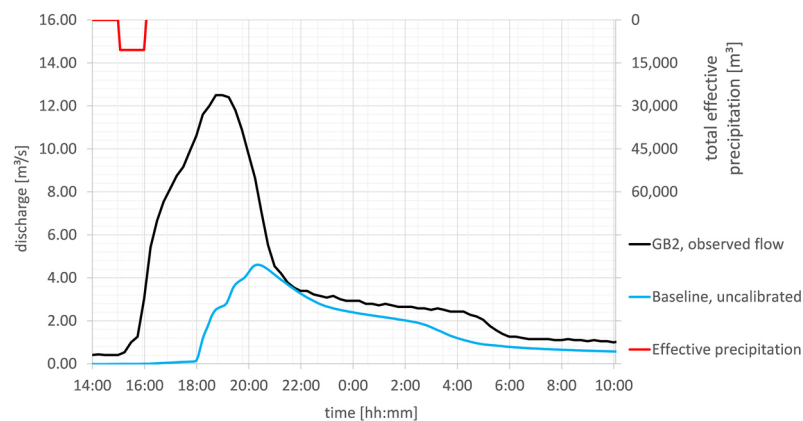
Figure 59: Simulated hydrograph and effective precipitation of uncalibrated baseline model in comparison to observed flow at GB2
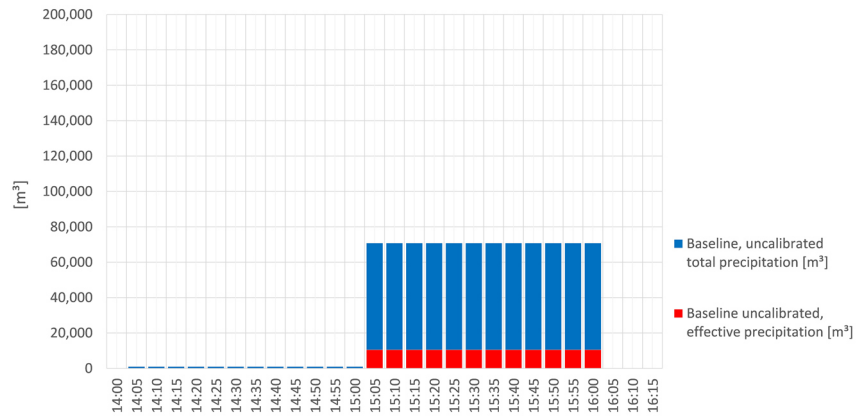
Figure 60: Input and effective precipitation data of uncalibrated baseline model

4.4.2 Results of Iterative Model Improvement

4.4.2.1 Precipitation

One hour radar rainfall

The model extension with spatially distributed input precipitation and unchanged parameterization of the runoff formation shows a faster increase of the hydrograph at the gauging station (**Figure 61**). In addition, a significant increase in input precipitation is detected, resulting in increased direct runoff at the gauging station. The effective precipitation (**Figure 62**) and the direct runoff volume continue to be significantly lower than the measured data. There is little time lag in the peak discharge compared to the measured discharge values. The significantly better agreement of the model results due to the spatially distributed input precipitation is also reflected in a significant improvement of the NSE to $NSE^2 = 0.65$.
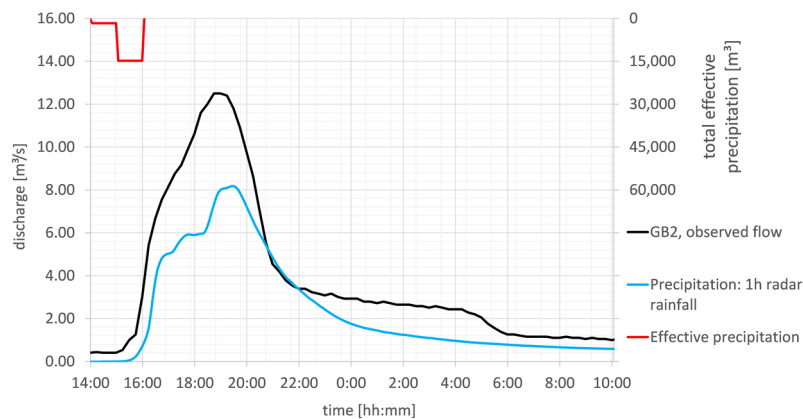
Figure 61: Simulated hydrograph and effective precipitation of model improvement with 1 h radar rainfall in comparison to observed flow at GB2
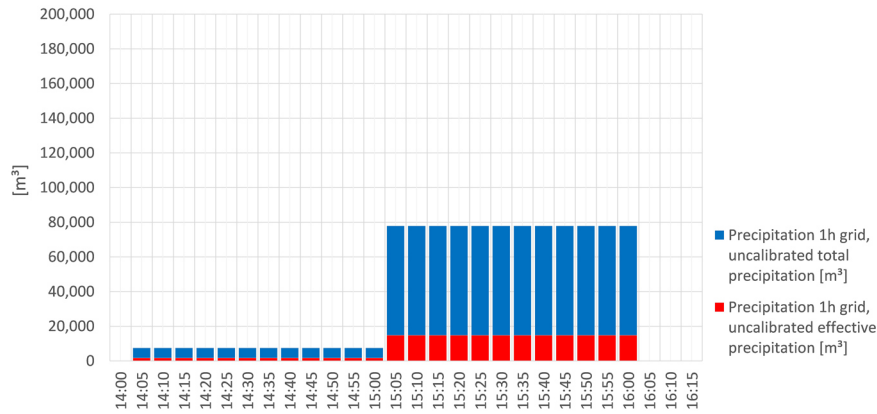
Figure 62: Input and effective precipitation data of model improvement with 1 h radar rainfall

Five minutes radar rainfall

The model extension of a spatially distributed precipitation with a temporal resolution of five minutes results again in a faster increase of the runoff hydrograph (**Figure 63**). The results correspondents well with the ascending branch of the measured hydrograph. The maximum discharge occurs with a short delay compared to the measured data at the gauging station. Due to the model extension, the temporal dynamics of the discharge event can be reproduced very well. This effect can be explained due to the change of temporal resolution of input precipitation data with higher and earlier effective precipitation rates (**Figure 64**). The improvement of the model results by adding a spatiotemporally finely resolved input precipitation is shown by an increase of the NSE. This is at NSE3=0.67. However, the calculated discharge quantities are still too low.
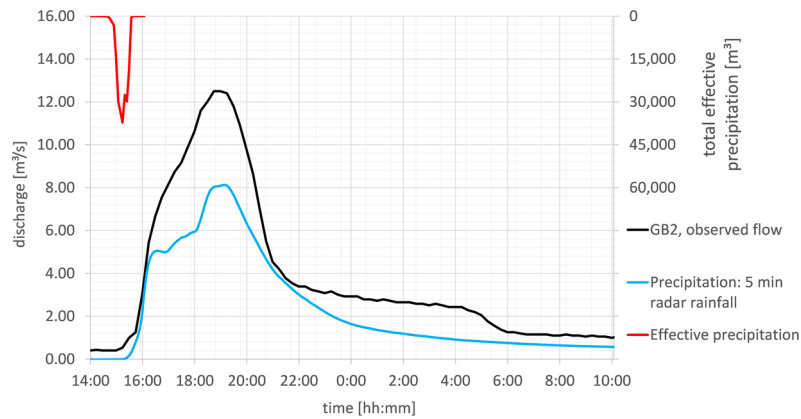
Figure 63: Simulated hydrograph and effective precipitation of model improvement with 5 min radar rainfall in comparison to observed flow at GB2
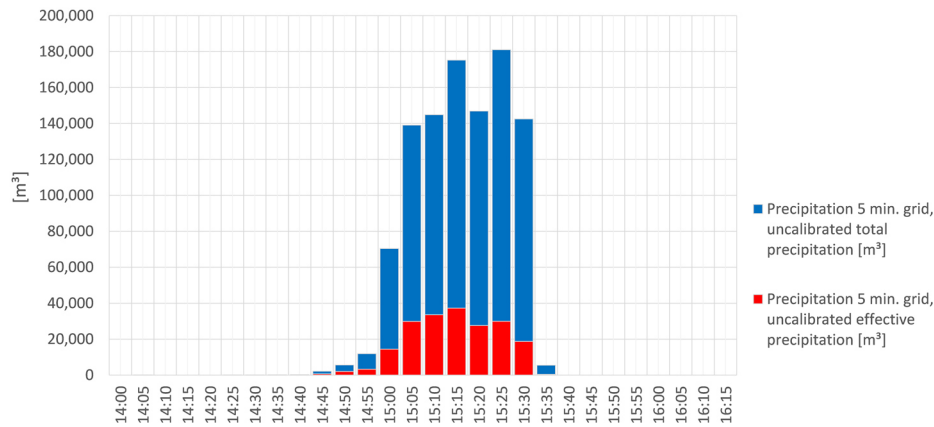
Figure 64: Input and effective precipitation data of model improvement with 5 min radar rainfall

4.4.2.2 Runoff Formation

Spatial SCS-CN values

The model extension of spatially distributed SCS-CN values and resulting runoff coefficients leads to a faster runoff response of the catchment at the gauging station (**Figure 65**). This results in a faster and higher increase of the discharge hydrograph. This effect is explained due to a more realistic coupling of the runoff effective areas to the stream course and thus higher effective precipitation rates (**Figure 66**). The model extension shows again an improvement of the agreement of the model results with the measured data. The NSE increases to $NSE^4 = 0.72$.
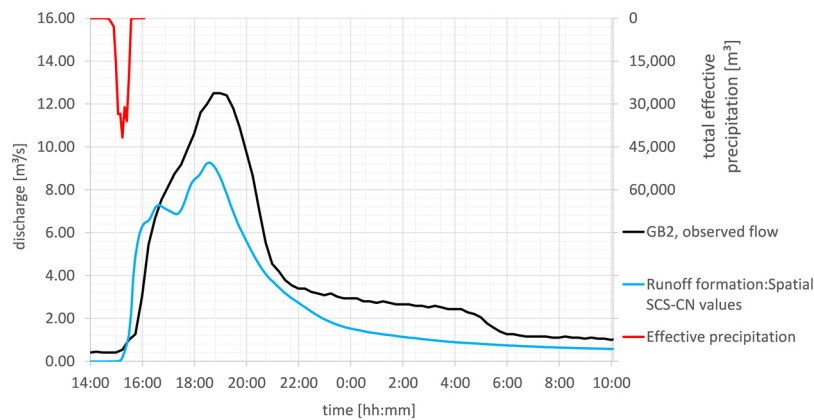
Figure 65: Simulated hydrograph and effective precipitation of model improvement with spatially distributed SCS-CN values in comparison to observed flow at GB2
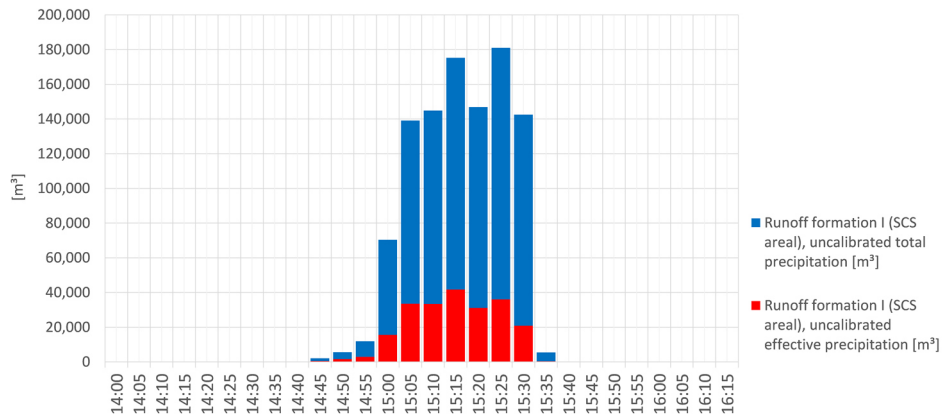
Figure 66: Input and effective precipitation data of model extension with spatially distributed SCS-CN values

Spatiotemporal SCS-CN values

By further adding a temporally distributed calculation of runoff formation, the effective precipitation increases significantly. The direct runoff volume increases by 27 % compared to a purely spatially distributed runoff formation. The temporal dynamics of the runoff event is maintained (**Figure 67**). While the total precipitation is equally distributed as in the previous simulation, the temporal dynamics of the effective precipitation changes significantly. At the beginning of the event, the impulses of the effective precipitation are lower than in the case of the temporally independent runoff formation. Toward the end of the event, effective precipitation increases and is higher than those from the simulation with a temporally constant runoff coefficient (**Figure 68**). This corresponds to a better representation of the catchment soil conditions during the event. In addition, losses due to depressions, swales, interception, wetting, etc. are reduced during the precipitation event, which in turn leads to an increasing runoff coefficient during the event. The increase in runoff volume due to the implementation of a time-dependent runoff formation process leads to a significant improvement of the model results. The NSE increases to NSE[5]=0.83.
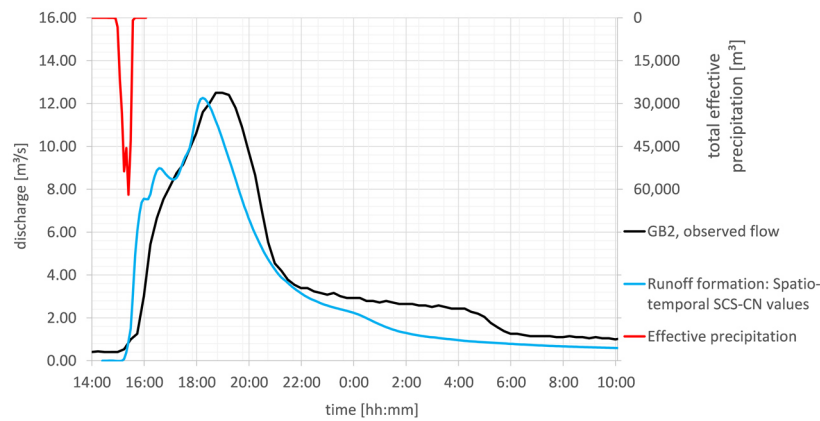
Figure 67: Simulated hydrograph and effective precipitation of model improvement with spatiotemporal SCS-CN values in comparison to observed flow at GB2
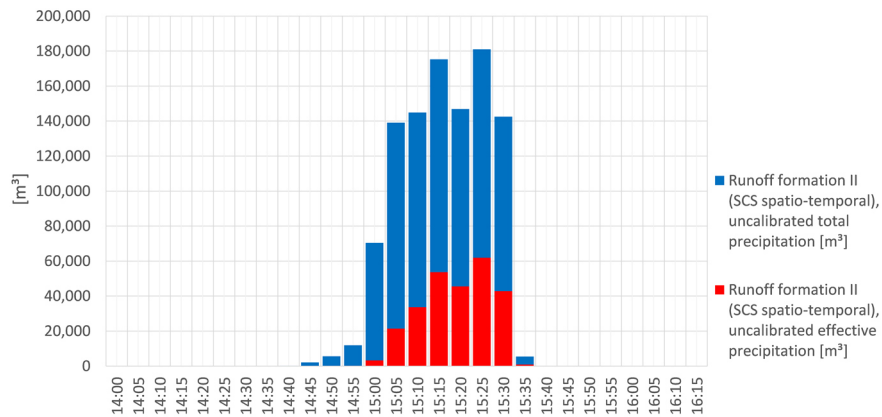
Figure 68: Input and effective precipitation data of model extension with spatiotemporal SCS-CN values

4.4.2.3   Interflow

Catchment based interflow

By implementing the process of interflow, the simulated runoff dynamics change significantly. While the time of the occurrence of the flood peak is preserved, the peak discharge is strongly reduced. The hydrograph flattens considerably and the concentration time of the falling branch increases significantly (**Figure 69**). A partitioning factor of α=0.18 was calculated as initial parametrization for the entire catchment area, so that the major part of the precipitation runs off as interflow (**Figure 70**). The model's representation of the catchment's runoff dynamics is significantly degraded by this model extension with respect to this heavy rainfall event. The quality criterion NSE decreases to $NSE^6=0.63$.
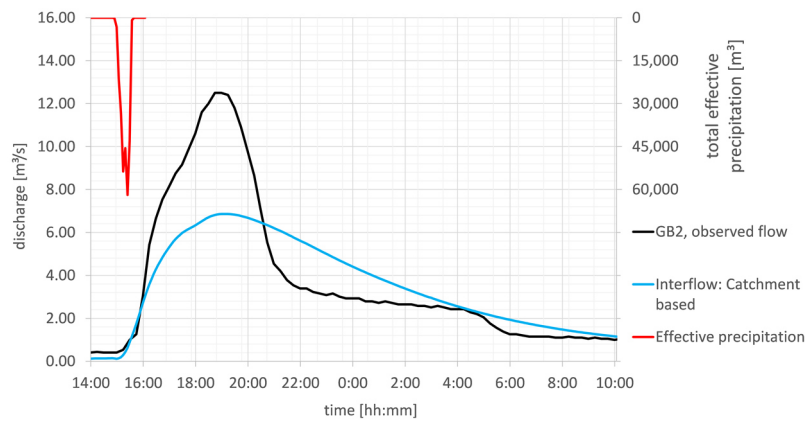
Figure 69: Simulated hydrograph and effective precipitation of model improvement with catchment based interflow in comparison to observed flow at GB2
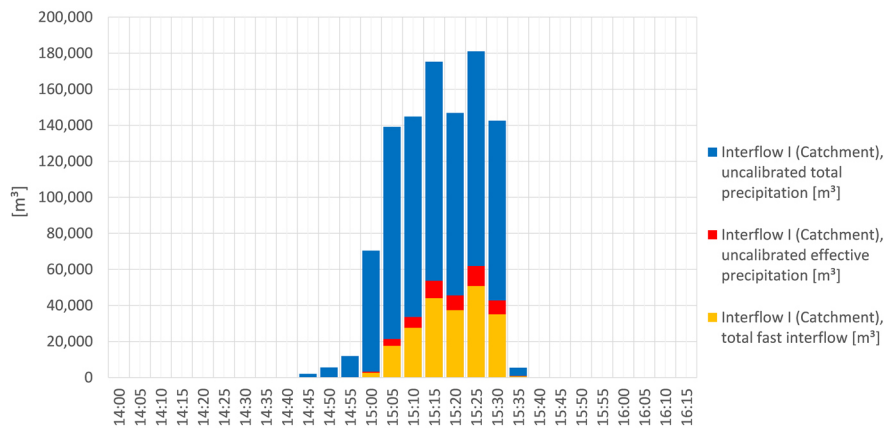
Figure 70: Input and effective precipitation data and proportion of interflow of model extension with catchment based interflow

Subcatchment based interflow

The implementation of a spatially distributed interflow results in a comparable calculated runoff hydrograph as the interflow uniformly distributed over the catchment. The peak discharge occurs with a time delay and is still clearly below the actual flood maximum (**Figure 71**). It can be seen that by adding the interflow, the storage coefficients and resulting concentration times are significantly overestimated. For the interflow, the mean value of the distribution of all subcatchments is at $\alpha=0.53$ which results in a higher proportion of surface runoff in comparison to event-related interflow (**Figure 72**). The poor agreement of the model results due to the implementation of the spatially distributed interflow is reflected in the quality criterion of the NSE. This is at $NSE^7=0.47$.
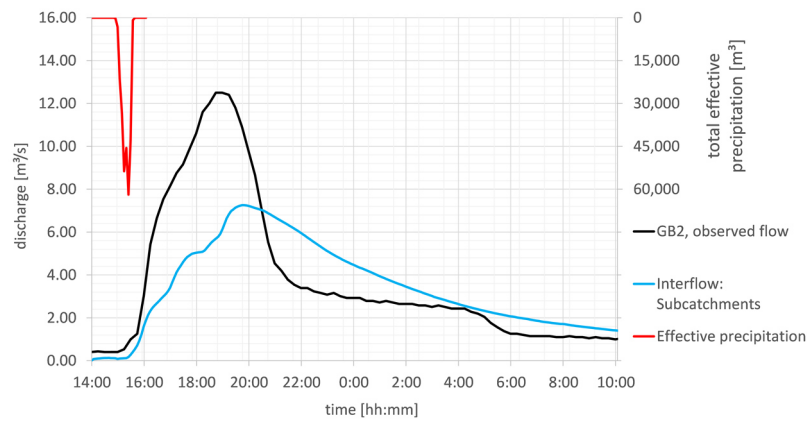
Figure 71: Simulated hydrograph and effective precipitation of model improvement with spatially distributed interflow in comparison to observed flow at GB2
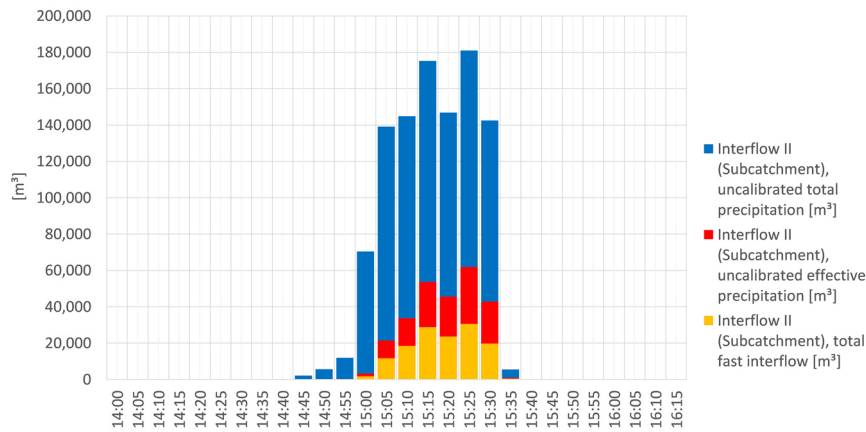
Figure 72: Input and effective precipitation data and proportion of interflow of model extension with spatially distributed interflow

4.4.3 Comparison of Uncalibrated Model Results

In the following five figures (**Figure 73 - Figure 77**), the quality criteria of the uncalibrated baseline model and the model runs of the applied model improvements presented in **Figure 51** (compare result hydrographs and precipitation rates in **Chapter 4.4.1** and **Chapter 4.4.2)** are compared. The designation of the quality criteria is based on the notations from **Table 27**. It can be seen that the general model performance of the uncalibrated baseline model is the worst for all quality criteria (NSE[1]=-0.36). There is a significant improvement in model performance for all determined quality criteria by adding the hourly radar rainfall (1.1. 1 h radar rainfall). The further model improvement due to five minutes precipitation data (1.2. 5 min radar rainfall) is minor compared the hourly input data. The integration of a spatially distributed SCS-CN values (2.1. Spatial SCS-CN values) leads to a significant improvement of the time of peak (ΔTP[4]=10 min). This effect is explainable since the runoff response of areas with higher runoff coefficients are not attenuated by an averaged runoff coefficient. By further implementing a time-dependent runoff coefficient (2.2. Spatiotemporal SCS-CN values), the NSE increases to NSE[5]=0.83. In addition, the delta to the measured direct runoff volume is strongly reduced and

at $\Delta DV^5 = 19$ %. It is explained due to more detailed capturing of total and effective precipitation rates. This effect is observed despite the model is still uncalibrated. Whereas the uncalibrated baseline model has a ΔDV of $\Delta DV^1 = 67$ %.
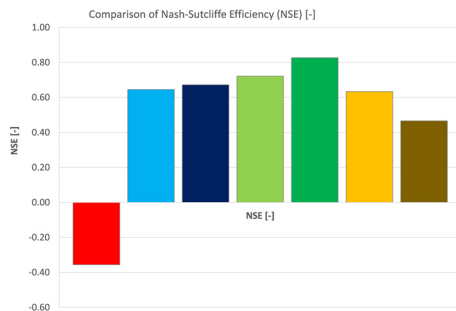
Figure 73: Comparison of Nash-Sutcliffe Efficiency (NSE) for uncalibrated baseline model (red) and model improvements of the approach of IMI-CaHyPro*
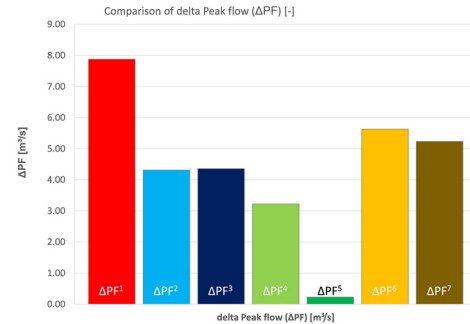
Figure 74: Comparison of delta peak flow (ΔPF) for uncalibrated baseline model (red) and model improvements of the approach of IMI-CaHyPro*
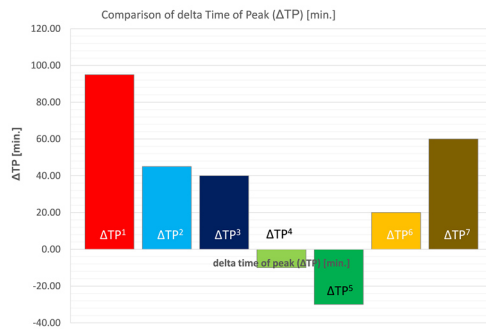
Figure 75: Comparison of delta time of peak (ΔTP) for uncalibrated baseline model (red) and model improvements of the approach of IMI-CaHyPro*
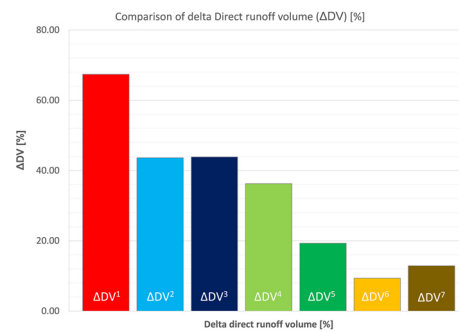
Figure 76: Comparison of delta direct runoff volume (ΔDV) for uncalibrated baseline model (red) and model improvements of the approach of IMI-CaHyPro*

- Uncalibrated baseline model, CN 72.1
- Precipitation: 1 h radar rainfall
- Precipitation: 5 min radar rainfall
- Runoff formation: Spatial SCS-CN values
- Runoff formation: Spatiotemporal SCS-CN values
- Interflow: Catchment based
- Interflow: Subcatchment based
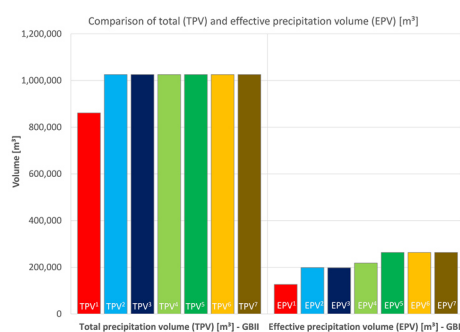
Figure 77: Comparison of total (TPV) and effective precipitation volume (EPV) for uncalibrated baseline model (red) and model improvements of the approach of IMI-CaHyPro*

* For notations and abbreviations of model runs, see **Table 27**

The general model performance reduces strongly due to the implementation of the additional process of interflow. The NSE decreases to $\text{NSE}^6 = 0.63$ for catchment based interflow (Interflow I) and $\text{NSE}^7 = 0.47$ for subcatchment based interflow (Interflow II). The strong flattening of the flood peak due to the delayed interflow leads to an increase of the delta peak flow to $\Delta \text{PF}^6 = 5.63$ m³/s and $\Delta \text{PF}^7 = 5.23$. The parametrization of the interflow process took place based on literature values and simplified equation sets (**Eq. 20** - **Eq. 27**). The used equations of the interflow component are only dependent on the catchment characteristics but not on the characteristics of the rainfall event. This event-independent generalization of the process can cause the overestimation of storage coefficients for the short lasting storm event. The subsequent calibration and adaptation of storage coefficients to the short lasting storm event of April 23, 2018 can improve the model results even for this additional process.

4.4.4 Model Calibration Process

4.4.4.1 Comparison of Hydrographs and Goodness of Fit Parameters

Baseline model

The baseline model was manually calibrated using two parameters (SCS-CN, Manning's n). Runoff formation was calculated for SCS-CN values of 82, 85, 86, 87 and ΔDV was determined after each model run (**Table 29**). Manning's n values were iteratively increased/decreased for the values (+ 10 %, - 10 %, - 20 %, - 30 %, - 40 %). The change in hydrograph was evaluated optically (**Figure 78**) and using the quality criteria, summarized in **Table 29**. The model performance increases with the increase of SCS-CN value from NSE=-0.36 (CN=72.1) for the original baseline model to NSE=0.55 for SCS-CN=87.

Table 29: Quality criteria of calibration model runs of baseline model

Loss values					
	Baseline [a]	CN82 [b]	CN85 [c]	CN86 [d]	CN87 [e]
NSE	-0.36	0.34	0.50	0.54	0.55
ΔPF	7.88	2.29	-0.34	-1.34	-2.26
ΔTP	95	45	20	15	10
ΔDV	67	29	13	7	1
TPV	861350	861350	861350	861350	861350
EPV	126431	228336	273278	291434	310289
Roughness values, CN=87					
	+10 % [f]	-10 % [g]	-20 % [h]	-30 % [i]	-40 % [j]
NSE	0.31	0.65	0.72	0.63	0.36
ΔPF	0.16	-2.21	-3.87	-5.96	-8.72
ΔTP	40	0	-25	-45	-65
ΔDV	2	0	-1	-2	-3
TPV	861350	861350	861350	861350	861350
EPV	310289	310289	310289	310289	310289

The direct runoff volume is correspondingly increased with increasing SCS-CN values. At the same time, ΔDV decreases by 66 % and the time of peak is shifted forward. Nevertheless, the runoff response of the catchment occurs with a strong time delay and the ascending branch of the hydrograph is not mapped by this model parametrization. By decreasing the roughness values in the model, the response time is reduced and the flood peak increases. The NSE increases from NSE=0.65 for 10 % reduction of roughness values to NSE=0.72 for 20 % reduction of roughness values. Further reduction of roughness values again decreases the agreement with the measured data due to too high peak discharge values. In summary, the simplified set-up of the baseline model (constant runoff coefficient, station data for precipitation, no integration of interflow) cannot represent the catchment-related processes for the investigated storm event. The subsequent calibration cannot compensate for the identified model deficits.
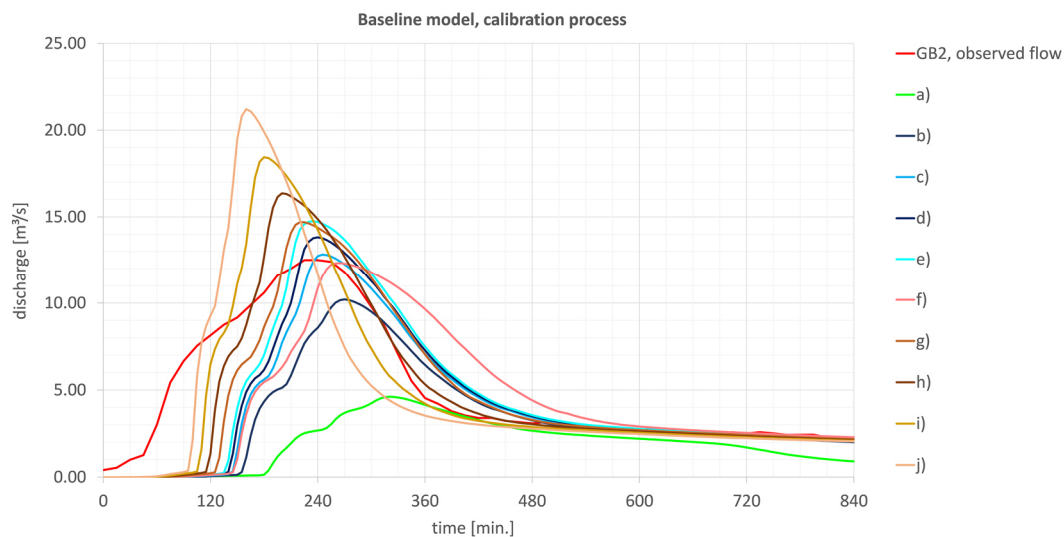
Figure 78: Hydrographs of calibration process of Baseline model for runoff formation (CN values) and runoff delay (n values)

IMI-CaHyPro model

The manual calibration routine of the IMI-CaHyPro model was performed for the three processes (runoff formation, interflow, runoff concentration) based on the three parameters: SCS-CN, k_2 and n. The parameter α (interflow) was identified in advance as low sensitive and therefore not included in the calibration process. During the calibration process, the NSE serves as a benchmark for performing the subsequent calculations (**Table 30**). By increasing the spatially distributed SCS-CN value by 4 %, ΔDV improves to 9 % (NSE=0.68). By increasing the SCS-CN value by 5%, ΔDV improves to -9 % (NSE=0.69). With further increase of CN values by 10 %, ΔDV decreases to -30 % (NSE=0.64). Therefore, CN=5 % is set for the subsequent calibration of the event-related interflow. By the catchment wide reduction of the retention constant k_2 for the slow cascades of the direct runoff (interflow), the agreement with the measured data improves considerably. The NSE increases from NSE=0.8 for a 40 % reduction of k_2 to NSE=0.88 for a 60 % reduction of k_2. At the same time ΔTP decreases to 0 minutes,

whereas ΔPF increases to -1.3 m³/s. The subsequent calibration of roughness values (+10 %, +5 %, -5 %, -10 %) again leads to an improvement in model performance to NSE=0.89 for -5% and NSE=0.90 for a 10 % reduction in roughness coefficients.

Table 30: Quality criteria of calibration model runs of IMI-CaHyPro model

Loss model (SCS-CN values)				
	IMI-CaHyPro [a]	+4 % [b]	+5 % [c]	+10 % [d]
NSE	0.47	0.68	0.69	0.64
ΔPF	5.23	3.98	2.81	0.75
ΔTP	60	45	45	25
ΔDV	13	9	-9	-30
TPV	1025557	1025557	1025557	1025557
EPV	263355	271950	282665	342375
Interflow, slow component k2, SCS-CN + 5 %				
	-40 % [e]	-50 % [f]	-60 % [g]	-70 % [h]
NSE	0.80	0.85	0.88	0.87
ΔPF	0.90	-0.11	-1.30	-2.70
ΔTP	25.00	15.00	0.00	-15.00
ΔDV	-11.63	1	-12	-12
TPV	1025557	1025557	1025557	1025557
EPV	282665	282665	282665	282665
Roughness values, SCS-CN + 5 %, k2 − 60 %				
	+10 % [i]	+5 % [j]	-5 % [k]	-10 % [l]
NSE	0.81	0.84	0.89	0.90
ΔPF	0.11	-0.19	-0.91	-1.32
ΔTP	25	25	5	0
ΔDV	-12	-12	-12	-13
TPV	1025557	1025557	1025557	1025557
EPV	282665	282665	282665	282665

A qualitative analysis of the hydrographs (**Figure 79**) shows that in particular the calibration of the parameter for the interflow provides a significant improvement of the representation of the processes in the catchment. The initial parameterization of the velocity of the interflow was significantly underestimated for the event.
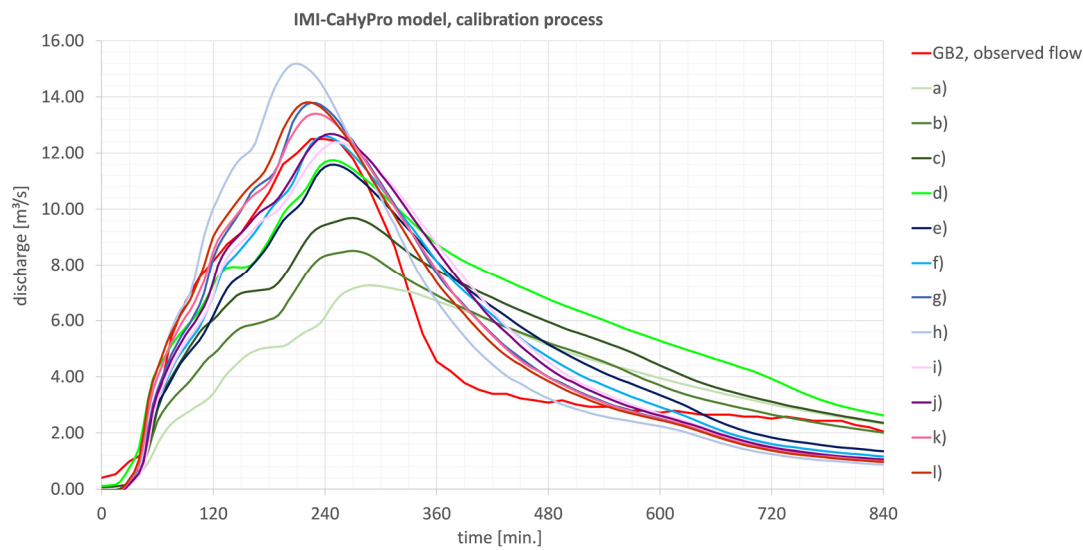
Figure 79: Hydrographs of calibration process of IMI-CaHyPro model for runoff formation (SCS-CN values) and runoff delay (Mannings'n values)

4.4.4.2 Comparison of Model Parametrization

A comparison of the calibrated parameters for the baseline model with the calibrated IMI-CaHyPro model shows that the additionally integrated CaHyPro (precipitation, runoff formation, interflow) leads to a completely different range of model parametrization. This applies in particular for the model parametrization of the SCS-CN values (**Table 31**). The calibrated SCS-CN value of the baseline model results in SCS-CN=87 which is far too high for a catchment with predominantly wooded and forestry land use. The average values of the calibrated IMI-CaHyPro model results in much lower mean value of SCS-CN=75.6. While the baseline model increased SCS-CN values by 20 %, the IMI-CaHyPro approach requires only a 5% increase to calibrate the direct runoff volume at the gauging station. For the roughness coefficients, the difference between the baseline model and the IMI-CaHyPro model is 10 %. In summary, it can be stated that a significant different model parameterization takes place due to the approach of IMI-CaHyPro. In this sense, the increase in SCS-CN values in the baseline model during calibration was used to compensate for the missing hydrologic processes in the catchment. Nevertheless, the results show that the calibration of the baseline model was not able to correct the model deficit.

Table 31: Initially and calibrated model parametrization of baseline model and IMI-CaHyPro model

SCS-CN values		Manning's n values	
$CN_{Baseline}$	72.1	$n_{Baseline}$	0.164*
$CN_{Baseline, calibrated}$	87	$n_{Baseline, calibrated}$	0.132*
$CN_{IMI-CyHyPro}$	75.6*	$n_{IMI-CyHyPro}$	0.148*

*mean value for total catchment

4.5 Conclusion and Outlook

In this study, the catchment hydrological processes (precipitation, runoff formation, interflow) for an observed storm event were iteratively added to a simplified baseline model. After each model extension, the results were evaluated for an observed storm event based on six criteria. Subsequently, the simplified baseline model and the improved model with the developed and implemented approach of IMI-CaHyPro were manually calibrated and the effect on the subsequent model parameterization was compared. In summary, the following, key findings were made:

- The integration of spatially distributed radar-based precipitation data leads to a significant improvement of the computational results and the mapped processes.
- The reduction of the time interval of the precipitation data from 1 h to 5 min has only a minor effect on the calculation results.
- The spatiotemporal implementation of the runoff formation in the model leads to an increase of the direct runoff volume, which is of great importance for a better representation of the analyzed storm event.
- The implementation of a purely conceptual, simplified interflow approach based on two parallel cascades of linear reservoirs leads to a significant overestimation of the cascade's storage retention times. Only the calibration of the storage retention times led to an improvement of the calculation results.
- The simplified baseline model is, despite calibration, not able to well represent the fast response time of the storm event. Only with the IMI-CaHyPro approach taking into account the processes in the catchment better results are achieved.
- There is a risk to generate processes not represented in the model by calibrating free parameters of other processes. This effect leads to an overestimation of the calibrated SCS-CN values in the baseline model.

The study has shown that for storm hazard analysis in combination with the application of the DRM, the integration of CaHyPro, especially the integration of radar precipitation data in combination with a spatiotemporal parametrization of the runoff formation routine leads to better model results. These findings correspond to the ongoing research activities of the integration of radar data in existing flood forecast systems (Pfister et al., 2015; Treis & Pfister, 2019).

5   Summary, Discussion and Outlook (Synthesis)

In the following, the results of the studies presented in Chapters 2 to 4 are summarized. Furthermore, the initially posed research question, whether the DRM is a suitable methodological approach to determine rain-related inundation areas in small, rural catchments, such as the low mountain range Fischbach catchment and whether the model system HEC-RAS can be applied as HHDRRM, is addressed.

In the following **Chapter 5.1**, the key findings are summarized for each study. Subsequently, they are discussed in the context of the overall research objective. Challenges and limitations of the study are pointed out in **Chapter 5.2**. **Chapter 5.3** provides an outlook and summarized recommendation for future research. **Figure 80** gives an overview of the structure of the subsequent section.
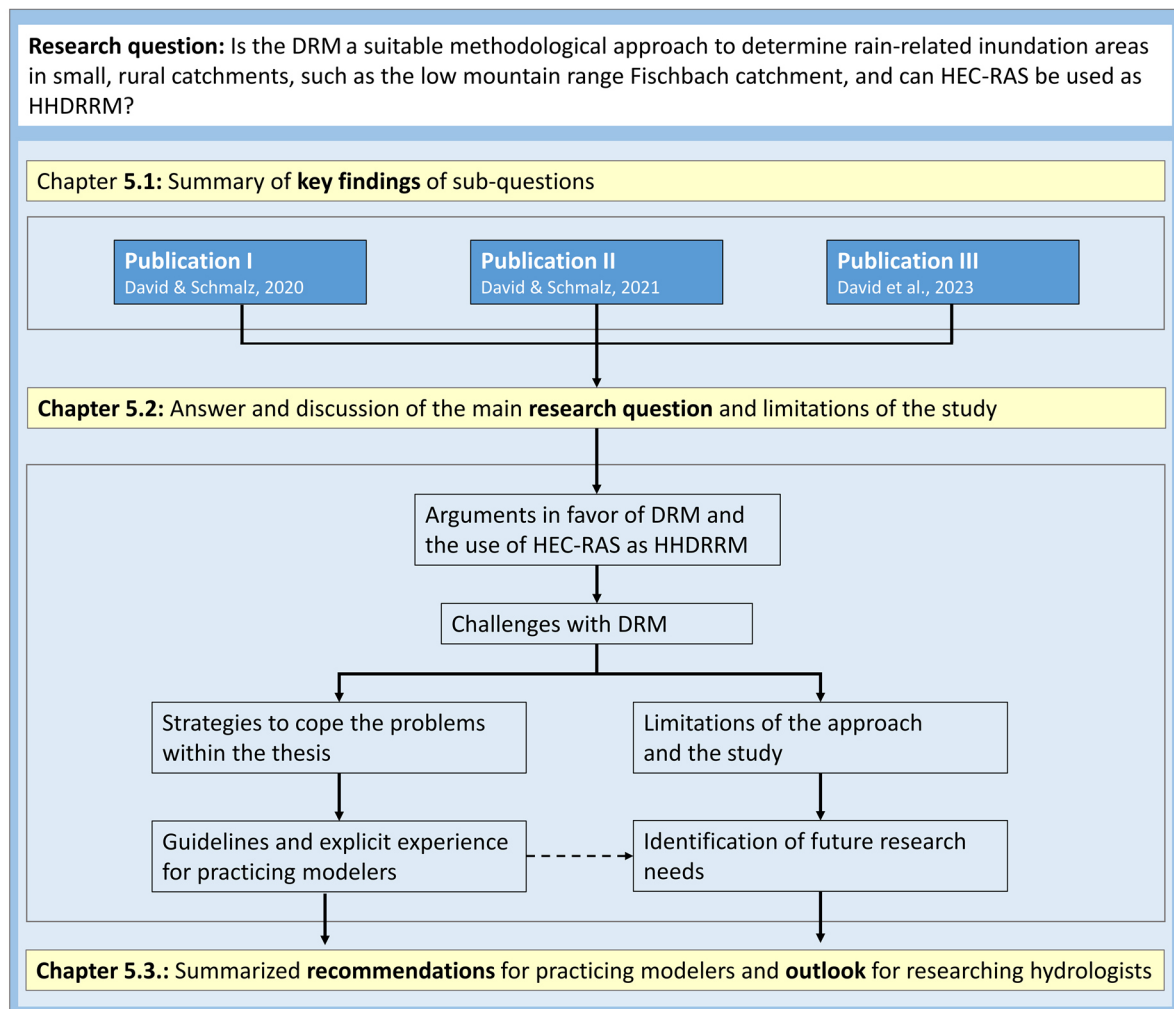
Figure 80: Framework of structure and content of Chapter 5 (Synthesis); DRM – Direct Rainfall Method, HHDRRM – Hydrological-Hydrodynamic Rainfall-Runoff Model, HEC-RAS – Hydrologic Engineering Center – River Analysis System

5.1 Summary of Key Findings

The following section summarizes the results of the three sub-questions presented in Chapter 1.2: Research questions and objectives.

1. **Question of Applicability:** Is it feasible to apply the DRM for the Fischbach River catchment using HEC-RAS? What are the challenges for small, rural catchments in terms of the model set-up, the approach of calibration and validation and the results compared to the classical, fluvial flood modeling approach?

Results of Publication I (pp. 9 - 39)

In 2016, the possibility to conduct the DRM was added in the HEC-RAS model system (HEC, 2016a). David & Schmalz applied the method to the Fischbach River catchment in 2020 with the goal of identifying storm-related inundation areas. Within the framework of this study, a methodological approach was developed by means of which it was possible to compare the model results of the DRM with the classical approach of hydrological-hydrodynamic modeling of fluvial flood hazards. Since little empirical data was available at the time of the study on the application of the new DRM and HEC-RAS method in a small, rural catchment, the model development was conducted using an iterative approach. In this process, the parameters of spatial resolution of topographic data, the time step, the integration of buildings, the settings of surface runoff, the equation approaches, the runoff formation, and the Manning's n roughness values were successively determined. The method performed resulted in a capable model dataset for the Fischbach River catchment that was used to compare the results of three rainfall-runoff events with the conventional approach for calculating floodplains of riverine floods. This procedure and the resulting model set-up generated spatially distributed information on flow paths, velocities and sinks for the research catchment. Especially in the upper part of the catchment, "flowing" transitions between surface and channel runoff were identified.

Regarding the model set-up of the integrated approach, the issue of finding a suitable model parameterization (parameter estimation) arose. This concerned the selection of the resolution of the computational grid, taking into account the subgrid implemented in HEC-RAS, and the simultaneous trade-off between model accuracy and long computation times. In addition, the study demonstrated the importance of appropriately estimating Manning's n values for the different flow regimes for surface and channel runoff. Hereby it was shown, that roughness model parametrization needs to be adapted to the expected flow regime and the recommendations on surface runoff roughness have to be considered regarding the representation of the upper hill flow processes (Engman, 1986; Downer & Ogden, 2006; Oberle et al., 2021).

Moreover, the study highlighted that the sensitivity of the model depends on the mesh resolution and the model-specific parameters. These in turn were found to be related to the

different flow behavior of surface runoff compared to the channel runoff. Based on a first investigation, the model's sensitivity in volume balance to cell size was determined. For the coarser mesh resolution of 100 m in the field and 5 m along the river course and within the settlements, a large volume difference between effective input precipitation and modeled direct runoff volume was identified. This difference decreased with a finer model resolution of 30 m in the field and 3 m in the river course and settlements.

In addition to the challenge of spatial model parameterization of the topographic data, the lack of possibility to implement precipitation in a spatially inhomogeneous manner and a non-existing routine for calculating runoff formation (until 2021) proved to be severe limitations. These missing processes challenged the adequate representation of the processes in the model. The oversimplification of hydrological processes due to technical model limitations together in combination with the application of the DRM were already determined by Hall (2015) for the model MIKE21. As a result, the precipitation data could not be added to the model domain in a spatially differentiated manner and a simplified approach had to be implemented to determine effective precipitation rates. This simplification turned out to be an oversimplification for the first analyzed storm event of long duration of 23 June 2007. The resulting poor calibration results for the event were related to the simplified representation of hydrological processes. Whereas for the event of short duration of April 23, 2018, good to very good modeling results were obtained. With respect to the simplified runoff formation approach and precipitation rates, the calibration results and the resulting model performance of DRM were dependent on the modeled event. Based on the study, it is not yet possible to say which processes exactly led to the significantly better representation of the event of April 23, 2018.

Finally, the answer to the first sub-question concerning the applicability of the DRM is summarized as follows: The application of DRM is possible in combination with the model system HEC-RAS. However, the study revealed challenges related to an appropriate model set-up, the oversimplification of CaHyPro and the method-adjusted parameter estimation. In particular, the issue of spatial resolution of topographic data interacting with low surface runoff heights requires detailed scientific consideration. This topic was further investigated in a second study (**Publication II:** *A Systematic Analysis of the Interaction between Rain-on-Grid-Simulations and Spatial Resolution in 2d Hydrodynamic Modeling*). Depending on the characteristics of the modeled storm event, the simplified integration of CaHyPro turned out to be a limitation. For longer duration rainfall-runoff events with more complex interactions between rainfall, runoff formation, runoff delay and a rather small fraction of surface runoff, the hydrological simplification was shown to likely lead to poor model results. For short, intense, fast-flowing storm events with a high proportion of effective precipitation and surface runoff, the new approach can provide good to very good model results. Thus, it can be stated that an event-dependent consideration of the respective hydrological processes dominating the event is necessary and that a consideration of the limits with respect to possible model simplification of the CaHyPro is required. This issue was addressed in more detail in a third study

(**Publication III:** *Importance of Catchment Hydrological Processes and Calibration of Hydrological-Hydrodynamic Rainfall-Runoff Models in Small Rural Catchments*).

2. **Question of Spatial Resolution of Topographic Data and Sensitivity:** Which model parameterization and spatial resolution with respect to the topographic data are reasonable when applying the DRM? Are there application-specific features and sensitivities regarding spatial resolution due to shallow water depths?

Results of Publication II (pp. 40 - 86)

The second research question focused on the model sensitivities of HEC-RAS with respect to the spatial resolution of the computational grid in interaction with the underlying subgrid and further model-specific parameters. Attempting to address this issue, application examples of the DRM were systematically compared with respect to the consideration of spatial resolution and model sensitivities in the context of a literature review. The evaluation of the studies showed that there are only very few application examples in which the model sensitivities are examined in terms of spatial resolution. Based on the results of the literature review, no transferable methodological approach was found to investigate the model sensitivities of HEC-RAS with the DRM. Therefore, a new methodological approach was developed that allowed for a systematic analysis of model sensitivities together with the DRM. To test this approach with reduced computational effort for a high number of model variants, the catchment size was reduced. For the detailed study, the DRM was applied to the 2.13 km² catchment area of the Messbach River. Seven different terrain models were used in combination with seven different computational grids. The following resolutions were used as the spatial resolution of the DEM: 0.25 m, 0.5 m, 1 m, 2 m, 3 m, 4 m and 5 m. These were combined with the following computational grids: 2 m, 3 m, 4 m, 5 m, 10 m, 20 m, 30 m and compared with a high-resolution benchmark computational run with a DEM of 0.25 m and a computational grid resolution of 1 m. A total of 50 simulations were run in the first part of the study. These runs were evaluated and compared using a total of six criteria.

Starting from a computational grid cell resolution of 10 m, a strong delay of the discharge and a decrease of the maximum discharge at the outlet of the catchment were observed. Based on the outcome evaluation indices, no indications were found for the cause of the strongly delayed and thus flattened discharge hydrograph at the outlet of the catchment. Through an additional catchment wide qualitative evaluation of the model results it was shown that the remaining water was computationally retained and only partly released with delay in the cells during the simulation. In terms of spatial resolution, it was found that up to a resolution of 5 m computational grid, model results comparable to the high-resolution benchmark run were achievable (NSE $\geq$ 0.8). Similar findings were obtained by evaluating the water levels in the channel. A very good agreement was achieved up to a resolution of the computational grid of 5 m (ΔWSE $\leq$ 0.03 m). With respect to the resolution of the terrain model, it was found that the very fine resolution terrain model with 0.25 m resolution contained a large number of

microsinks, which influenced the comparative values of the volume deficit. Water retained in the microsinks did not contribute to the runoff hydrograph, or contributed only after a significant delay. Due to this effect, the volume deficit was largest for the high-resolution benchmark run at 6.4 % and was of a similar magnitude to the volume deficit of the coarse computational grid at 30 m resolution in combination with the terrain model of 0.25 m resolution. However, two different effects caused the same magnitude of volume deficit in the two model runs. The high-resolution benchmark model was able to identify the large number of microsinks actually contained in the terrain model, whereas the coarse-resolution model produced artificial sinks. These resulted from an unfavorable combination of a fine terrain model together with a coarse computational grid. The artificial sinks formed in areas where the cell edges were higher than the terrain within the cells. This resulted in the water being trapped in the cell when the water level was low. The resulting puddles were found to have no or only with significant delayed effect for the runoff formation. The catchment wide qualitative evaluation of the inundation depths together with an analysis of the elevation data of the DEM provided an explanation for the differences in the effective model outputs. Thus, it was possible to increase the process understanding through the identified model deficits. The volume balance in terms of volume accuracy was fulfilled, regardless of the resolution of the model for all model runs.

In the second part of the study, a selection of simulations was made from the 50 that showed good to very good agreement with the high-resolution benchmark run (see **Figure 10, Chapter 3.4.3**). These were used for the detailed investigation of the model sensitivity with respect to the further parameters of Laminar flow depth, Manning's n values, Filter settings and Precipitation distribution. Three computational grids (3 m, 4 m, 5 m) in combination with three different resolutions of terrain models (0.25 m, 0.5 m, 1 m) were selected for the further investigation on model sensitivity. The evaluation of the results of the sensitivity analysis demonstrated that the laminar flow depth can be classified as weakly sensitive in relation to the maximum discharge height. The roughness values were shown to be sensitive with respect to the discharge height. The filter settings indicated a very low sensitivity for the calculated resolutions with respect to the runoff height and the inundation areas. With regard to the precipitation distributions, it was shown that the precipitation event with higher precipitation rates at the beginning of the event only had a very small influence on the runoff height. Whereas the rainfall event with the intensity peak at the end of the event resulted in the highest peak flow.

Finally, the answer of the second sub-question concerning the spatial resolution of topographic data and sensitivity is summarized as follows: Based on the second study, a recommendation for the catchment-wide, spatial discretization of the computational grid and topographic data was elaborated for the HEC-RAS model system. At a resolution of the computational grid exceeding 10 m, the agreement of the results with the finely resolved benchmark run was shown to be significantly lower due to the artificially generated sinks. For

this reason, when applying the DRM in HEC-RAS, a minimum spatial discretization of 5 m is recommended. In terms of computation time, a trade-off between the latter and the model accuracy is required. Depending on the size of the catchment, a finer resolution should be chosen. With respect to the terrain model, resolutions up to 1 m are recommended. When considering the water volume balance the large number of microsinks must be taken into account with very fine resolution DEMs. The sinks may lead to a volume deficit in the direct runoff hydrograph. With regard to the other model sensitivities investigated, it became apparent that the model-specific adjustments to surface runoff hardly impacted the model results.

3. **Question of Catchment Hydrological Processes and Calibration:** What is the influence of the spatiotemporal resolution of the CaHyPro of precipitation and runoff formation? Is there a possibility to integrate the event-based interflow into the model system through an existing computational approach? How does the resolution and integration of the CaHyPro into the model domain interact with parameter estimation based on model calibration?

Results of Publication III (pp. 87 - 119)

In the third study, a methodological approach was developed with the aim of answering the third sub-question. With this aim, the influence of the integration of CaHyPro into the DRM modelling process on the results was determined. Moreover, it was examined how the integration or refinement of the processes interact with the model parameterization after calibration. For this purpose, a storm event that occurred on the April 23, 2018 in the Fischbach catchment was analyzed in more detail. This event was proven to be the most recent with significant surface and channel runoff, which fit well with the expected rainfall-runoff dynamics of a hazardous storm. The study was conducted as an event-based case study. To compare and analyze the optimized model setups, a simplified baseline model was created using the model experience gained in the first and second studies of this thesis.

With the initial parameter estimation based on literature values, the baseline model did not perform well. The difference in the modeled and measured hydrograph resulted primarily from a significant underestimation of the input and effective precipitation. The initially determined NSE was -0.36, indicating a poor agreement of the model results.

The first model optimization using spatially distributed radar data significantly improved the model performance to an NSE of 0.65 for precipitation data with a temporal resolution of 1 h and to an NSE of 0.67 with a temporal resolution of five minutes. The subsequent integration of a spatially distributed calculation of the runoff formation routine increased the model performance to a NSE=0.72. The incorporation of the time-dependent runoff coefficients increased the NSE to NSE=0.83. These four model optimizations were conducted without calibrating the model. Thus, for the analyzed event it may be concluded that the integration of the CaHyPro radar rainfall and spatiotemporal runoff formation produced significant model improvements beyond the calibration process. The inclusion of the higher spatio-temporal

resolution of the processes led to a significantly better agreement between the model output and the observed data.

As a further model optimization, a procedure was developed, by which a simplified approach for the calculation of event-related interflow was integrated into the model domain. For this purpose, the Fischbach catchment was subdivided into 19 subcatchments based on comparable catchment characteristics and separate inflows to the main stream. With this method, characteristic values (division factor α and storage coefficient k_2) were determined for each subcatchment and characteristic inflow hydrographs for the slow component of the direct runoff were created.

The integration of the event-based interflow first led to a significant deterioration of the model results for the analyzed event. This effect is explained by the fact that the parameters originally used overestimate the calculated storage coefficients for the fast-response storm event. Only through a subsequent calibration, an increase of surface runoff volume through an adjustment of the SCS-CN values and a strong reduction of the storage coefficients of the interflow component, the model performance improved to an NSE of 0.90.

Finally, the integration of the CaHyPro resulted in a range of calibrated parameter values for the optimized model being of a significantly different order of magnitude than for the baseline model. Therefore, it can be concluded that by the integration and refinement of the additional processes, a model improvement was carried out independent of the parameter based calibration process.

Finally, the answer to the third sub-question concerning the catchment hydrological processes and calibration is summarized as follows: With the increase of the spatio-temporal resolution of the CaHyPro of radar precipitation and runoff formation, an improvement of the model results for the analyzed event were achieved. In particular, the representation of the rapidly rising runoff hydrograph and the magnitude of the runoff volume were significantly improved through the integration of the additional processes. Moreover, a procedure was developed to include a simplified approach of event-related interflow into the model domain. The integration of this process initially led to a deterioration of the model results. Only through the succeeding model calibration and a significant reduction of the initially estimated storage constants, the runoff hydrograph was improved. Moreover, it was shown that the integration of the CaHyPro into the model domain has a great impact on the estimation of the model parameters.

5.2 Discussion of the Results and Limitations of the Study

The following subchapter discusses the central research question based on the results of the three sub-studies. The research question is:

Is the DRM a suitable methodological approach to determine rain-related inundation areas in small, rural catchments, such as the low mountain range Fischbach catchment, and can HEC-RAS be used as HHDRRM?

By carrying out the three sub-studies on the topic of the application of the DRM in combination with the HEC-RAS model system in the Fischbach catchment, the great potentials, challenges and limitations with regard to the identification of floodplains in small, rural catchments were revealed. In the following, the suitability of the DRM approach and of HEC-RAS as HHDRRM for the identification of storm-related floodplains is discussed based on the studies presented. Furthermore, the current challenges, which arise in the application, as well as the extent to which the thesis has developed approaches and solution strategies to cope with these challenges are elaborated. These results can serve as explicit experiences and guidelines for practicing modelers dealing with the DRM. Based on the limitations of the model and the studies as well as their approaches, future research needs are discussed and an assessment is given whether HEC-RAS may be applied as HHDRRM. For details on the framework and the contents of the chapter, compare **Figure 80** in the introduction to the Chapter 5.

The Application of the DRM in the Fischbach catchment and the use of HEC-RAS as HHDRRM

Within the scope of the thesis, a HEC-RAS model was set-up for the Fischbach catchment and the subcatchment of the Messbach to investigate the applicability of the DRM. The iterative model optimizations in the first study, the sensitivity analysis in the second study and the detailed study on the integration of CaHyPro in the third study made it possible to systematically gain explicit model experience with HEC-RAS in the use as a HHDRRM. As part of this work, the rainfall-runoff event of April 23, 2018 was successfully modelled, with a very good agreement between the modelled and observed data. Through the integrated modeling of catchment processes and the combined modeling of surface runoff and channel flow, a modeling strategy was developed which allowed the use of the HEC-RAS model as HHDRRM. With the proposed modelling strategy, the runoff processes in the catchment and the local danger spots caused by heavy rainfall were identified for the entire catchment. The improved predictive capability of the HHDRRM for flood inundation areas in comparison to the convential approach of fluvial flood modeling is also stated in Cea & Rodriguez (2016) for the 2d model GUAD-2d.

Within the scope of the first study, the model-specific peculiarities of HEC-RAS with respect to the spatial resolution of topographic data, application-specific parameter sensitivities, as well as the simplified integration of CaHyPro were identified (**Publication I**: David & Schmalz, 2020). In the following studies on the spatial resolution of the topography in combination with

model sensitivity (**Publication II:** David & Schmalz, 2021) and catchment hydrological processes and calibration (**Publication III:** David et al., 2023) two identified research questions were investigated with individual methodological approaches. Through this iterative process involving two follow-up studies, methodological approaches and solution strategies were developed to address the prior identified application challenges.

A conclusive explanation was proposed for the investigated dependency between mesh resolution, delay times in the entire catchment and modeled peak discharges by the methodological approach of the second study. The determined model sensitivity was explained by the specifics of surface runoff with low runoff heights and the subgrid approach implemented in HEC-RAS. If the model is too coarsely discretized, the water is either computationally kept in the cells and artificial pools are generated (compare **Chapter 3.4**: **Figure 28** and **Figure 29**) or the water is released from these pools with a significant delay. This effect causes longer concentration times and thus a flattening and delay of the hydrograph's peak. Zeiger & Hubbart (2021) confirmed that a coarse grid representation can artificially trap water in the cells in HEC-RAS. Similar findings were made in Clark et al. (2008) regarding the model sensitivity towards discharge volumes for the 2d models SOBEK and TUFLOW. The observed effect is expected to be dependent on the topographic characteristics of the catchment. As stated in Yu & Coulthard (2015), this model sensitivity is expected to be higher for catchments with a sloped terrain. Nevertheless, our study has also shown that artificial sinks can occur in flat regions (s. **Figure 28** and **Figure 29**), so that it is necessary to look individually for each catchment area to see whether there is an unfavorable combination of computational grid and terrain topography that produces such non-existing puddles.

Based on the second study, recommendations were made for spatial mesh and DEM resolutions. The results of the study showed that mesh resolutions of 5 m and finer were suitable in combination with a DEM resolution of up to 1 m. In the latest applications of HEC-RAS as HHDRRM, spatial resolutions smaller than 1 m are recommended for the DEM for urban flood inundation maps (Shah et al., 2022). The results of Shah et al. (2022) fall in a similar range to those of the present study, however, they suggest an even finer spatial resolution. This difference can be explained by the need to represent topographic details when modeling urban flooding.

In the field of fluvial urban flood modeling the effects of the DEM resolution was investigated in Muthusamy et al. (2021) for a 1 m to 50 m grid resolution. The coarsening of the DEM resolution led to much higher flood depths and flood extents. As coping strategy it was proposed to merge fine river channels with coarse DEMs (Muthusamy et al., 2021). By this method, a significant improvement of the modeling results was achieved. This coping strategy cannot be transferred 1:1 to rain-on-grid simulations since shallow overland flow is determined all over the catchment. The coarsening of the DEM leads to a flattening of microstructures in the field which might represent important flow structures. Therefore, David & Schmalz (2021) recommended 1 m and finer DEM resolutions for rain-on-grid simulations.

Further, David & Schmalz (2021) proposed a consistent explanation regarding the origin of the flood volume and the flood extent sensitivity on mesh resolution and topographic resolution. For the applied model system HEC-RAS, the observed phenomena are explained to be mainly connected to the inner model structure and interplay between subgrid and computational grid. The given explanation is seen to be model-specific. For other model systems, there can be different explanations for volume differences of the catchment's outflow volume and delayed or flattened runoff hydrographs together when applying the DRM. The differences in discharge volume can also be related to numerical errors resulting from too low water depths, the implemented roughness loss approach or too high Manning's n parameter estimation. Lim & Brandt (2019) analyzed the correlation between grid resolution and Manning's n values for fluvial flood inundation mapping together with the model system CEASAR-LISFLOOD. Different combinations of DEM resolutions and Manning's n values were compared. The model results showed sensitivities towards friction values and the DEM resolution. These sensitivities can be seen as model specific and were determined in the field of fluvial flood modeling (Lim & Brandt, 2019). For this reason, the further investigation of the interplay between meshing, resolution of topography, catchment topography and the parametrization of the implemented roughness loss approach is seen as an important field for future research in rainfall-runoff applications of 2d hydrodynamic models.

In the first study, it was technically not possible to integrate spatially distributed precipitation data and runoff formation values into the model domain due to the model-specific technical limitations. The model extension covering the spatially distributed precipitation and runoff formation values was released in 2021 (HEC, 2021). By this technical model optimization, the model system HEC-RAS was enhanced to include spatially distributed hydrological processes. The model limitations that occurred in the first study in David & Schmalz (2020) led to the fact that the relatively long lasting investigated event (Basin Lag Time, BLag=540 min.) from June 23, 2007 could only be represented with moderate model performance. After model calibration, the NSE was 0.73 for a time constant runoff coefficient and 0.61 for a time dependent runoff coefficient. The simplified model set-up caused the problem that the two discharge peaks of the two-peaked event were not differentiated and thus the hydrological simplification was seen as a model limitation. The hydrological component was not able to reproduce the increase of the first discharge peak. Calibrating the model with Manning's n values resulted in a delayed discharge at the gauging station and had the effect of blurring the two-peak event with a delayed first peak. Whereas for the short-lasting runoff event measured on April 23, 2018 with a higher overland flow and peak rates, very good model results were obtained.

The third study intended to give an explanation on the impact of the integration of the catchment hydrological processes in a stepwise manner. To this end, an approach was developed to analyze the influence of the integration of radar rainfall, spatiotemporal runoff formation and event-dependent interflow. The model improvement was analyzed together with their respective interaction with the subsequent model calibration routine and the parameter

estimation. For this purpose, the event of April 23, 2018 was used. At the time of the conceptualization of the third study, this event was the most recent storm event measured in the research catchment. This event led to significantly high overland and peak flow rates and was shown to be a suitable, representative storm event for the purpose of this study.

Briefly summarized, the study revealed that the detailed spatiotemporal integration of the processes rainfall and runoff formation led to a considerable improvement of the model results (David et al., 2023). Through the investigation, it became apparent that the limitation existing in the first study of David & Schmalz (2020) was eliminated by the model extension of 2021 (HEC, 2021). It became clear that the integration of catchment hydrological processes was necessary for a better representation of an event.

The mentioned technical limitations of HEC-RAS also apply to other 2d hydrodynamic models and are considered to be restrictive with respect to the application of a 2d hydrodynamic model as HHDRRM. In Jia et al. (2019) a similar recommendation for further research in terms of the consideration of the catchment hydrological processes interception, evapotranspiration, and infiltration together with the DRM and the model system CCHE2d is given. Hall (2015) identified the lack of soil infiltration as a limitation to the use of MIKE21 as a HHDRRM. This limitation has since been addressed and the process was added to the model system (DHI, 2022). Zeiger & Hubbart (2021) confirmed these findings on model limitations in terms of infiltration rates for the model system HEC-RAS. Tyrna et al. (2018) stated the need for a more profound analysis of the model sensitivity of pre-event soil moisture condition in the application of the DRM with FloodAreaHPC. Also Taylor et al. (2014), identified this research gap for the model Mike Flood. It is seen as an important field of research in terms of parameter estimation and hydraulic design tasks.

Integration of Catchment Hydrological Processes and Calibration

In David & Schmalz (2021) the calibration of the two-peak event by Manning's n values with the integrated simplified runoff formation routine revealed a limitation of the initial model set-up. It was found that the calibration based on the roughness values was not possible. The model contained simplified hydrological processes, which defined a model deficit. The simplified model set-up was seen as the source of the model deficit. The deficit cannot be eliminated by calibration. By the methodology developed in the third publication (David et al., 2023) a more profound investigation was possible to improve the model results apart of a parameter based calibration. The interaction between the runoff-formation parameters, their spatiotemporal resolution and the procedure for calibration was investigated. Based on the model improvement, a procedure was developed which iteratively increases the spatiotemporal resolution of the processes precipitation, runoff formation and interflow. By this methodology, it was possible to give an alternative to the calibration strategy of the first publication that was based purely on parameter changes.

As a result, it is shown that the integration of radar data and the spatiotemporal refinement of runoff formation parameters leads to a significant model improvement. The improvement was

observed before the performed parameter based calibration technique. When applying DRM, the event-dependent, the fine spatiotemporal integration of the investigated processes is necessary. Otherwise, there is a risk that processes not represented in the model domain are quasi forced into the model by parameters of other processes during calibration. Cea & Rodriguez (2016) mention that the sensitivity of the model output to the pre-event soil moisture state is an additional important hydrological process, which should be taken into account when performing an event based storm hazard analysis in combination with the DRM. This additional process was not implemented in this study and should further be investigated.

The mentioned model deficits cannot be resolved by calibration. The improved model has been calibrated with very good accordance with the measurements at the gauge. As additional source of calibration data to improve the model performance and the validation process are satellite techniques. It is recommended to use for validation in Shah et al. (2022) and in Yu & Coulthard (2015). By this additional spatially distributed data source of measured inundation areas, there is seen a possibility to reduce the risk of forcing not included hydrological processes into the model. The additional data set for model validation can improve the validation process and give more profound explanations in terms of model strengths and weaknesses.

Weighing Up Between Computational Time and Calibration Outcome

It was shown that the computational costs of modeling a large model area with ca. 40 h for an event of 21 h with a normal Desktop-PC (Intel processor: i7-8700K, 3.7 GHz, 6 cores, 16 GB RAM) are rather high, making calibration of the additional model parameters added by the hydrological component unfeasible. The long computational time reduces the number of possible calibration and validation runs. The model limitation of HEC-RAS was also noted in Zeiger & Hubbart (2021). In the field of fluvial flood hazard mapping, the hydrological model and the hydraulic model are calibrated separately, which benefits the computational time of the large number of free parameters of the rainfall-runoff models. By this separation, the calibration of the hydrodynamic model can usually be reduced to Manning's n values. For the integrated consideration of hydrological and hydrodynamic processes in one model system for pluvial flooding, the computational times in relation to the additional model parameters pose a challenge. As a result, the model calibration in this study had to be performed iteratively. To reduce the number of calibration runs, the parameter range of the expected SCS-CN values was limited in advance. A further strategy in dealing with computational times is the reduction of the size of the model area for a detailed study on model sensitivity. By this approach, which was carried out in the second sub-study, a detailed analysis of the model sensitivity was possible. A further approach, which was not examined in the thesis, is a hybrid modeling strategy between the integrated and the decoupled modeling methods. For this purpose, sub-areas in which no hydrodynamic simulation is required can be modeled purely hydrologically to save computational time. The points of interest are then modeled using the DRM. This modeling strategy was proposed, for example, by Kaiser et al. (2018) in the HiOS ('HiOS' - Hinweiskarte Oberflächenabfluss/Surface runoff guidance map) project for storm hazard

analysis in the federal state of Bavaria in Germany. The approach is considered a useful way to reduce computational costs by focusing on areas of interest. This is especially true for larger catchments where calculation time is a constraint.

Despite the idea of intelligently splitting and combining the two modeling strategies, the need for further development of the model in terms of increasing computational speed, as noted in Zeiger & Hubbart (2021), is considered an important improvement of using the 2d model HEC-RAS together with rainfall-grid simulations.

Equation Sets and Manning's n Values

One limitation of the work identified when using the DRM in conjunction with HEC-RAS was dealing with the fixed-implemented equation approaches with respect to the specific characteristics of surface runoff. This restriction stems from the fact that the selected model is a freely available, but not open source, model. This becomes evident, for example, in the roughness approach implemented in HEC-RAS on the basis of Manning's n values. In Broich et al. (2019) an example is given for the implementation and comparison of four additional roughness approaches for the open source model TELEMAC-2d. Oberle et al. (2021) discuss the limitations of model parameterization of the commonly used equation sets to determine friction losses. Thereby, the limitations of the parametrization of the used approaches (e.g. Gauckler-Manning-Strickler, Darcy-Weisbach) in fluvial flood hazard analysis are presented. As a result, recommendations were made with respect to the different characteristics of surface runoff (steep slope, shallow water depth, high roughness in comparison to water depth) in comparison to the processes in channel hydraulics. In Hall (2015) the missing of depth-dependent definition of Manning's n values together with the model system MIKE21 was stated as limitation of the use of the analyzed model system as HHDRRM. Since constant Manning's n values are used in HEC-RAS, this aspect was resolved in this study using a pragmatic approach for model parameterization. In the first study, there was no differentiation of model parameterization for the two different flow processes of surface and channel runoff. This resulted in the need to significantly increase Manning's n values throughout the calibration process, aligning them with the roughness values recommended for surface runoff from Engman (1986) and Downer & Ogden (2006). For further model applications, two different water level-dependent zones for assigning Manning's n values were defined to establish a procedure for the parameter estimation. For the areas in the catchment with surface runoff and lower water depths, the model parameterization was carried out based on the recommendations for surface runoff, and for channel hydraulics. The parameterization took place based on literature parameters for channel hydraulics. Thus, the problem of fixed Manning's n values in HEC-RAS was circumvented by a pragmatic approach. This is a common modeling strategy to handle the missing depth-dependent definition of Manning's n values in 2d hydrodynamic models and was also applied in Muncaster et al. (2006). Nevertheless, this solution does not represent a physically based satisfactory result, since the transitions between surface and channel flow are continuous and no clear boundary can be drawn in terms of water depth between the two flow

processes. For this reason, further research is needed to determine a flow consistent approach to roughness losses along with DRM and shallow water flow. The specific research needs and limitations of the model for other 2d hydrodynamic models in conjunction with the DRM were mentioned previously by Muncaster et al. (2006), Caddis et al. (2008), Clark et al. (2008), Broich et al. (2019) or Zeiger & Hubbart (2021). A more detailed discussion of the parameter estimation and limitations of the implemented roughness loss equations for shallow water flow together with 2d hydrodynamic modeling can be found in Oberle et al. (2021). Here, a water level dependent definition of Manning's n values in the hydrodynamic model for pluvial (rainfall-related) flood inundation modeling and shallow water flow is recommended. In James et al. (2016), a more sophisticated proposal is presented to improve the solution of the SWE for laminar flows based on an interactive boundary layer, which takes into account the viscous boundary layer for shallow water flows. In the case of HEC-RAS, this study identified the limitations of the model and proposed a pragmatic coping strategy to overcome its technical limitations. Nevertheless, the need for more detailed consideration of flow-specific approaches to determine roughness losses is considered a necessary model improvement to HEC-RAS and other 2d models for overland flow.

Subsurface Stormflow

For an event-based rainfall-runoff computation using a hydrological model, the runoff-relevant components are determined based on the processes of the hydrological cycle. HEC-RAS was originally developed to determine water levels along the river. By extending the model to include precipitation as a source term and integrating the approaches to runoff formation, HEC-RAS can be used as a 2d HHDRRM. However, no approach is taken to add an event-based consideration of subsurface runoff. The contribution of that flow component to the runoff hydrograph is dependent on the event and catchment characteristics and can contribute significantly to the runoff process (Weiler et al., 2005). Subsurface flow has a longer runoff delay than the rapid surface runoff due to the higher flow resistance in the soil. In David et al. (2023), a simplified approach for determining event-based interflow based on the concept of linear storage was integrated into the model domain. The integrated approach assumes a division of runoff-effective precipitation into a fast component and a slow component. Storage coefficients are then determined for each subcatchment. The determination of the characteristic values of the partitioning factor α, as well as the temporal delay (storage coefficient k_2) is based on the surface catchment characteristics (flow path, slope and channel density). This applied approach does not capture additional properties, such as soil type, soil structure (morphodynamics), or vegetation. In addition, the determination of the factors is independent of the characteristics of the precipitation event. Although this information may impact the amount and velocity/delay of the subsurface stormflow. Therefore, the implemented approach needs to be seen as a simplified approach and a proposal on how a routine for subsurface stormflow in the model domain may be integrated. Le et al. (2015)

proposes suggestions for high-resolution, physically based hydrologic modeling by coupling surface and subsurface flow modeling in one model system.

The limitation of the HEC-RAS model system in terms of its use as a HHDRRM and the missing hydrological processes of subsurface stormflow was identified by the means of the third publication. As a coping strategy, a procedure was proposed to compensate for the model deficit by integrating an existing conceptual approach, which can be applied by practicing modelers.

Final Resume

Overall, the work generated an extensive repository of modeling and methodological experiences using HEC-RAS in combination with the DRM for the Fischbach River Basin. This allowed for model parameterization recommendations to be derived, specific model sensitivities to be determined, and model limitations to be identified. It was further shown that the newly implemented approach enables a variety of new use cases and offers a large potential for storm hazard analysis in small, rural catchments. Based on the results of this work, the DRM as a methodological approach to determine pluvial (rainfall-related) inundation in small, rural watersheds was successfully established. In particular, for the parameter estimation of surface runoff in the catchment, solution strategies for the spatial resolution of topographic data as well as for the treatment of spatial hydrological processes were demonstrated. These enable the application of HEC-RAS as HHDRRM. Based on the research presented in this study, the DRM is considered an appropriate approach for determining storm-related floodplains in small, rural watersheds. The proposed modeling approach is particularly suitable for small, upstream catchments, such as that of Fischbach. The work has confirmed and highlighted the challenges and limitations of the new approach and provided recommendations for future research needs.

5.3 Summarized Recommendations for Practicing Modelers and Outlook for Research Hydrologists

The application of the DRM in the Fischbach River catchment demonstrated not only the great potentials of the approach, but also its limitations. In this thesis, a variety of coping strategies were proposed for practicing modelers to overcome these limitations. Together with the results of the scientific analyses in the three sub-studies, these can serve as explicit model experience and recommendations for future engineering applications. For the limitations and model deficiencies that were not further explored in this study, a summary outlook on future research needs in the area of technical and scientific improvement of model-based pluvial (rainfall-related) flood analysis is presented in this chapter. Together with the social-communicative embedding of the research results in daily applications, these recommendations can contribute towards the development of an effective storm risk management (**Figure 81**).
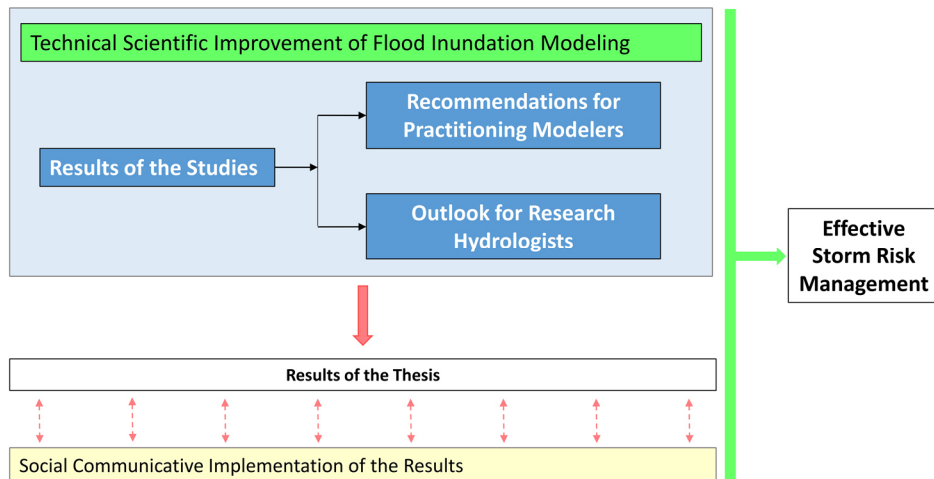
Figure 81: Framework of Summarized Recommendations for Practicing Modelers and Outlook for Research Hydrologists (Chapter 5.3)

For practicing modelers in pluvial (rainfall-related) flood analysis, the following recommendations for the application of the DRM and the use of HEC-RAS as HHDRRM are derived from the findings of this thesis:

1. The DRM in implementation with the model system HEC-RAS represents a promising approach to compute catchment-wide precipitation-related inundation areas in small rural catchments. The model results are suitable as a basis for planning tasks in water management and for the subsequent analysis in storm risk management.

2. For the application of the DRM, the recommendations for the model parameterization elaborated in this thesis should be considered. The special attention to model parametrization mainly concerns the spatial resolution of the computational grid (recommended resolution ≤ 5 m) and the topography (recommended resolution ≤ 1 m). These recommendations are related to the shallow depth of surface runoff (< 10 cm) and low elevation differences of the terrain and are specific to the application of the DRM in HEC-RAS. They will need to be verified in advance for other model systems by means of a sensitivity analysis.

3. With respect to the analyzed rainfall-runoff event, a prior analysis of the dominant processes of the event is necessary. HEC-RAS as a surface runoff model is recommended in the use as HHDRRM for short-term events with high rainfall intensity in combination with high effective runoff heights. For longer lasting precipitation events, surface-subsurface processes might play an important role in the rainfall-runoff process. These processes are not implemented in the HEC-RAS model system at the time (version HEC-RAS 6.0) and cannot be represented by the model. This limitation must be taken into account in the assessment of the suitability of the method for modelling a respective rainfall-runoff event.

4. The integration of basin-wide distributed precipitation input data (radar data) and spatiotemporally variable runoff coefficients plays an important role in determining total and effective precipitation and the resulting runoff response of the basin. It is recommended to perform a preliminary evaluation of the storm event with respect to its location and extent in the considered catchment area. The selection of precipitation data and distribution over the model domain as input data must be consistent for optimal model results.

Outlook for Research Hydrologists

Based on the results as well as the model deficiencies and limitations of the DRM identified in the three sub-studies, the following outlook is provided for research hydrologists:

1. Approaches for hydrodynamic simulations on High Performance Computing Clusters (HPC clusters) and GPU-based parallelized computations are needed. These are already under development and need to be further implemented as a standard for the 2d hydrodynamic models widely used in water management (Kalyanapu et al., 2011; Le et al., 2015; Loretz & Volz, 2017; Tyrna et al., 2018; García-Feal et al., 2018). The improvements need to be complemented by assessments on more efficient mathematical solvers for hydrodynamic rainfall-runoff simulations (Leandro et al., 2014; Cea & Bladé, 2015; Caviedes-Voullième et al., 2020).

2. Further research is needed to integrate hydrological processes in the watershed to fully represent the runoff-related components of the precipitation-runoff process. This refers to the integration of subsurface processes to be able to model a larger variety of rainfall runoff events by means of the DRM. This should be complemented by event-based research on initial conditions, which is important for hydraulic design tasks (Le et al., 2015) and reliable storm hazard analyses.

3. The study showed the need for more fundamental research, but also the need for the technical implementation of existing hydrological research results into 2d hydrodynamic models. This concerns particularly the application-related model parameterization and implemented equation sets. The research need stems from the demand for adequate parameter estimation considering the different runoff conditions in pluvial (rainfall-related) flood modeling compared to flood hazard analyses in rivers. Most mathematical approaches and empirically determined parameters in flood modeling were originally derived from channel runoff. This fact pushes the application of existing approaches in the field of surface runoff modeling to their limits (Oberle et al., 2021).

Implementation of an Effective Storm Risk Management

This thesis deals with the technical-scientific analysis of implementing the DRM in HEC-RAS as HHDRRM. The results of the DRM can serve for a variety of water management tasks and are

valuable to practitioners from a variety of disciplines. Nevertheless, it must be kept in mind that improving model systems by scientific-technical optimization is only one part of a successful storm risk management. Only together with communication, dissemination and translation of the results to users and communities, as stated in LAWA (2018b) an understanding of the value and effective use of the map content, thus a successful and effective storm risk management can be achieved.

Bibliography

Arcement, G. J. & Schneider, V. R. (1989). *Guide for Selecting Manning's Roughness Coefficients for Natural Channels and Flood Plains*. *2339*. https://doi.org/10.3133/wsp2339

Aronica, G., Bates, P. D. & Horritt, M. S. (2002). Assessing the uncertainty in distributed model predictions using observed binary pattern information within GLUE. *Hydrological Processes, 16*(10), 2001–2016. https://doi.org/10.1002/hyp.398

Assmann, A., Fritsch, K. & Jäger, S. (2012). Starkregengefahrenkarten und Risikomanagement im Glems-Einzugsgebiet. In J. Strobl, T. Blaschke, & G. Griesebner (Eds.), *Angewandte Geoinformatik 2012: Beiträge zum 24. AGIT-Symposium Salzburg* (pp. 576–585). Wichmann.

Ball, J., Barton, C., Bishop, W., Gray, S., Jones, R. H., McCowan, A., Murtagh, J., Peirson, B., Phillips, B., Rigby, T., Retallick, M., Smith, G., Syme, B., Szylkarski, S. & Thompson, R. (2012). *Australian Rainfall & Runoff Revision Projects (Project 15)—Two Dimensional Modelling in Urban and Rural floodplains* (Stage 1 and 2 Draft Report P15/S1/009; pp. 184–202). Engineers Australia.

Bates, P. D. & De Roo, A. P. J. (2000). A simple raster-based model for flood inundation simulation. *Journal of Hydrology, 236*(1–2), 54–77. https://doi.org/10.1016/S0022-1694(00)00278-X

Becker, A. & Glos, E. (1969). *Grundlagen der Systemhydrologie*. Verlag für Bauwesen.

Beven, K. (2012). *Rainfall-runoff modelling: The primer* (2nd ed). Wiley-Blackwell.

Beven, K. & Binley, A. (1992). The future of distributed models: Model calibration and uncertainty prediction. *Hydrological Processes, 6*(3), 279–298.

https://doi.org/10.1002/hyp.3360060305

Bickelhaupt, M. (2018). *Photos from storm event at 23.04.2018*. Voluntary fire brigade Groß-Bieberau in Hesse (Germany).

Blume, T., Zehe, E. & Bronstert, A. (2007). Rainfall—Runoff response, event-based runoff coefficients and hydrograph separation. *Hydrological Sciences Journal, 52*(5), 843–862. https://doi.org/10.1623/hysj.52.5.843

Broich, K., Kaiser, M., Lin, Q., Mitterer, J., Nguyen, H., Pflugbeil, T., Trentini, F. von, Willkofer, F., Disse, M. & Ludwig, R. (2018). Starkregen und Sturzfluten – Erfassen, Erforschen, Evaluieren. Beiträge zum Seminar am 6. Juni 2018 an der Technischen Universität München. *Starkregen und Sturzfluten – Erfassen, Erforschen, Evaluieren Beiträge zum Seminar am 6. Juni 2018 an der Technischen Universität München, 40.18*. https://doi.org/10.14617/for.hydrol.wasbew.40.18

Broich, K., Pflugbeil, T., Disse, M. & Nguyen, H. (2019, October 17). Using TELEMAC-2D for Hydrodynamic Modeling of Rainfall-Runoff. 26th *TELEMAC-MASCARET User Conference 2019*. Toulouse. https://doi.org/10.5281/ZENODO.3611524

Bronstert, A., Agarwal, A., Boessenkool, B., Fischer, M., Heistermann, M., Köhn-Reich, L., Moran, T. & Wendi, D. (2017). Die Sturzflut von Braunsbach am 29. Mai 2016 - Entstehung, Ablauf und Schäden eines "Jahrhundertereignisses", Teil 1: Meteorologische und hydrologische Analyse. *Hydrologie und Wasserbewirtschaftung, 61*(3), 150–162. https://doi.org/10.5675/hywa_2017,3_1

Caddis, B. M., Jempson, M. A., Ball, J. E. & Syme, W. J. (2008). *Incorporating Hydrology into 2D Hydraulic Models—The Direct Rainfall Approach*. 57–64.

Casulli, V. (2009). A high-resolution wetting and drying algorithm for free-surface hydrodynamics. *International Journal for Numerical Methods in Fluids, 60*(4), 391–408. https://doi.org/10.1002/fld.1896

Caviedes-Voullième, D., Fernández-Pato, J. & Hinz, C. (2020). Performance assessment of 2D Zero-Inertia and Shallow Water models for simulating rainfall-runoff processes. *Journal of Hydrology, 584*, 124663. https://doi.org/10.1016/j.jhydrol.2020.124663

Cea, L. & Bladé, E. (2015). A simple and efficient unstructured finite volume scheme for solving the shallow water equations in overland flow applications. *Water Resources Research, 51*(7), 5464–5486. https://doi.org/10.1002/2014WR016547

Cea, L., Garrido, M. & Puertas, J. (2010). Experimental validation of two-dimensional depth-averaged models for forecasting rainfall–runoff from precipitation data in urban areas. *Journal of Hydrology, 382*(1–4), 88–102. https://doi.org/10.1016/j.jhydrol.2009.12.020

Cea, L., Garrido, M., Puertas, J., Jácome, A., Del Río, H. & Suárez, J. (2010). Overland flow computations in urban and industrial catchments from direct precipitation data using a two-dimensional shallow water model. *Water Science and Technology*, *62*(9), 1998–2008. https://doi.org/10.2166/wst.2010.746

Cea, L., Puertas, J., Pena, L. & Garrido, M. (2008, September 1). *Hydrologic forecasting of fast flood events in small catchments with a 2d-swe model. Numerical model and experimental validation*. World Water Congress 2008, Montpellier, France.

Cea, M. & Rodriguez, M. (2016). Two-Dimensional Coupled Distributed Hydrologic–Hydraulic Model Simulation on Watershed. *Pure and Applied Geophysics*, *173*(3), 909–922. https://doi.org/10.1007/s00024-015-1196-5

Chang, T.-J., Wang, C.-H. & Chen, A. S. (2015). A novel approach to model dynamic flow interactions between storm sewer system and overland surface for different land covers in urban areas. *Journal of Hydrology*, *524*, 662–679. https://doi.org/10.1016/j.jhydrol.2015.03.014

Chen, A. S., Djordjević, S., Leandro, J. & Savić, D. A. (2010). An analysis of the combined consequences of pluvial and fluvial flooding. *Water Science and Technology*, *62*(7), 1491–1498. https://doi.org/10.2166/wst.2010.486

Chifflard, P. (2016). Subsurface Stormflow—A well-recognized but still challenging process in Catchment Hydrology. *University of Marburg - Department of Geography*. https://www.online.uni-marburg.de/ssf/index.html

Chow, V. T. (1985). *Open-channel hydraulics: International student edition* (21st print). McGraw-Hill.

Chow, V. T., Maidment, D. R. & Mays, L. W. (1988). *Applied hydrology*. McGraw-Hill.

Clark, K., Ball, J. & Babister, M. (2008). *Can Fixed Grid 2D Hydraulic Models Be Used as Hydrologic Models?* 2496–2507.

https://search.informit.org/doi/10.3316/informit.594590466843451

Costabile, P., Costanzo, C., Ferraro, D. & Barca, P. (2021). Is HEC-RAS 2D accurate enough for storm-event hazard assessment? Lessons learnt from a benchmarking study based on rain-on-grid modelling. *Journal of Hydrology*, *603*, 126962.

https://doi.org/10.1016/j.jhydrol.2021.126962

David, A. & Schmalz, B. (2020). Flood hazard analysis in small catchments: Comparison of hydrological and hydrodynamic approaches by the use of direct rainfall. *Journal of Flood Risk Management*, *13*(4). https://doi.org/10.1111/jfr3.12639

David, A. & Schmalz, B. (2021). A Systematic Analysis of the Interaction between Rain-on-Grid-Simulations and Spatial Resolution in 2D Hydrodynamic Modeling. *Water*, *13*(17), 2346. https://doi.org/10.3390/w13172346

David, A., Ruiz Rodriguez, E. & Schmalz, B. (2023). Importance of Catchment Hydrological Processes and Calibration of Hydrological-Hydrodynamic Rainfall-Runoff Models in Small Rural Catchments. Journal of Flood Risk Management, e12901. https://doi.org/10.1111/jfr3.12901

Djordjević, S., Prodanović, D. & Maksimović, Č. (1999). An approach to simulation of dual drainage. *Water Science and Technology*, *39*(9), 95–103. https://doi.org/10.2166/wst.1999.0451

Djordjević, S., Prodanović, D., Maksimović, Č., Ivetić, M. & Savić, D. (2005). SIPSON – Simulation of Interaction between Pipe flow and Surface Overland flow in Networks. *Water Science and Technology*, *52*(5), 275–283. https://doi.org/10.2166/wst.2005.0143

Downer, C. W. & Ogden, F. L. (2006). *Gridded Surface Subsurface Hydrologic Analysis (GSSHA) User's Manual, Version 1.43 for Watershed Modeling System 6.1* (ERDC/CHL SR-06-1; System-Wide Water Resources Program). U.S. Army Engineer Research and Development Center.

DVWK. (1984). Arbeitsanleitung zur Anwendung von Niederschlag-Abfluß-Modellen in kleinen Einzugsgebieten. In *DVWK-Regeln zur Wasserwirtschaft* (Vol. 113). Deutscher Verband für Wasserwirtschaft und Kulturbau e.V.

DWA. (2006). *Hydraulische Bemessung und Nachweis von Entwässerungssystemen, DWA-Regelwerk A 118* (März 2006). Deutsche Vereinigung für Wasserwirtschaft, Abwasser und Abfall (DWA).

DWA. (2008). Abflüsse aus Außengebieten der Kanalisation. *Korrespondenz Abwasser, Abfall*, *2008*(8), 850–859. https://doi.org/10.3242/kae2008.08.001

DWD. (2017). *KOSTRA-DWD-2010R - Starkniederschlagshöhen für Deutschland (Bezugszeitraum 1951 bis 2010)*. Deutscher Wetterdienst (DWD) "German Weather Service."

DWD. (2018). *Precipitation data from Reinheim station (ID: 4134), hourly Data*. Deutscher Wetterdienst (DWD) "German Weather Service."

DWD. (2022). *Precipitation data from Reinheim station (ID: 4134), hourly Data*. Deutscher Wetterdienst (DWD) "German Weather Service."

Echo Zeitungen GmbH. (2018, April 23). Gewitter bringt Starkregen nach Südhessen—Vollgelaufene Keller in Seeheim-Jugenheim, Fischbachtal und Modautal. *Echo Online*. http://www.echo-online.de/lokales/suedhessen/gewitter-bringt-starkregen-nach-suedhessen-vollgelaufene-keller-in-seeheim-jugenheim-fischbachtal-und-modautal_18700339.htm

EEA. (2016). *CORINE Land Cover (CLC) 2012*. European Environment Agency (EEA) - Copernicus - Land Monitoring Service. https://land.copernicus.eu/pan-european/corine-land-cover/clc-2012

Elfeki, A., Masoud, M. & Niyazi, B. (2017). Integrated rainfall–runoff and flood inundation modeling for flash flood risk assessment under data scarcity in arid regions: Wadi Fatimah basin case study, Saudi Arabia. *Natural Hazards, 85*(1), 87–109. https://doi.org/10.1007/s11069-016-2559-7

Engman, E. T. (1986). Roughness Coefficients for Routing Surface Runoff. *Journal of Irrigation and Drainage Engineering, 112*(1), 39–53. https://doi.org/10.1061/(ASCE)0733-9437(1986)112:1(39)

ESRI Inc. (2021a). *An overview of the TIN Dataset toolset*. ArcGIS Pro. https://pro.arcgis.com/en/pro-app/2.6/tool-reference/3d-analyst/an-overview-of-the-tin-dataset-toolset.htm

ESRI Inc. (2021b). *LAS-Dataset in Raster (Conversion)*. ArcGIS Pro.

https://pro.arcgis.com/de/pro-app/tool-reference/conversion/las-dataset-to-raster.htm

EU. (2007). *Directive 2007/60/EC of the European Parliament and of the Council of 23 October 2007 on the assessment and management of flood risks* (2007/60/EC). European Parliament, Council.

Faber, R., Fuchs, M. & Puchner, G. (2012). Numerische Simulation von Hochwässern: Von 1D zu 3D aus Anwendersicht im Ingenieurbereich. *Österreichische Wasser- Und Abfallwirtschaft, 64*(5–6), 307–313. https://doi.org/10.1007/s00506-012-0404-0

Falconer, R. H., Cobby, D., Smyth, P., Astle, G., Dent, J. & Golding, B. (2009). Pluvial flooding: New approaches in flood warning, mapping and risk management. *Journal of Flood Risk Management*, *2*(3), 198–208. https://doi.org/10.1111/j.1753-318X.2009.01034.x

Fan, Y., Ao, T., Yu, H., Huang, G. & Li, X. (2017). A Coupled 1D-2D Hydrodynamic Model for Urban Flood Inundation. *Advances in Meteorology*, *2017*, 1–12. https://doi.org/10.1155/2017/2819308

Fernández-Pato, J., Caviedes-Voullième, D. & García-Navarro, P. (2016). Rainfall/runoff simulation with 2D full shallow water equations: Sensitivity analysis and calibration of infiltration parameters. *Journal of Hydrology*, *536*, 496–513. https://doi.org/10.1016/j.jhydrol.2016.03.021

Fraga, I., Cea, L. & Puertas, J. (2015). Validation of a 1D-2D dual drainage model under unsteady part-full and surcharged sewer conditions. *Urban Water Journal*, *14*(1), 74–84. https://doi.org/10.1080/1573062X.2015.1057180

Fraga, I., Cea, L., Puertas, J., Suárez, J., Jiménez, V. & Jácome, A. (2016). Global Sensitivity and GLUE-Based Uncertainty Analysis of a 2D-1D Dual Urban Drainage Model. *Journal of Hydrologic Engineering*, *21*(5), 04016004. https://doi.org/10.1061/(ASCE)HE.1943-5584.0001335

Fritsch, K., Assmann, A. & Tyrna, B. (2016). *Long-term experiences with pluvial flood risk management* (M. Lang, F. Klijn, & P. Samuels, Eds.; Vol. 7). https://doi.org/10.1051/e3sconf/20160704017

García-Feal, O., González-Cao, J., Gómez-Gesteira, M., Cea, L., Domínguez, J. & Formella, A. (2018). An Accelerated Tool for Flood Modelling Based on Iber. *Water*, *10*(10), 1459. https://doi.org/10.3390/w10101459

GDV. (2017). *Naturgefahrenreport 2017—Die Schaden-Chronik der deutschen Versicherer in Zahlen, Stimmen und Ereignissen* (pp. 30–31). Gesamtverband der Deutschen Versicherungswirtschaft e.V. (GDV).

Grismer, M. (2016). Surface Runoff in Watershed Modeling—Turbulent or Laminar Flows? *Hydrology*, *3*(2), 18. https://doi.org/10.3390/hydrology3020018

Grosser, P. F. & Schmalz, B. (2021). Low Flow and Drought in a German Low Mountain Range Basin. *Water*, *13*(3), 316. https://doi.org/10.3390/w13030316

Gül, G. O., Harmancıoğlu, N. & Gül, A. (2010). A combined hydrologic and hydraulic modeling approach for testing efficiency of structural flood control measures. *Natural Hazards*, *54*(2), 245–260. https://doi.org/10.1007/s11069-009-9464-2

Guse, B., Pilz, T., Stoelzle, M. & Bormann, H. (2019). Charakterisierung und Analyse hydrologischer Modelle im deutschsprachigen Raum. *Wasser und Abfall*, *21*(5), 43–52. https://doi.org/10.1007/s35152-019-0043-x

Hall, J. (2015). Direct rainfall flood modelling: The good, the bad and the ugly. *Australasian Journal of Water Resources*, *19*(1), 74–85. https://doi.org/10.7158/W14-016.2015.19.1

HEC. (1998). *HEC-1 Flood Hydrograph Package User's Manual*. U.S. Army Corps of Engineers - Hydrologic Engineering Center (HEC).

HEC. (2000). *Hydrologic Modeling System HEC-HMS - Technical Reference Manual*. U.S. Army Corps of Engineers - Hydrologic Engineering Center (HEC).

HEC. (2011). *HEC-GeoRAS GIS Tools for Support of HEC-RAS using ArcGIS - User ' s Manual*. U.S. Army Corps of Engineers - Hydrologic Engineering Center (HEC).

HEC. (2012). *HEC-GeoHMS - Geospatial Hydrological Modeling Extension—Version 10.1* (User's Manual CPD-77). U.S. Army Corps of Engineers - Hydrologic Engineering Center (HEC).

HEC. (2016a). *HEC-RAS River Analysis System 2D Modeling User's Manual—Version 5.0*. U.S. Army Corps of Engineers - Hydrologic Engineering Center (HEC).

HEC. (2016b). *HEC-RAS River Analysis System Hydraulic Reference Manual—Version 5.0*. U.S. Army Corps of Engineers - Hydrologic Engineering Center (HEC).

HEC. (2016c). *HEC-RAS River Analysis System User's Manual Version 5.0*. U.S. Army Corps of Engineers - Hydrologic Engineering Center (HEC).

HEC. (2016d). *Hydrologic Modeling System HEC-HMS - User's Manual (Version 4.2)*. U.S. Army Corps of Engineers - Hydrologic Engineering Center (HEC).

HEC. (2017). *Workshop Material, Application of HEC-HMS using Gridded Precipitation in Watersheds Outside of the United States*. U.S. Army Corps of Engineers - Hydrologic Engineering Center (HEC).

HEC. (2018). *Benchmarking of the HEC-RAS Two-Dimensional Hydraulic Modeling Capabilities*. U.S. Army Corps of Engineers - Hydrologic Engineering Center (HEC).

HEC. (2020). *HEC-RAS River Analysis System Hydraulic Reference Manual—Version 6.0 Beta*. U.S. Army Corps of Engineers - Hydrologic Engineering Center (HEC).

HEC. (2021). *HEC-RAS River Analysis System 2D Modeling User's Manual Version 6.0*. U.S. Army Corps of Engineers - Hydrologic Engineering Center (HEC).

HLNUG. (2011). *Gewässerkundliches Jahrbuch 2011—Station: Groß-Bieberau2 (GBII); ID: 24761005*. Hessisches Landesamt für Naturschutz, Umwelt und Geologie (HLNUG). http://www.hlnug.de/static/pegel/wiskiweb2/#

HLNUG. (2017a). *Digital soil map of Hesse 1:50.000 (BFD50)*. Hessisches Landesamt für Naturschutz, Umwelt und Geologie (HLNUG).

HLNUG. (2017b). *Rating curve—Station: Groß-Bieberau2 (GBII); ID: 24761005*. Hessisches Landesamt für Naturschutz, Umwelt und Geologie (HLNUG).

HLNUG. (2020a). *Discharge time series—Station: Groß-Bieberau2 (GBII); ID: 24761005*. Hessisches Landesamt für Naturschutz, Umwelt und Geologie (HLNUG).

HLNUG. (2020b). *Precipitation data time series—Station: Modautal-Brandau-Kläranlage (Modautal); ID: 2396108*. Hessisches Landesamt für Naturschutz, Umwelt und Geologie (HLNUG).

Hornberger, G. M. & Spear, R. (1981). An Approach to the Preliminary Analysis of Environmental Systems. *Journal of Environmental Management, 12(1)*.

Howes, D. A., Abrahams, A. D. & Pitman, E. B. (2006). One- and two-dimensional modelling of overland flow in semiarid shrubland, Jornada basin, New Mexico. *Hydrological Processes, 20*(5), 1027–1046. https://doi.org/10.1002/hyp.5922

Hübener, H., Bülow, K., Fooken, C., Früh, B., Hoffmann, P., Höpp, S., Keuler, K., Menz, C., Mohr, V., Radtke, K., Ramthun, H., Spekat, A., Steger, C., Toussaint, F., Warrach-Sagi, K. & Woldt, M. (2017). ReKliEs-De Ergebnisbericht. *World Data Center for Climate (WDCC)*. https://doi.org/10.2312/wdcc/rekliesde_ergebnisbericht

Hunter, N. M., Bates, P. D., Neelz, S., Pender, G., Villanueva, I., Wright, N. G., Liang, D., Falconer, R. A., Lin, B., Waller, S., Crossley, A. J. & Mason, D. C. (2008). Benchmarking 2D hydraulic models for urban flooding. *Proceedings of the Institution of Civil Engineers - Water Management, 161*(1), 13–30. https://doi.org/10.1680/wama.2008.161.1.13

HVBG. (2017a). *Amtliches Topographisch-Kartographisches Informationssystem (ATKIS®)*. Hessische Verwaltung für Bodenmanagement und Geoinformation (HVBG).

HVBG. (2017b). *Digital Elevation Model (ATKIS® DGM)—1m resolution*. Hessisches Landesamt für Bodenmanagement und Geoinformation (HVBG).

HVBG. (2019). *Luftgestütztes Messverfahren Airborne Laserscanning (ALS)*. Hessische Verwaltung für Bodenmanagement und Geoinformation (HVBG). https://hvbg.hessen.de/geoinformation/landesvermessung/geotopographie/3d-daten/airborne-laserscanning-als

IHWB. (2020). *Water level measurements of Groß-Bieberau, 5 min time interval*. Chair of Engineering Hydrology and Water Management (Fachgebiet Ingenieurhydrologie und Wasserbewirtschaftung - IHWB), Technical University of Darmstadt, Germany.

JAVAD. (2017, June 21). *Javad GNSS - TRIUMPH-LS - Data Sheet*. JAVAD: TRIUMPH-LS - The Ultimate RTK Land Survey Machine. http://javad.com/jgnss/products/receivers/triumph-ls.html

Jia, Y., Shirmeen, T., A. Locke, M., E. Lizotte Jr., R. & Douglas Shields Jr., F. (2019). Simulation of Surface Runoff and Channel Flows Using a 2D Numerical Model. In V. Hrissanthou & K. Kaffas (Eds.), *Soil Erosion—Rainfall Erosivity and Risk Assessment*. IntechOpen. https://doi.org/10.5772/intechopen.80214

Kaiser, M., Broich, K., Pflugbeil, T., Mitterer, J., Lin, Q., Sheikhy, T., Trentini, F. von, Willkofer, F., Nguyen, H., Ludwig, R. & Disse, M. (2018). Sturzflutforschung in Bayern – Ziele und Ansätze des Projekts HiOS. *Sturzflutforschung in Bayern – Ziele und Ansätze des Projekts HiOS*, *2018*(11), 685–690. https://doi.org/10.3243/kwe2018.11.005

Kalyanapu, A. J., Shankar, S., Pardyjak, E. R., Judi, D. R. & Burian, S. J. (2011). Assessment of GPU computational enhancement to a 2D flood model. *Environmental Modelling & Software*, *26*(8), 1009–1016. https://doi.org/10.1016/j.envsoft.2011.02.014

Kissel, M. & Schmalz, B. (2020). Comparison of Baseflow Separation Methods in the German Low Mountain Range. *Water*, *12*(6), 1740. https://doi.org/10.3390/w12061740

Kivva, S. L. & Zheleznyak, M. J. (2005). Two-Dimensional Modeling of Rainfall Runoff and Sediment Transport in Small Catchment Areas. *International Journal of Fluid Mechanics Research*, *32*(6), 703–717. https://doi.org/10.1615/InterJFluidMechRes.v32.i6.50

Kleiber, G. (2018). *Flächenhafte GIS-basierte Analyse der Sturzflutgefährdung im Gersprenz-Einzugsgebiet* [Bachelor thesis]. Chair of Engineering Hydrology and Water Management (Fachgebiet Ingenieurhydrologie und Wasserbewirtschaftung - IHWB), Technical University of Darmstadt, Germany.

Knebl, M. R., Yang, Z.-L., Hutchison, K. & Maidment, D. R. (2005). Regional scale flood modeling using NEXRAD rainfall, GIS, and HEC-HMS/RAS: A case study for the San Antonio River Basin Summer 2002 storm event. *Journal of Environmental Management*, *75*(4), 325–336. https://doi.org/10.1016/j.jenvman.2004.11.024

Krvavica, N. & Rubinić, J. (2020). Evaluation of Design Storms and Critical Rainfall Durations for Flood Prediction in Partially Urbanized Catchments. *Water*, *12*(7), 2044. https://doi.org/10.3390/w12072044

LAWA. (2010). *Empfehlungen zur Aufstellung von Hochwassergefahrenkarten und Hochwasserrisikokarten—Recommendations for the development of flood hazard maps and flood risk maps*. Bund/Länderarbeitsgemeinschaft Wasser (LAWA).

LAWA. (2018a). *Empfehlungen zur Aufstellung von Hochwassergefahrenkarten und Hochwasserrisikokarten* (p. 77). Bund/Länder-Arbeitsgemeinschaft Wasser (LAWA), Thüringer Ministerium für Umwelt, Energie und Naturschutz.

LAWA. (2018b). *LAWA-Strategie für ein effektives Starkregenrisikomanagement* (p. 86). Bund/Länderarbeitsgemeinschaft Wasser (LAWA).

Le, P. V. V., Kumar, P., Valocchi, A. J. & Dang, H.-V. (2015). GPU-based high-performance computing for integrated surface–sub-surface flow modeling. *Environmental Modelling & Software*, *73*, 1–13. https://doi.org/10.1016/j.envsoft.2015.07.015

Leandro, J., Chen, A. S., Djordjević, S. & Savić, D. A. (2009). Comparison of 1D/1D and 1D/2D Coupled (Sewer/Surface) Hydraulic Models for Urban Flood Simulation. *Journal of Hydraulic Engineering*, *135*(6), 495–504. https://doi.org/10.1061/(ASCE)HY.1943-7900.0000037

Leandro, J., Chen, A. S. & Schumann, A. (2014). A 2D parallel diffusive wave model for floodplain inundation with variable time step (P-DWave). *Journal of Hydrology*, *517*, 250–259. https://doi.org/10.1016/j.jhydrol.2014.05.020

Leandro, J. & Martins, R. (2016). A methodology for linking 2D overland flow models with the sewer network model SWMM 5.1 based on dynamic link libraries. *Water Science and Technology, 73*(12), 3017–3026. https://doi.org/10.2166/wst.2016.171

Leandro, J., Schumann, A. & Pfister, A. (2016). A step towards considering the spatial heterogeneity of urban key features in urban hydrology flood modelling. *Journal of Hydrology, 535*, 356–365. https://doi.org/10.1016/j.jhydrol.2016.01.060

Li, W., Chen, Q. & Mao, J. (2009). Development of 1D and 2D coupled model to simulate urban inundation: An application to Beijing Olympic Village. *Chinese Science Bulletin, 54*(9), 1613–1621. https://doi.org/10.1007/s11434-009-0208-1

Lim, N. J. & Brandt, S. A. (2019). Flood map boundary sensitivity due to combined effects of DEM resolution and roughness in relation to model performance. *Geomatics, Natural Hazards and Risk, 10*(1), 1613–1647. https://doi.org/10.1080/19475705.2019.1604573

Loretz, B. & Volz, C. (2017). Strukturierte Netze in der hydraulischen Modellierung mit Grafikkarten. *Wasserwirtschaft, 107*(6), 45–50. https://doi.org/10.1007/s35147-017-0081-9

LUBW. (2003). *Hydraulik naturnaher Fließgewässer Teil 3—Rauheits- und Widerstandsbeiwerte für Fließgewässer in Baden-Württemberg* (No. 78; Oberirdische Gewässer, Gewässerökologie, p. 104). Landesanstalt für Umwelt, Messungen und Naturschutz (LUBW).

LUBW. (2012). *Hochwassergefahrenkarten in Baden-Württemberg—Leitfaden* (Version 2.3). Landesanstalt für Umwelt, Messungen und Naturschutz (LUBW). https://www.hochwasser.baden-wuerttemberg.de/publikationen

LUBW. (2016). *Leitfaden Kommunales Starkregenrisikomanagement in Baden-Württemberg.* Landesanstalt für Umwelt, Messungen und Naturschutz Baden-Württemberg (LUBW).

Maidment, D. & Hoogerwerf, T. (2002). *Parameter Sensitivity in Hydrologic Modeling* [Technical Report]. Center for Research in Water Resources, The University of Texas at Austin.

Makkonen, L. (2006). Plotting Positions in Extreme Value Analysis. *Journal of Applied Meteorology and Climatology, 45*(2), 334–340. https://doi.org/10.1175/JAM2349.1

Mandlburger, G., Höfle, B., Briese, C., Ressl, C., Otepka, J., Hollaus, M. & Pfeifer, N. (2009). Topographische Daten aus Laserscanning als Grundlage für Hydrologie und Wasserwirtschaft. *Österreichische Wasser- und Abfallwirtschaft*, *61*(7), 89–97. https://doi.org/10.1007/s00506-009-0095-3

Melenti, I. L., Keri, A. A. & Rusu, T. (2011). Soil Conservation Service Curve Number Method for Surface Runoff Estimation Using GIS Techniques, in Rosia Poieni Mining Area (Romania). *ProEnvironment*, *4*, 240–246.

MKULNV. (2014). *Bericht zu den Hochwassergefahrenkarten und Hochwasserrisikokarten (HWGK/HWRK) im Rahmen der EG-Hochwasserrisikomanagement-Richtlinie (EG-HWRM-RL) in NRW*. Ministerium für Klimaschutz, Umwelt, Landwirtschaft, Natur- und Verbraucherschutz des Landes Nordrhein-Westfalen (MKULNV).

Muncaster, S., Bishop, W., & McCowan, A. (2006). Design Flood Estimation in Small Catchments Using Two-dimensional Hydraulic Modelling: A Case Study. *30th Hydrology & Water Resources Symposium: Past, Present & Future.* https://search.informit.org/doi/10.3316/informit.499152388058951

Muthusamy, M., Casado, M. R., Butler, D. & Leinster, P. (2021). Understanding the effects of Digital Elevation Model resolution in urban fluvial flood modelling. *Journal of Hydrology*, *596*, 126088. https://doi.org/10.1016/j.jhydrol.2021.126088

Neal, J. C., Fewtrell, T. J., Bates, P. D. & Wright, N. G. (2010). A comparison of three parallelisation methods for 2D flood inundation models. *Environmental Modelling & Software*, *25*(4), 398–411. https://doi.org/10.1016/j.envsoft.2009.11.007

Néelz, S. & Pender, G. (2013). *Benchmarking the latest generation of 2D hydraulic modelling packages—Report* (No. SC120002; p. 194). Environment Agency - UK.

Nguyen, H., Degener, J. & Kappas, M. (2015). Flash Flood Prediction by Coupling KINEROS2 and HEC-RAS Models for Tropical Regions of Northern Vietnam. *Hydrology*, *2*(4), 242–265. https://doi.org/10.3390/hydrology2040242

Nguyen, P., Thorstensen, A., Sorooshian, S., Hsu, K., AghaKouchak, A., Sanders, B., Koren, V., Cui, Z. & Smith, M. (2016). A high resolution coupled hydrologic–hydraulic model (HiResFlood-UCI) for flash flood modeling. *Flash Floods, Hydro-Geomorphic Response and Risk Management*, *541*, 401–420. https://doi.org/10.1016/j.jhydrol.2015.10.047

Oberle, P., Kron, A., Kerlin, T., Nestmann, F. & Rodriguez, E. R. (2021). Diskussionsbeitrag zur Fließwiderstandsparametrisierung zur Simulation der Oberflächenabflüsse bei Starkregen. *Wasserwirtschaft, 2021*(4), 12–21.

Ouédraogo, W., Raude, J. & Gathenya, J. (2018). Continuous Modeling of the Mkurumudzi River Catchment in Kenya Using the HEC-HMS Conceptual Model: Calibration, Validation, Model Performance Evaluation and Sensitivity Analysis. *Hydrology, 5*(3), 44. https://doi.org/10.3390/hydrology5030044

Ozdemir, H., Sampson, C., De Almeida, G. & Bates, P. (2013). Evaluating scale and roughness effects in urban flood modelling using terrestrial LIDAR data. *Hydrology and Earth System Sciences Discussions, 10*, 5903–5942. https://doi.org/10.5194/hessd-10-5903-2013

Palmer, V. J. (1946). Retardance coefficients for low flow in channels lined with vegetation. *Transactions, American Geophysical Union, 27*(2), 187. https://doi.org/10.1029/TR027i002p00187

Pappenberger, F., Beven, K. J., Ratto, M. & Matgen, P. (2008). Multi-method global sensitivity analysis of flood inundation models. *Advances in Water Resources, 31*(1), 1–14. https://doi.org/10.1016/j.advwatres.2007.04.009

Patt, H. & Jüpner, R. (Eds.). (2013). *Hochwasser-Handbuch: Auswirkungen und Schutz* (2., neu bearb. Aufl). Springer Vieweg.

Pfister, A., Treis, A. & Teichgräber, B. (2015). Der Einsatz von Radardaten für wasserwirtschaftliche Zwecke bei Emschergenossenschaft und Lippeverband. *Korrespondenz Wasserwirtschaft, 2015*(2), 115–124. https://doi.org/10.3243/kwe2015.02.005

Pina, R., Ochoa-Rodriguez, S., Simões, N., Mijic, A., Marques, A. & Maksimović, Č. (2016). Semi- vs. Fully-Distributed Urban Stormwater Models: Model Set Up and Comparison with Two Real Case Studies. *Water, 8*(2), 58. https://doi.org/10.3390/w8020058

Rangari, V. A., Umamahesh, N. V. & Bhatt, C. M. (2019). Assessment of inundation risk in urban floods using HEC RAS 2D. *Modeling Earth Systems and Environment, 5*(4), 1839–1851. https://doi.org/10.1007/s40808-019-00641-8

Rauchlatner, P. & Höppl, W. (2009). Anforderungen an die Fernerkundung und die Abfluss-modellierung aus Sicht der wasserwirtschaftlichen Planung. *Österreichische Wasser- und Abfallwirtschaft*, *7–8*, 105–109.

Rehmann, H. U., Zollinger, M. W. & Collings, G. B. (2003). *Hydrological vs. Hydraulic Routing—Possibilities with Two-Dimensional Hydraulic Modelling*. 3311–3316.

Saltelli, A. (2004). *Sensitivity analysis in practice: A guide to assessing scientific models*. Wiley.

Saltelli, A. (2008). *Global sensitivity analysis: The primer*. John Wiley.

Savage, J., Bates, P., Freer, J., Neal, J. & Aronica, G. (2016). When does spatial resolution become spurious in probabilistic flood inundation predictions?. *Hydrological Processes*, *30*(13), 2014–2032. https://doi.org/10.1002/hyp.10749

Savage, J., Pianosi, F., Bates, P., Freer, J. & Wagener, T. (2016). Quantifying the importance of spatial resolution and other factors through global sensitivity analysis of a flood inundation model. *Water Resources Research*, *52*(11), 9146–9163. https://doi.org/10.1002/2015WR018198

Schanze, J. (2018). Pluvial flood risk management: An evolving and specific field: Editorial. *Journal of Flood Risk Management*, *11*(3), 227–229. https://doi.org/10.1111/jfr3.12487

Schmalz, B. & Kruse, M. (2019). Impact of Land Use on Stream Water Quality in the German Low Mountain Range Basin Gersprenz. *Landscape Online*, *72*, 1–17. https://doi.org/10.3097/LO.201972

Scholand, D. & Schmalz, B. (2021). Deriving the Main Cultivation Direction from Open Remote Sensing Data to Determine the Support Practice Measure Contouring. *Land*, *10*(11), 1279. https://doi.org/10.3390/land10111279

Schröder, W. & Euler, G. (Eds.). (1999). *Grundlagen des Wasserbaus: Hydrologie, Hydraulik, Wasserrecht* (4., völlig überarb. und erw. Aufl). Werner.

Schürmann, L. (2018). *Auswirkung der Aufbereitung und Verwendung verschiedener Niederschlagseingangsdaten auf die Ergebnisse in der Starkregenmodellierung (Effect of the preparation and use of different precipitation input data on the results in heavy rainfall modeling)* [Master thesis]. Chair of Engineering Hydrology and Water Management (Fachgebiet Ingenieurhydrologie und Wasserbewirtschaftung - IHWB), Technical University of Darmstadt, Germany.

Segura-Beltrán, F., Sanchis-Ibor, C., Morales-Hernández, M., González-Sanchis, M., Bussi, G. & Ortiz, E. (2016). Using post-flood surveys and geomorphologic mapping to evaluate hydrological and hydraulic models: The flash flood of the Girona River (Spain) in 2007. *Journal of Hydrology*, 541, 310–329. https://doi.org/10.1016/j.jhydrol.2016.04.039

Senarath, S. U. S., Ogden, F. L., Downer, C. W. & Sharif, H. O. (2000). On the calibration and verification of two-dimensional, distributed, Hortonian, continuous watershed models. *Water Resources Research*, *36*(6), 1495–1510. https://doi.org/10.1029/2000WR900039

Seyoum, S. D., Vojinovic, Z., Price, R. K. & Weesakul, S. (2012). Coupled 1D and Noninertia 2D Flood Inundation Model for Simulation of Urban Flooding. *Journal of Hydraulic Engineering*, *138*(1), 23–34. https://doi.org/10.1061/(ASCE)HY.1943-7900.0000485

Shah, Z., Saraswat, A., Samal, D. R. & Patel, D. (2022). A single interface for rainfall-runoff simulation and flood assessment—A case of new capability of HEC-RAS for flood assessment and management. *Arabian Journal of Geosciences*, *15*(18), 1526. https://doi.org/10.1007/s12517-022-10721-2

Tahmasbine, H., Feyzolahpo, M., Mumipour, M. & Zakerhosei, F. (2012). Rainfall-runoff Simulation and Modeling of Karun River Using HEC-RAS and HEC-HMS Models, Izeh District, Iran. *Journal of Applied Sciences*, *12*(18), 1900–1908. https://doi.org/10.3923/jas.2012.1900.1908

Taylor, A., Johnson, C. & Kapugama, D. (2014). Never mind the subcatchments, here's the rain on grid. In Engineers Australia & National Committee on Water Engineering (Eds.), *Hydrology and Water Resources Symposium 2014* (pp. 86–93). ACT: Engineers Australia.

Thakur, B., Parajuli, R., Kalra, A., Ahmad, S. & Gupta, R. (2017). Coupling HEC-RAS and HEC-HMS in Precipitation Runoff Modelling and Evaluating Flood Plain Inundation Map. *World Environmental and Water Resources Congress 2017*, 240–251. https://doi.org/10.1061/9780784480625.022

Treis, A. & Pfister, A. (2019). Flächenhafte Niederschlagserfassung mittels Radar—Erfahrungen aus 25 Jahren Radardatennutzung bei Emschergenossenschaft und Lippeverband. *Wasserwirtschaft*, *109*(7–8), 56–59. https://doi.org/10.1007/s35147-019-0190-8

Tyrna, B., Assmann, A., Fritsch, K. & Johann, G. (2018). Large-scale high-resolution pluvial flood hazard mapping using the raster-based hydrodynamic two-dimensional model FloodAreaHPC. *Journal of Flood Risk Management*, *11*, 1024–1037. https://doi.org/10.1111/jfr3.12287

UMBW. (2016). *Leitfaden—Hochwassergefahrenkarten in Baden-Württemberg*. Ministerium für Umwelt, Klima und Energiewirtschaft Baden-Württemberg (UMBW).

USDA. (1986). *Urban Hydrology for Small Watersheds, Technical Release (TR)—55*. United States Department of Agriculture, Natural Resources Conservation Service.

USDA. (2010). *National Engineering Handbook, Part 630 Hydrology Chapters* (Issue Chapter 15-Time of Concentration). United States Department of Agriculture.

Van Drie, R., Milevski, P. & Simon, M. (2010). *ANUGA: Identifying Real Hazard by Direct Hydrology in 2D Hydraulic Model and the role of roughness*. 7th International Conference on sustainable techniques and strategies for urban water management, Lyon.

Van Drie, R; Milevski, P and Simon, M. Validation of a 2-D Hydraulic Model - ANUGA, to Undertake Hydrologic Analysis. *Proceedings of the 34th World Congress of the International Association for Hydro- Environment Research and Engineering: 33rd Hydrology and Water Resources Symposium and 10th Conference on Hydraulics in Water Engineering.* Barton, A.C.T.: Engineers Australia, 2011: 450-457.

Veneziano, D. & Villani, P. (1999). Best linear unbiased design hyetograph. *Water Resources Research*, *35*(9), 2725–2738. https://doi.org/10.1029/1999WR900156

Vogel, K., Ozturk, U., Riemer, A., Laudan, J., Sieg, T., Wendi, D., Agarwal, A., Rözer, V., Korup, O. & Thieken, A. (2017). Die Sturzflut von Braunsbach am 29. Mai 2016 - Entstehung, Ablauf und Schäden eines "Jahrhundertereignisses", Teil 2: Geomorphologische Prozesse und Schadensanalyse. *Hydrologie und Wasserbewirtschaftung*, *61*(3), 163–175. https://doi.org/10.5675/HyWa_2017,3_2

Wackermann, R. (1981). Eine Einheitsganglinie aus charakteristischen Systemwerten ohne Niederschlags-Abfluß-Messungen—A unit hydrograph developed from characteristic parameters without the aid of rainfall-runoff readings. *Wasser und Boden*, *1981*(1), 23–28.

Walega, A., Rutkowska, A. & Policht-Latawiec, A. (2014). Sensitivity of Beta and Weibull synthetic unit hydrographs to input parameter changes. *Polish Journal of Environmental Studies*, *23*(1), 221–229.

Weiler, M., McDonnell, J. J., Tromp-van Meerveld, I. & Uchida, T. (2005). Subsurface Stormflow. In M. G. Anderson & J. J. McDonnell (Eds.), *Encyclopedia of Hydrological Sciences* (p. hsa119). John Wiley & Sons, Ltd. https://doi.org/10.1002/0470848944.hsa119

Willems, P. (2012). Model uncertainty analysis by variance decomposition. *Physics and Chemistry of the Earth, Parts A/B/C*, *42–44*, 21–30. https://doi.org/10.1016/j.pce.2011.07.003

Willis, T., Wright, N. & Sleigh, A. (2019). Systematic analysis of uncertainty in 2D flood inundation models. *Environmental Modelling & Software*, *122*, 104520. https://doi.org/10.1016/j.envsoft.2019.104520

Winterrath, T. (2022, February 24). *Starkregen kann überall auftreten*. Für und Wider einer Versicherungspflicht gegen Elementarschäden - Sachverständigenrat für Verbraucherfragen, Online.

Winterrath, T., Brendel, C., Hafer, M., Junghänel, T., Klameth, A., Lengfeld, K., Walawender, E., Weigl, E. & Becker, A. (2018a). *Radar climatology (RADKLIM) version 2017.002; gridded precipitation data for Germany: Radar-based gauge-adjusted one-hour precipitation sum (RW)* (Version 1, p. approx. 40 MByte per gzip compressed ascii or binary archive with monthly data) [Gzip compressed and tar packed ascii and binary]. Deutscher Wetterdienst (DWD). https://doi.org/10.5676/DWD/RADKLIM_RW_V2017.002

Winterrath, T., Brendel, C., Hafer, M., Junghänel, T., Klameth, A., Lengfeld, K., Walawender, E., Weigl, E. & Becker, A. (2018b). *Radar climatology (RADKLIM) version 2017.002; gridded precipitation data for Germany: Radar-based quasi gauge-adjusted five-minute precipitation rate (YW)* (Version 1, p. approx. 500 MByte per gzip compressed ascii or binary archive with monthly data) [Gzip compressed and tar packed ascii and binary]. Deutscher Wetterdienst (DWD). https://doi.org/10.5676/DWD/RADKLIM_YW_V2017.002

Yu, D. & Coulthard, T. J. (2015). Evaluating the importance of catchment hydrological parameters for urban surface water flood modelling using a simple hydro-inundation model. *Journal of Hydrology, 524,* 385–400. https://doi.org/10.1016/j.jhydrol.2015.02.040

Zaiß, H. (1989). *Simulation ereignisspezifischer Einflüsse des Niederschlag-Abfluß-Prozesses von Hochwasserereignissen kleiner Einzugsgebiete mit N-A-Modellen, Dissertation.* TH Darmstadt - Institut für Wasserbau.Zeiger, S. J. & Hubbart, J. A. (2021). Measuring and modeling event-based environmental flows: An assessment of HEC-RAS 2D rain-on-grid simulations. *Journal of Environmental Management, 285,* 112125. https://doi.org/10.1016/j.jenvman.2021.112125

Appendix

A Mathematical model description

In this study, the hydrological processes are simulated using the model HEC-HMS from the U.S. Army Corps of Engineers (USACE). All model components and their mathematical description are documented in detail in the technical reference manual (HEC, 2000). HEC-HMS has implemented several routines to determine the rainfall-runoff process of a catchment. In the following, the routines used in our study are briefly summarized. In each catchment, the runoff formation is determined via SCS-CN method. The basic equations (**Eq. 1 - Eq. 4**) to determine the excess rainfall P_e are listed in the following **Table 1**. The direct runoff is determined for each subcatchment by the use of the Clark Unit Hydrograph. This approach makes use of the concept of a linear storage with the storage coefficient R and the time-area relationship A/At for each subcatchment. The watershed specific relationship can be determined by the catchment specific time of concentration t_c which was determined by the use of the Watershed lag time USDA (2010). The basic equations (**Eq. 5 – Eq. 7**) to determine the catchment specific Unit Hydrograph are listed in the following **Table 1**. For the runoff routing in the channel, the Kinematic Wave Equation was used. The approach makes use of a simplified combination of the momentum (Energy gradient Sf is set equal bottom slope S0) and the continuity equation for shallow flow (**Eq. 8 – Eq. 9**). The kinematic-wave approximation can be used for stream flow where the dominant force is associated with the bottom slope and the channel roughness. The energy gradient Sf is determined via Manning's equation and calibrated by the Manning's n value (**Eq. 10**). The partial differential equation (**Eq. 11**) is solved for the specified initial and boundary condition and channel geometries (**Eq. 12 - Eq. 13**) with a standard finite-difference scheme which is described in the model's technical reference manual (HEC, 2000). The baseflow is set as a constant baseflow Q0 during the event.

Table 1: Mathematical model description of the applied hydrological model HEC-HMS (HEC, 2000)

Hydrological process: *calculation routine*	Mathematical model (HEC, 2000)		
Runoff formation: *SCS-Curve Number*	Precipitation excess P_e	$P_e = \dfrac{(P - I_a)}{P - I_a + S}$	**(Eq. 1)**
	Initial abstraction I_a	$I_a = 0.2 * S$	**(Eq. 2)**
	Maximum retention S	$S = \dfrac{25400 - 254 * CN}{CN}$	**(Eq. 3)**
	Composite Curve number CN for the drainage area A_i of subdivision i	$CN_{composite} = \dfrac{\sum A_i * CN_i}{\sum A_i}$	**(Eq. 4)**
Runoff concentration: *Clark Unit Hydrograph*	Linear storage S_{linear}	$\dfrac{dS}{dt} = I_t - O_t \; ; \; S_t = R * O_t$	**(Eq. 5)**
	Storage coefficient R	calibration parameter	-
	Time of concentration t_c	Watershed lag time (SCS), (USDA, 2010)	-
	Outflow O_t, Inflow I_t	$O_t = \dfrac{\Delta t}{R + 0.5\,\Delta t} * I_t + (1 - \dfrac{\Delta t}{R + 0.5\,\Delta t}) * O_{t-1}$	**(Eq. 6)**
	Time-area relationship $\dfrac{A_t}{A}$	$\dfrac{A_t}{A} = \begin{cases} 1.414 \left(\dfrac{t}{t_c}\right)^{1.5} & for\ t \leq \dfrac{t_c}{2} \\ 1 - 1.414\left(1 - \dfrac{t}{t_c}\right)^{1.5} & for\ t \geq \dfrac{t_c}{2} \end{cases}$	**(Eq. 7)**
Runoff routing: *Kinematic Wave*	Simplified momentum equation (1D)	$S_f = S_0$ $S_f -$ Energy gradient $S_0 -$ Bottom slope	**(Eq. 8)**
	Simplified continuity equation (1D)	$\dfrac{\partial A}{\partial t} + \dfrac{\partial Q}{\partial x} = q$ $A -$ Cross sectional area $Q -$ flow $q -$ lateral inflow	**(Eq. 9)**
	Energy gradient S_f (Manning's equation)	$v = \dfrac{C * R^{\frac{2}{3}} * S_f^{\frac{1}{2}}}{n}$ $R -$ Hydraulic radius $S_f -$ Energy gradient $C -$ Conversion constant $n -$ Manning's roughness coefficient	**(Eq. 10)**
	Kinematic wave approximation	$\dfrac{\partial A}{\partial t} + \alpha m A^{(m-1)} \dfrac{\partial A}{\partial x} = q$ $\alpha, m -$ Parameters for flow geometry and surface roughness	**(Eq. 11)**
	e.g. Rectangular channel section	$\alpha = \dfrac{1.49}{n} S^{\frac{1}{2}} * W^{-\frac{2}{3}} ; m = \dfrac{5}{3}$ $S -$ Slope $W -$ Channel width	**(Eq. 12)**
	e.g. Triangular channel section	$\alpha = \dfrac{0.94}{n} S^{\frac{1}{2}} * (\dfrac{Z}{1 + Z^2})^{\frac{1}{3}} ; m = \dfrac{4}{3}$ $Z -$ Bank slope	**(Eq. 13)**
	Further channel shapes	s. Technical Reference Manual (HEC-HMS), (HEC, 2000)	-
Baseflow: *Constant Monthly*	Baseflow Q_0,	constant flow	-

2d overland flow is determined by the 2d hydrodynamic model HEC-RAS from the U.S. Army Corps of Engineers (USACE). The theoretical basis for the 2d unsteady flow hydrodynamics is documented in detail in the technical reference manual (HEC, 2016b). The mathematical model (s. **Table 2**) consists of the 2d equations of the continuity of mass (**Eq. 14** and **Eq. 15**) and momentum (**Eq. 17**), the 2d Shallow Water Equation and their simplification, the Diffusion Wave Approximation (**Eq. 19**). For both equation sets the model makes use of the subgrid bathymetry approach (Casulli, 2009). The approach takes into account the fine underlying topography of each cell by a characteristic cell volume property table (**Eq. 16** and **Eq. 20**). This makes it possible to define a coarser mesh resolution than the resolution of the digital elevation model. The basic equations to determine overland flow are listed in the following **Table 2**. HEC-RAS solves the equations by a hybrid discretization scheme combining finite differences and finite volumes. The hybrid discretization makes advantage of the orthogonality of the grid. If the grid is orthogonal, the normal derivatives are determined by a finite difference approximation. If the grid is not orthogonal, a finite volume approximation is used. The numerical methods to solve the underlying mathematical equations are described in detail in the hydraulic reference manual of the model (HEC, 2016b).

Table 2: Mathematical model description of the applied hydrodynamic model HEC-RAS (HEC, 2016b)

Hydrodynamic process	Mathematical model (HEC, 2016b)		
	Continuity equation (2d)	$$\frac{\partial H}{\partial t} + \frac{\partial (hu)}{\partial x} + \frac{\partial (hv)}{\partial y} + q = 0$$	**(Eq. 14)**
		H − Water surface elevation h − Water depth u, v − velocity in x/y − direction q − source / sink term	
	Continuity equation (2d) - Integral form	$$\frac{\partial}{\partial t}\iiint_\Omega d\Omega + \iint_S V \bullet n dS + Q = 0$$	**(Eq. 15)**
		Ω − 3D space of the fluid V (u, v) − Velocity vector n − Boundary normal vector S − Side boundaries Q − Inflow/outflow	
	Subgrid bathymetry mass conservation	$$\frac{\Omega(H^{n+1}) - \Omega(H^n)}{\Delta t} + \sum_k V_k \bullet n_k A_k(H) + Q = 0$$	**(Eq. 16)**
		$\Omega (H)$ − Cell volume $A_k(H)$ − Face areas $V_k(H)$ − Average velocity of face k $n_k(H)$ − Normal vector of face k	
	Momentum equation (2d)	$$\frac{\partial u}{\partial t} + u\frac{\partial u}{\partial x} + v\frac{\partial u}{\partial y} = -g\frac{\partial H}{\partial x} + v_t\left(\frac{\partial^2 u}{\partial x^2} + \frac{\partial^2 u}{\partial y^2}\right) - c_f u + fv$$ $$\frac{\partial v}{\partial t} + u\frac{\partial v}{\partial x} + v\frac{\partial v}{\partial y} = -g\frac{\partial H}{\partial y} + v_t\left(\frac{\partial^2 v}{\partial x^2} + \frac{\partial^2 v}{\partial y^2}\right) - c_f v + fu$$	**(Eq. 17)**
		u, v − velocity in x/y − direction v_t − Eddy viscosity coefficient c_f − Bottom friction coefficient g − Gravitational acceleration f − Coriolis parameter	
	Bottom friction	$$c_f = \frac{n^2 g |V|}{R^{4/3}}$$	**(Eq. 18)**
		$|V|$ − Magnitude of the velocity n − Roughness coefficient (Manning's n) R − Hydraulic radius	
	Diffusion Wave Approximation – Differential form	$$\frac{\partial H}{\partial t} - \nabla \bullet \beta \nabla H + q = 0 \qquad \beta = \frac{(R(H))^{5/3}}{n|\nabla H|^{1/2}}$$	**(Eq. 19)**
	Diffusion Wave Approximation – Subgrid bathymetry	$$\frac{\Omega(H^{n+1}) - \Omega(H^n)}{\Delta t} - \sum_k \alpha \nabla H \bullet n + Q = 0 \text{,}$$ $$\alpha = \alpha(H) = \frac{(R(H))^{2/3} A_k(H)}{n|\nabla H|^{1/2}}$$	**(Eq. 20)**
		$\Omega (H^n)$ − Cell volume at time n $A_k(H)$ − Area of face k	